HEALTH & SAFETY LABORATORY

Review of Vapor Cloud Explosion Incidents

MH/15/80

Lead Authors: **Graham Atkinson and Jonathan Hall**
Contributing Authors: **Alison McGillivray**
Technical Reviewer: **Jill Wilday**
Editorial Reviewer: **Mike Wardman**
Report Authorised for Issue By: **Rosemary Gibson**
Date Authorised: **April 11th 2016**

DISTRIBUTION

Simon Rose	ORNL
Julie Halliday	PHMSA
David Painter	HSE
Edmund Cowpe	HSE

PRIVACY MARKING:

Commercial in confidence

CONTENTS

1 ACKNOWLEDGEMENTS

Additional Reviewers

Kelly Thomas, Baker Engineering & Risk Consultants
David Moore, AcuTech
Brad Fuller, AcuTech

2   EXECUTIVE SUMMARY

This review of major vapor cloud incidents has been jointly commissioned by the US Pipeline and Hazardous Materials Safety Administration (PHMSA) and the UK Health and Safety Executive (HSE). The primary objective was to improve understanding of vapor cloud development and explosion in order to examine the potential for these hazards to exist or develop at LNG export plants that store substantial quantities of these flammable gases for use in the liquefaction process or as a by-product from the liquefaction.

Many of the findings of the review are also relevant to other types of site including: gasoline storage depots, tanker terminals, refineries and chemical processing sites. There are also implications for the assessment of risks from pipelines.

2.1   POTENTIAL FOR VAPOR CLOUD EXPLOSIONS AT LNG SITES

This review has not found any historical records of LNG (methane) vapor cloud explosions in open areas with severity sufficient to cause secondary damage to tanks and pipes and consequently rapid escalation of an incident from a minor process leak to a major loss of inventory.

On the other hand some LNG sites (especially export sites) also hold substantial amounts of refrigerant gases and blends containing ethane, propane, ethylene and iso-butane. Higher hydrocarbons may also be produced and stored on LNG export sites as by-products of gas condensation. There are numerous examples of Vapor Cloud Explosions (VCEs) in open areas involving these higher molecular weight materials and the storage and use of higher molecular weight hydrocarbons on LNG export sites may (if not managed adequately) introduce an additional set of incident scenarios in which VCEs trigger rapid escalation of loss of containment.

This study involves a review of 24 major VCE incidents focussing on source terms, cloud development and explosion mechanics. The incidents studied are split between permanent fuel gases C2-C4 (e.g. LPG) and volatile liquids C4-C6 (e.g. gasoline). The source terms for leaks of gases and liquids are different but once a stable current of cold heavy vapor forms, the subsequent development of LPG and gasoline clouds are similar. The fundamental combustion properties of all the saturated hydrocarbons in the range C2-C6 are very similar (Table 1) and this is reflected in the explosion damage observed in VCEs. Those operating sites handling LPG should be interested in records of cloud development and VCEs at gasoline sites and vice versa.

Table 1: Burning velocities recommended for use in venting assessments NFPA 68 (2013 Ed)

Gas	Laminar Burning velocity (cm/s)
Methane	40
Ethane	47
Propane	46
Butane	45
Pentane	46
Hexane	46
Heptane	46

It is worth noting that the siting of new LNG export terminals with large liquefaction facilities is subject to significant regulatory control especially through 49 CFR Part 193. Application of a range of other standards (especially NFPA 59A) is intended to minimize risks through strong requirements in the areas of: design, materials, construction, testing, fire protection (detection, notification, extinguishment), operating, training and maintenance. Furthermore, all LNG export terminals covered by DOT would also be under USCG safety and security regulations and likely under FERC regulations and safety reviews. LNG export terminals within navigable waters are not under DOT 49 CFR 193, but under FERC/OSHA/EPA if within state waters and USCG/MARAD if within federal waters.

2.2 FINDINGS RELEVANT TO THE ASSESSMENT OF VAPOR TRANSPORT AND DISPERSION

An important finding from the review is that a high proportion of vapor cloud incidents occurred in nil/low wind conditions. By the term "nil/low wind" we mean a wind that was so weak close to the ground that it only detrained (stripped away) a small proportion of the vapour accumulating around the source – this is discussed quantitatively in Section 6.2. Rather than being picked up and moved downwind, the vapor flow in these case was gravity driven; spreading out in all directions and/or following any downward slopes around the source.

In many of cases examined, 50% (12/24), there is clear evidence from the well-documented transport of vapor in all directions and/or meteorological records that the vapor cloud formed in nil/low-wind conditions. In a further 21% (5/24), the pattern of vapor transport suggests nil/low-wind conditions but there is insufficient data available to be sure. In the remaining 29% (7/24) vapor dispersion appears to have occurred in light or moderate winds. The latter cases corresponded to large releases that were ignited almost immediately.

At first sight these results are surprising because nil/low-wind weather conditions are relatively rare: at most temperate latitudes they usually correspond to stable conditions that develop at night in high pressure weather systems. The overall frequency is around 5%. This frequency will vary on a site by site basis around the world but the frequency is always fairly low. Notwithstanding such low frequencies, incidents in nil/low wind conditions apparently make up the majority of historical records of the most serious VCEs.

The likely explanation for this finding is that a wider range of smaller losses of containment (with much higher frequency) have the potential to cause a large cloud in these conditions, if the releases are not stopped and the vapor is allowed to accumulate around the source.

The potential importance of nil/low-wind conditions in an overall risk assessment has been investigated theoretically using a simple test case that might be of relevance at LNG sites: 2" and 4" liquid releases from a 30,000 gallon tank containing propane at 288K. Dispersion in windy conditions was modelled using PHAST and nil/low-wind vapor transport was assessed using the method described in FABIG Technical Note 12 (Atkinson and Pursell, 2013).

For wind speeds of 2 m/s and 5 m/s (F2 and D5 in the Pasquill classification scheme – Pasquill, 1961) the contour defining the lower flammable limit (LFL) reaches a maximum extent within a period of less than 30 seconds. In nil/low-wind conditions the cloud continues to grow throughout the time that the tank takes to empty (which is 350 -1500 seconds)[1] .

---

[1] *In practice the provision of gas detection and remotely operated shut–off valves at LNG export sites provides important protection against this kind of release.*

The maximum area covered by the flammable cloud is typically several hundred times greater in nil/low-wind conditions than in light winds.

The implication of this type of analysis is that if the density of ignition sources is constant and quite low in the area around the tank, the chances of ignition in nil/low-wind conditions would be hundreds times greater for a given release. This illustrates why nil/low-wind conditions dominate records of major vapor cloud incidents even though the weather frequency is low.

Losses of containment in nil/low-wind conditions are also particularly dangerous because a highly homogeneous cloud can be formed that may spread by gravitational slumping (without significant dilution) for hundreds of metres. High and low pressure releases of LPG or gasoline can form such clouds: seal failures or pipeline faults are typical high pressure failures, and tank overfills are typical low pressure events.

A very large cloud that is all close to the stoichiometric ratio increases the risk of flame acceleration to a high pressure regime capable of seriously damaging storage and process facilities, when compared with clouds that are entraining air because of wind-driven dilution. This is because fundamental burning rates fall off rapidly for concentrations away from the stoichiometric ratio (Poinsot and Veynante 2005). Once a high pressure regime is established explosions are not confined to congested areas of a site. In many of the cases reviewed almost all the footprint of the cloud was exposed to pressures in excess of 2000 mbar (29 psi). In at least one case the cloud detonated, causing extremely severe damage over the area covered by the cloud.

2.3   IMPLICATIONS FOR THE SCOPE OF RISK ASSESSMENT OR REGULATION

The worst case for dispersion of a very large release of short duration (e.g. complete failure of a large tank or a very short discharge from a large bore, high pressure pipe) may be a low (non-zero) wind in an unfavourable direction. However the complete failure of a tank whether it be an ASME storage vessel or an LNG tank is not generally considered a credible scenario.

For a wide range of smaller leaks that can be sustained over a long period (e.g. seal failures, spot corrosion failure or over-fills) nil/low-wind conditions are likely to pose the highest risks all around the source. These smaller leaks are *much more common* than catastrophic failures. Risks of sustained leaks at LNG export sites are minimised by the use of gas detection and shut-off systems and other standards e.g. for overfill protection.

In principle risk assessments (or regulation) and emergency planning should consider both types of incident – considering different types of release together with the weather conditions in which they could produce large clouds.

Different approaches to mitigation may be appropriate if nil/low-wind scenarios are considered. For example: detection of gas plumes in windy conditions generally requires a large number of closely spaced devices and the chances of limiting maximum cloud size and risk of ignition by shut-down are low – because the cloud reaches its maximum size very quickly. Investment in such systems may not be warranted. On the other hand, in nil/low-wind conditions the cloud develops slowly and can be reliably detected by a small number of sensors. Shut-down on detection may be a key element of a site's safety planning.

The problem of laminarised nil/low-wind vapor transport at medium and long distance from the source is generally better defined and easier to solve than the more familiar dispersion in windy conditions. Approximate methods suitable for fairly level sites are available in FABIG

Technical Note 12 (Atkinson and Pursell, 2013). These methods require no specialist software and assessors require a minimum of training. Some examples of application of these methods in incident analysis are given in this report.

Near-field dispersion (before laminarisation of the heavy current) is not well understood for high momentum sources e.g. releases of pressure liquefied gas. Releases that lead to fuel re-entrainment (i.e. jets that are released or deflected upwards) give the highest fuel concentrations when the flow laminarises.

2.4 FORENSIC ANALYSIS OF EXPLOSION DAMAGE

Forensic techniques for the interpretation of blast effects have improved greatly in the last ten years – especially for low lying vapor clouds. Pressure-impulse diagrams are now available for some standard objects like drums and steel boxes that are sensitive to over-pressure (crushing) damage (Chen, 2013). It is possible to identify severe explosions (defined here as those generating overpressures in excess of 2000 mbar or 29 psi) with confidence by examining such objects. Detonation tests have also demonstrated the type of damage to be expected where this has occurred.

In low-lying clouds, over relatively flat open areas, the direction of breakage of trees and posts gives a useful indication of the direction of explosion propagation. This type of analysis has been used in some of the cases reviewed to identify the location of the point of transition where a flash fire accelerated to become a severe explosion.

The review has uncovered a new means of discriminating between different types of severe explosion based on examination of slender columnar objects such as lamp posts, scaffold tubes, fence posts etc. In detonation tests and vapor cloud explosions that detonated, these objects display a characteristic pattern of distributed plastic deformation which leads to continuous curvature along the length rather than concentration of plastic deformation in "hinges". This behaviour is associated with the very high impulsive loads experienced during the normal impingement of a detonation. These loads accelerate lightweight elements on a time scale that is short compared with the transit of (elastic) flexural waves from points of restraint. Continuous curvature is very easy to spot in incident photographs and, if it can be established that an element has not been affected by a prolonged fire, it is a very good indicator that detonation has occurred. Fast deflagrations do not produce the highly impulsive forces required. Some further experimental testing and finite element analysis in this area would be useful to assist forensic work at future incidents.

2.5 PROPAGATION OF SEVERE EXPLOSIONS IN OPEN AREAS

The regular occurrence of severe explosions extending to the whole cloud has been recognised in the years since Buncefield. There has been a general presumption that this means that all such incidents were detonations. This was the only established theory that allows sufficiently rapid burning to be sustained in open areas. The results of this review cast doubt on this presumption: there are serious discrepancies between the effects of experimental detonations on a variety of objects and what has been observed at most VCE incidents. For example, as noted above, normal impact by a detonation typically leaves slender column-like objects with continuous curvature. No objects with this type of deformation have been observed at the sites presumed to have been detonations e.g. Buncefield, Jaipur, Amuay and San Juan. Similar discrepancies have been noted for all of the other types of damage reviewed.

It is consequently appropriate to critically examine the assumption that has underpinned VCE assessment for the last 30 years, namely that (unless deflagration to detonation transition or DDT occurs) high overpressures are confined to congested areas. The data suggests that severe explosions can progress by a different mechanism: one that has not yet been observed in experimental tests on congestion arrays in gas tents. There is a very large gap between the scale of clouds in real incidents and available test data and it was always possible that very-large scale phenomena might have been missed.

The data reviewed also suggests that this new type of explosion is episodic in nature. Rapid phases of burning are punctuated by pauses. The overall rate of progress of the flame is sub-sonic. This effect is shown directly in CCTV footage of the explosion at San Juan.

It is suggested in an Appendix to this report that, at very large scale, thermal radiation may play a key role in driving explosions. Pressure waves from a severe localised explosion may disturb particles on the ground and other surfaces. Thermal radiation impacting on such re-suspended particles would lead to pre-warming of the surrounding gas and the development of an area ahead of the flame (and pockets of unburned gas within the turbulent flame) where gas is warmer and consequently more reactive. Warming of propane/air by 230°C increases the laminar flame speed to that of acetylene/air. At some point this warmed gas could react violently – producing a localised explosion capable of re-elevating more particles and sustaining the episodic combustion.

There is a need for continued research effort in this area. Additional detonation testing is required to better understand how a range of targets are affected – this should include cases where the cloud concentration was stratified. If discrepancies with incident data remain, then we will need to recognise that our fundamental understanding of the mechanisms that operate in large VCEs is incomplete. There may be ways, other than DDT, in which severe explosions can be sustained in open areas. In this case other types of experiment will be needed to develop the understanding needed for reliable explosion risk assessment.

2.6 EMPIRICAL EVIDENCE ON THE TRANSITION TO SEVERE EXPLOSIONS

In the absence of a consistent fundamental understanding of all of the mechanisms that may operate in very large vapor cloud explosions, one option is to use empirical evidence from previous incidents to guide plant design and risk assessment.

The transition to a severe (but not detonative) explosion regime seems to involve some degree of congestion or confinement. Based on the incidents studied the following may act as triggers: confined explosions in buildings (e.g. pump houses), dense vegetation, pipe racks and other moderately congested plant. The extent and density of congestion required are substantially less than that required for DDT.

There are very few, if any, reports of very large premixed gasoline clouds (R>200 m) which have burned slowly as flash fires. Notwithstanding the lack of pressure effects such flash fires could cause deaths or injuries and would certainly leave a huge burned area: it seems likely that a high proportion of such occurrences would be reported. The lack of such reports suggests that if a very large cloud develops in the context of a fuel depot the probability of a severe explosion is high. A high proportion of incidents have been in fuel depots because there are larger numbers of them worldwide than refineries or other processing plants.

Our observations of the circumstances under which transition has occurred in the past provide an explanation for this: the density of pipework and other plant and the type of buildings that have provided triggers for transition are typical of fuel storage sites and could be expected in and around almost all sites. Again the conclusion is that if a very large gasoline cloud develops in a normal site, it is currently appropriate to assume that the risk of transition to a severe (non-detonative) explosion is high (close to unity). With careful design and operation of sites it may be possible to reduce the risk of such transition but currently we lack the fundamental understanding required to specify what level of control of congestion and confinement is needed.

By contrast with gasoline clouds at storage depots, the incident history for LPG pipeline failures suggests that even if a very large cloud develops and is ignited, the risk of a VCE is probably less than 50%. This appears to be because some clouds are very rich or even over the UFL. It may be that there is a significant probability that, even if a large LPG cloud does accumulate in nil/low-wind conditions, it will be too rich to undergo transition to a VCE. This is clearly of relevance to the assessment of risk at LNG sites. Additional experimental and modelling work would be useful to establish what kinds of LPG spray releases in nil/low-wind conditions result in clouds within the flammable range.

The evidence at Flixborough strongly suggests that, in this case, DDT occurred in highly confined and congested areas. The resulting detonation propagated widely through the extensive cloud around the plant, causing massive damage. Avoiding the potential for DDT by appropriate plant layout remains a priority. Significant new work in this area is underway at the time of writing (Davis et al 2016).

2.7 FURTHER WORK

A detailed review of the specific circumstances of one or more LNG export sites would be useful to assess the frequency and consequences of a range of incidents – including nil/low-wind scenarios and the potential for VCEs. Such a review would provide the basis for regulation of sites and the specification of appropriate mitigation measures.

3   INTRODUCTION

This review of major vapor cloud incidents has been jointly commissioned by the US Pipeline and Hazardous Materials Safety Administration (PHMSA) and the UK Health and Safety Executive (HSE). The primary objective was to improve understanding of vapor cloud development and explosion in order to examine the potential for these hazards to exist or develop at LNG export plants that store substantial quantities of these flammable gases for use in the liquefaction process or as a by-product from the liquefaction.

Many of the findings of the review are also relevant to other types of site including: gasoline storage depots, tanker terminals, refineries and chemical processing sites. There are also implications for the assessment of risks from pipelines carrying pressure liquefied gases and volatile liquids.

3.1   POTENTIAL VCE SCENARIOS AT LNG EXPORT SITES

This review has found no historical records of LNG vapor cloud (methane) explosions in the open with severity sufficient to cause secondary damage to tanks and pipes and consequently rapid escalation of an incident from a minor process leak to a major loss of inventory.

On the other hand, there are numerous examples of such VCEs in open areas involving higher molecular weight materials and mixtures, especially common materials such as LPG (Liquid Petroleum Gas) and gasoline. Refrigerants commonly used at LNG facilities would come within these categories. Losses of containment in very low wind conditions are particularly dangerous because a highly homogeneous flammable cloud can be formed that may spread (without significant entrainment) for hundreds of metres. Both high and low pressure releases can form such clouds: seal failures or pipeline faults are typical high pressure failures and tank overfills are typical low pressure events. Low pressure releases of refrigerants are not expected to be likely events at LNG sites.

A very large, homogeneous cloud within the flammable range greatly increases the risk of flame acceleration to a high pressure regime potentially capable of seriously damaging storage facilities. Once a high pressure regime is established explosions are not confined to congested areas of a site. In many of the cases to be reviewed almost all the footprint of the cloud is exposed to pressures in excess of 2000 mbar (29 psi). In at least one case the cloud has detonated causing extremely severe damage over the area covered by the cloud.

It follows from the above that storage and use of higher molecular weight hydrocarbons on LNG export sites may introduce an additional set of major incident scenarios in which VCEs trigger rapid escalation of loss of containment. Refrigerant gases of particular relevance are ethane, propane/ethane blends, propane, ethylene, ethylene blends, propane/isobutane blends and isopentane. Some higher hydrocarbons may also be produced and stored on LNG export sites as by-products of gas condensation.

The source terms in LPG and gasoline releases are very different but if a stable current of cold heavy vapor forms in nil/low wind conditions the subsequent (gravity driven) development of LPG and gasoline clouds is very similar. If this cloud is close to stoichiometric the explosion damage observed in a variety of objects (e.g. drums and vehicles) is also closely similar. The fundamental combustion properties of all of the aliphatic hydrocarbons C2 – C6 are comparable and for this reasons propane has long been used as a test substance in large-scale tests to be applied to a wide range of other substances. The combustion properties of propane are also commonly used to represent those of other hydrocarbons in combustion models.

Given the above observations and experience it is likely that learning about the mechanisms of flame acceleration is largely transferable between substances. Those operating sites handling LPG should be interested in records of cloud development and VCEs at gasoline sites and vice versa. The incidents studied in this project are roughly equally split between LPG and gasoline.

The reactivity of methane is lower than that of higher hydrocarbons. This leads to lower flame speeds and explosion severity. This is discussed in more detail in Section 4.3.

3.2   INCIDENTS TO BE REVIEWED

Four very large vapor cloud incidents from the last 10 years stand out as deserving particular attention:

- Buncefield (UK, 2005)   Fuel storage depot - Gasoline overfill

- Jaipur (India, 2009)   Fuel storage depot – Gasoline spray

- Amuay (Venezuela, 2012)   Refinery tank farm – Light hydrocarbon spray

- San Juan (Puerto Rico, 2009)   Fuel storage depot - Gasoline overfill

In the first three cases HSL has a substantial collection of photographic and other unpublished evidence on which to draw. The San Juan incident was investigated by the CSB and their contribution to the current work by making this data available is gratefully acknowledged.

All four of the above incidents involved very extended clouds with typical diameters in the range 400-1000 m (1300 – 3280 ft). References are given in Section 5 – where each of the incidents is described in turn.

Other earlier VCE incidents are also important in illustrating the risks involved and have been included in this review. A proportion of these have already been the subject of peer reviewed journal papers. HSE has recently assembled and digitised its archive of images from Flixborough and these have allowed a significant reassessment of this explosion.

- Skikda (Algeria, 2004)   LNG facility

- Ufa (Russia, 1989)   LPG pipeline fault

- Port Hudson (US, 1970)   LPG pipeline fault

- Newark New Jersey (US, 1983)   Fuel depot - Gasoline overfill

- St Herblain (France, 1991)   Fuel depot - Seal failure – Gasoline spray

- Naples (Italy, 1995)   Fuel depot - Gasoline overfill

- Brenham Texas (US, 1992)   LPG storage cavern – Spray release

- Flixborough (UK, 1974)   Process plant – Cyclohexane release

A number of other significant vapor cloud explosions were included in the review scope. The amount of publicly available information on these is variable.

- La Mede (France 1992)   Refinery, light hydrocarbon release

- Norco, Louisiana (1988)   Refinery, propane release

- Pasadena, Texas (1989)   HDPE unit, Ethylene/isobutane release

- Big Spring, Texas (2008)   Refinery, propylene splitter

- Geismer Louisiana (2013)   Petrochemical plant, propylene fractionator

HSE have published a review of U.S. pipeline incidents 1970 – 2000 (HSE Research Report RR036). This includes a section on flashing liquids most of which were LPG. Of 12 major incidents in this category investigated by the NTSB, 8 incidents involved delayed ignition and the development of a vapor cloud. These incidents have also been reviewed.

3.3 INFORMATION SOUGHT

The primary objective of this work was to gather together records of a selection of the most significant historic and recent examples of VCEs. The first priority was to establish the basic circumstances of the loss of containment and explosion:

1. Substances (LNG, gasoline, LPG, hydrocarbons used as refrigerants);

2. Source term (e.g. tank overfill, sprays, seal failure, hole size and release pressure);

3. Release size (duration of release, inventory);

4. Weather conditions (wind speed, stability);

5. Near field dispersion – especially the formation of a low entrainment, gravity-driven flow;

6. Cloud development (footprint, depth and influence of topography and surface roughness);

7. Explosion severity (flame speed and overpressure, distance of flame travel);

8. Blast damage to plant and other structures within and outside the cloud footprint;

9. Harm to on and off-site personnel;

10. Information about the facility:

    a. Location (latitude/longitude). To clearly identify the site and to develop an understanding of the socio-economic characteristics of the location;

    b. Characteristics of area where the event occurred (e.g. close to ports, urban, rural, industrial, etc.);

    c. Maps of facility showing the property and surrounding area with distances;

      d. Category of facility (possible categories - refineries, petrochemical, gas processing, terminals and distribution, and upstream). Description of facility;

      e. Number of similar facilities in the world;

11. Information about the incident and the engineering practices at the site:

      a. Description and cause of the release (operator error, equipment malfunction, material failure, construction or design error, weld failure);

      b. What mitigation measures were in place? Did they work?

3.4   ARCHIVES OF PRIMARY DATA

An additional objective of the project was, where possible, to make publically available more detailed primary records of what happened in the incidents. These records include photographs of the aftermath and any video records of cloud accumulation and explosion.

Four electronic multimedia packages have been prepared to allow wider access to primary data from the following incidents:

- Buncefield
- Jaipur
- Flixborough
- San Juan

3.5   REPORT STRUCTURE

Section 4 comprises a basic introduction to vapor cloud explosions. It is aimed at those with limited initial knowledge of the subject - to assist interpretation of the review data presented later on.

Section 5 comprises the bulk of the report and is taken up with reviews of specific incidents.

Section 6 covers findings arising from the review that are relevant to the analysis of vapor cloud development

Section 7 covers findings relevant to the analysis of vapor cloud development

Section 8 provides a summary of all findings

Further sections contain appendices that explore additional issues arising from the review

Section 9 comprises a survey of observed explosion damage to a range of common objects including fencing, buildings, drums, boxes, vehicles etc.

Section 10 comprises an analysis of the extent to which radiative heat transfer can affect the propagation of very large scale vapor cloud explosions.

Section 11 is a preliminary analysis of the response of slender columnar objects (e.g. lamp posts, scaffold poles, fence posts etc.) to blast loading.

4　BACKGROUND INFORMATION ON VCES

4.1　THE SIGNIFICANCE OF PRE-MIXING OF FUEL AND AIR

When an accumulation of a combustible gas with a concentration above the upper flammable limit (UFL) is ignited at its surface a mixing process has to take place before full combustion occurs and this mixing is usually relatively slow and limits the rate of combustion. Such events produce fire balls rather than explosions and combustion is normally spread out over a period of several seconds. This is too slow to cause a blast wave and the main risk is from thermal radiation.

Vapor Cloud Explosions are possible where air and fuel gases are **pre-mixed** in a proportion that is within the flammable range. All that is required to initiate and spread combustion is for the unburned mixture to be heated to the point where ignition occurs. Depending on the circumstances VCE events can consume very large quantities of gas in a short period. The rapid expansion associated with combustion leads to the generation of blast waves.

Flammable concentrations for some common fuel gases are shown in Table 1.

Table 2: Flammability limits for common hydrocarbons

	Lower flammable limit (g/m^3)	Upper flammable limit (g/m^3)
Methane	36	126
Ethane	41	190
Propane	42	210
n-Butane	48	240
n-Pentane	46	270
Hexane	47	310

The rest of this section presents some basic background information on the development of pre-mixed explosion events that can lead to blast effect in vapor clouds. A summary of three types of severe events is provided at the end - on a single page.

4.2　SUB-SONIC DEFLAGRATIONS

The three parameters that determine the overpressure generated and destructive power of a VCE are:

- Burning velocity

- Degree of confinement

- Cloud geometry – e.g. linear, flat layer, hemispherical

Burning velocity

This is the rate at which the flame spreads into unburned mixture. It depends on the fuel reactivity, the turbulence intensity and the temperature of the unburned gas. It is not always the same as the observed flame speed because the burned and unburned gas are generally moving relative an observer (or the ground). However, for a similar geometry e.g. a spherical cloud flame or a flat "pancake" cloud a higher burning velocity will produce a higher flame speed. Burning rate is the fundamental quantity: flame speed is a combination of burning rate and geometric factors. The reactivity of methane is lower than higher hydrocarbons such as propane. This means the burning velocity at ambient temperature and pressure is lower and, even more importantly, the burning rate increases less rapidly with compression as an explosion develops. Obstacles play a key role in increasing the turbulent burning rate – this is discussed in more detail in 4.2.4.

Degree of confinement

Confinement is provided by strong boundaries around the gas cloud; these could be the walls of a tube, the floor and roof of a multi-storey process area or just the ground in the open. Expansion cannot occur through these boundaries and it is therefore concentrated into open boundaries. Higher velocities are required at the open boundaries and these generally imply higher driving pressures.

Cloud geometry

The rate of combustion and therefore rate of expansion depends on the area over which the flame can progress. The pressure developed depends on the size of this area in comparison with the area available for the burned gas to vent. The area for flame spread is small if the cloud is in a long line or the flame is running fast down a linear array of obstacles.

On the other hand in a spherical cloud the burning occurs over the whole surface of the flame and there is nowhere else for the expansion to occur. For a given burning rate the pressure in a spherical flame is much larger than in an open sided linear or flat one.

Linear flame	Spherical flame
Red – Area where flame is spreading	Red – Area where flame is spreading
Blue – Additional burned gas surface area available for expansion	Blue – Additional burned gas surface area available for expansion (none in this case)
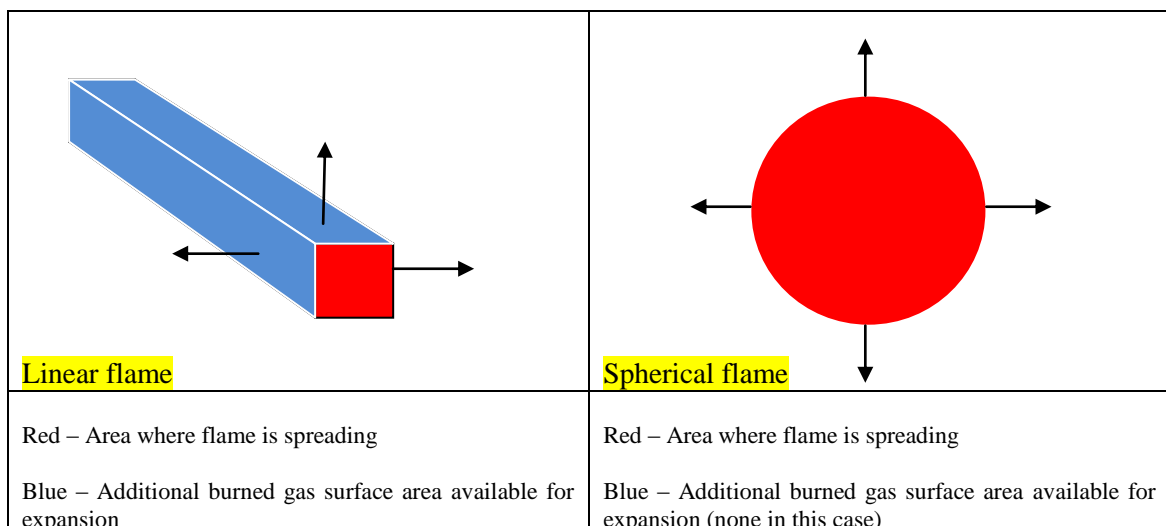
Figure 1: Areas available for flame spread and gas expansion

Some simple quantitative results are useful here to illustrate the difference between spherical and flat clouds.

Table 3 shows how the flame speed depends on burning velocity and overpressure depends on flame speed, for flame speeds well under the speed of sound. Coincidentally the expression for overpressure in both spherical and flat clouds is similar $P \sim \rho_u V_f^2$. But the fundamental quantity is the burning velocity: this is what is determined by fuel reactivity, turbulence intensity, obstacle density etc. For a given burning velocity the overpressure in a spherical cloud is larger by a factor of σ. σ is the expansion ratio in combustion, which is about 7 for a stoichiometric mixture of most hydrocarbons.

This means that clouds which are deep enough to allow 3D (spherical) explosion propagation generally produce much higher overpressures for the same gas reactivity and obstacle density.

Table 3: Flame speeds and overpressures for a spherical and flat clouds. S_u is the burning velocity, σ is the expansion ratio, ρ_u is the unburned denisty

	Flame speed V_f	Overpressure (as a function of V_f)	Overpressure (as a function of S_u)
Spherical flame spread	$S_u \ \sigma$	$\sim \rho_u V_f^2$	$\sigma^2 . \rho . S_u^2$
Flame spread in an open flat cloud	$S_u . \sigma^{1/2}$	$\sim \rho_u V_f^2$	$\sigma . \rho . S_u^2$

4.2.1 Determining the burning velocity

The above expressions for overpressure are simple, and equivalent estimates for duration of pressure pulse are also relatively straightforward to derive. The difficulty arises in the calculation of S_u (the burning velocity). Much useful empirical information is available to guide estimation of S_u in various special cases but the general problem of calculation of burning velocities remains unsolved.

4.2.2 Laminar burning

If the gas cloud is still, and the distance to the ignition point is small, the flame will be laminar (smooth surfaced). In this case the burning velocity is largely a function of the reactivity of the gas mixture[2] , which in turn depends on: type of gas, concentration, temperature and pressure.

Some measured laminar flame speeds are listed in Table 4 and Table 1. The laminar flame speed is highest for stoichiometric mixtures, declining if the mixture is lean or rich.

---

[2] *Any curvature of the flame front may also have an effect see Bradley et al. 1980. It is worth noting that there is significant scatter in reported values of laminar burning rate. Much of this is associated with variation in the extent of flame curvature in the tests or the corrections made to allow for this effect.*

Table 4: Laminar burning velocity *(equivalence ratio is the ratio of fuel volume fraction to the stoichiometric fraction)*

Gas (ϕ = equivalence ratio)	Laminar burning velocity (cm/s) (ambient pressure, 25˚C, in air)
Methane ϕ =1	38 (Proc. Comb. Inst. 1998, v27, p513)
Propane ϕ =1	42 (Proc. Comb. Inst. 1994, v25, p1341)
Propane ϕ =0.8	32 (Proc. Comb. Inst. 1994, v25, p1341)
Propane ϕ =1.2	35 (Proc. Comb. Inst. 1994, v25, p1341)
Butane ϕ =1	40 (Comb. Sci. Tech. 1998, v140, p427)
Ethylene ϕ =1	63 (Proc. Comb. Inst. 1994, v30, p193)
Acetylene ϕ =1	125 (Proc. Comb. Inst. 1990, v23, p471)

Data in Table 1 (in the Executive Summary) reinforce the point that explosion mechanics of gasoline vapor (a mixture of butane, pentane, hexane and heptane) is not expected to different markedly from that of LPG (a mixture of propane and butane).

Laminar burning velocities increase strongly with temperature (Section 10). This is very important as there are number of ways in which unburned gas may be preheated as it approaches the flame. Adiabatic compression of approaching unburned gas increases temperature and the effect on burning rate leads to higher rates of compression. This is an important positive feedback mechanism that operates as flames accelerate to produce severe explosions.

Another mechanism that can raise the temperature of unburned gas ahead of the flame is thermal radiation (Section 10).

4.2.3   Turbulent burning

If the flame grows larger or encounters turbulence the flame surface becomes distorted. In comparison to a flat sheet or smooth sphere the distorted flame surface has a higher area over which the flame can spread (Figure 2) and the burning velocity is correspondingly greater.
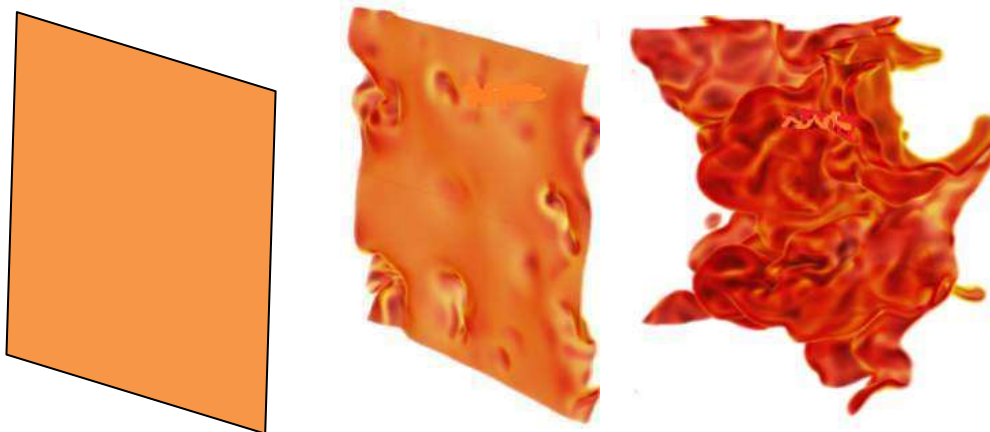
Figure 2: Laminar flame, flame with minor wrinkling and flame deformed by strong turbulence

By simply increasing the turbulence intensity (e.g. by stirring the mixture before ignition) the burning velocity can be increased by a factor of about 15- 20. To do this requires turbulent velocities of about ten times the laminar burning velocity (see Figure 3). There is significant scatter in these turbulent velocity plots. In addition to the difficulties associated with the determination of laminar burning velocity, the introduction of turbulence introduces a range of new variables (associated with the turbulence structure: length-scale and intensity) that are difficult to control.

The increase in burning velocity does not continue with ever more vigorous stirring: if the surface of the flame becomes too distorted the flame may be partially or completely extinguished by the stretching processes involved.
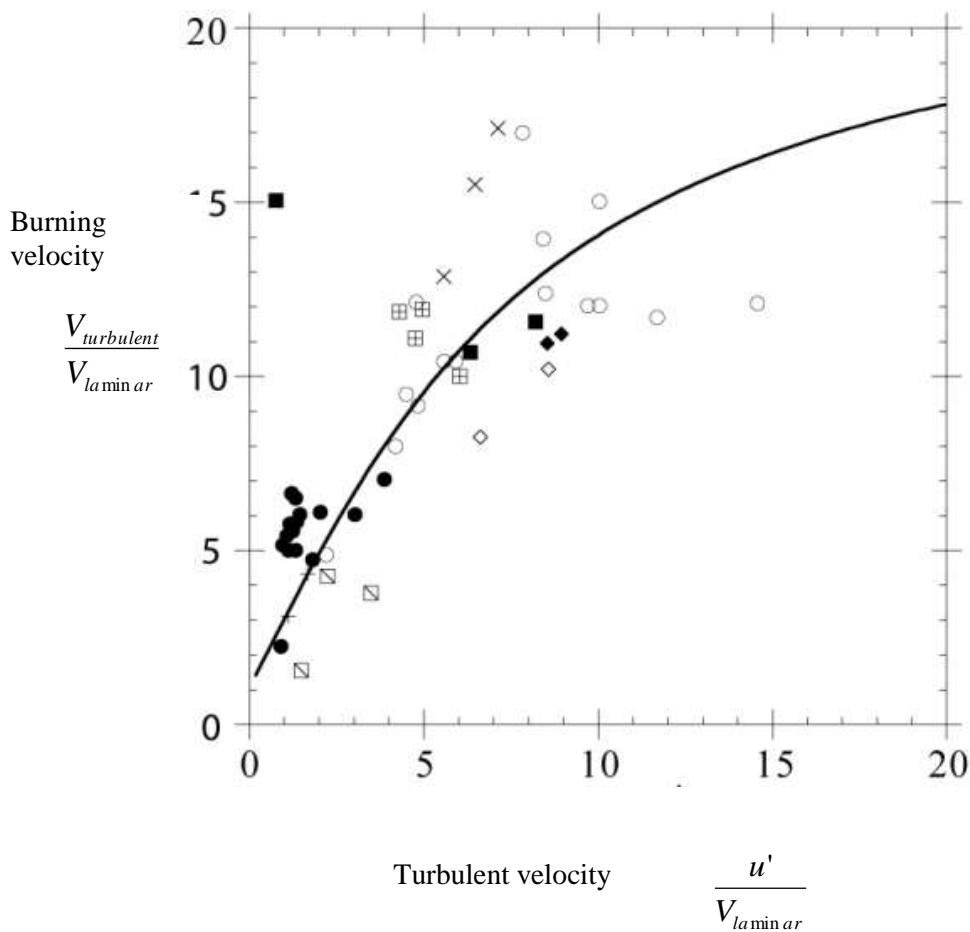
Figure 3: Turbulent burning velocity $V_{turbulent}$ as a function of turbulence velocity u' (both expressed as ratios of laminar burning velocity $V_{laminar}$).

4.2.4   Interaction with obstacles

Much higher burning rates may be reached if the flame interacts with obstacles or the flame interacts with strong large scale vortices. In this case the flame divides around the obstacles or is

stretched and folded by large scale vortices and this can further increase the area available for flame spread.

Figure 4 shows data from Gardner et al (1998) showing measured burning velocities as premixed flames pass through grids of obstacles[3]. Different turbulence levels correspond to different obstacle densities in the grids.
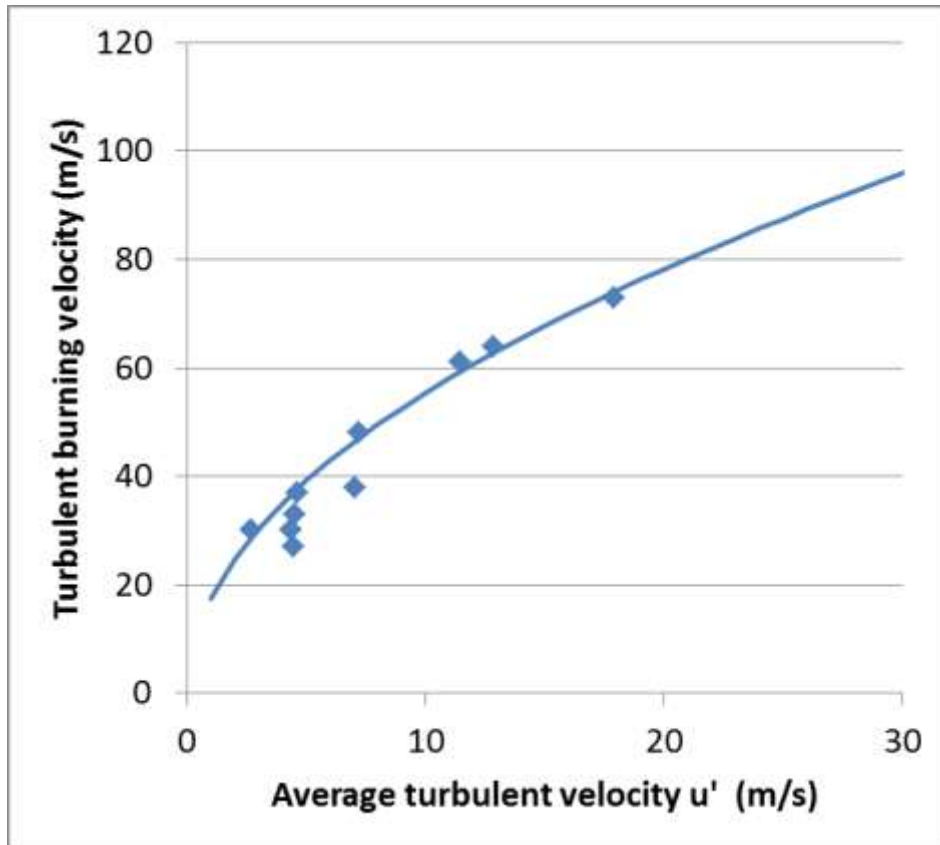
Figure 4: Increases in burning velocity with turbulent velocity.

(Note in spherical geometry flame speeds exceed burning velocities by a factor of around 7)

The higher values of turbulent velocity shown in Figure 4 correspond to severe (super-sonic) explosions in spherical flames. In this case the flame speed is approximately σ times the burning velocity so a turbulent burning velocity of greater than about 50 directly implies a flame speed greater than the speed of sound.

Table 3 suggests that, for low lying clouds, flame speed is $\sigma^{1/2}$ times the burning velocity so a turbulent burning velocity of 70 m/s (with σ = 7) implies a flame speed of around 185 m/s. In fact for C2+ hydrocarbons such flames would be unstable: the compression and heating associated with the pressure rise would increase the underlying laminar flame speed. This would feed back to increase the turbulent velocity which would again increase compression and so on (Atkinson 2015b). Flame speeds over about 150 m/s are not stable for this reason but will tend to run away to produce severe explosions.

---

[3] These data refer to low values of the Karlowitz number where flame extinction is not expected to significantly restrict the increase in burning rate with turbulence intensity.

4.3 HIGH–ORDER (SUPER-SONIC) DEFLAGATIONS

For more reactive gases (e.g. C2+ hydrocarbons) explosions in both flat and spherical clouds in highly congested environments can accelerate to produce high flame speeds. In many cases the flame acceleration continues to the point where the explosion exhibits deflagration to detonation transition (DDT). It is not clear whether stable higher order deflagrations are possible in uniformly congested environments without leading to DDT for more reactive gases. No such stable severe burning was observed in the Buncefield JIP tests (SCI 2014); whenever flame runaway occurred in these tests it was rapidly followed by DDT. The critical level of flame speed when DDT finally occurred was around 600 m/s and the pressure around 5 bar (72 psi).

In more realistic environments where obstacle densities are variable it is possible that flames could accelerate in more congested areas before decelerating in more open areas. If DDT did not occur, such an explosion would have the character of a sustained severe deflagration.

The reactivity (laminar flame speed) of methane is much less sensitive to adiabatic compression. It is unlikely that explosions in flat clouds (in the open) will ever run away to give a severe explosion. However large-scale tests by British Gas on methane air mixtures have shown that if high flame speeds (>500 m/s) are generated by strong confinement of a methane explosion (in a "bang box") then high flame speeds may be sustained even if the flame emerges into a congested area that is not confined (Harris and Wickens, 1989). DDT was not observed in the British Gas tests and it appears that in this case stable super-sonic explosions[4] are possible. When such flames reach uncongested areas the flame speed rapidly declines.

The pressure associated with super-sonic deflagration rises instantaneously in a leading shock. However if the explosion strikes a surface normally the reflected pressure is much less than would be observed for a non-reacting shock of a similar strength – because the burned gas has low density. The maximum reflected pressure for a fast deflagration is of order 10 bar (145 psi). Outside the reaction zone, reflected pressures are typically about twice the shock pressure.

4.4 EPISODIC DEFLAGRATIONS

If a flame encounters separate blocks of obstacles it is possible for the flame to generate high overpressures within the congested areas whilst the overall speed of the flame is subsonic – because of the low rate of propagation between blocks. In his case a target ahead of the flame would experience a series of separate blasts that increased in strength as the flame approached.

It is suggested in Appendix 1 (Section 10) that in some circumstances this type of burning might be possible for very large clouds in the open (i.e. with relatively low level of congestion) as a result of natural flame instability. One possible mechanism that might allow such a burning pattern is the effect of preheating of unburned gas ahead of a flame by thermal radiation. This mechanism is investigated in detail in Section 10. One characteristic of such events (in comparison with normal fast deflagrations) is that they would be unlikely to trip over into DDT: this is because fast burning would be confined to finite volumes of gas preheated by radiation. When such preheated material was consumed there would be a pause until thermal radiation had regenerated the conditions necessary for fast burning.

4.5 DETONATIONS

In deflagrations the heating of unburned gas to the ignition point occurs as a result of a combination of thermal conduction across the flame front, adiabatic compression and (in some

---

[4] *Not all super-sonic flames are detonations*

circumstances) thermal radiation. A completely separate combustion regime is possible for many gas mixtures in which ignition is triggered by a powerful shock. Initially this shock may arise from a high explosive or the combination of weaker shocks from a fast deflagration (DDT). However rapid energy release associated with the combustion can sustain a shock moving forwards at the speed of sound relative to the combustion products. A self-sustaining compression/reaction wave of this sort is known as a detonation.

The concentration ranges of mixtures of some common gases that will sustain a detonation in the open are shown in shown in Table 5. For hydrocarbons the detonation limits are somewhat narrower than the overall flammability limits (for deflagration). The ratio of flammability limits to detonability limits are similar for the components of gasoline vapor (butane – heptane) to those for LPG (Ethane – butane).

Table 5: Upper and lower detonation and deflagration flammability limits

Fuel	Lower detonation limit (%v/v)	Upper detonation limit (%v/v)	Lower flammable limit (%v/v)	Upper flammable limit (%v/v)
Methane	5.3	15.5	5	16
Ethane	4.0	9.2	3	12.4
Propane	3.0	7.0	2.1	9.5
Butane	2.5	5.2	1.8	8.4
Hydrogen	15	90	4	75

The flame speed and overpressure of detonations are high - some values for propane mixtures are shown in Table 6. Values for other hydrocarbons are similar

Table 6: Detonation velocity and pressure for propane/air mixtures (4.1% is stoichiometric)

Propane concentration	4% (v/v)	5% (v/v)	6% (v/v)	7% (v/v)
Detonation velocity (m/s)	1795	1840	1825	1790
Detonation pressure	17.3 bar 251 psi	18.2 bar 264 psi	18.0 bar 261 psi	17.4 bar 252 psi

Once established, detonations do not require any obstacles to sustain the high pressure burning regime. If DDT occurs the detonation may spread to all of the cloud which has a concentration within the detonable range. There is good evidence that this occurred in the Flixborough incident – which is reviewed in Section 5.4.

The duration of the positive pressure phase in a low lying cloud is a function of the cloud depth. In a 3m deep cloud forwards flow lasts about 5 ms.

Where a detonation impacts normally on a surface there is a marked increase in pressure because of shock reflection. The maximum sustained pressure at the surface for a reflected detonation is 35-40 bar (507 – 580 psi) but higher pressures are possible for short periods.

Some important properties of three types of severe combustion that can give blast damage effects in VCEs are summarised in Figure 5.

Detonation

Distance / Time

Steady flame propagation
Speed ~1800 m/s
Pressure ~18 bar
Reflected pressure ~35 bar
No congestion required

Pressure field calculated with a hydrocode

Fast Deflagration

Distance / Time

Steady flame propagation
Speed ~ up to about 600m/s
Pressure up to about 5 bar
Reflected pressure up to about 10 bar
Dense congestion required

Pressure field calculated with compressible CFD

Episodic Deflagration

Distance / Time

Unsteady flame propagation
Average speed 150 - 250 m/s
Max Pressure ~2-5 bar
Max Reflected pressure up to about 10 bar
Dense congestion not required
Particulate contamination required (?)

Pressure field calculated by summing the effects of fast combustion episodes with allowance for phase.

Figure 5: Summary of properties of three types of severe VCE that can cause blast damage

Note the following equivalent pressures: 5 bar = 72 psi,   10 bar = 145 psi,   18 bar = 261 psi, 35 bar = 507 psi,

5 REVIEW OF SPECIFIC INCIDENTS

5.1 JAIPUR

5.1.1 Summary of incident data

Time and date:	29th October 2009 (Thursday) Release started at approximately 18:10 i.e. just after dusk
Location	Jaipur, India (26˚46'46.2" N 75˚50'17.54" E)
Company	Indian Oil Company (Gasoline Terminal)
Narrative :	Mal-operation of a valve at the foot of a tank of gasoline led to a fountain of gasoline driven by the head of liquid in the tank. There was no wind and over a period of 75-90 minutes a vapor cloud spread in all directions to cover the whole site – approximately 700 x 700 m (2300 x 2300 ft). A boundary wall (height 2.5m – 8 ft) prevented spillage of vapor from the site into the neighbourhood. The leak was detected immediately and the tank was fitted with a remote shutoff valve that could have been used to stop the loss of containment but this valve had not been operational for several years. The large site was sparsely occupied: tanks, loading gantries, pump houses offices etc. were separated by large open areas of semi-arid scrub land. A severe VCE occurred that caused overpressure in excess of 2000 mbar (29 psi) and drag damage across almost all of site. Severe explosion effects were confined an area within a few tens of metres from the site but minor damage (e.g. windows breaking) extended to a range of 2 km (6500 ft). Six people were killed on the IOC site and five others in buildings immediately adjacent to the site. Thanks to the efforts of a number of investigators the incident has provided one of the most complete records of the progress of a severe explosion in a very extended, low-lying vapor cloud. Hundreds of smallish trees scattered across the site provided very detailed evidence of the direction of explosion propagation.
Incident Cause	
Category Categorize incident cause (e.g. operator error, equipment malfunction, material failure, construction error, design error, weld failure)	Operator error Equipment malfunction (Remote shut-off valve not in service)

Source Term	Type of release (e.g. gas, evaporating liquid or a gas-liquid (two phase) flow)	Description of equipment/piping	Hole size or pipe diameter if it was a guillotine failure	Substance(s) released	Release pressure and temperature
	Volatile liquid (gasoline) Jet directed upwards from near ground level	Valve (Hammer blind)	Rectangular slot/opening 2" x 10" (0.05 x 0.25m)	Gasoline	~0.8 bar (11.6 psi) Temperature not known probably 20-25 ˚C. (68 - 77 F)
Release	Quantity released	Migration of substance from release source		Duration of release	
	450-540 m^3 340 – 400 tonnes (*Calculated from release duration*)	Gravitational slumping		Not known exactly Incident report gives estimate of 75 to 90 minutes (4500 to 5400 seconds)	
Cloud development	Cloud footprint	Depth and influence of topography under and near the vapor cloud.	Surface roughness	Substance which formed a vapor cloud	Near field dispersion
	700 x 700 m (2300 x 2300 ft)	Site surrounded by a 2.5 m (8.2 ft) high solid wall - which confined vapor	Semi-urban	Gasoline	Upward jet settling into a gravity driven non-entraining flow
Weather conditions	Atmospheric stability		temperature	Wind speed	
	Stable – release happened during the evening inversion layer.		Approx. 25˚C (77 F)	Nil	
Ignition	Ignition strength	Source of ignition		Ignition location	
	No known. Apparently not highly energetic	Not known.		Appears to be at NE corner of site boundary	
Explosion severity	Overpressure	Distance of flame travel		Flame speed	
	Damage consistent with >2000 mbar (29 psi) observed	Approximately 800 m		Not known directly. Overpressure indicates detonation, fast	

	over the whole site		deflagration (FD) or episodic deflagration (ED). Details of drag damage suggest ED.
Consequences	Fatalities, injuries, health effects, property damage within and outside of the plant property. Heavy damage – structural collapse Moderate damage- cladding loss, cracking of vulnerable masonry, purlin deformation Light damage - cladding damage, window breakage,		Blast damage to plant and other structures within and outside of cloud footprint.
	6 on-site fatalities 5 off-site fatalities Heavy damage approx. 30 m Moderate damage approx. 300 m (Limited information) Light damage up to around 2000 m		i. All product tanks set on fire. Tanks deformed above the liquid line but not split below liquid level. ii. Displacement of exposed pipe runs. iii. Destruction of all site buildings. iv. Severe damage to buildings immediately adjacent to site boundary

	Cloud mitigation measures	Performance and/or reasons for poor performance		
Mitigating Measures				
	Vapor detection	Not installed – but not a key issue in this case. Site operators were aware of the leak immediately but not able to control it.		
	Vapor barrier surrounding site	2.5m high wall gave excellent performance – probably prevented mass casualties. The wall completely confined cloud to site.		
	On-site vapor fencing	Not installed		
	Active vapor dispersal	Not installed		
Facility Information	Other Hydrocarbons at Facility	Quantity stored (is amount >10,000 lbs?)	Type of storage vessel/container	End product or used for a process
	Lubricants	Approx 200 tonnes (440,000 lb)	Drummed	End product
	Characteristics of the area where the event occurred	Urban, rural, suburban	Industrial, residential	Proximity to ports/marine

	Fairly high occupancy	Suburban	Mostly commercial but some residential	Inland
	Facility description	Category (refinery, petrochemical, gas processing, terminal and distribution, upstream)		Number of similar facilities worldwide
	Gasoline terminal	Terminal and distribution		Approx 10000

Some basic information on: site layout prior to explosion; site layout after explosion; important site locations and pattern of explosion development are given in Figure 6 to Figure 9.

Figure 6: IOC Terminal site prior to explosion

Figure 7: IOC Terminal site in 2015

Detailed information on the damage to this site is available in the form of a multi-media package.

Further reading:

MoPNG Committee (2010) (constituted by Govt. of India) Independent Inquiry Committee Report on Indian Oil Terminal Fire at Jaipur on 29th October 2009; completed 29th January 2010. Available from http://oisd.nic.in, accessed 19 August 2013.

Johnson, D.M., (2012) *Characteristics of the vapor cloud explosion at the IOC terminal in Jaipur.* Global Congress of Process Safety, Chicago, April 2012.

Figure 8: Important parts of site

1. Water tank and Pipelines Division fire water pump house
2. Ponds and site fire pumps
3. Pipelines Division control room
4. Pipeline pump house
5. Tank from which gasoline released
6. Road tanker loading gantries
7. Water tanks
8. Lubrication oils storage
9. Central administration
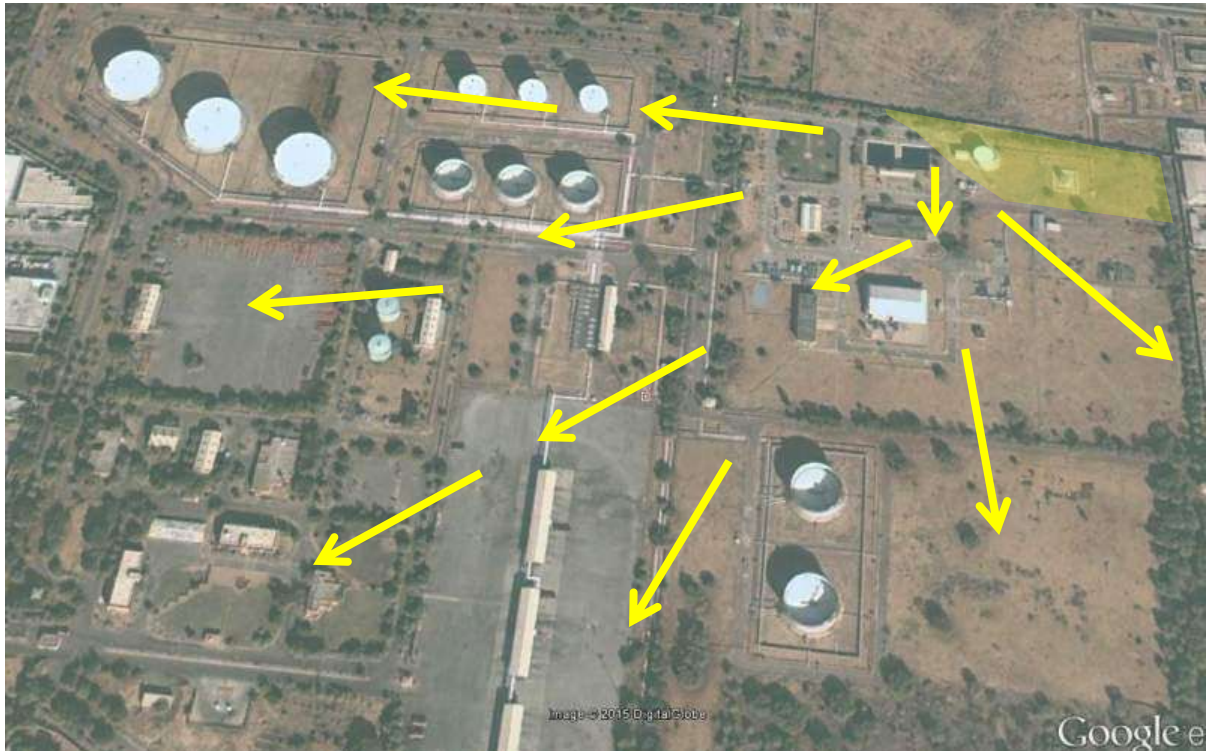
Figure 9: Explosion development

Note 1: Area affected by initial flash fire shaded yellow – there is little pressure damage in this area.

Note 2: The direction of propagation of a severe explosion (derived from forensic evidence) is indicated by arrows.

5.1.2   Vapor cloud production at Jaipur

For reasons that have not been explained a site operator manually initiated the opening of a valve at the foot of a full tank of gasoline. Product immediately reached a blind valve from which both the blind and passing inserts had been removed – leaving an upward facing slot opening of size 2" x 10". Gasoline was forced upwards out of this slot by the hydrostatic pressure exerted by fluid in the tank. Because of the gasoline spray the operator and others in the area were not able to access the controls to shut off the flow. At least two people were overcome by fumes and collapsed within the bund whilst attempting to reach the valve controls. A remotely operated shut-off valve had been installed but had been out of service for several years prior to the incident.

The loss of containment continued for a period between 75 and 90 minutes and a very large flammable vapor cloud was formed extending to more than 500 m from the source in some directions. The vapor was confined by a 2.5m high stone wall that ran around the site boundary; the whole of the area within this wall filled up with vapor.

In contrast with other VCE incidents at Buncefield , San Juan and Amuay the humidity was so low that there was no condensation of atmospheric moisture and hence no visible mist. This

made it even more difficult for those on the site to appreciate where vapor was accumulating. The Pipelines Division control room was not evacuated and after a time the depth of the vapor cloud made this impossible – trapping those inside.

The wall around the site was extremely effective in preventing vapor flow off the site and this certainly reduced the number of off-site fatalities. However the depth of the cloud on the site was increased and travel distances through the cloud to evacuate the site were very large (~700 m) because an opening in the NE corner to allow emergency access and egress had been walled up.

It is worth noting that FERC staff have recommended additional access/egress points at US LNG facilities where this was required. Also the NFPA 101 Life Safety Code which is incorporated by reference in NFPA 59A 2001 – 2016 has significant requirements for means of egress and limits to the distance between these egress locations.

5.1.2.1   Modelling of the Jaipur release

PHAST
The dispersion of vapors from the release was modelled by the IOC Accident Committee (MoPNG Committee, 2010) using PHAST. Typical results are shown in Figure 10. The IOC committee was aware that the wind speed was low and used the lowest value possible in PHAST (DNV, 2013). For some reason the modelling assumed a full bore release rate from a 250 mm pipe – rather than allowing for the restriction at the slot outlet. The assumed outflow rate of 1000 tonnes/hr (611 lb/s) was consequently overestimated by a factor of about 4.
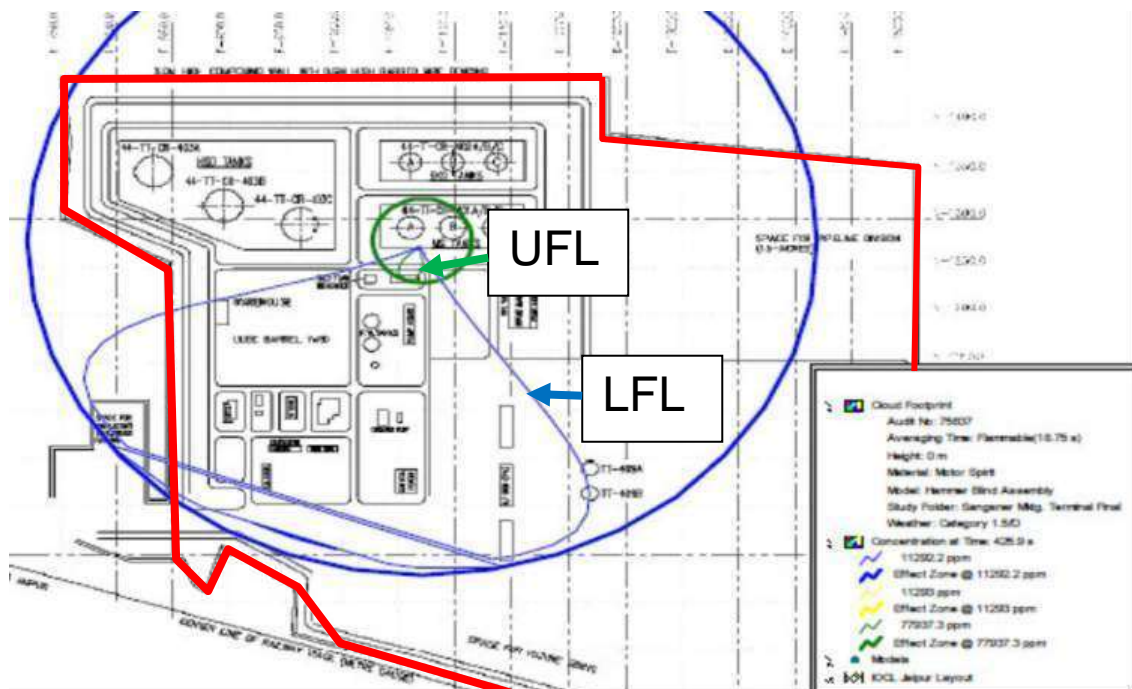
Figure 10: IOC committee modelling of vapor dispersion using PHAST (1.5 m/s). Cloud boundary observed in the incident marked in red.

Even though the outflow rate was grossly over-estimated PHAST significantly underestimates the extent of the cloud. The movement of the cloud against the wind was not predicted. The code is simply not suitable for the modelling of nil/low wind dispersion.

Using CFD and the FABIG TN12 VCA (Vapor Cloud Assessment) Method

No CFD treatment of vapor dispersion in this incident has been undertaken – to the authors' knowledge.

Many of the physical processes that apply in such a release are common with the overfilling tank problem. Entrainment of air into the liquid spray occurs on the way up and on the way down. For relatively low-pressure, high-volume releases, the area covered by the liquid spray is larger on the downward part of the trajectory, and this is where most air is entrained.

The vertical extent of the drop is often comparable with that in a tank overfill cascade and for hydrocarbons it would be expected that the droplets would be sufficiently fine to bring the liquid fairly close to equilibrium with the entrained gas – as was the case for overfill cascades. There is also an impact zone in which enhanced heat and mass transfer after splashing brings the liquid and vapor phases even closer to equilibrium.

The FABIG TN12 method (Atkinson and Pursell, 2013) can be adapted to determine the maximum volume of near stoichiometric cloud that could be produced by the release. Table 7 shows output from the TN12 model in which a notional tank overfill is used as the source term. The fuel flow matches the incident but the notional perimeter over which this liquid is discharged (and hence the air entrainment) has been adjusted to give a vapor cloud hydrocarbon concentration of 80 g/m^3. The assumptions about diameter and perimeter wetted are equivalent to assuming the spray covered an area 5.5 x 5.5 m (18 x 18 ft).

Table 7: Output from the TN12 VCA model for the Jaipur case.

Input		unit
Compound	**Winter Grade Gasoline**	
Notional Tank Diameter	**26**	(m)
Tank Height	**15**	(m)
Overspill % of Tank Rim	**100**	(%)
Air Temp	**25**	(°C)
Fuel Temp	**25**	(°C)
Fuel Mass Flowrate (Mfuel)	**76**	(kg/s)
Output		**unit**
Air Mass Flowrate (Mair)	247	(kg/s)
Ccascade	12.18	(%)
Mvap	34.3	(kg/s)
Msplash	0.65	(kg/s)
Vcloud	434	(m3/s)
Ccloud	0.080	(kg/m3)
Cloud depth assumed	2.5	(m)
Time	4500	(m)

| Cloud Radius | 499 | (m) |

The predicted radius of a 2.5 m (8.2 ft) deep cloud at 80 g/m^3 is 499 m (1640 ft).

The observed reach of the cloud to the South and East was about 460 m (1510 ft). The fuel temperature is not known and the assumption that the cloud concentration was near stoichiometric is arbitrary but the method does give a reasonable first estimate of the volume of the cloud – on the assumption that the concentration was close to stoichiometric.

5.1.3   Explosion development at Jaipur

The explosion site at Jaipur offers a remarkable opportunity to study the effects of a very large VCE and to identify the area in which the explosion made a transition from a low speed flash fire to a severe explosion. Such information is particularly valuable as it provides an opportunity to test our understanding about what conditions are required to initiate a severe explosion.

The vapor cloud explosion covered almost the whole site but did not extend beyond the perimeter wall. Only a very small proportion of the area affected by the VCE was subsequently damaged by sustained tank fires. The site was very large with tanks, loading gantries, offices etc. being separated by extensive open areas of semi-arid scrub land. Much of this land was covered by small isolated trees that provided excellent indicators of net drag impulse during the explosion (Figure 11). As at Buncefield posts and trees were broken backwards by the reverse flow after the explosion passed: this means they pointed towards the point of initiation. This type of damage is observed for both detonations and deflagrations (Section 9.4)

Figure 11: Small trees indicating explosion direction in open areas (explosion passed from left to right)

A full appreciation of the damage at the site requires access to a substantial number of photographs. HSL has produced a multi-media package that presents all of the available pictures of the incident site and identifies the locations shown.

Ignition and initiation of a severe explosion occurred in the Pipeline Division area in the NE corner of the site. Figure 12 summarises the evidence from scores of deformed objects in

photographs like Figure 11. The arrows indicate the direction of deflection and consequently point back towards the point of initiation.
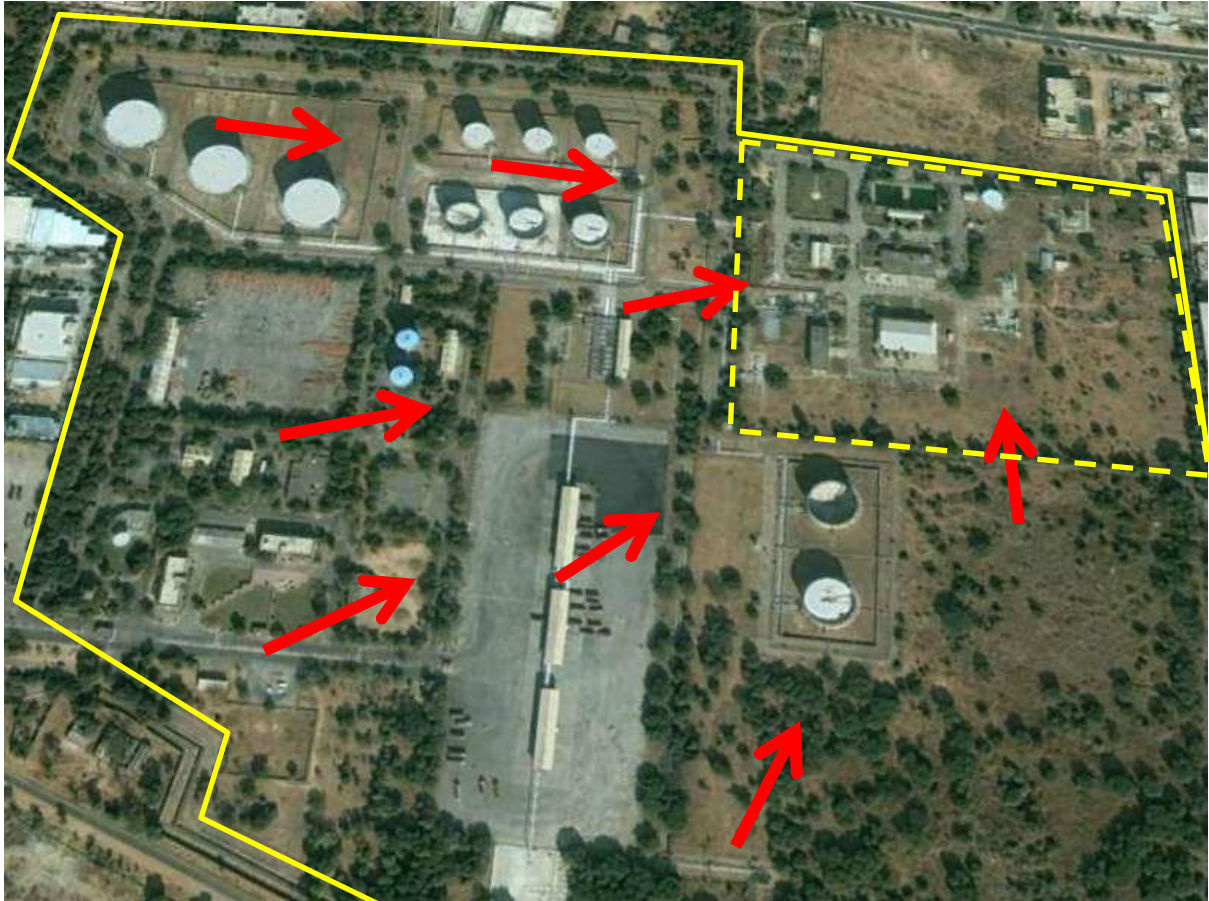
Figure 12: Summary of site-wide directional evidence at Jaipur. *Yellow line indicates site boundary. Dashed line indicates the Pipelines Division Area in the NE part of the site.*

In the Northeast part of the Pipelines Division Area there was an area that was burned but did not suffer high overpressures or strong drag forces (Figure 13). This low pressure area was defined by damage to the bounding wall and light damage to trees and enclosures. Combustible objects showed damage consistent with exposure to a flash fire.

Figure 13: Area shaded in yellow was burned but showed no signs of a severe explosion. Pump house circled in red.

Figure 14: Views of the end of the stretch of intact wall in the NE corner of the Jaipur site – marked X on Figure 13 . *From the North (left) and from the South (right)*

Directional indicators in the Pipelines Division area are shown in Figure 15. Details of individual indicators are shown in the multimedia package associated with this report. There are a number of points to note in this figure:

1. There are clear changes in the direction of drag impulse over short distances – especially near the point X. This illustrates the important point that strong drag forces, as well as high overpressures, are a consequence of *local* explosion conditions i.e. within approximately 5-10 m of the indicator. This is also illustrated by the damage to trees just outside the area covered by the VCE. Figure 16 and Figure 17 show examples: the area within the boundary wall was fully involved in the VCE with trees broken and stripped of twigs and leaves. However, within a few metres of the wall the drag forces associated with the explosion have weakened to the point where many twigs and leaves

(above the level of the wall) survived. Very similar patterns of damage were observed at Buncefield with tree damage being confined to an area within or immediately adjacent to the cloud.

It is important to reiterate the need to distinguish between overpressure and drag sensitive indicator objects in this connection. Overpressure effects are local in both detonation and deflagration cases (local means length scale equal to cloud depth). Drag forces are not local for detonation – they can only vary on a length scale at least 10 times the cloud depth.

2. The directional evidence suggests the pattern of early explosion development illustrated in Figure 18.

These observations summarised in Figure 18 are unexpected and challenge conventional expectations about the type of environment that can lead to flame acceleration and transition to a severe explosion. The area in Figure 18 where the high speed flame originates is certainly not filled with congested pipework or dense vegetation. It does not appear to include a strong bang-box although the transition to a severe flame appears to correspond to the passage of the flame through a site pump house.

The rest of this section presents some more details about the area where severe VCE appeared; with a view to understanding what mechanisms might have operated.

Figure 15: Directional indicators in the Pipeline Division area

Figure 16: Rapid decline in drag related damage with distance from the explosion

Figure 17: Rapid fall off in damage to trees near point Y (see Figure 13)

Figure 18a: Ignition near the NE corner of the site. Flame spread along the wall/tree line

Figure 18b: Transition to severe explosion as flame passes through the pump house

Figure 18c: Severe explosion propagates outwards across the site.

Figure 19 shows the remains of the pump house.

Figure 19: Remains of the pump house on the edge of area affected by the severe explosion.

Prior to the explosion the roof and upper half of the walls of the building were clad with profiled cement sheets. All of these have been displaced. Fragments of cladding in a relatively undisturbed area close to the pump house are shown in Figure 20. The typical fragment size is 10 – 100 mm.

Figure 20: Cladding fragments

Figure 21: Trees in the area of the pump house

Figure 22: Broken trees near the pump house. Arrows show direction indication

There was a significant amount of congestion within and around the pump house and the cladding on the walls and roof provided partial confinement of the expansion of combustion products. The failure pressure for such cladding systems is typically only of order 10 mbar (0.15 psi) and it is very likely that the explosion within the pump house displaced the panels, which would have fragmented on failure. If the explosion progressed more quickly into the pump house at low level, unburned gas would have been displaced upward through the cloud of cladding fragments. Explosion within the pump house and panel failure would have also elevated a large amount of dust.

A substantial area of the unignited vapor cloud around the pump house would have been disturbed by high speed panel fragments and pressure waves. Impacts of fragments with the ground and with nearby trees would also have raised more dust (Figure 21 and Figure 22).

The pump house and surrounding trees would consequently have had a number of effects on flame propagation:

1. Increased congestion and confinement would have increased the burning rate and associated pressure;
2. Failure of the cladding panels would have injected a large number of fragments into the unburned gas; these would act as additional turbulence generators;
3. Both gas flow driven by expansion and fragments have the potential to re-elevate dust ahead of the flame front.

Section 10 includes an analysis of the rate of propagation of pre-mixed turbulent flames where the mixture is contaminated with dust. It is shown that in such mixtures thermal radiation within the flame is effective in significantly heating pockets of unburned gas. The effect of this is that the latter stages of combustion accelerate. The magnitude of temperature rise predicted may be sufficient to raise the laminar flame speed of propane to that of acetylene or higher.

The normal heat transfer mode in flames is conduction, and this acts only on gas immediately beyond the flame front. Thermal radiation acts much more broadly on the unburned gas wherever it is contaminated with dust. The general heating of volumes of gas means there is a strong tendency for the burning to be unstable: short periods of rapid burn-out of a volume of pre-heated gas are associated with high pressures and correspond to an episode of localised severe explosion. When the pre-heated gas is consumed the burning rate will fall and there will be a pause until the large-scale mixing processes operating within the flame reform areas of dust contamination and radiation gets to work on them

This mechanism provides a possible explanation for the observation that flames can generate local areas of high pressure whilst propagating in relatively open areas. It could explain some of the key features of damage at Jaipur, Buncefield and other sites:

1. Very localised pressure and drag effects – corresponding the pockets of high pressure and high speed flow that act on objects within a few metres;
2. The absence of high pressure asymmetry in objects and permanent forward deformations that would be associated with a detonation;
3. Sub-sonic average flame speeds – which is consistent with CCTV and witness evidence where this is available.

5.2 BUNCEFIELD

5.2.1 Summary of incident data

Time and date:	11th December 2005 (Sunday) Release started at approximately 05:30 i.e. well before dawn
Location	Buncefield, UK (51˚45'56" N 0˚25'35.57" W)
Company	HOSL (Hertfordshire Oil Storage Ltd). Terminal for Gasoline, Diesel and Jet Fuel
Narrative :	The site was importing gasoline from a long-distance pipeline. Mal-operation of a tank process level indicator and automatic high level shut-off system led to a tank being overfilled at a rate of 550 m^3/hr, rising to around 900 m^3/hr, for a total of 23 minutes. There was no wind and a vapor cloud spread in all directions to cover most of the HOSL site and a substantial area of an off-site industrial estate. The maximum extent of the cloud was approximately 500 x 350 m (1640 x 1150 ft). Eventually the vapor cloud reached the tanker loading gantry and was reported by a tanker driver. The site emergency system was activated but this involved starting the site fire pump, which ignited the vapor cloud. A severe VCE occurred that caused overpressure in excess of 2000 mbar (29 psi) and drag damage across all of area covered by the vapor cloud. Severe explosion effects were confined to an area within a few tens of metres from the edge of the cloud but minor damage (e.g. windows breaking) extended to a range of more than 1 km (3280 ft). Damage to the site and surrounding businesses amounted more than £1 billion but fortunately no-one was killed.
Incident Cause	
Category Categorize incident cause (e.g. operator error, equipment malfunction, material failure, construction error, design error, weld failure)	Equipment malfunction and operator error

Source Term	Type of release (e.g. gas, evaporating liquid or a gas-liquid (two phase) flow)	Description of equipment/piping		Hole size or pipe diameter if it was a guillotine failure	Substance(s) released	Release pressure and temperature
	Volatile liquid (gasoline) Overfill from tank top	Atmospheric tank. Fixed roof - floating deck		Overflow from 30% of tank top perimeter. Gravity driven cascade.	Gasoline	Low pressure release. Temperature 14'C (57 F)
Release	Quantity released	Migration of substance from release source			Duration of release	
	260 m^3 195 tonnes (430,000 lb)	Gravitational slumping			23 minutes 1380 seconds	
Cloud development	Cloud footprint	Depth and influence of topography under and near the vapor cloud.	Surface roughness		Substance which formed a vapor cloud	Near field dispersion
	500 x 350 m	CCTV images show cloud depth 2-3 m (6.5 – 9.8 ft) . Deeper close to source. Vapor travel arrested by rises in ground level >3 m (9.8 ft)	Semi-urban		Gasoline	Gasoline cascade settling into a gravity driven non-entraining flow
Weather conditions	Atmospheric stability		temperature		Wind speed	
	Stable – release happened during the night time inversion layer.		Approx. 0 ˚C		Nil	
Ignition	Ignition strength		Source of ignition		Ignition location	
	Moderately high All (steel) cladding lost from pump house which was at low level (completely immersed in cloud)		Fire pump starter		Site fire pump	

Explosion severity	Overpressure	Distance of flame travel	Flame speed
	Damage consistent with >2000 mbar (29 psi) observed over the whole site	Approximately 300 m	Not known directly. Overpressure indicates detonation, fast deflagration (FD) or episodic deflagration (ED). Details of damage and CCTV evidence suggest ED.
Consequences	Fatalities, injuries, health effects, property damage within and outside of the plant property. Heavy damage – structural collapse Moderate damage- cladding loss, cracking of vulnerable masonry, purlin deformation Light damage - cladding damage, window breakage,		Blast damage to plant and other structures within and outside of cloud footprint.
	No fatalities Heavy damage approx. 20 m (65 ft) from cloud edge Moderate damage approx. 300 m (984 ft) Light damage up to around 1500 m (4920 ft)		i. All product tanks engulfed by the cloud were set on fire. Tanks deformed above the liquid line but not split below liquid level. ii. On-site damage to pipe runs obscured by fire damage. iii. Destruction of all engulfed site buildings. iv. Severe damage to buildings which were exposed to the cloud (at their bases). These had to be demolished. v. Houses within about 100 m (328 ft) were wrecked. vi. Substantial economic damage associated with loss of weather tightness of very large commercial premises.

Mitigating Measures	Cloud mitigation measures	Performance and/or reasons for poor performance		
	Vapor detection	Not installed. Vapor detection is particularly cost effective protection against nil/low wind dispersion; vapor goes everywhere and only a small number of detectors can provide good coverage.		
	Hedging surrounding site	Did not significantly restrict vapor flow		
	On-site vapor fencing	Not installed		
	Active vapor dispersal	Not installed		
Facility Information	Other Hydrocarbons at Facility	Quantity stored (is amount >10,000 lbs?)	Type of storage vessel/container	End product or used for a process
	Diesel, Jet fuel	Of order 100,000 tonnes	Atmospheric storage tanks	End product
	Characteristics of the area where the event occurred	Urban, rural, suburban	Industrial, residential	Proximity to ports/marine
	Mostly commercial. Occupancy in cloud area very variable from O(1000) to nil (at time of incident)	Suburban	Commercial but some residential fairly close to cloud area	Inland
	Facility description	Category (refinery, petrochemical, gas processing, terminal and distribution, upstream)		Number of similar facilities worldwide
	Gasoline terminal	Terminal and distribution		Approx 10000

Further Reading

Buncefield Major Incident Investigation Board (2007) The Buncefield Incident – 11th December 2005 – The Final Report of the Major Incident Investigation Board, Vol. 1., ISBN 978-07176-6270-8. Available from http://www.buncefieldinvestigation.gov.uk, accessed 19 August 2013

Atkinson G., Coldrick S., Gant S.E. and Cusco, L. (2015)a *Flammable vapor cloud generation from overfilling tanks: Learning the lessons from Buncefield,* Journal of Loss Prev., Vol 35, p329-338.

These provide a good general introduction. A large number of additional references on specific issues are given in the sections below on cloud development and explosion mechanics.

Figure 23 to Figure 26 show the site layout before and after explosion and the relationship between the cloud size and the topography of the site.
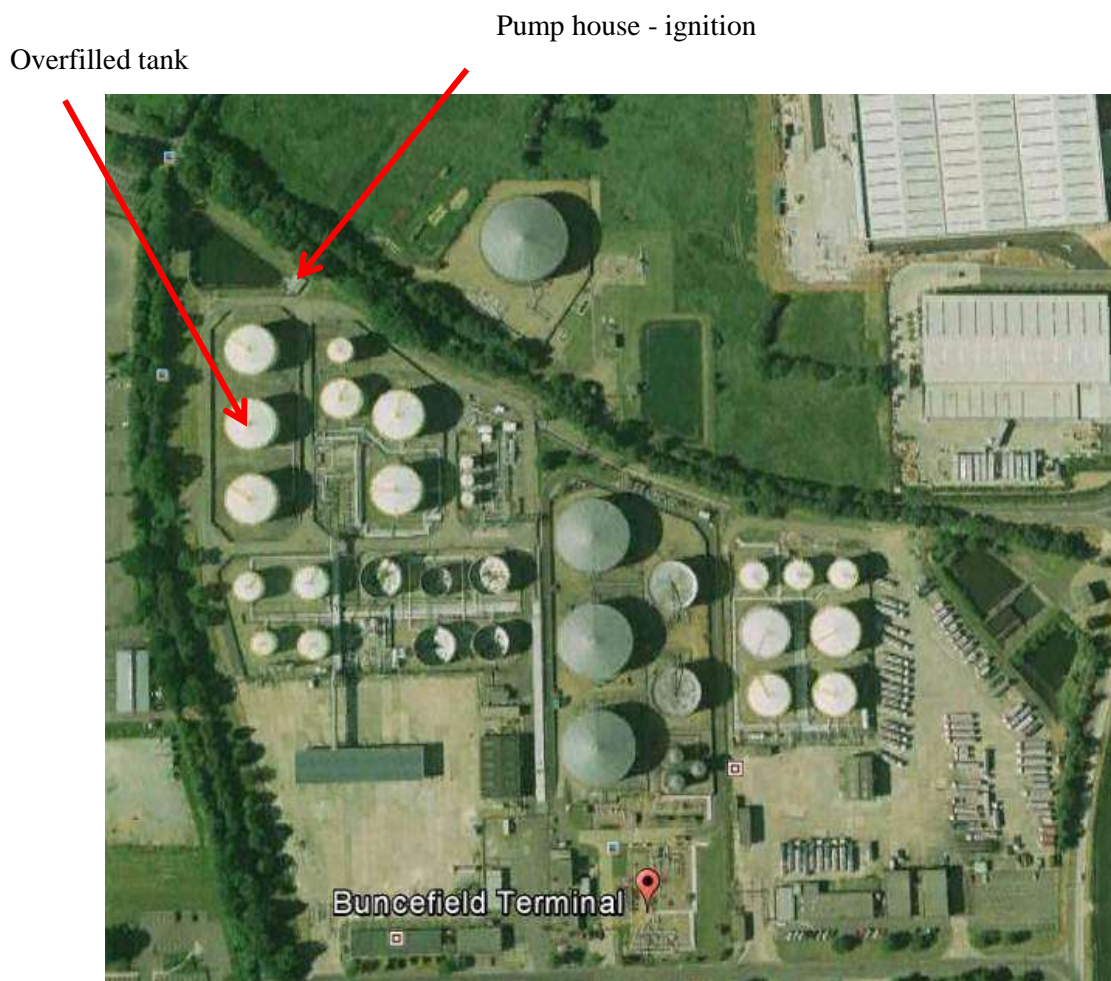
Figure 23: Buncefield HOSL Terminal site prior to explosion

Figure 24: Terminal site and wider area after the explosion – final extent of vapor cloud explosion marked in yellow.

The area indicated by a question mark was inside a tank bund: there were relatively few pressure makers and even those were so badly damaged by a fire lasting several days that it was not possible to tell whether a severe explosion had occurred in the area.
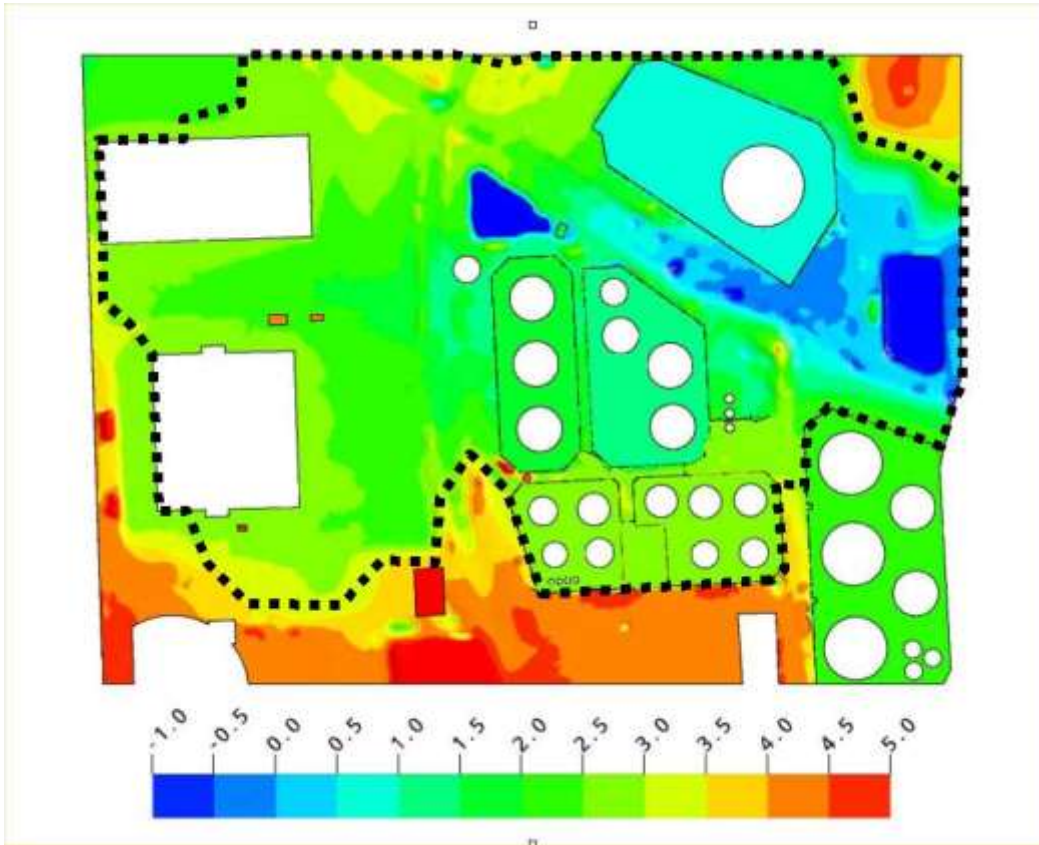
Figure 25: Correspondence between cloud geometry and topography.
Scale shows terrain height in metres

Figure 26: Approximate final depths of the visible mist. Solid colours indicate observed depths of the mist taken directly from the CCTV cameras. Transparent colours indicate cloud heights inferred from the surrounding levels.

5.2.1 Vapor cloud production at Buncefield

Examination of the blast affected area around the site showed that a large continuous area surrounding the site was uniformly affected by both blast and heat i.e. all vegetation was scorched and all pressure sensitive objects were affected. The area powerfully affected by blast (e.g. vehicles crushed, trees stripped) did not extend more than a few tens of meters beyond the edge of the burned zone.

Aerial photographs confirmed the observations on the ground: the site was surrounded by a blackened area (all plant leaves scorched) extending to a distance of up to around 250 m (820 ft) (Figure 27). All of this ground had been exposed (briefly) to a vapor flash and contained crushed cars and severely damaged buildings. Outside the area affected by the flash, damage to vehicles and vegetation was minimal; buildings were affected only by damage to vulnerable elements such as windows and cladding. This is explained in Steel Construction Institute, SCI 2104 - *Dispersion and Explosion Characteristics of Large Vapor Clouds Volume 1 – Summary Report*. This report on the post-Buncefield research also provides a method for calculating the overpressure outside pancake shaped clouds.

Figure 27: The edge of the vapor cloud marked by scorching and blast damage

It was dark at the time of the release but the areas covered by CCTV were well lit. Conditions were clear but the temperature was close to the dew point. About 25 minutes before the explosion, cameras close to Bund A (containing 3 large gasoline tanks) captured a current of dense white mist flowing westwards out of the bund; outside the bund the mist continued to spread smoothly in all directions at a speed of order 1 m/s. After a few minutes cameras in the large car parks of nearby buildings showed the mist initially flowing in a very shallow, smooth topped layer. In one location around 200 m (656 ft) West from Bund A, there are remarkable pictures of a worker arriving by car for an early shift. He successfully parked the car and then walked away out of a cloud that extended to around his knees but no higher. Over time, the depth of this layer increased until it reached about 2m over most of the areas covered by cameras (Figure 28).

The area where a cloud could be seen closely matched the area in which burning occurred. There was no extended area around the burned area in which a (more dilute) cloud could be seen.

Figure 28: Accumulation of vapor cloud around the lowest parts of the Northgate Building

The upper surface of the vapor cloud was visible over large distances and it was apparently undisturbed by any vortices. This, and the symmetry of the spreading cloud, confirmed that the incident had occurred in nil/low wind conditions, with the spread of vapor being driven by buoyancy forces.

At the time of the incident, Tank 912 was being filled with winter grade gasoline at a rate of 550 m^3/hr. The level reached the top of the tank and liquid began to run out of the vents in the fixed tank roof. The overflow continued for around 1400 seconds (23.3 mins) with the flow rate being increased to between 800 and 960 m^3/hr for about 8 minutes before the explosion.

Examination of the CCTV images and blast damage levels (indicating cloud concentration at distance) convinced the investigation team that there was very little entrainment into parts of the cloud further than about 20 m (65 ft) from the tank. Explosion severity (and therefore presumably gas concentrations) appeared to be close to uniform over more than 95% of the area covered by the cloud. The conclusion was that all of the air (as well as the gasoline vapor) was entrained into the vapor current very close to the tank and thereafter the vapor cloud spread out in a buoyancy current with minimal further increase in volume flux.

Previous assessments of vapor risks around bulk tanks had focused on pool evaporation in a range of wind speeds: nil/low wind conditions were not considered as there would be no movement of contaminated vapor away from the surface of a pool in a bund. It became clear that a crucial aspect of the source term had been overlooked – of particular significance for low wind speeds.
In a tank overfilling release, such as that from Tank 912, a stream of liquid from the top of a tank breaks up into a cascade of small droplets. As these droplets fall through the air, there is a transfer of momentum from the liquid to the air; the droplets are retarded by the air and the air is driven into downward movement. This was not a previously unknown phenomenon; many people must have noticed that large waterfalls drive a strong current of air outwards from the area where the cascade impacts the ground at the foot of the waterfall. However, the significance of this effect for industrial safety had not been appreciated.

The entrainment of large volumes of air by freely falling cascades of a volatile liquid produces a large and continuous flow of vapor. For overfilling releases from tanks of the size typically found on fuel storage sites, the initial speed in the vapor current is of order 5-8 m/s. The shear between this current of vapor and the surrounding air produces some initial mixing and dilution – depending on the extent of recirculation in the immediate vicinity of the tank. Moving further away from the tank, as the velocity of the cold, heavy vapor current falls, mixing is progressively reduced (due partly to stable stratification which suppresses turbulent mixing). In very low wind speeds, the amount of dilution on the top surface of the spreading vapor cloud may vanish completely, with only a small degree of mixing at the front of the gravity current. Under these conditions, the vapor current may run for very large distances without diluting significantly. If the (constant) concentration of this extensive flow is in the flammable range, there is potential for the production of a very large, hazardous cloud which could sustain an explosion throughout.

5.2.1.1   Modelling of the Buncefield vapor cloud

Since the incident HSE and others have developed a reasonably complete understanding of the various important stages of vapor cloud production during overfilling:

- Liquid outflow;

- Fragmentation in the liquid cascade;
- Entrainment of air;
- Heat and mass transfer between fuel and air;
- Splashing;
- Near field air entrainment;
- Interaction between vapor currents and bunds;
- Long-range dispersion.

Long-range dispersion is the most difficult aspect because it is controlled by the site topography and any obstacles – in general it requires CFD analysis. Some useful general methods have been developed that can be used to estimate the cloud *volume* (at a given time). These methods are described in FABIG Technical Note 12 (Atkinson and Pursell, 2013).

The cloud depth in the Buncefield case was around 2m with roughly symmetrical spread from the source. Assuming this cloud geometry (i.e. a circular with constant depth 2m) allows the radius to be calculated from the cloud volume. For reasonably level, unconfined sites this allows an estimate to be made of the range of a vapor cloud as a function of time. More details are given in FABIG TN12.

Application of the VCA method in FABIG TN12 to Buncefield

Table 8 shows application of the VCA method to the Buncefield case. The radius of a 2m deep cloud predicted is 210 m (689 ft).

The actual cloud was not circular – the maximum size East-West was about 500 m (1640 ft) and North–South 350 m (1150 ft). The average radius was consequently around (500 + 350)/2 = 212m (695 ft).

The correspondence is fortuitous as the assumed depth in the VCA method is arbitrary. Nevertheless the method gives a reasonably good estimate of the volume of the cloud. As expected the shape requires knowledge of the site topography.

It is worth noting that the analysis of cloud volume in the VCA method is based on a combination of large scale experiments, thermodynamics and CFD. It was not tuned to the Buncefield case.

Table 8: Application of the VCA method to the Buncefield case

Input		unit
Compound	**Winter Grade Gasoline**	
Tank Type	**Fixed with internal floating deck - Type1**	-
Tank Diameter	**25**	(m)
Tank Height	**15**	(m)
Overspill % of Tank Rim	**30**	(%)
Air Temp	**0**	(°C)
Fuel Temp	**14**	(°C)
Fuel Mass Flowrate (Mfuel)	**115**	(kg/s)
Output		**unit**
Air Mass Flowrate (Mair)	108	(kg/s)
Ccascade	15.42	(%)
Mvap	19.7	(kg/s)
Msplash	0.98	(kg/s)
Mcloud	257	(kg/s)
Vcloud	198	(m3/s)
Ccloud	0.104	(kg/m3)
Cloud depth assumed	2	(m)
Time	1400	(m)
Cloud Radius	210	(m)

FABIG TN12 also extends the scope of the VCA method to liquids other than gasoline. Parameterized thermodynamic analyses are available for hexane, acetone, ethyl acetate, benzene, MEK, toluene, methanol, ethanol and a range of mixtures with defined compositions: naphtha, winter grade gasoline, raw gasoline, F3 condensate, stabilized Brent Crude, reformate and heavy reformate. The assessment method is also suitable for other liquids but a simple thermodynamic analysis is required.

FABIG TN12 also provides some preliminary advice on the integration of cascade vaporization into the source term for the assessment of windy conditions.

CFD analysis of the Buncefield cloud

The first CFD modelling of the Buncefield cloud is reported by Gant and Atkinson (2011)

Details of extensive subsequent CFD modelling of overfills can be found in the works of Coldrick *et al.* (2011) and Atkinson and Coldrick (2012a). Further background to the development and validation of the CFD model for sprays and tank overfilling cascades can be found in the works of Gant *et al.* (2007) and Gant and Atkinson (2012). Some examples of CFD predictions of vapor cloud spreading are shown in Figure 29 which compares the results with CCTV records.
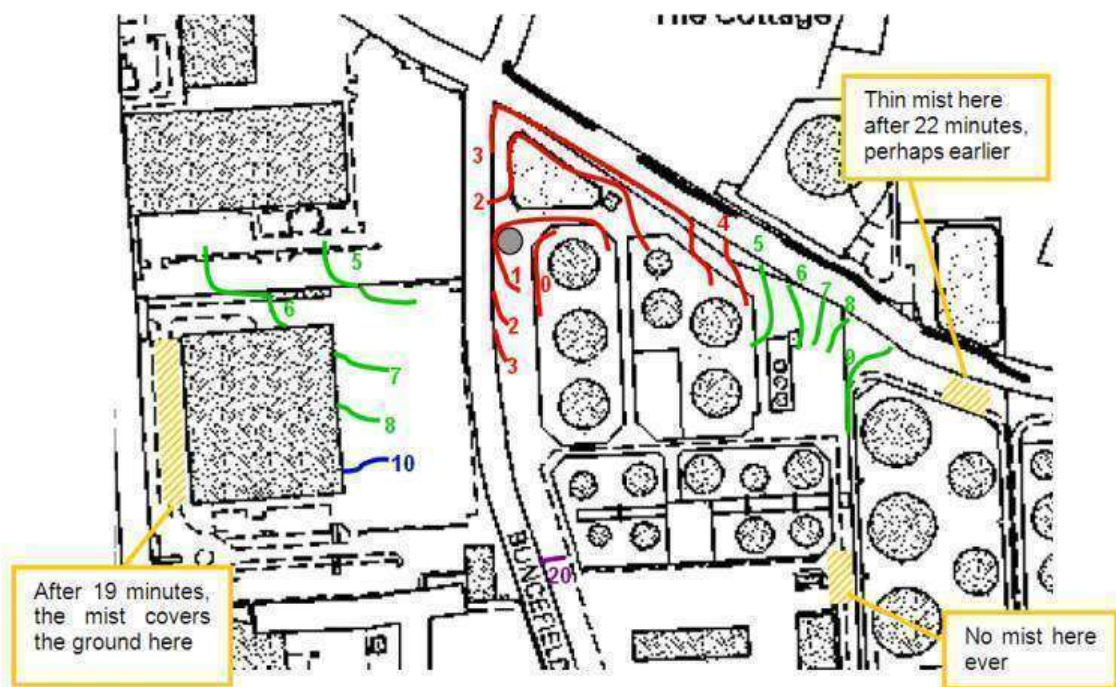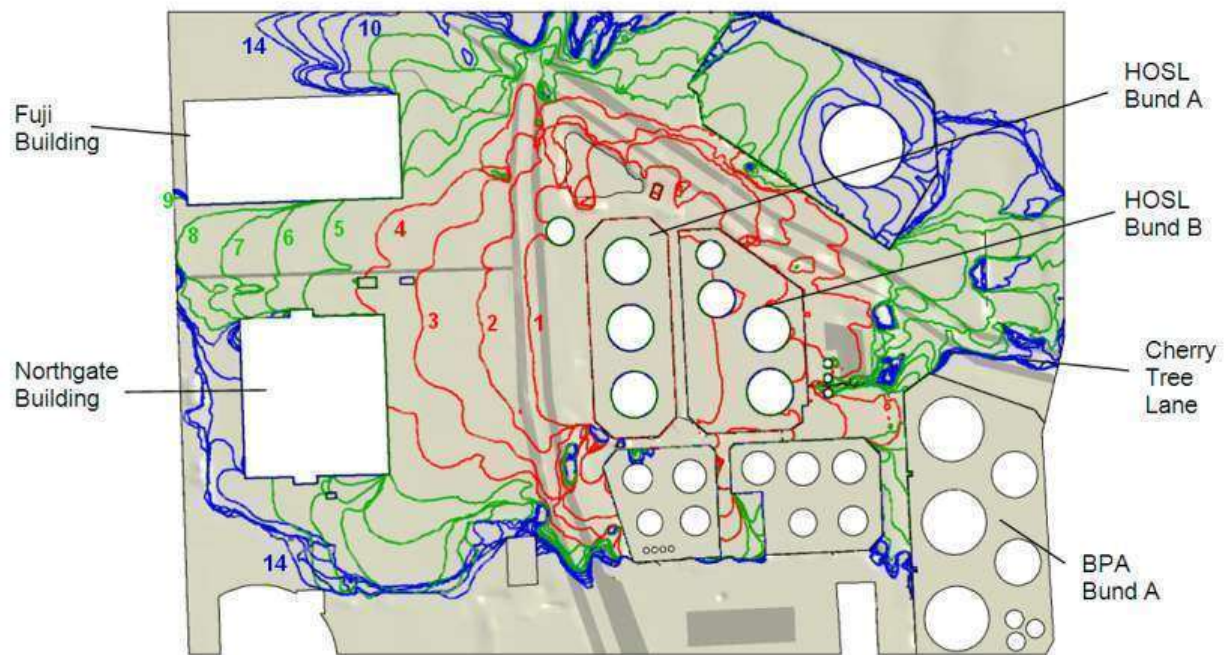
Figure 29: Comparison of CFD predictions (top) and CCTV observations (bottom) for the progress of the vapor cloud or mist across the Buncefield site - Gant and Atkinson (2011). Times shown are in minutes from the moment the mist appeared over the wall of Bund A,

5.2.2 Explosion Development at Buncefield

The explosion occurred immediately after the site alarm was raised – which automatically started the diesel fire pump. Witness statements, structural examination of steelwork and CCTV

records show that the fire started in the fire water pump house. A detailed description of the pump house is provided by Atkinson (2006). Some images are reproduced in Figure 30 because of the importance of the building in the early stages of explosion development.

	Pump house prior to the incident
	Front view after the explosion. Remains of hedge in the background The front half of the building was affected by a fire – caused by seepage of hydrocarbons from a nearby bund after the explosion.
	View of the rear of the pump house. The rear half of the building escaped fire damage. All of the cladding sheets had been lost without purlin deformation.

Figure 30: Views of the Buncefield firewater pump-house

The pump house building lost all of its cladding by failure of fixings and those purlins that had escaped fire damage were undamaged by inward force from the explosion. This strongly suggests that all of the cladding was lost before the building was exposed to external pressure and drag forces i.e. that the explosion started within.

Figure 31 shows the locations of sections of pump house cladding that were recovered. The distribution relative to the axis of the building suggests that the final location was largely determined by the internal blast rather than being a result of large scale gas movements during the explosion.

Both the range of cladding fragments and the fact that all of the sheets were simultaneously lost suggest a relatively strong internal explosion.

Figure 31: Final location of pump house cladding sheets

The front to the diesel pump starter box showed that there had been an internal explosion in this enclosure (Figure 32) and this must have acted as a strong ignition source within the rest of the pump house. The building also contained significant congestion and it is not surprising that the initial internal explosion was quite powerful.

CCTV images show that the (sunken) building was completely submerged by the cloud. The jetting of unburned gas between cladding sheets during failure would have introduced high levels of turbulence into the gas surrounding the pump house and this would have driven a significant external explosion. Figure 33 shows a still from a recent HSL test programme on explosions in clad structures. In this case the maximum overpressure in the external explosion was around 200 mbar (2.9 psi) and the duration of the pressure pulse was 30-40 ms. At a distance the external explosion sounded like a bang – and did not correspond to the descriptions of an extended pressure event provided by witnesses to the Buncefield explosion.

Figure 32: Pressure damage to the front of the enclosure of the diesel pump starter

Figure 33: Explosion test in a steel clad structure

In contrast to Jaipur and San Juan no substantial areas indicating low overpressures were recorded around the ignition point at Buncefield. It is clear that the explosion started at the pump house and made a transition to a severe explosion almost immediately.

Figure 34 compares metal enclosures from the Buncefield and Jaipur pump houses. Moderate pressure damage is apparent suggesting overpressures of around 1 bar (14.5 psi). It is seems

likely that these pressures were a result of severe explosions initiated very close to the pump house in both cases

Figure 34: Steel enclosures in pump houses at Buncefield (Left) and Jaipur (Right)

Inward deflection of the sidewall is visible directly in the Buncefield case and indirectly through the curving of the shadow of a straight pipe in the case of Jaipur.

The direction of propagation of the severe explosion at Buncefield was indicated by drag-sensitive objects such as trees and posts. The evidence is not as complete as at Jaipur because of the relative scarcity of suitable marker objects and because a sizable proportion of the area affected by the VCE was subsequently badly damaged by a severe and prolonged fire. Nevertheless it is clear that the explosion did originate somewhere close to the pump house - Figure 35.
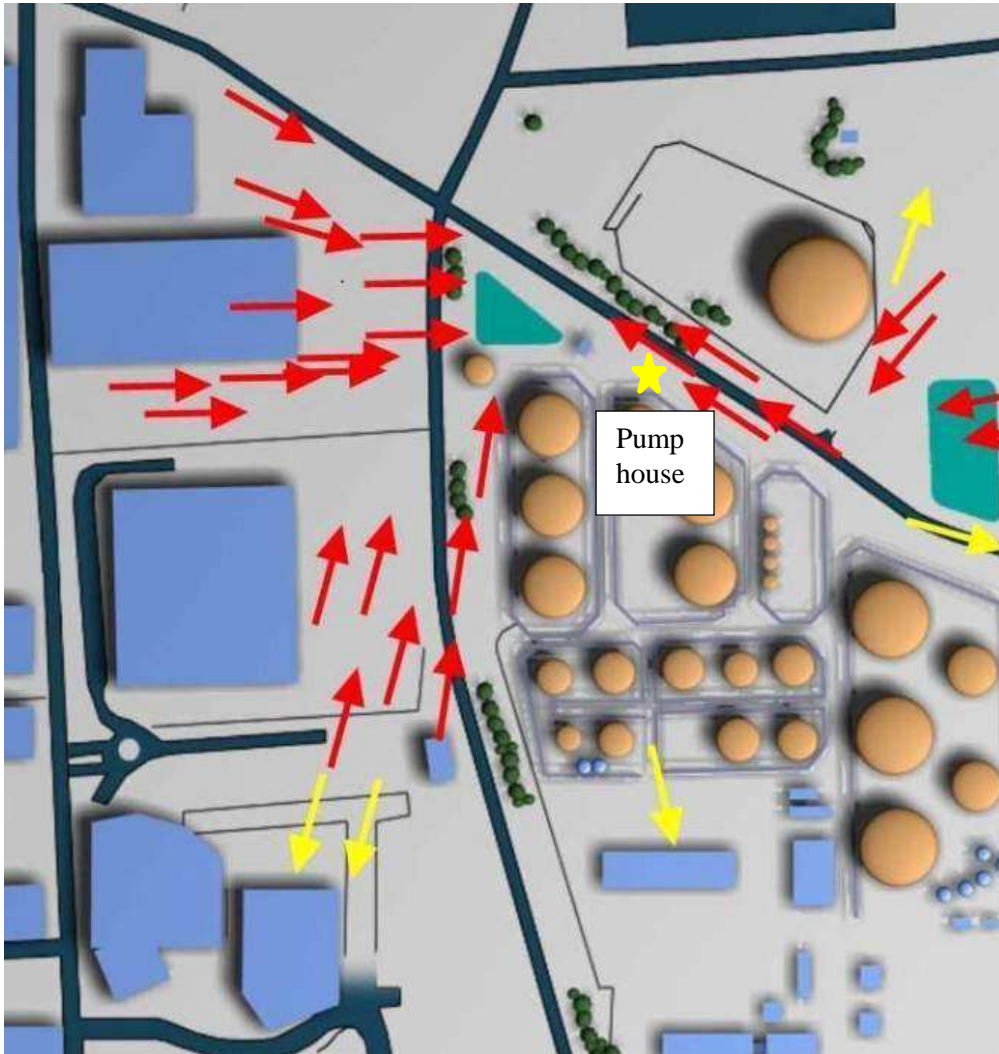
Figure 35: Directional evidence from the Buncefield site. Outward indicators (yellow arrows) are found within about 5m of the edge of the cloud.

Figure 35 was based on directional evidence recorded during the investigation – which started a few days after the explosion when fire-fighting was finished. One set of directional indicators was omitted: these were large trees that had been felled across the road (Three Cherry Trees Lane) running close to the pump house and were removed by the Fire Service (Figure 36).

These anomalous indicators are confined to the area close to the lagoon. This is probably reflection of the fact (also illustrated at Jaipur) that directional indicators are a function of local explosion conditions: in a flat, open environment explosions all around the object are of similar magnitude but the backwards impulse operates last (when the object may already be weakened) and with marginally higher impulse. This produces the pattern of damage observed over large open areas in Jaipur and at Buncefield.

Local explosion conditions are different for the trees shown in Figure 36: the depth of the cloud is greater in the lagoon and impulse of explosions from this side would have been significantly larger. Figure 37 gives an impression of the vegetation along Three Cherry Trees Lane prior to

the explosion[5]. Vegetation was dominated by a line of large trees forming a high level canopy that closed over the road – most of the foliage and or fine branches would have been above the cloud.

Figure 38 shows a CCTV view immediately prior to the overflow. A pool of light thrown by a lamp (next to Tank 12 bund) beyond the hedgerows bordering Three Cherry Trees Lane shows that the obstruction presented by vegetation is dominated by isolated tall trunks.

Figure 36: Area surrounding pump house lagoon soon after the explosion

Figure 37: Tree cover prior to the explosion – a canopy covers Three Cherry Trees Lane

Figure 38: View of through the hedge rows bordering Three Cherry Trees Lane

5.2.2.1   CCTV evidence

Some CCTV records with high time resolution were recovered that allow a reasonably accurate measurement of the time between the first light from the explosion and the arrival of the first shock (when the camera first moved). This allows the distance of the initial event from the camera to be calculated - within the accuracy of the time measurement. Figure 39 shows the results for two different cameras – it is clearly very likely that the initial explosion event occurred at the pump house.

Frustratingly no cameras captured the progress of flame but they did give consistent results for the total time over which light was emitted by the explosion – this was 1620 ms +/- 60 ms. Cameras shook over a time interval of about 900 ms. Typical results are shown in Figure 40.
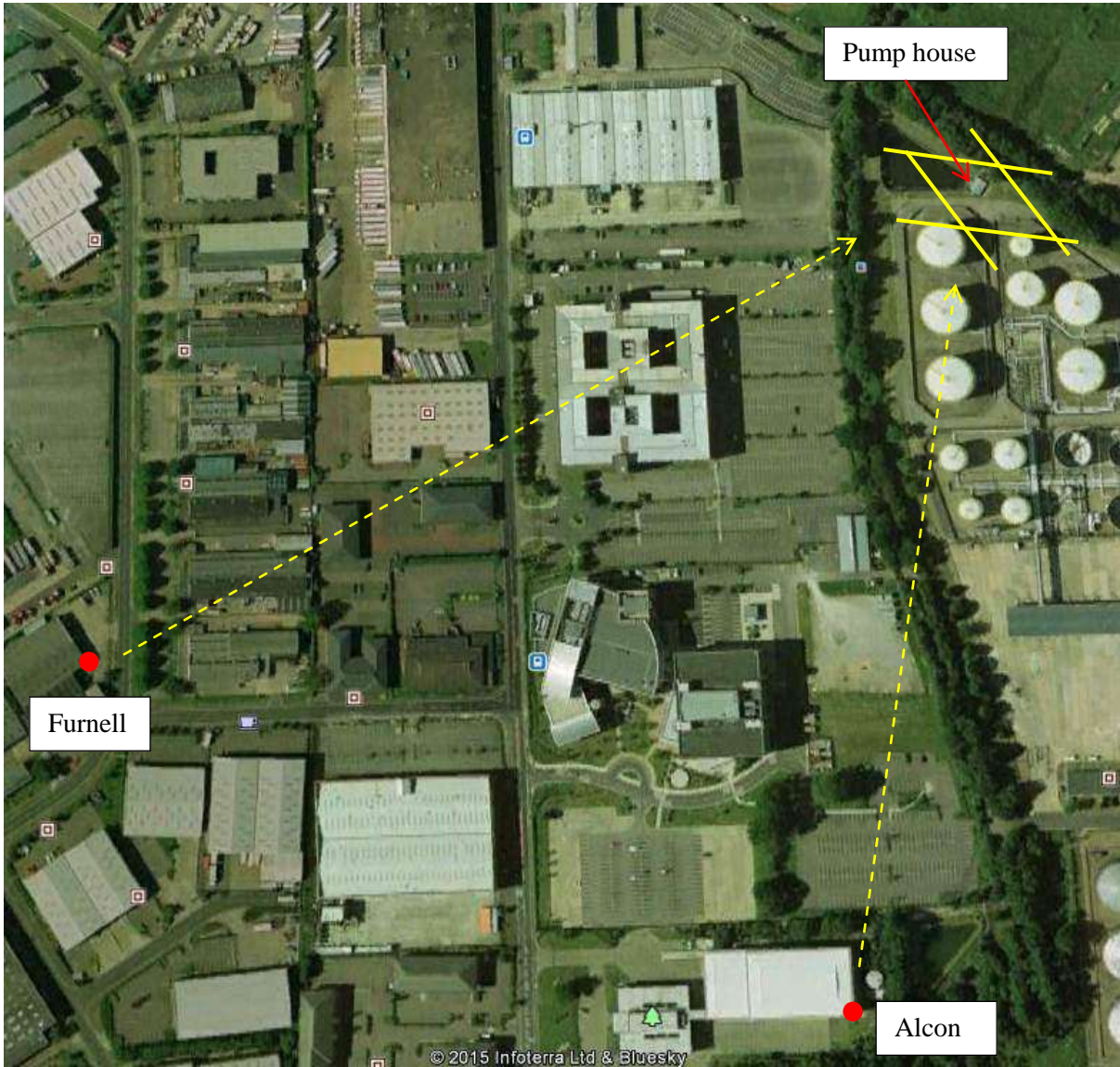
Figure 39: Time of flight analysis for pressure disturbances recorded by two cameras
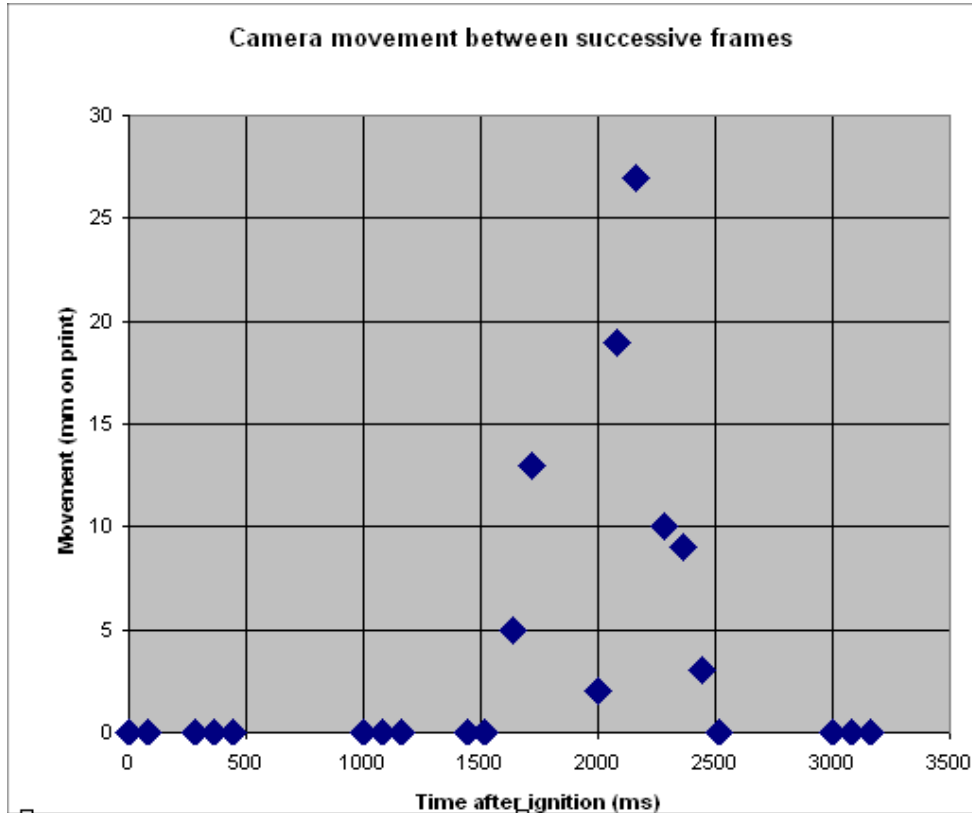
Figure 40: Camera movements between frames driven by the explosion

5.2.2.2 *Deflagration interpretation*

Both of these results can be understood if the explosion front travels at an average rate of about 150 m/s.

1. Duration of light emission

   The average velocity is given by the distance of flame propagation (L_{flame} =240 m i.e. the distance from the pump house to the western edge of the cloud) divided by the time over which the explosion emits light (T_{light} = 1.62 s - see previous page).

   $$V_{flame} = \frac{L_{flame}}{T_{light}} = \frac{240}{1.62} = 148m/s$$

2. Duration of pressure pulse

   The duration of the pressure pulse T_{press} (see Figure 40) is shortened by the Doppler effect, because the flame is moving at a significant proportion of the speed of sound V_{sound}.

   $$V_{flame} = \frac{V_{sound}}{\dfrac{V_{sound}T_{press}}{L_{flame}} + 1} = \frac{331}{2.24} = 147m/s$$

The uncertainty in the latter calculation is around 10 m/s because of uncertainties in determination of T_{press}.

Other features of the emissions of light can also be understood on the basis of a flame travelling at this speed. Consideration of the light path to the yard monitored by the Furnell cameras suggests that the intensity of light should increase with the appearance of strong shadows after approximately 1000 ms (prior to this the Northgate building intercepts light). An increase in light intensity and appearance of shadows is in fact observed – Figure 41.

The observed timing of the onset of rarefaction (made visible by the appearance of a fine mist) and the duration of negative phase are also well predicted by the deflagration mechanism.
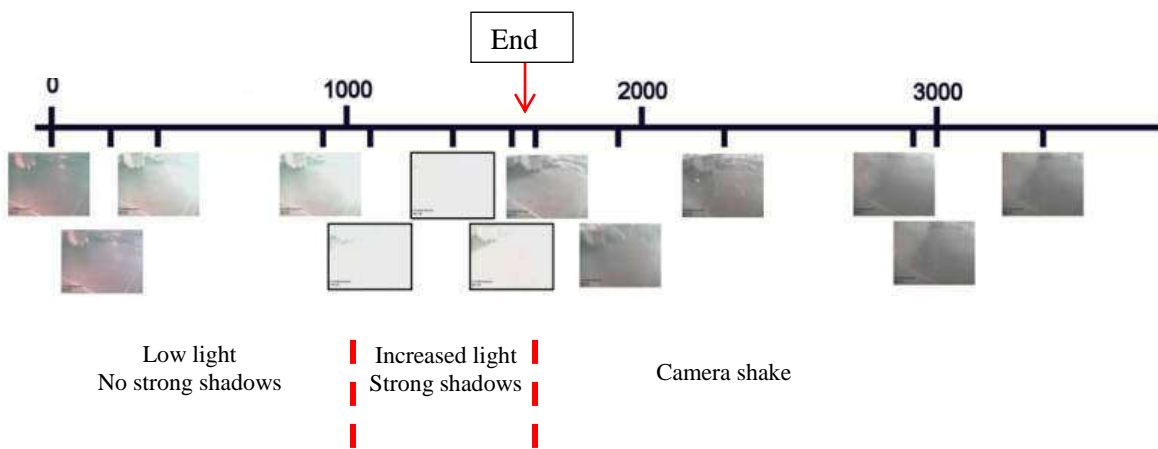
Figure 41: Time line of images from a Furnell camera.
Scale indicates time in milliseconds. T= 0 is the appearance of first light.

5.2.2.3   Detonation interpretation

The Buncefield Explosion Mechanism Group (EMG) Final Report (SCI, 2009) proposed an alternative interpretation of the data based on the assumption that the explosion was a detonation. The onset of camera movement was interpreted as marking the arrival of the detonation pressure wave. The duration of camera shake was taken to indicate the duration of vibration in the building or camera mounting. The more intense period of illumination is too long to correspond to the progress of a detonation and it was suggested that this corresponded to a period of after burning of fuel rich areas of the cloud. Because a detonation travels much more rapidly than the speed of sound, the time of flight calculations illustrated in Figure 39 do not apply. The EMG report suggested that the identification of the pump house as the point of origin by this method was fortuitous.

This particular version of the detonation interpretation is very unlikely to be correct for a number of reasons:

1. It would imply that early pressure effects reported by witnesses close to the cloud (see 5.2.2.4 e.g. shaking of a tanker) had no effect on any of the cameras.
2. The camera vibration is not consistent with an initial impulsive load. It becomes more violent as time progresses.
3. Detonation modelling with fuel rich clouds shows that after-burning progresses and cuts off too slowly to explain the recorded light data (Fluid Gravity, 2009).
4. Transition to detonation would have had to occur after about 600 ms on the time line in Figure 41. The images before and after are almost identical which is difficult to believe given the enormous difference in flame size and location.

Another, more plausible, interpretation assumes that transition to detonation occurred about 1000 ms after ignition. In this case pressure waves from the early stages of the explosion (starting with the pump house explosion) would have arrived at cameras and witnesses before the detonation blast. Objection 1(in the list above) is resolved and the time of flight calculations can be reinstated. However in this case a new objection to the detonation theory arises: all of the CCTV views shows strong pressure effects following the first camera movement – for example substantial displacement of light objects such as a pieces of paper. This implies that a sizable proportion of the total amount of gas had been combusted in the period prior to detonation which is inconsistent with the observation that a severe explosion was established close to the point of origin.

This interpretation also leads to a very low estimate for the duration of the positive phase – which is not consistent with detonation modelling of very wide flat clouds.

5.2.2.4   Witness evidence

There were a number of people very close to the edge of the cloud and who were consequently well placed to see and feel the effects of the explosion. Witnesses 1 to 8 (see below) were formally interviewed by police within a few days of the incident and the resulting statements are of high quality. At the time of the interviews the explosion was being investigated as a potential bomb blast. Open questions were asked about witnesses' experiences – the interviewers had no knowledge of or interest in VCEs.

Locations of key eyewitnesses to the explosion are shown in Figure 42

Figure 42: Witness locations and the point of ignition

Witness 1 (Control room)

"As I picked up the phone and hit the button I looked out of the window [of the control room]. I immediately saw a massive explosion in front of me that got bigger and bigger towards the control room. The noise was unbelievable and I was blown across the room.
The initial explosion was very broad and at low level. It was the width of the horizon. It appeared to cover the whole site, concentrated in the middle but getting bigger. It was followed by the blast with a massive vacuum noise and then the terrific bang"

Witness 2 (Mess room)

"We were sitting facing the rear wall of the mess room. Suddenly something happened. It wasn't like an actual explosion but it seemed like all the air was sucked out of the room. Almost at the same time there was a massive 'boom', there was at most a second or so gap between these. The ceiling disintegrated and all the lights smashed. Everything in the room was thrown around."

 Witness 3 (tanker loading area)

"I had only walked a few steps when all of a sudden I heard and felt a whoosh coming from behind me; I had the main tanks to my back. The whoosh was like a strong wind thudding me in the back. Immediately after the whoosh came a massive and loud explosion, the force of this blew me from my feet onto the floor."

Witness 4 (tanker loading area)

"All of a sudden there was a very loud crackling noise followed by an almighty explosion from somewhere on the site."

Witness 5(tanker loading area)

"My lorry began to shake. My immediate thought was that there was something wrong with the lorry and the pistons were going to come through and that the cab was going to blow up. At the same time I recall hearing a noise that I can only describe as a huge pressure sound, similar to that of a jet engine. This was followed by a very loud bang, which sounded like metal being hit with a large club hammer."

Witness 6 - about 30 m (98 ft) SW of Junction of Boundary Way and Three Cherry Trees Lane

"The whole area was suddenly engulfed by a large bright fireball. This fireball seemed to take away the fog I had witnessed, the fireball I believe had come from the direction of the oil depot. I turned and started to run back from where I had just come from. As I ran I could hear a sound similar to thunder and then I felt and heard a massive explosion which knocked me from my feet and onto the floor."

Witness 7 (Northgate Building Gatehouse)

"Without any warning I heard a whoosh of air and a loud bang afterwards.
A few moments later I looked around to see that the doors to the gatehouse had come inside the building and the glass from the windows had smashed."

Witness 8 - Three Cherry Trees Lane – 50 m (164 ft) NW of the junction with Boundary Way)

"I began dialling 999 I was looking in my driver's mirror to see whether XXXX had got to the corner. As I dialled the number, it blew. I clasped my hands over my ears and kept an eye on the mirror, seeing the flame coming towards me. I continued to look, to see whether the flames went past me, being concerned due to the fact my window was still down….The flames came from the direction of the Buncefield Lane; the initial fire ball filled the whole of the lane, all I could see was the flame engulfing the cars. There was a flash, the flames came towards me and then receded – it lasted for two seconds."
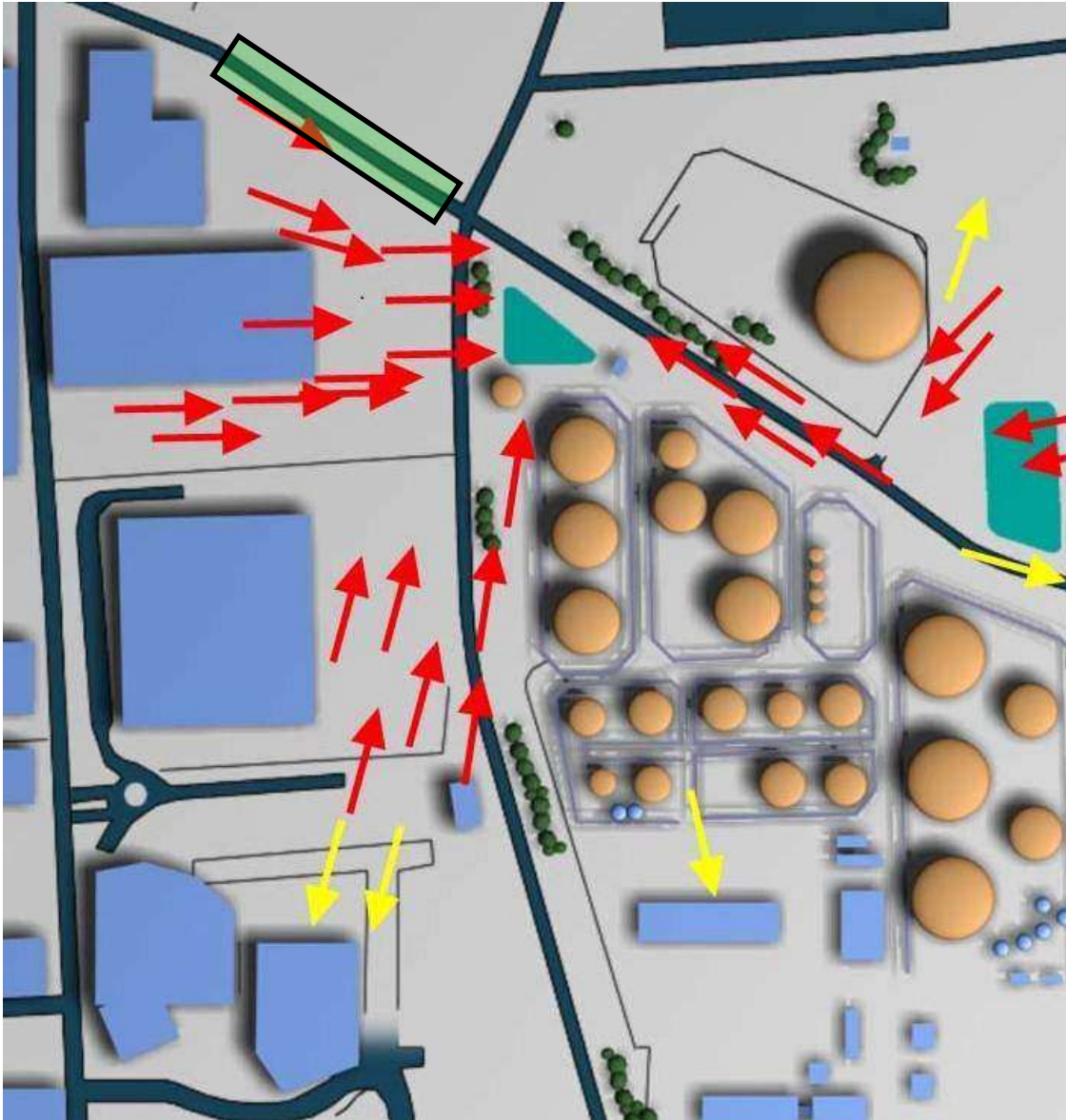
Figure 43: Location of cars that Witness 8 saw engulfed by the flame (marked by green box)

All of the witnesses report noise, drag forces or other sustained pressure effects prior to the arrival of the most powerful blast wave. These sounds are variously described as like:

- a vacuum noise
- a jet engine noise
- a very loud crackling noise
- thunder
- a whoosh

The initial drag forces were perceived as:

- A strong wind thudding me in the back

- A lorry shaking

The arrival of the most intense part of blast wave was characterised by:

- Destruction of buildings
- Witnesses being thrown around

The witnesses who had the earliest visual warning of the explosion were Witness 1 (Control room) and Witnesses 6 and 8 (Junction of Boundary Way and Three Cherry Trees Lane). Each provided detailed description of the advancing explosion. Witness 6 appears to have had time to turn and start to run before being bowled over by the explosion.

Those witnesses who did not have visual warning of the explosion have independently provided descriptions of the sustained noise and pressure effects that preceded it. For the character of these noises to be sufficiently well fixed in their minds to prompt recall and description in a statement, suggests that the noise must have lasted a sizable fraction of a second. No-one described the *initial* phase as a "bang" and no–one reported hearing loss after the main blast passed.

Some of these witnesses were very close to the edge of the cloud. Figure 44 and Figure 45 show calculated blast waves 10 m (32 ft) outside the edge of a 200 m (656 ft) radius vapor cloud, for an episodic deflagration and a detonation respectively. The cloud depth has been chosen so that each blast has the same impulse at a distance corresponding to the building shown in Figure 46. The magnitude of this impulse is consistent with movement of the front wall of this building.

Both of the mechanisms predict rapid increases in pressure. In a detonation this occurs without warning: in the case of of a deflaration there are significant pressure effects in advance of the final blast from the closest part of the cloud. The deflagration mechanism can account for the sustained pressure effects reported by witnesses.
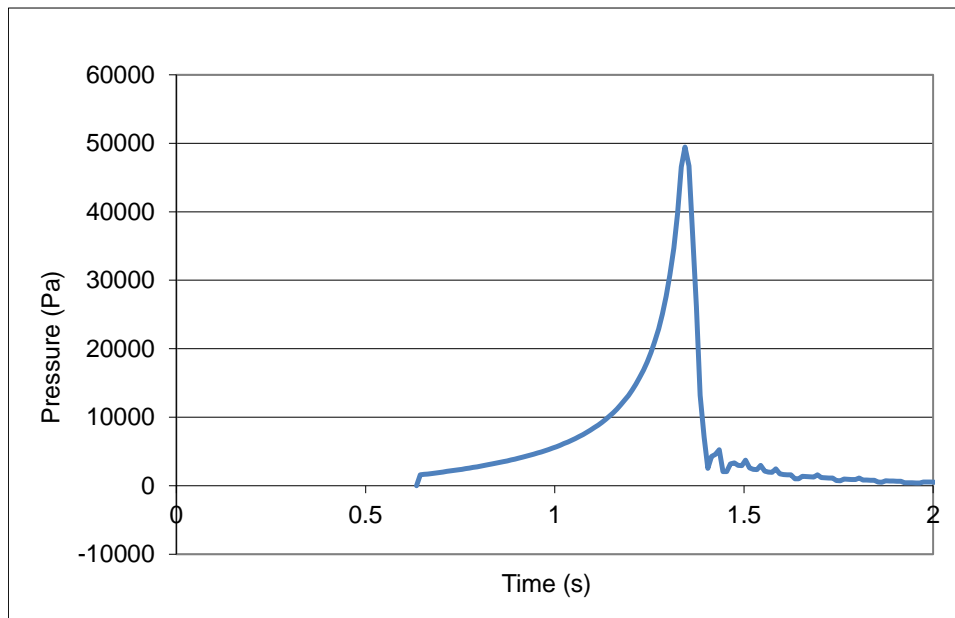
Figure 44: Blast wave from an episodic deflagration (flame speed 150 m/s)

Note 50,000 Pa is equivalent to 0.5 bar and 7.3 psi
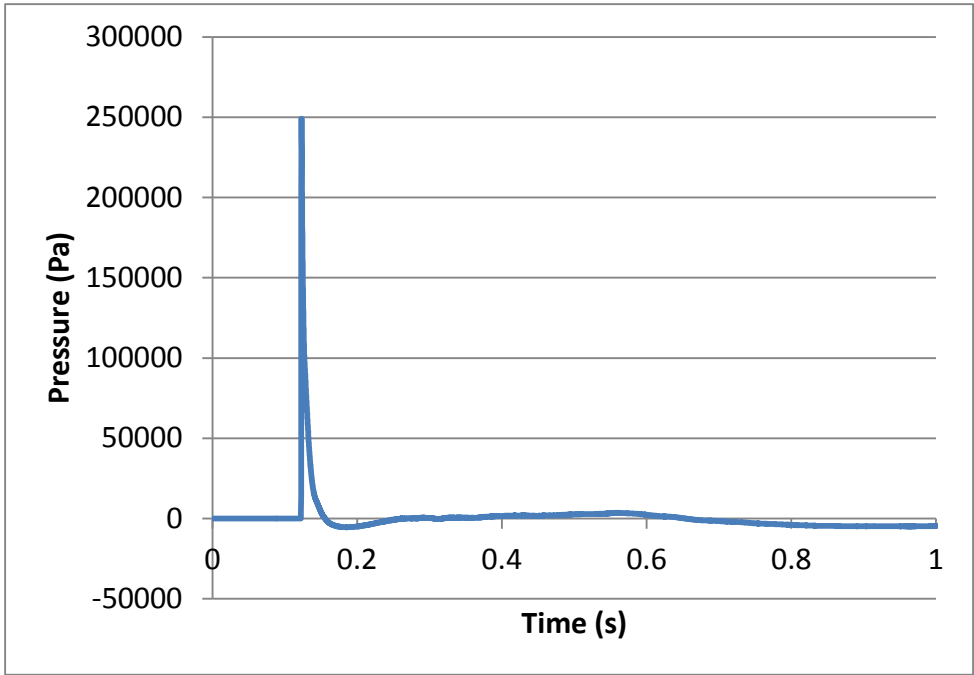
Figure 45: Blast wave from a detonation

Note 250,000 Pa is equivalent to 2.5 bar and 36.7 psi

An impulsive blast capable of causing the deformations shown in Figure 46 would produce very high pressures close to the cloud – for a detonation. It is difficult to understand how those close to the cloud edge escaped without permanent hearing loss or more serious injury if they were exposed to blast pressures like those in Figure 45.

Figure 46: Deformation of the front face of a building about 300 m (984 ft) from the edge of the Buncefield cloud.

5.2.2.5   Explosion testing

Experimental work following the Buncefield explosion showed that it was possible to get rapid flame acceleration and DDT in dense obstacle arrays formed by packing together fine branches in an array of width 4 m (13.1 ft) . The remains of vegetation close to the point of ignition in the two tests that led to DDT are shown in Figure 47.

It is not clear how these results relate to the vegetation near the point of ignition at Buncefield (Figure 48). At Buncefield vegetation close to the pump house was dominated by a greatly overgrown hedge. Individual trees had been planted close together in a line but had grown into substantial trees of height around 8m that formed a dense canopy at high level (Figure 37). A low density network of side branches would (in summer) have suppported a screen of leaves on the sides of the hedge.

The density of fine branches and twigs growing under such a cover would have been low because of low light levels and little evidence of dense undergrowth was observed in the aftermath of the explosion. In other parts of the Buncefield site there were patches of dense vegetation that had developed in open (unshaded) areas Figure 50. These were clearly visible after the explosion. The fact that dense undergrowth was not observed after the explosion in the hedge near the pump house suggests that there never was any.

Overall the situation at Buncefield was quite similar to that at Jaipur: in both case there was a building filled with gas that (for different reasons) would have generated a moderately powerful localised explosion. In both cases there were some substantial trees close by. Not only was the character of the developed explosion very similar but it is likely that the circumstances of transition to a severe explosion were also similar.

Figure 47: Vegetation post-explosion near the point of ignition in the two JIP tests that gave DDT

Figure 48a: Vegetation post-explosion near the point of ignition at Buncefield

Figure 498b: Vegetation post-explosion near the point of ignition at Buncefield – a new fence has been erected between pump house and hedge in this shot.
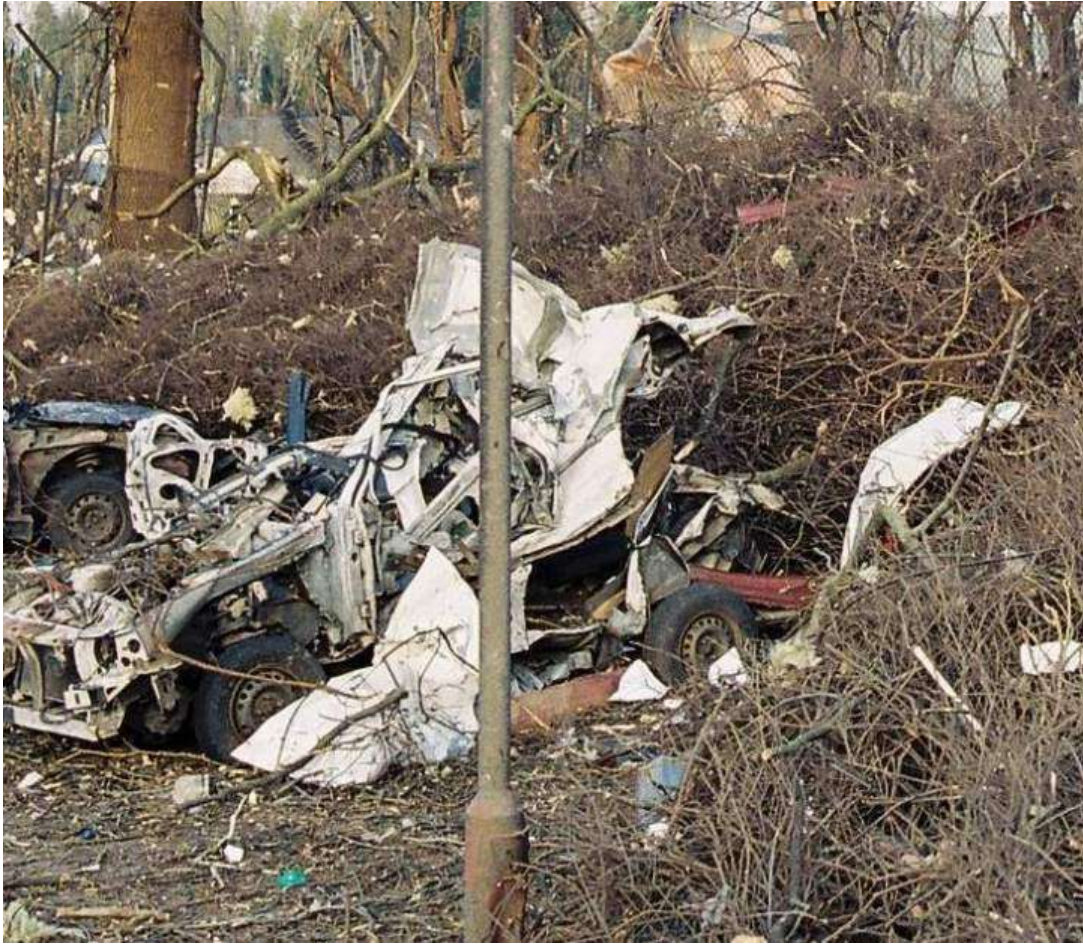
Figure 50: Patch of dense vegetation in the Buncefield site

Figure 51: Location of the patch of dense vegetation – outside the overgrown hedge

5.3   AMUAY REFINERY (VENEZUELA)

5.3.1   Summary of incident data

Time and date:	August 25 2012 (Saturday) around 1:10 AM
Location	Punt Fijo, Falcon State, Venezuela Site of leak at 11˚44'32.7" N 70˚11'13.57" W
Company	Paraguana Refinery Complex (PDVSA)
Narrative :	There are two accounts of this incident produced by : RMG (Risk Management Group) and PDVSA (the plant operators). These reports agree about the location of the leak and the extent o the vapor cloud but differ on the events leading up to the VCE. RMG Report: This report appeared very soon after the incident and was based on unnamed industrial contacts and various media sources. According to the RMG report, the leak occurred at a pump handling light hydrocarbons. This was in the vicinity of storage spheres in a tank farm area- about 400 m (1310 ft) east of the main refinery. This identification of the leak point matches the location of the ongoing jet fire immediately after the explosion. According to the RMG report a leak had been in progress for several days prior to the explosion but the refinery continued to operate as normal without the leak being fixed – the leak probably corresponded to a small proportion of refinery output . This was possible because prevailing winds diluted the released vapor and carried it out to sea. The day before the VCE the wind became weaker and unstable; high (>LEL) levels of flammable gas were detected outside the site boundary. An off-site lube oil plant south of the leak point was evacuated. Conditions in this area improved somewhat as the wind picked up and some workers returned to the lube oil plant. In the evening of August 24th in the hours before the blast it appears the external wind dropped out completely. Judging from the clear pattern of off-site explosion damage, vapor spread out up to 700 m (2296 ft) from the source, in directions covering an arc of 135 - 180˚. PDVSA Report: According to this report a serious seal failure occurred in a pump at 00:00am on August 25th. Inventory information for the associated olefin tank is presented suggesting a large leak of 67 kg/s lasting for 68 minutes until the explosion (273 tonnes total loss). The report identifies the location of ignition form CCTV records. Judging from the on-site damage to tanks the cloud did not spread far towards the main process areas of the refinery. This may reflect the effect of residual wind, but it possible that the convective flow driven by heat released around the refinery may have been sufficient to prevent

	accumulation of a cloud on this side (refinery) of the leak. Some annotated views of the area affected by the cloud are shown at the end of this summary. Cloud development is discussed further below. The cloud affected industrial, commercial and residential areas. More than 50 people were killed by the blast and many other were badly burned. It appears that all but one of the casualties were off-site.				
Incident Cause	Leaking pump				
Category Categorize incident cause (e.g. operator error, equipment malfunction, material failure, construction error, design error, weld failure)	Equipment malfunction				
Source Term	Type of release (e.g. gas, evaporating liquid or a gas-liquid (two phase) flow)	Description of equipment/piping	Hole size or pipe diameter if it was a guillotine failure	Substance(s) released	Release pressure and temperature
	Two-phase release of pressure liquefied products	Pump	About 2" diameter equivalent Judging by size of residual jet fire	C3/C4 hydrocarbons	Pressure is not known - likely to be a few bar (a few tens of psi). Temperature Not known
Release	Quantity released	Migration of substance from release source		Duration of release	
	At least 200 tonnes (440,000 lb)	Gravitational slumping		More than one hour	
Cloud development	Cloud footprint	Depth and influence of topography under and near the vapor cloud.	Surface roughness	Substance which formed a vapor cloud	Near field dispersion
	1100 x 800 m (approx. max dimensions)	Vapor accumulation in some areas may have been prevented by convective flows driven by the	Semi-urban	C3/C4 hydrocarbons	Hydrocarbon spray settling into a gravity driven non-entraining flow

		refinery. There appears to have been some channelling of the vapor current by bund walls .		
Weather conditions	Atmospheric stability		temperature	Wind speed
	Stable		Not known Approx. 20 ˚C	Nil
Ignition	Ignition strength	Source of ignition		Ignition location
	Not known	Not known		Highway
Explosion severity	Overpressure	Distance of flame travel		Flame speed
	Damage consistent with >2000 mbar (29 psi) observed over the whole site	Approximately 1000 m (3280 ft)		Not known directly. Overpressure indicates detonation, fast deflagration (FD) or episodic deflagration (ED).
Consequences	Fatalities, injuries, health effects, property damage within and outside of the plant property. Heavy damage – structural collapse Moderate damage- cladding loss, cracking of vulnerable masonry, purlin deformation Light damage - cladding damage, window breakage,		Blast damage to plant and other structures within and outside of cloud footprint.	
	50+ fatalities Heavy damage approx. 20 m from cloud edge (65 ft) Moderate damage approx. 300 m (984 ft) Light damage up to around 1500 m (4920 ft) (not much information)		i. Product tanks engulfed by the cloud were set on fire. Tanks deformed above the liquid line but not split below liquid level. ii. Destruction of all engulfed site buildings. iii. Severe damage to off- site buildings which were exposed to the cloud iv. Houses within about 100 m (328 ft) of cloud edge were wrecked. v. Substantial economic damage associated with on and off-site damage and loss of production.	

		Marsh large loss register(2013 Ed) gives insured loss as $330 million.		

Mitigating Measures	Cloud mitigation measures	Performance and/or reasons for poor performance		
	Vapor detection	Installed in offsite premises. More than an hour prior to the blast a worker in an off-site lube–oil plant sent a text: "Methane 24% -We are going to die" This person did not evacuate and was subsequently killed in the explosion. It is not known what vapor detection was in operation within the site.		
	Hedging/wall surrounding site	No		
	On-site vapor fencing	Not installed. Some unhelpful channelling of the vapor current by bund walls appears to have occurred.		
	Active vapor dispersal	Not installed		
Facility Information	Other Hydrocarbons at Facility	Quantity stored (is amount >10,000 lbs?)	Type of storage vessel/container	End product or used for a process
	Full range of refinery products	Of order 1,000,000 tonnes	Atmospheric storage tanks and bullets	Crude oil and refined products
	Characteristics of the area where the event occurred	Urban, rural, suburban	Industrial, residential	Proximity to ports/marine
	The bulk of the cloud was off-site. Topography – flat	Sub-urban	Industrial, commercial and residential. The death rate in	Marine

Climate semi-arid		areas exposed to the cloud appears to have been high.	
	Facility description	Category (refinery, petrochemical, gas processing, terminal and distribution, upstream)	Number of similar facilities worldwide
	Storage area of refinery	Refinery	Approx 700

Figure 52 and Figure 53 are aerial views showing the extent of the cloud.

Figure 52: Area affected by the vapor cloud – aerial photograph after the incident

Figure 53: Area affected by the explosion imaged in 2015 – source marked in red

5.3.2   Cloud development at Amuay

The leak apparently occurred at a pump handling light C3/C4 hydrocarbons. This was in the vicinity of storage spheres in a tank farm area- about 400 m (1312 ft) east of the main refinery. This identification of the leak point matches the location of the ongoing jet fire immediately after the explosion.

Figure 54: Ongoing fire around the site of the leak

Inventory information presented in the PDVSA report suggests the leak rate was 67 kg/s and the vapor cloud accumulated for 68 minutes (4080 secs) prior to ignition. The total release was consequently 273 tonnes.

In the evening of August 24th in the hours before the blast it appears the external wind dropped out completely. Judging from the clear pattern of off-site explosion damage, vapor spread out up to 700 m (2296 ft) from the source, in directions covering an arc of around 135˚. Judging from the on-site damage to tanks the cloud did not spread far towards the main process areas of the refinery. This may reflect the effect of residual wind but it possible that the convective flow driven by heat released around the refinery may have been sufficient to prevent accumulation of a cloud on this side (refinery) of the leak.

5.3.2.1   Effects on dispersion of convection driven by process heat

On the basis of its throughput the process heat released by the refinery complex has been estimated at 1.5 GW. The plant where this heat production would have been located is spread out over an area of approximately 500,000 m^2. Entrainment of air has been estimated by representing the heat release as a grid of thermal sources spaced at 50 m (164 ft) intervals. The strength of each source is 7 MW. Entrainment would be most active in the lowest 150 m (490 ft) of the up-flow where individual thermals are separate − above this level the plumes would

coalesce and the perimeter of the combined plume over which entrainment could occur would be relatively small.

Based on standard plume entrainment correlations (Drysdale, 1986) the entrainment rate up to the 150 m (490ft) level would be around 1.5×10^6 m^3/s. At moderate distances from the refinery area the associated in-flow will approximate to a sink flow i.e. it will be roughly symmetrically distributed on a hemispherical surface centred on the refinery. Table 9 shows the air flow driven by the convection at different distances from the centre of the refinery.

Table 9: Flow induced by the convection of refinery process heat

Distance to refinery centre	Inward air flow (m/s)
500 m (1640 ft)	0.95
1000 m (3280 ft)	0.24
1500 m (4920 ft)	0.1

As far as one can tell from aerial views of tank damage the cloud did not accumulate closer than about 500 m (1640 ft) from the centre of the refinery. At this location Table 9 suggests the air flow imposed by convection would have exceeded the rate of flow driven by the gravity - which is typically of order 0.5 m/s. It is possible therefore that in direction towards the refinery the convection driven flow drew away and diluted the cloud – preventing it from accumulating.

The cloud spread away from the refinery to a range of around 1300 m. At this distance the cloud would not have been have been significantly disturbed by the convective flow driven by the refinery.

This analysis is clearly approximate but does provide an explanation for the observed development of the cloud which appears to have been driven by gravity over a wide area in directions away from the refinery but not much towards the plant.

There are important implications for the probability of development of very large gravity driven clouds on refineries. The typical convection rates driven by process heat are likely to prevent such gravity-driven transport in substantial areas of the plant.

This might be an important consideration in the analysis of LNG export facilities. Convective heat release is likely to be intermediate between that at refineries and tank farms but might still effectively prevent accumulation of gas in nil/low wind conditions in some areas. Cooling fans are extensively used in LNG export facilities and these will further restrict the accumulation of gas in some important locations.

If it assumed that half of the vapor released was drawn away by convective flows driven by the heat island over the refinery, then the hydrocarbon content of the cloud would have been about 136 tonnes – this figure is very uncertain. The area of the observed cloud was approximately 600,000 m^2. Table 10 compares the mass of hydrocarbons in various clouds and their size (burned area). The figures suggest that if the mass of hydrocarbons per unit area is around 200 g/m^2 there is a risk of a VCE. This would correspond to a flammable cloud of depth around 2m deep which is consistent with CCTV records of visible cloud depth.

Overall these figures show that the source term parameters in the PVDSA report are consistent with the observed cloud size.

Table 10: Cloud mass and dimensions

	Mass in cloud (tonnes)	**Area of cloud (m^2)**	**Mass/unit area (g/m^2)**	**Vapor cloud explosion?**
Buncefield	26	150,000	173	Yes
San Juan	78	450,000	170	Yes
Amuay	~136	600,000	226	Yes
Donnellson	~150	300,000	500	No (over rich cloud?)

5.3.3   Explosion development at Amuay

Records of this incident come from photo-journalists and members of the public. Many of the images are of great interest but understandably the photographs were not taken to identify and record directional evidence. Two rare examples of directional evidence are shown in Figure 55 and .

Evidence of the sort shown in Figure 55 (showing a car shelter and fence) at Jaipur and Buncefield consistently indicated an explosion propagating form left to right (West to East). This location and direction are identified on Figure 57. Drums in the background of this shot showed moderate levels of crush damage consistent with those observed in Buncefield and Jaipur.

Figure 55: Directional damage to a car shelter (main supports) and fence post. Suggests severe explosion propagation from left to right. Location marked A in Figure 57

 shows inclined posts which again suggest a direction of propagation from West to East. This location and direction is also shown on Figure 57 – marked B. However the cloud is clearly propagating across a road at this point and disturbance of the depth and concentration of the cloud is to be expected.

Figure 56: Angled posts (some leaning on a wall). Marked B in Figure 57

A CCTV image presented in the PVDSA report shows that ignition actually occurred towards the Eastern edge of the cloud (Figure 57). This shows that directional indicators should be

treated with caution; local effects of variations in cloud structure can be confusing. Preferably indicators should be numerous (and consistent) and located in open, level undisturbed sites.

Figure 57: Limited indicators of direction of explosion propagation at Amuay – inconsistent with the observed location of ignition point.

Witness evidence from near the point of ignition has unusual features.

Edino Rafael Muñoz Lambertino was apparently on a jeep close to the observed point of ignition. The jeep's engine stuttered and when the driver tried restarting the vehicle, there was an explosion.

"*It seems that it* [the jeep] *had lifted...*"

Edino reported jumping from the car and running down the street to a corner.

"*When I look over there it came as a wave of fire, I laid down and prayed…It went over and then returned again."*

After the explosion had passed, Edino looked back at the jeep: it was burning with all its passengers as well as another vehicle with military guards and a lady with a 5-month-old girl.

"*All died. I saw them the next day in the newspaper…It is strange that they stay put and did not run away"*

"*I had glass fragments in my skin.*"

This witness apparently was located close to the point of ignition but several seconds later reports an energetic flame propagating towards his location. Possibly this might indicate a secondary ignition or fast flame spread in a drain that triggered transition to a severe explosion at a distant vent point. This might explain the discrepancy in explosion indicators.

5.3.4 Explosion severity

There is evidence of a severe explosion in all of the areas covered by photographic records. Damage to trees, drums, buildings etc. matches that observed at Buncefield and Jaipur. Some examples are shown in Section 9 of this report which deals with characteristic damage patterns.

Figure 58 shows damage to trees and a vehicle.

Figure 58: Explosion damage towards the NE edge of the cloud at Amuay

The cloud affected industrial, commercial and residential areas. More than 50 people were killed by the blast and many other were badly burned. It appears that all but one of the casualties were off-site.

5.4 FLIXBOROUGH, UK

5.4.1 Summary of incident data

Time and date:	Saturday 1st June 1974 4.53 pm
Location	Flixborough, UK 53˚37'18.42" N 0˚41'54.63" W
Company	NYPRO (UK)
Narrative :	The plant operating company was a joint venture between Dutch State Mines (DSM), the UK National Coal Board and Fisons (UK). It produced Caprolactam – a main component of Nylon 6. The section where the release took place was devoted to the production of cyclohexanone and cyclohexanol by the oxidation of cyclohexane with air in the presence of a catalyst. The reaction normally took place in a connected series of 6 adjacent reactors. At the time of the incident the fifth reactor had been removed for repair and replaced with a bypass pipe. This bypass was connected to the reactors on either end using a flexible bellows type fitting. It appears that the temporary connection was not subject to appropriate structural analysis or pressure test. On Saturday 1st June 1974 at 4.53 pm the 20" bypass pipe failed completely and there was a massive double ended release of cyclohexane at a pressure of at least 9 bar (130 psi) and a temperature of 155°C (311 F). Prior to the rupture the 5 remaining reactors would have contained approximately 120 tonnes (264,000 lb) of cyclohexane of wihich 80 tonnes (176,000 lb) was recovered after the incident. Of the 40 tonnes (88,000 lb) that was lost it has been estimated that 30 tonnes (66,000 lb) contributed to the cloud prior to ignition. Workers in the site laboratory, which was 75 m (246 ft) from the leak point, saw and heard the release and were able to evacuate to a distance of about 150 m (492 ft) before ignition – these people survived. Eighteen workers in the adjacent control room did not evacuate and were all killed. The delay before ignition appears to have been 45 seconds. It is not known precisely where ignition occurred but rapid flame acceleration occurred and damage to objects within parts of the cloud is consistent with a transition to detonation. Of the 72 people working on the site at the time, 28 were killed and 36 others suffered injuries. If the explosion had occurred on an ordinary working day, many more people would have been on the site, and the number of casualties would have been much greater.

	Outside the Works injuries and damage were widespread but no-one was killed. Fifty-three people were recorded as casualties by the casualty bureau which was set up by the police; hundreds more suffered relatively minor injuries which were not recorded. Property damage extended over a wide area: 1000 houses were damaged within a range of 1500 m (4,921 ft) and a further 800 houses at a range between 1500 to 4500 meters (4,921 – 14,760 ft). 167 shops and factories were damaged to a greater or lesser degree.
Incident Cause	Failure of dog leg by-pass pipe with bellows connections
Category Categorize incident cause (e.g. operator error, equipment malfunction, material failure, construction error, design error, weld failure)	Design error – no proper design analysis of pressure system or appropriate pressure test.

Source Term	Type of release (e.g. gas, evaporating liquid or a gas-liquid (two phase) flow)	Description of equipment/piping	Hole size or pipe diameter if it was a guillotine failure	Substance(s) released	Release pressure and temperature
	Two-phase release of superheated cyclohexane at around 9 bar (130 psi)	Bypass pipe with bellows connections	20"	Cyclohexane	9 bar (130 psi). Of which roughly half CHX and half nitrogen 155˚C (311 F)

Release	Quantity released	Migration of substance from release source	Duration of release
	About 30 tonnes (66,000 lb)prior to ignition	Complex two phase release from two slightly offset facing pipes. Jets would have impacted on reactors close to release point. Flow in the outer parts of the vapor cloud would have been affected by gravity and external wind	45 seconds

Cloud development	Cloud footprint	Depth and influence of topography under and near the vapor cloud.	Surface roughness	Substance which formed a vapor cloud	Near field dispersion
	300 x 200 m Plan area See map	Cloud driven by initial momentum , gravity and a light wind.	Rural (outside the confines of the plant)	Cyclohexane	Two phase spray developing into a largely gravity driven flow

Weather conditions	Atmospheric stability		temperature	Wind speed
	NK		Not known	Low

Ignition	Ignition strength	Source of ignition	Ignition location
	Not known	Not known	Not known

Explosion severity	Overpressure	Distance of flame travel	Flame speed
	Damage consistent with detonation in areas at ground level	Approximately 300 m (984 ft)	Not known directly. Damage indicates fast deflagration leading to detonation

Consequences	Fatalities, injuries, health effects, property damage within and outside of the plant property. Heavy damage – structural collapse Moderate damage- cladding loss, cracking of vulnerable masonry, purlin deformation Light damage - cladding damage, window breakage,	Blast damage to plant and other structures within and outside of cloud footprint.
	28 fatalities Heavy damage approx. 100 m from cloud edge (328 ft) Moderate damage approx. 1000 m (3280 ft) Light damage up to around 4500 m (14,763 ft) (not much information)	

Mitigating Measures	Cloud mitigation measures	Performance and/or reasons for poor performance		
	Vapor detection	Not relevant. The catastrophic release was immediately obvious to most of those on site. Cloud accumulation was very rapid.		
	Hedging/wall surrounding site	No		
	On-site vapor fencing	N/A		
	Active vapor dispersal	N/A		
Facility Information	Other Hydrocarbons at Facility	Quantity stored (is amount >10,000 lbs?)	Type of storage vessel/container	End product or used for a process
	NK	Of order 1,000 tonnes	Tank farm Drum storage Solids warehouse	Cyclohexane was a process fluid
	Characteristics of the area where the event occurred	Urban, rural, suburban	Industrial, residential	Proximity to ports/marine
	The cloud was on-site. The footprint included substantial heavily congested plant areas Topography – flat	Rural (beyond site boundary)	Industrial .	In land (45 km from the coast)
	Facility description	Category (refinery, petrochemical, gas processing, terminal and distribution, upstream)		Number of similar facilities worldwide
	Manufacturer of plastic precursor	Chemical manufacture		

Further reading

The Flixborough Disaster: Report of the Court of Enquiry, Department of Employment (1975)

HSE holds an archive of 900+ photographs from the incident investigation. A selection of the most important have been assembled as part of a media package as part of this project. This locates the images on the incident site and provides notes.

Figure 59 to Figure 64 show maps and aerial views of the layout of the site and the nature of the damage.
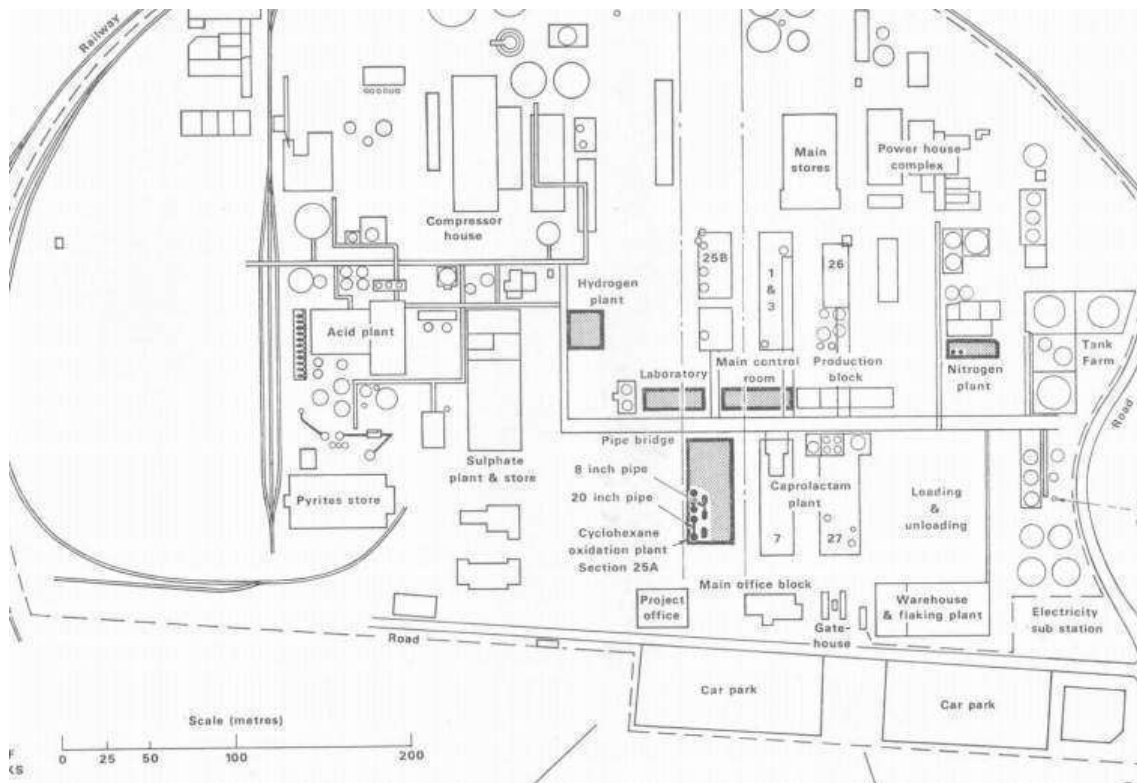
Figure 59: Overall view of Flixborough site
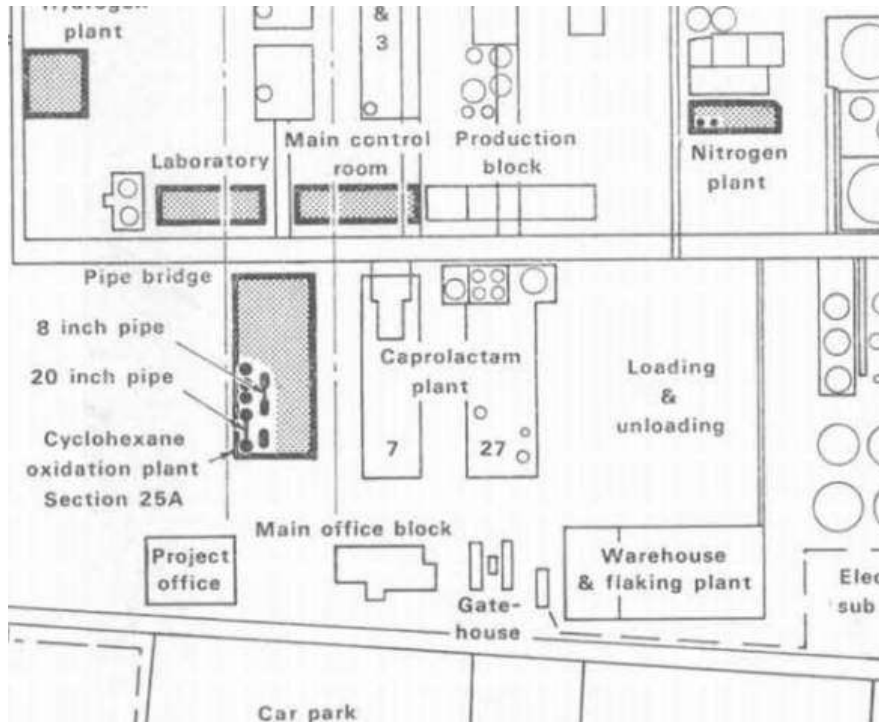
Figure 60: Close-up view of area where the vapor cloud accumulated
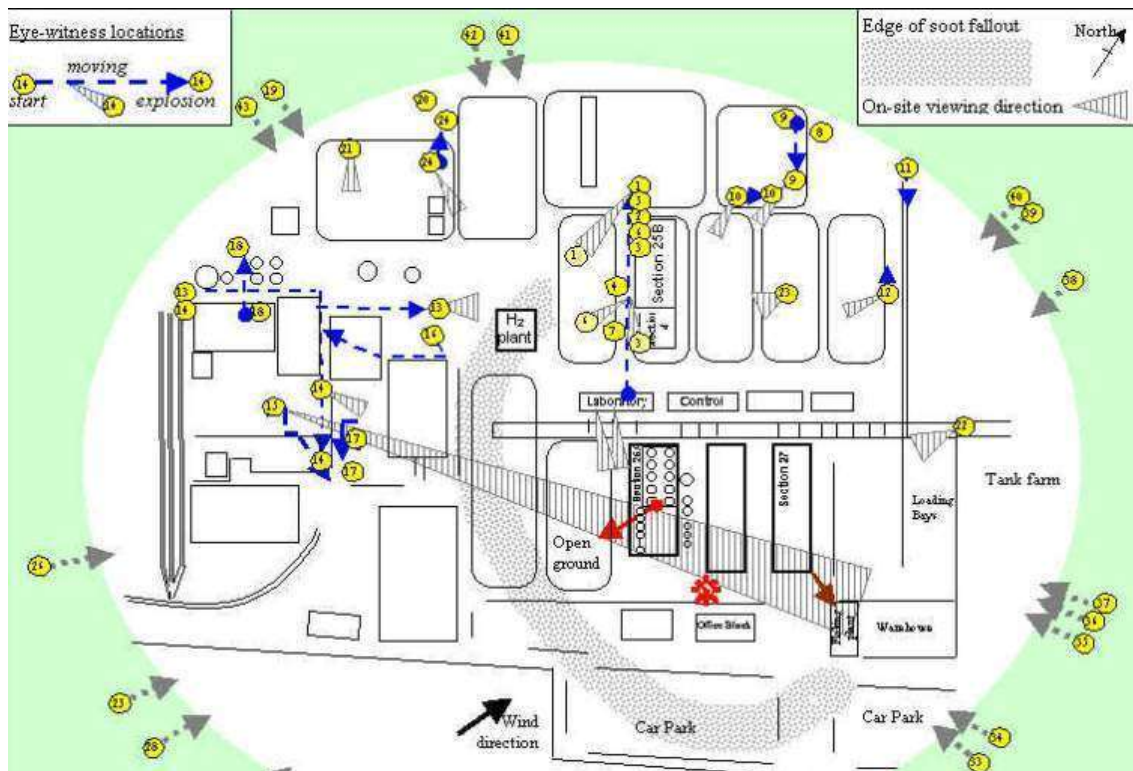
Figure 61: Graphic showing edge of soot fall out – which marks edge of the rich part of cloud

Figure 62: Flixborough site prior to the incident – release point marked X

Figure 63: Aerial view of the Flixborough site after the incident – release point marked X

Figure 64: Aerial view of the Flixborough site after the incident – release point marked X

Key:

1. Reactor 5 –scaffolded for repair in an open part of the site

2. Ruins of main office block (unoccupied as the incident occurred on Saturday)

3. Ruins of warehouse – drums and solids

5.4.2   Vapor cloud production at Flixborough

The series of reactors forming the pressure system that failed is illustrated schematically in Figure 65 and shown in a photograph in Figure 66.
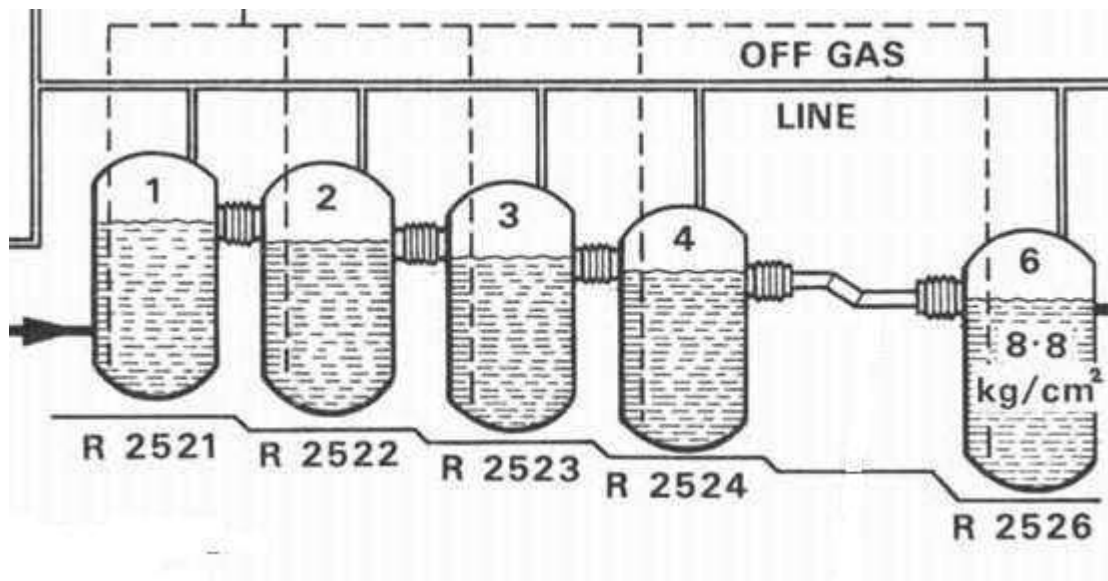
Figure 65: Schematic of reactor train including by-pass

Figure 66: Photograph of part of the reactor train after the incident the dog leg bypass was lost completely. Scaffolding has been erected after the incident.

Figure 67 shows a close-up of the 28" flanges left after the failure of the 20" by-pass. It can be appreciated that the source term would have been complex with expanding, two-phase jets issuing from both holes in opposite directions. These off-set jets would have collided, forming an angled fan of vapor and fine droplets. Later in the release the combination of tanks 1-4 would have depressurised less quickly than Tank 6: the release would have increasingly resembled a jet directed towards the car parking areas.

Entrainment of air would have progressively reduced the outward jet speed and the resulting diluted jet would have started to slump since it would still be significantly heavier than air. The typical downward velocities driven by buoyancy forces on the accumulating heavy cloud near the source would have been of order 5-10 m/s for pure vapor and 3-4 m/s for a vapor/air mixture close to the stoichiometric ratio. These estimates can be derived from equating the potential energy of the elevated heavy gas to the accumulated downward kinetic energy.

The release time of 30-60 seconds would have been sufficient for gravity to drive the establishment of a vapor current – with much of the accumulated vapor being concentrated in a relatively shallow layer at ground level.
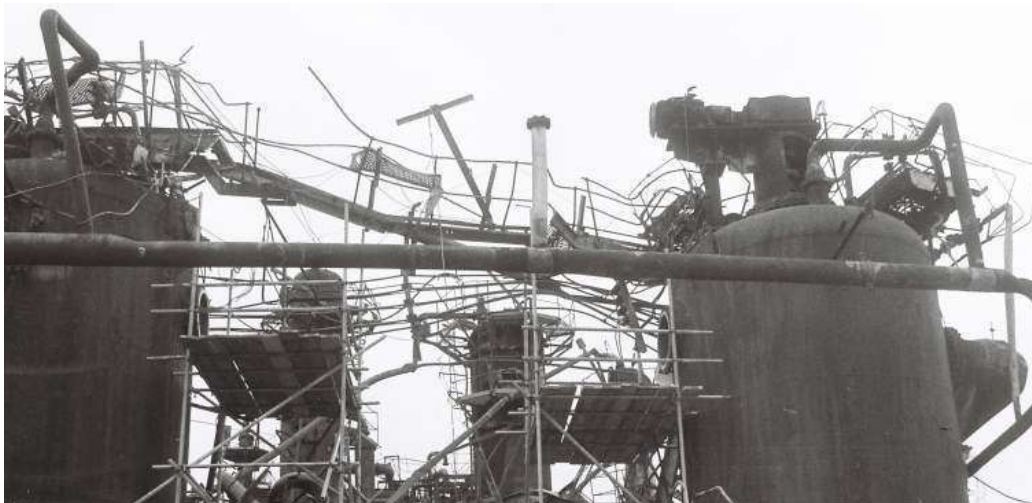
Figure 67: Openings left after loss of bypass pipe

The total mass of cyclohexane released was around 30 tonnes (66,000 lb) and overall plan area of the cloud was around 60,000 m^2. **Table 11** shows how the average depth of the cloud varies with its average concentration.

Table 11: Cloud depth derived from mass release rate and plan area

Average concentration (g/m^3)	Average depth (m)
85 (stoichiometric)	5.8
170	2.9

There was noticeable fall out of soot from the explosion – even at the upwind edge - which suggests the cloud was quite rich. It seems likely that the average cloud depth over much of its plan area was around 3-4 m (9.8 – 13.1 ft). The depth close to the source would have been much greater i.e. >15m (>49 ft).

5.4.3 Explosion development at Flixborough

Figure 66 illustrates the high level of congestion and confinement in the plant areas at Flixborough. Many more photographs are available in the archive application that will be produced to accompany this report.

The area where the release occurred would have been almost completely filled with flammable vapor – even at high levels. It is to be expected that a severe explosion would have been sustained in this area. The combination of large flame path lengths and highly confined and congested areas provided the potential for transition from a fast deflagration to a detonation (DDT). If this occurred the detonation could propagate away from plant areas into the open low lying areas of the cloud.

There is good evidence that this did in fact occur and spread to most of the areas of the cloud in the open. The sequence of images in Figure 68 to Figure 71,show the damage to the equivalent parts of the skirts of Reactors 2,3 6 and finally Reactor 5 with the wreckage of associated scaffolding. Reactor 5 had been relocated to an open area of the site for repair (necessitating the installation of the temporary by-pass pipework that failed).

The level of damage clearly increase as the reactors step down in elevation and (presumably) further away from the ignition point in the sequence 2,3, and 6. The damage to the vessel in an **open area** (Reactor 5) is noticeably more severe than those on the plant. This side of the reactor was facing the plant so if the cloud engulfing Reactor 5 detonated, then the reflected pressure on the upstream face would be around 35-40 bar (507 – 580 psi) – compared with the side-on overpressure in a detonation of around 15-18 bar (217 – 261 psi).

Figure 72 shows the back face of Reactor 5. Comparison with Figure 71 confirms that there is the clear asymmetry in damage level to be expected for an impinging detonation.

Figure 68: Reactor 2. Limited pressure damage to reactor skirt
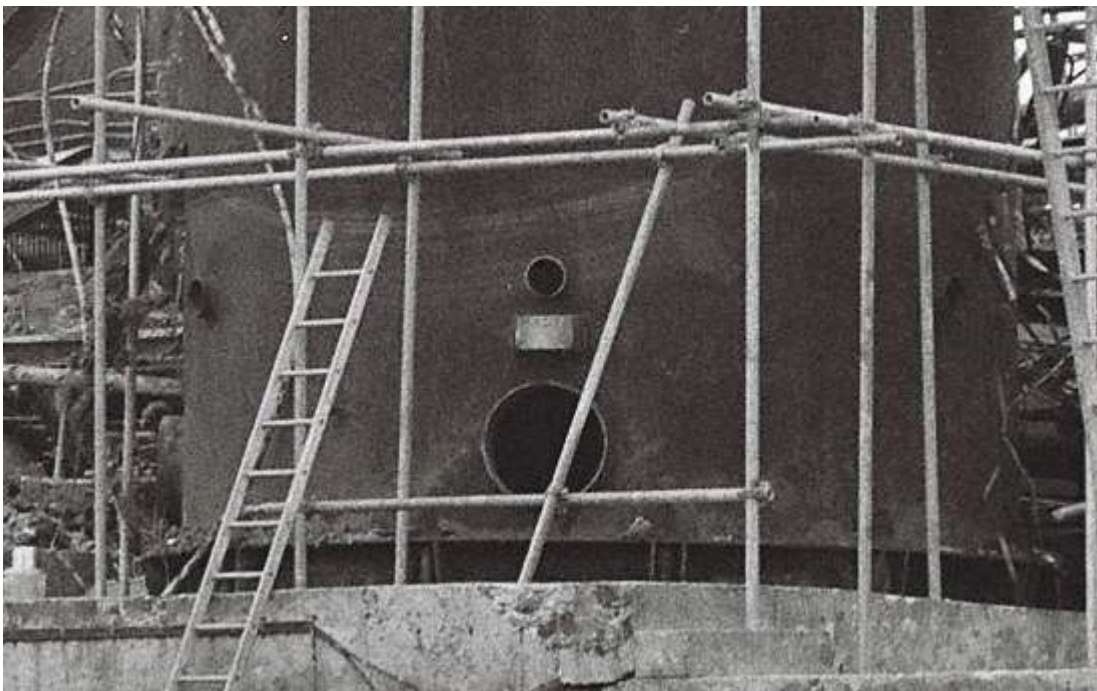
Figure 69: Reactor 3. Limited pressure damage to reactor skirt

Figure 70: Reactor 6 (Number 5 missing). Significant pressure damage to the skirt

Figure 71: Reactor 5 - Located in open ground approximately 40 m (131 ft) from the leak. Substantial damage to the reactor skirt on the side facing the plant

Figure 72: Reverse face of Reactor 5 showing asymmetry in damage

The curved scaffold tubes in the wreckage surrounding Reactor 5 are also significant (Figure 71 and Figure 72). Numerous pieces of scaffold boarding are visible in their midst and it is clear that there was no sustained fire around the vessel. It follows that the curvature of the tubes was caused by the explosion not by any subsequent fire.

The weight, second moment of area and degree of end constraint of these tubes is comparable with the angle iron used to fabricate the tents in Buncefield JIP detonation tests. The general character of the deformation and extent of deformation are also comparable (Figure 73).

Figure 73: Angle iron deformed by a detonation (depth 3m)

It is highly likely that damage to Reactor 5 and the scaffolding that surrounded it was caused by the progress of a detonation through the cloud in this area. At this point the detonation was apparently travelling outwards from a point close to the south end of the oxidation plant.

Similar examples of continuous curvature are seen in fence posts and barriers to the south of the cyclohexane oxidation plant (Figure 74, Figure 75 and Figure 76).
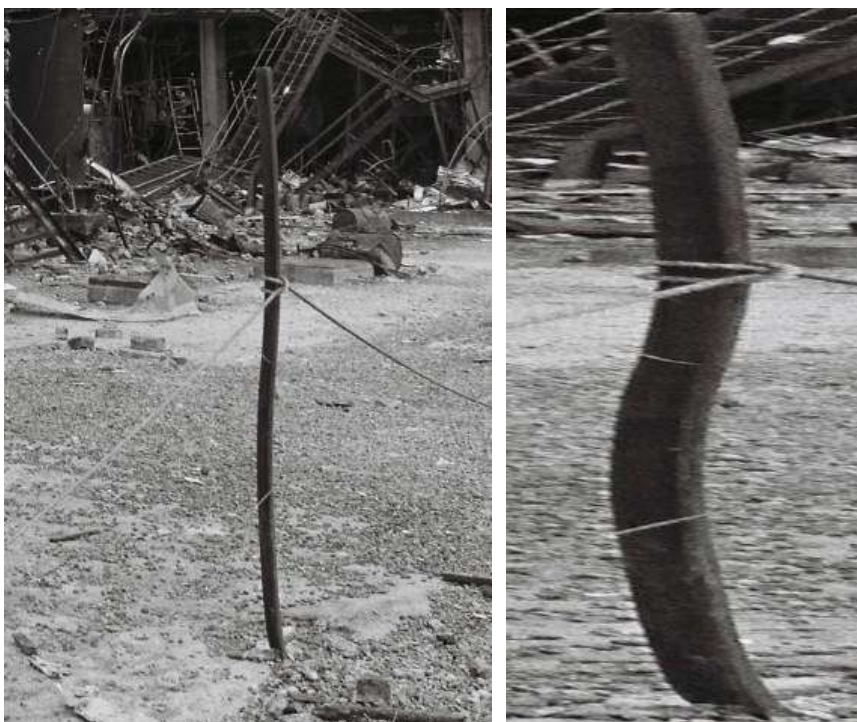
Figure 74: Curved fence posts in open areas to the south of the cyclohexane oxidation plant

The original images are on the left. The images on the right are digitally stretched by 500% in the horizontal direction to allow the curvature to be seen.

Figure 75: Curved fence posts in open areas to the south of the cyclohexane oxidation plant

The original image is above. The image below is digitally stretched by 500% in the vertical direction to allow the curvature to be seen.

Figure 76: Curved barriers

The original image is above. The image below is digitally stretched by 500% in the vertical direction to allow the curvature to be seen.

Continuous curvature was also observed in lamp posts within the cloud (Figure 77 and Figure 78). The most pronounced curvature along the length of the posts was observed around the fringes of the cloud where the mixture would have been detonable through the whole depth.

Figure 77: Lamp post within the cloud – approx. 130 m (426 ft) south of vapor source

Figure 78: Lamp post within the cloud – approx. 180 m (590 ft) NE of vapor source

Outside the cloud the posts did not exhibit plastic deformation along the whole length (Figure 79 and Figure 80). Plastic deformation was concentrated near the base of the main stem – where the moment of blast forces would have been greatest.

Figure 79: Lamp post outside the cloud to the East

Figure 80: Lamp post outside the cloud to the North

It is useful to examine why the occurrence of continuous curvature disappears so rapidly beyond the edge of the cloud. Figure 81 shows dynamic pressure just inside and just outside a 3m deep propane/air detonation (Fluid Gravity, 2009). The maximum pressure falls off very quickly.
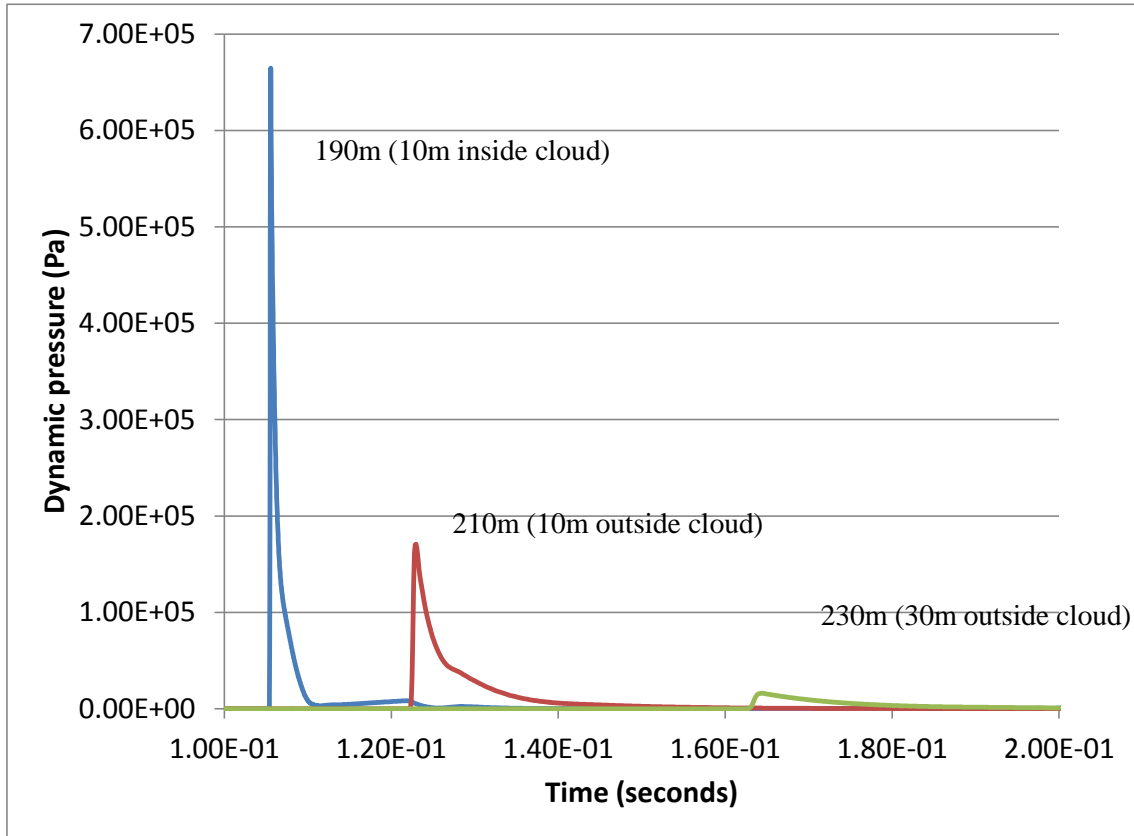
Figure 81: Dynamic pressure in and close to the edge of a 3m deep detonation (cloud radius 200m, measurement height 1.5m, measurement radius 190, 210 and 230 m)

The kinetic energy (per unit length) absorbed from the drag impulses in the first 5ms is shown in Table 12; expressed as the proportion of the energy required to cause local plastic deformation (Section 11):

Table 12 : Energy absorbed from a detonation shock

Distance from cloud edge	Energy absorbed (as a proportion of that required to cause local plastic deformation)
-10 m (within the cloud)	270%
+10 m (outside the cloud)	109%
+30 m (outside the cloud)	27%

This suggests that local plastic deformation is confined to areas very close to the edge of the cloud and this type of damage effectively marks the edge of the detonation.

Page | 110

Anticipating Section 9 it is worth pointing out that this type of continuous curvature, with plastic deformation distributed along the length rather than being concentrated in hinges, is only observed for extremely high impulsive load profiles. No continuously curved spars or posts were observed at the Buncefield, Jaipur, Amuay or San Juan sites[6]. Some elements suffered mid-span failure but closer examination shows these were mono-modal hinged failure characteristic of application of force over a longer period compared with the natural frequency of the element –Figure 82 and Figure 83.

Figure 82: Deformed steels outside and within the Buncefield cloud exhibit hinged failure – characteristic of loads applied over a long period relative to the natural frequency

---

[6] *The top reinforcing bar in a skip (Figure 244) developed several hinge points and could be viewed as exception. This bar has a particularly low stiffness to effective mass ratio and the natural frequency is low for this reason – this is discussed further in Section 9.5*

Figure 83: Deformed steels at Buncefield exhibit hinged failure – characteristic of loads applied over a long period relative to the natural frequency. Images on the right and below stretched digitally in the horizontal and vertical directions respectively – to visualise strain distribution.

Figure 84: Typical deformation of a lamp post at Buncefield

5.4.4 Extent of the detonation at Flixborough

Deformation of lamp posts is a useful means of determining which open areas were affected by cloud detonation. Figure 85 shows results of this analysis.

Red arrows indicate continuous curvature of the main lamp post stems or mid-span hinging and probably indicate direct exposure to detonation of the surrounding cloud. The direction of arrows indicates the final direction of the stem in the photographs. Numbers correspond to the ID numbers chalked on boards and included in the original photographs.

Blue arrows correspond to lamp posts where plastic deformation was confined to an area near the base of the main stem.
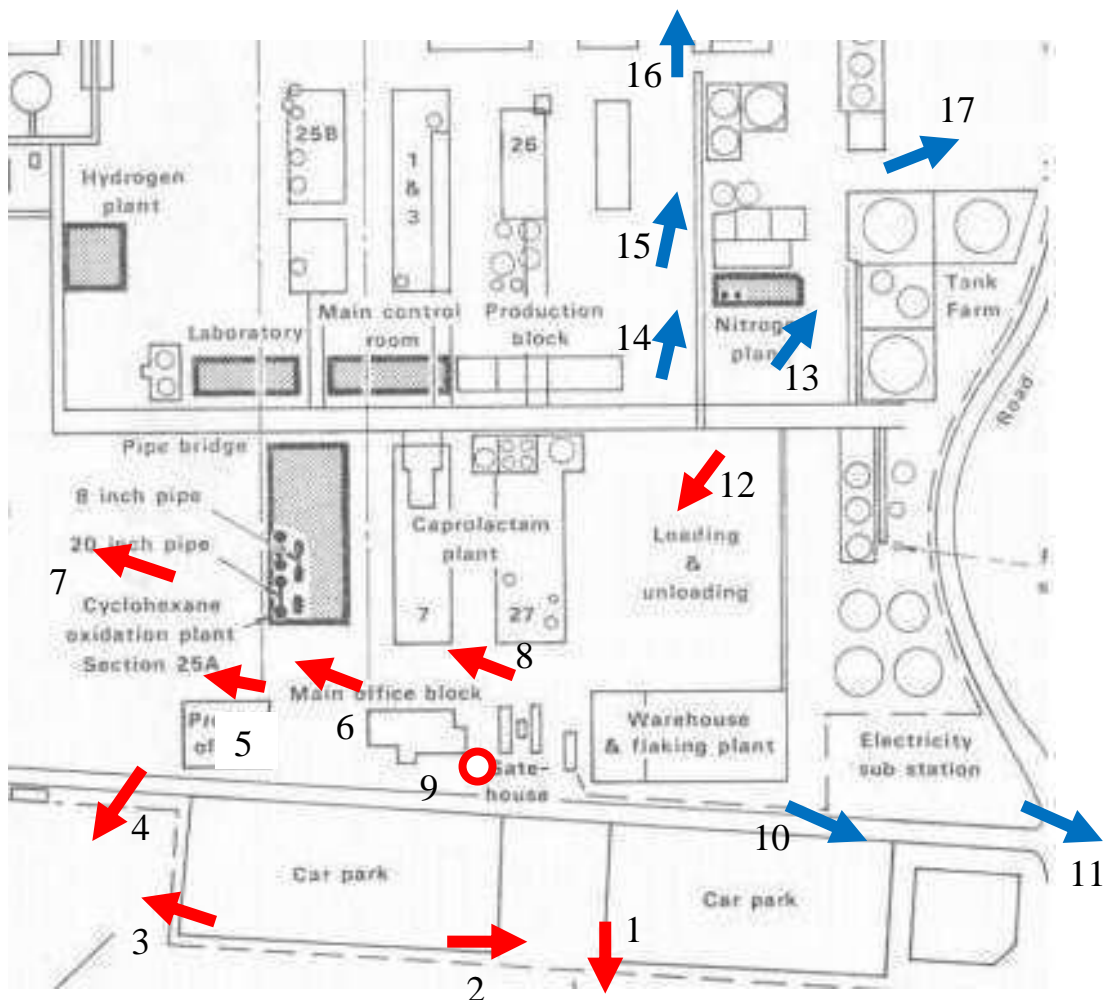
Figure 85: Deformation of lamp posts at Flixborough

It appears that detonation affected a high proportion of the cloud away from the main plant areas. However no clear pattern emerges from the direction of the red arrows that might allow the tracking of detonation's progress.

Because of the directional nature of the source term and the relatively short release period, gravity would certainly not have had time to even out horizontal concentration gradients around the site – especially in areas where there were substantial buildings. For this reason it is likely that the cloud would have been very patchy. Once initiated a detonation would thread its way through such a cloud via a circuitous route. The extremely high drag forces exerted on an exposed lamp post reflect the local direction of explosion propagation and it is perhaps not surprising that such widely spaced markers cannot resolve the way the detonation propagated.

Blue arrows correspond to much smaller and slower impulses and the direction is generally radially away from the cloud, as is to be expected.

Lamp post 9 (LP 9) is a curiosity: although well within the general outline of cloud, it was not flattened by the blast - Figure 86. This post was originally close to the Main Office Building – which lay between LP 9 and the vapor source. This three storey building was reduced to the rubble pile visible in the top left of Figure 86. It is plausible that there was minimal vapor in this particular area at the time of the blast. On the other hand there was certainly vapor in areas surrounding LP8, LP2, L1 etc. as these posts were both bent and flattened.

Some previous investigators have imagined a large cloud high up in the air above this post to explain the lack of massive deformation. It seems more likely that minimal deflection simply reflects the cancellation of longer time scale pressure waves from areas all around.

Figure 86: Low levels of deformation and deflection damage to LP 9

This post is, in fact, neither vertical nor straight as shown in the digitally stretched image shown in Figure 87.

Figure 87: Digitally stretched image of LP9

5.4.5 Summary

The cyclohexane oxidation plant at Flixborough contained some heavily congested and confined areas. The release would have filled the part of the plant where it occurred to full depth giving a 3D character to the developing explosion – which would also have increased overpressures.

There is clear evidence that the cloud detonated when the flame reached the area around the leak. The detonation then progressed into the lower lying areas of the cloud in open areas around the plant. Characteristically high impulsive loads were exerted on posts and spars that were perpendicular to the direction of detonation propagation.

The imposed loads were massively higher than the minimum level required to cause failure and were imposed in a time very much shorter than the natural period of vibration of the elements. The result was the propagation of a zone of plastic deformation along the length of elements, leaving them with continuous curvature.

The short duration and directional character of the release resulted in a patchy cloud. The detonation would have had to propagate around areas where cloud conditions could not support it. This produced a complex pattern in the extent and direction of high impulse damage.

5.5 SAN JUAN, PUERTO RICO

Time and date:	00:23 23rd October 2009
Location	Luchetti Industrial Park, Bayamón, Puerto Rico
Company	Caribbean Petroleum Corporation (CAPECO)
Narrative :	On the night of October 23, 2009, a large explosion occurred at the Caribbean Petroleum Corporation (CAPECO) facility in Bayamón, Puerto Rico, during offloading of gasoline from a tanker ship, the *Cape Bruny*, to the CAPECO tank farm onshore. A 5-million gallon aboveground storage tank (AST) overflowed into a secondary containment dike. The gasoline cascade formed a large vapor cloud, which ignited after reaching an ignition source in the western fringes of the cloud. The blast and fire from multiple secondary explosions resulted in significant damage to 17 of the 48 petroleum storage tanks and other equipment onsite and in neighbourhoods and businesses offsite. The fires burned for almost 60 hours. Petroleum products leaked into the soil, nearby wetlands and navigable waterways in the surrounding area.
Incident Cause	An overfill of Tank 409 was likely caused by a combination of: • Malfunctioning of the tank side gauge or the float and tape apparatus during filling operations led to recording of inaccurate tank levels; • Variations in the gasoline flow rate from the *Cape Bruny* may have contributed to the overfill; • Potential failure of the tank's internal floating roof due to turbulence and other factors.
Category Categorize incident cause (e.g. operator error, equipment malfunction, material failure, construction error, design error, weld failure)	Deficiency in Safety Management System

Source Term	Type of release (e.g. gas, evaporating liquid or a gas-liquid (two phase) flow)	Description of equipment/piping	Hole size or pipe diameter if it was a guillotine failure	Substance(s) released	Release pressure and temperature
	Cascade of volatile liquid	Overflow from Tank 409 through six vents		Gasoline	Low pressure overfill

Release	Quantity released	Migration of substance from release source		Duration of release
	200,000 gallons	Gravitational slumping from the secondary containment dike		26 minutes
Cloud development	Cloud footprint	Depth and influence of topography under and near the vapor cloud.	Surface roughness	Substance which formed a vapor cloud	Near field dispersion
	115 acres			Gasoline	
Weather conditions	Atmospheric stability		Temperature	Wind speed
	Data from Luis Munoz Marin International Airport (8.5 miles East) Calm and partly cloudy		79degF 26.7degC	Nil wind
Ignition	Ignition strength	Source of ignition		Ignition location
	Not known	Not known (area of ignition not electrically classified)		Somewhere within the decommissioned refinery Not known precisely. Probably secondary ignition (about 7 seconds later) in E part of site.
Explosion severity	Overpressure	Distance of flame travel		Flame speed
	Severe explosion in the latter stages. Explosion measured 2.8 on the Richter scale	Substantial flash fire prior to transition into a severe explosion. Transition to a VCE occurred as the flame entered a deeper area of the cloud containing a pipe rack.		
Consequences	Fatalities, injuries, health effects, property damage within and outside of the plant property. Heavy damage – structural collapse Moderate damage- cladding loss, cracking of vulnerable masonry, purlin deformation Light damage - cladding damage, window breakage,		Blast damage to plant and other structures within and outside of cloud footprint.	

	No fatalities Minor injuries to 3 people off-site Heavy damage: Within cloud Moderate damage: Within 50m of cloud Light damage: Within 500m of cloud	17 of 40 storage tanks were ignited

Mitigating Measures	Cloud mitigation measures	Performance and/or reasons for poor performance		
	Vapor barrier surrounding site	No		
	On-site vapor fencing	No		
	Active vapor dispersal	No		
Facility Information	Other Hydrocarbons at Facility	Quantity stored (is amount >10,000 lbs?)	Type of storage vessel/container	End product or used for a process
	Gasoline Fuel oil Kerosene Diesel	Capable of storing up to 90,000,000 gallons of product	Storage	End product
	Characteristics of the area where the event occurred	Urban, rural, suburban	Industrial, residential	Proximity to ports/marine
	Industrial area in the centre of the city limits	Urban	Commercial with some residential nearby	2.5km from port
	Facility description	Category (refinery, petrochemical, gas processing, terminal and distribution, upstream)		Number of similar facilities worldwide
	Gasoline terminal	Terminal and distribution		≈ 10,000
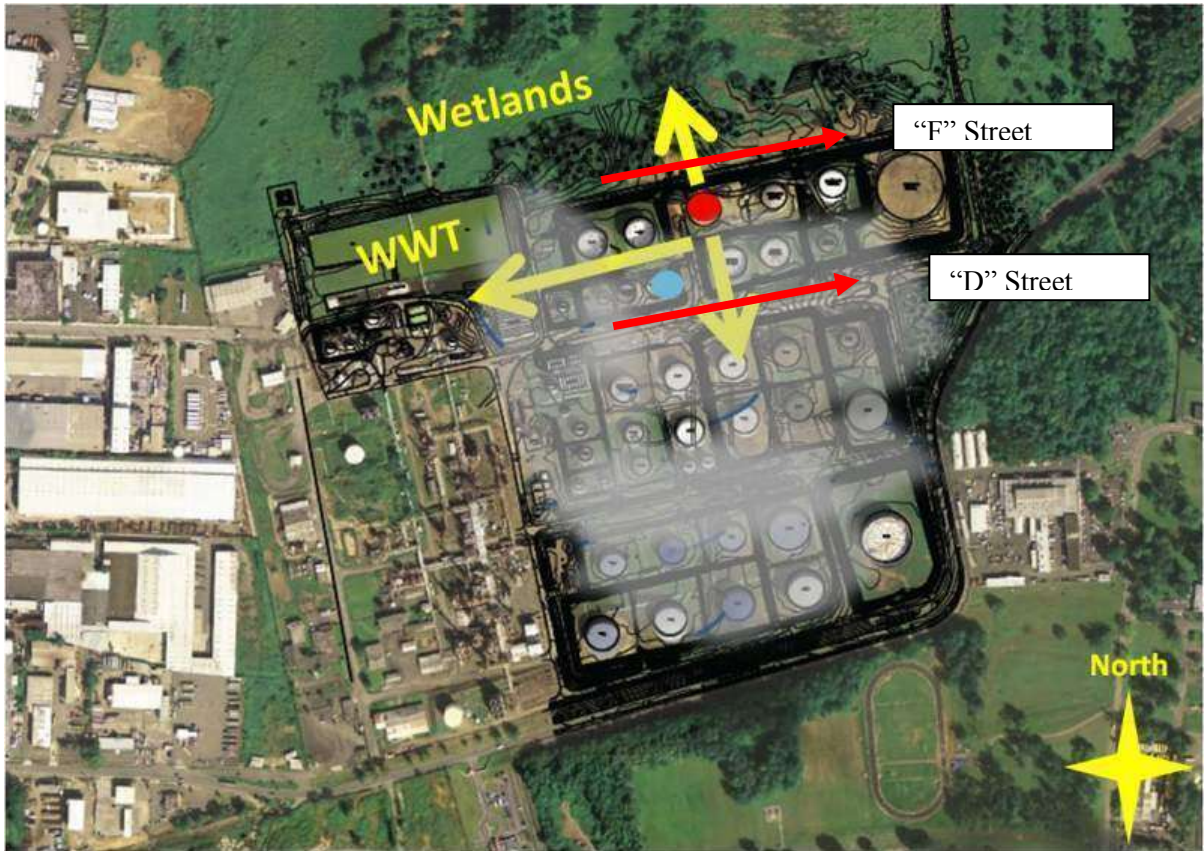
Figure 88: Topographic Survey of CAPECO Tank Farm

Reproduced from CSB Report - CSB (2015)

Figure 89: CAPECO multiple tank farm fire, October 23, 2009

Figure 90: Impact of the explosion and multiple tank fires after the October 23, 2009 incident

Reproduced from CSB report – CSB (2015)

Figure 91: Aerial view showing cloud footprint

Figure 92: Derived cloud footprint

(Area enclosed is 115 acres = 465,000 m², Equivalent radius = 385 m)

Daily Weather History Graph
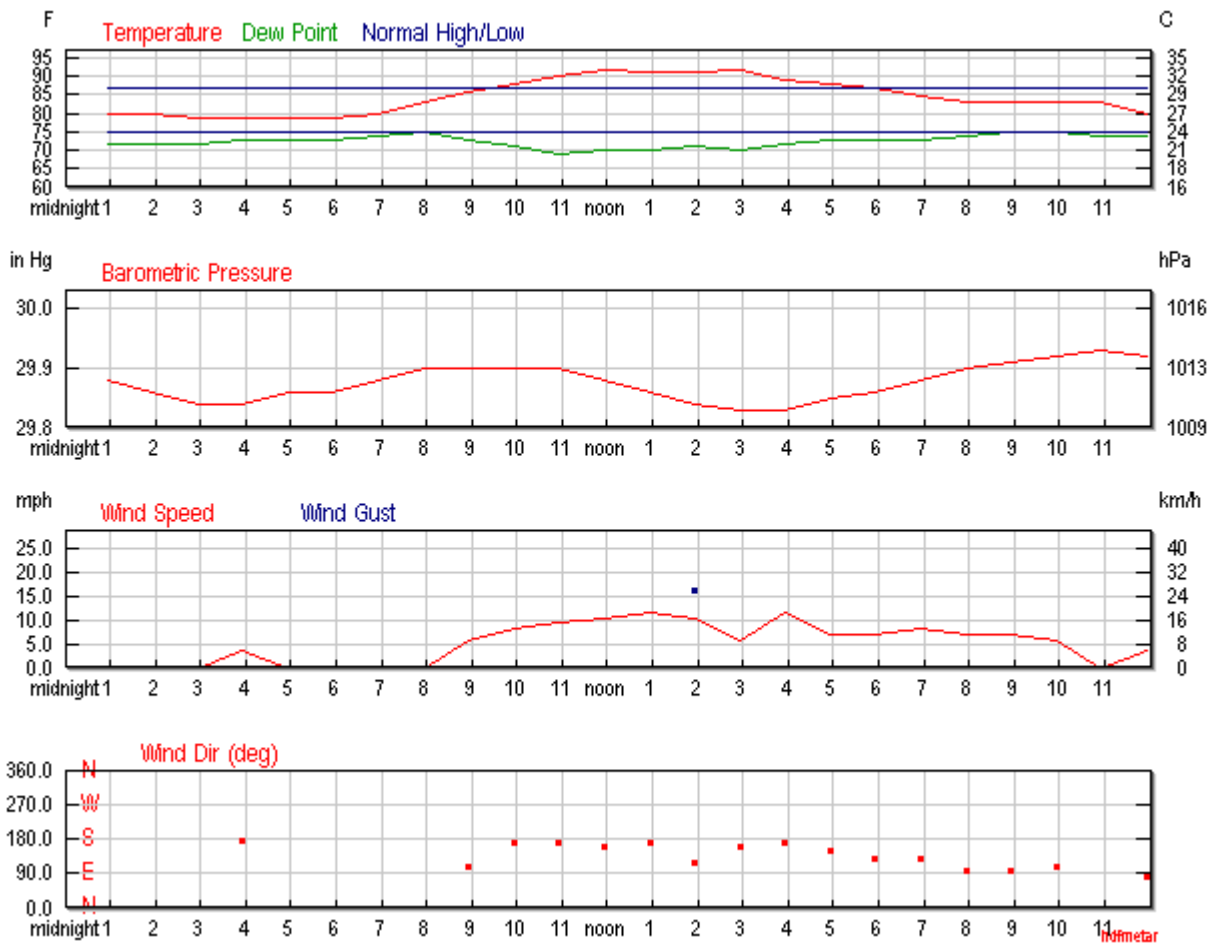
Figure 93

Hourly Weather History & Observations

Time(AST)	Temp.	Dew Point	Humidity	Pressure	Wind Dir	Wind Speed	Conditions
12:56 AM	**26.7** °C	**22.2** °C	76%	**1011.6** hPa	Calm	Calm	Partly Cloudy
1:56 AM	**26.7** °C	**22.2** °C	76%	**1011.0** hPa	Calm	Calm	Partly Cloudy
2:56 AM	**26.1** °C	**22.2** °C	79%	**1010.4** hPa	Calm	Calm	Partly Cloudy
3:56 AM	**26.1** °C	**22.8** °C	82%	**1010.5** hPa	South	**5.6** km/h /**1.5** m/s	Partly Cloudy
4:56 AM	**26.1** °C	**22.8** °C	82%	**1010.9** hPa	Calm	Calm	Partly Cloudy
5:56 AM	**26.1** °C	**22.8** °C	82%	**1011.2** hPa	Calm	Calm	Scattered Clouds
6:56 AM	**26.7** °C	**23.3** °C	81%	**1011.7** hPa	Calm	Calm	Scattered Clouds
7:56 AM	**28.3** °C	**23.9** °C	77%	**1012.3** hPa	Calm	Calm	Scattered Clouds
8:56 AM	**30.0** °C	**22.8** °C	65%	**1012.5** hPa	ESE	**9.3** km/h /**2.6** m/s	Scattered Clouds

Time(AST)	Temp.	Dew Point	Humidity	Pressure	Wind Dir	Wind Speed	Conditions
9:56 AM	**31.1** °C	**21.7** °C	57%	**1012.5** hPa	South	**13.0** km/h/ **3.6** m/s	Scattered Clouds
10:56 AM	**32.2** °C	**20.6** °C	50%	**1012.4** hPa	South	**14.8** km/h/ **4.1** m/s	Scattered Clouds
11:56 AM	**33.3** °C	**21.1** °C	48%	**1011.7** hPa	SSE	**16.7** km/h/ **4.6** m/s	Scattered Clouds
12:56 PM	**32.8** °C	**21.1** °C	50%	**1011.0** hPa	South	**18.5** km/h/ **5.1** m/s	Scattered Clouds
1:56 PM	**32.8** °C	**21.7** °C	52%	**1010.5** hPa	ESE	**16.7** km/h/ **4.6** m/s	Scattered Clouds
2:56 PM	**33.3** °C	**21.1** °C	48%	**1010.1** hPa	SSE	**9.3** km/h / **2.6** m/s	Scattered Clouds
3:56 PM	**31.7** °C	**22.2** °C	57%	**1010.1** hPa	South	**18.5** km/h/ **5.1** m/s	Scattered Clouds
4:56 PM	**31.1** °C	**22.8** °C	61%	**1010.6** hPa	SSE	**11.1** km/h /**3.1** m/s	Scattered Clouds
5:56 PM	**30.6** °C	**22.8** °C	63%	**1011.1** hPa	SE	**11.1** km/h /**3.1** m/s	Scattered Clouds
6:56 PM	**29.4** °C	**22.8** °C	67%	**1011.6** hPa	SE	**13.0** km/h/ **3.6** m/s	Scattered Clouds
7:56 PM	**28.3** °C	**23.3** °C	74%	**1012.5** hPa	East	**11.1** km/h /**3.1** m/s	Scattered Clouds
8:56 PM	**28.3** °C	**23.9** °C	77%	**1012.7** hPa	East	**11.1** km/h /**3.1** m/s	Scattered Clouds
9:56 PM	**28.3** °C	**23.9** °C	77%	**1013.2** hPa	ESE	**9.3** km/h /**2.6** m/s	Scattered Clouds
10:56 PM	**28.3** °C	**23.3** °C	74%	**1013.3** hPa	Calm	Calm	Scattered Clouds
11:56 PM	**26.7** °C	**23.3** °C	81%	**1013.2** hPa	East	**5.6** km/h /**1.5** m/s	Scattered Clouds

5.5.1 Vapor cloud development at CAPECO, San Juan

The footprint of the vapor cloud is shown in Figure 91. The area affected is roughly circular and roughly centred on the tank that was overfilled. The equivalent radius of the cloud (derived from its footprint) was 385m. The extent to which the burned area corresponded to a circle centred on the source must be regarded as coincidental as the site included some gradients. But these gradients were most significant at some distance (>250m) from the source. The strong flow of vapor in all directions close to the source was to be expected in this area – which was locally fairly flat.

The CSB report indicates that gasoline would have been discharged from six vents on the top of Tank 409. The tank is shown in Figure 94 together with the presumed range of trajectories of over-spilled gasoline. The discharge pattern is significantly different to that at Buncefield where vents discharged onto the top of the tank. For Tank 409 the speed of the liquid at the level of the wind girder would have been around 7 m/s and some liquid could have been projected away from the tank by about 10m (at ground level). Sideways spreading of the cascade would have been much less pronounced: based on experience from the post-Buncefield tests it would be reasonable to assume a lateral width of around 0.5 m.

Results from a standard application of the FABIG TN12 VCA method are shown in Table 14: Standard application of FABIG VCA method to the San Juan Case. The default distribution of the release around 30% of tank perimeter (suitable for the Buncefield case) has been used. Winter gasoline of the same composition as that at Buncefield has been used as the released material. The predicted cloud radius is 85% of that observed. The concentration of hydrocarbons is very high; which is probably a result of underestimating the area of the liquid cascade and overestimating the volatility of the gasoline.

Results using raw gasoline as the released product are shown in Table 15 for comparison. As expected the cloud size is similar but the hydrocarbon concentration is much less.

The standard VCA method in this case involves liquid cascade spread over a total area of around 14 m². In fact it is likely that at San Juan the cascade area was about twice this value (6 x 10 m x 0.5 m). Table 16 shows results for the San Juan case obtained by adjusting the liquid distribution parameter appropriately to model the enhanced cascade spread. The predicted radius increases because of the additional entrainment and is quite close to the observed value.

This level of agreement is fortuitous in this case as site elevations vary significantly and the cloud depth must have varied widely around the assumed average value of 2m. Nevertheless even the standard VCE method does give a reasonable idea of the extent of the cloud.

Figure 94: Tank geometry and presumed range of trajectories of over-spilled gasoline

Table 13: Composition of liquids used in modelling

	Paraffins							Aromatics				Naphthenes	
	C3	C4	C5	C6	C7	C8	C10	C6	C7	C8	C9	C5	C6
Winter Grade Gasoline		9.6	17.2	16			57.2						
Raw Gasoline		1	9	21				35	13	7	14		

Table 14: Standard application of FABIG VCA method to the San Juan Case

Input		unit
Compound	**Winter Grade Gasoline**	
Tank Type	**Fixed with internal floating deck - Type1**	-
Tank Diameter	**37**	(m)
Tank Height	**20**	(m)
Overspill % of Tank Rim	**30**	(%)
Air Temp	**20**	(°C)
Fuel Temp	**20**	(°C)
Fuel Mass Flowrate (Mfuel)	**340**	(kg/s)
Output		**unit**
Air Mass Flowrate (Mair)	216	(kg/s)
Ccascade	23.09	(%)
Mvap	64.9	(kg/s)
Msplash	2.91	(kg/s)
Mcloud	568	(kg/s)
Vcloud	437	(m3/s)
Ccloud	0.155	(kg/m3)
Cloud depth assumed	2	(m)
Time	1560	(s)
Cloud Radius	329	(m)

Table 15: Application of FABIG VCA method to the San Juan Case using raw gasoline as the released substance

Input		unit
Compound	**Raw Gasoline**	
Tank Type	**Fixed with internal floating deck - Type1**	-
Tank Diameter	**37**	(m)
Tank Height	**20**	(m)
Overspill % of Tank Rim	**30**	(%)
Air Temp	**20**	(°C)
Fuel Temp	**20**	(°C)
Fuel Mass Flowrate (Mfuel)	**340**	(kg/s)
Output		**unit**
Air Mass Flowrate (Mair)	216	(kg/s)
Ccascade	16.54	(%)
Mvap	42.9	(kg/s)
Msplash	5.85	(kg/s)
Mcloud	530	(kg/s)
Vcloud	408	(m3/s)
Ccloud	0.119	(kg/m3)
Cloud depth assumed	2	(m)
Time	1560	(s)
Cloud Radius	318	(m)

Table 16: Application of FABIG VCA method to the San Juan Case: by doubling the liquid spread parameter to account for enhanced spreading of the liquid cascade.

Input		unit
Compound	**Raw Gasoline**	
Tank Type	**Fixed with internal floating deck - Type1**	-
Tank Diameter	**37**	(m)
Tank Height	**20**	(m)
Overspill % of Tank Rim	**60**	(%)
Air Temp	**20**	(°C)
Fuel Temp	**20**	(°C)
Fuel Mass Flowrate (Mfuel)	**340**	(kg/s)
Output		**unit**
Air Mass Flowrate (Mair)	364	(kg/s)
Ccascade	14.42	(%)
Mvap	61.3	(kg/s)
Msplash	5.85	(kg/s)
Mcloud	862	(kg/s)
Vcloud	663	(m3/s)
Ccloud	0.101	(kg/m3)
Cloud depth assumed	2	(m)
Time	1560	(s)
Cloud Radius	406	(m)

CSB noted that valves on drains leading out (northwards then westward) from the 409 bund to the lagoon were open at the time of the incident. Some liquid and vaporised gasoline accumulated in the East end of the lagoon – and fuelled a pool fire after ignition.

Experience with CFD modelling the Buncefield incident suggests that a very deep cloud would be established within and just outside the 409 bund. This occurs where rapidly moving currents of vapor collide or strike bunds or other tanks. Beyond the bund the deep cloud rapidly slumps under the influence of gravity.

According to the tanker's log the explosion occurred about three minutes after the period of overfilling finished (off-loading terminated at the dock). The tank would still have been emptying (through the vents) but at a reduced rate after this delay. An analysis using the Bazin weir equation (Horton 1967) and the normal scaling of entrainment rate with liquid flow (FABIG TN 12 Atkinson and Pursell), suggests that (if the vents were unobstructed) the rate of cloud accumulation would have fallen to about 80% that during the overfill. It is possible that

the vents would have been partially obstructed by seals on the floating deck. In this case liquid may have accumulated to a somewhat higher level in the tank and the outflow would have been sustained at a higher level for longer when the supply was cut. In any case it is to be expected that at the time of the explosion the cloud depth would be greater in the vicinity of the tank and the fuel concentration somewhat less than was the case during the main part of overfill.

5.5.2   Explosion damage at San Juan

A severe explosion affected a substantial proportion of the site. Two types of evidence are available on this explosion:

1. Physical evidence – crushed and bent objects in the areas affected by the severe explosion and objects that were scorched but not affected by high pressure in the areas which burned as a flash fire.

2. CCTV records from several angles.

Although this section focusses on physical damage some references to basic facts derived from CCTV records are made – for example that the primary ignition was near the western edge of the cloud in the area occupied by a decommissioned refinery. There was a secondary ignition towards the East end of "D" Street some 7 seconds later.

5.5.2.1   Area around the point of ignition

The whole of the burned area is shown in **Figure 95** (yellow line).

Figure 95: Extent of the burned area (yellow). Area around the point of primary ignition (blue)

The ignition occurred somewhere in the North part of the decommissioned refinery (North-West corner of the whole site). The exact point of ignition is not known but CCTV records suggest it was somewhere in the area marked by the blue line.

Figure 96 shows typical damage close to the ignition point. Part of the edge of the cloud is shown in Figure 97. The burned vegetation shows the extent of the vapor cloud but there are no signs of severe overpressure effects. Figure 96 shows some doors have been blown off where vapor penetrated enclosures, but corrugated iron covers and other vulnerable structures have not been affected. The cloud would have been shallow in this area.

Figure 96: Typical damage around the ignition point

Figure 97: Part of the edge of the cloud – showing character of unburned ground cover

5.5.2.2   *Other areas affected before transition to a severe explosion*

Figure 98 shows the **approximate** extent of fire spread prior to the first signs of a severe explosion on the CCTV record. The flame took about 8 seconds to reach this stage. The maximum extent of flame spread was around 250 m corresponding to an average rate of flame spread of order 30 m/s.
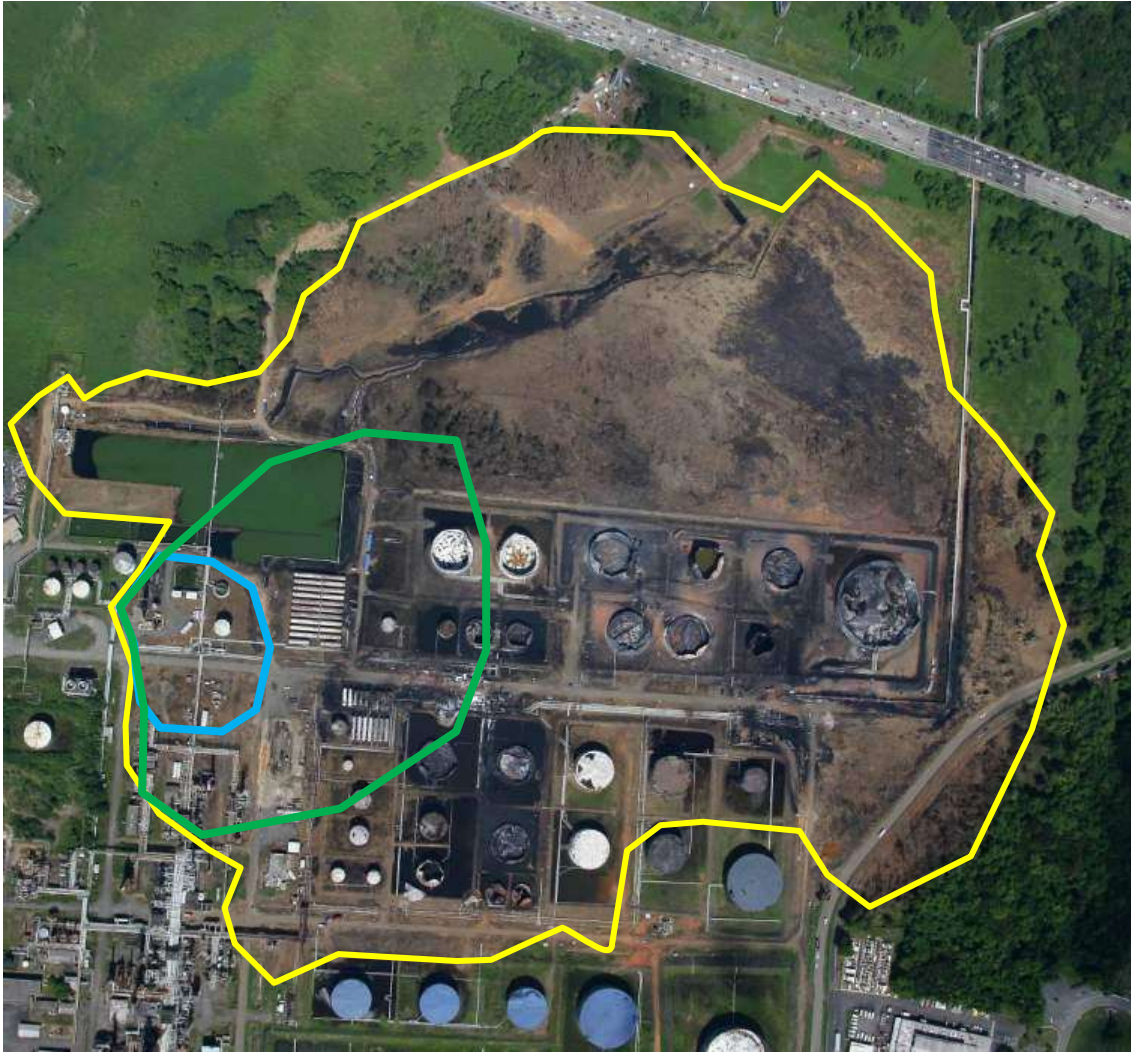
Figure 98: Extent of the burned area (yellow). Approximate extent of flame spread prior to transition to a severe explosion (green).

Within this area there was generally a low or moderate level of pressure damage. Examples are shown in Figure 99 and Figure 100. Figure 100 also shows the effects of fire damage to some tanks – such fire damage effectively masked the true level of pressure damage in a number of locations, making it difficult to say whether they were affected by high pressures or not.

Figure 99: Low level of pressure damage to pipes and steel box

Figure 100: Low level of pressure damage to weather cover sheets (left hand side) and small bore pipe work (right hand side).

Important exceptions to the generally low or moderate level of pressure damage in the area indicated in Figure 98 were associated with the local effects of explosions in drains. The courses of the main enclosed drains that suffered internal explosions are shown in Figure 101. Water was pumped from the East end of "D" Street back to the lagoon whereas from the West end it ran directly. These two drains were apparently not connected along "D"Street (Figure 102). On the other hand, the drains at the West end of "D" Street do appear to have a connection to those running N-S along the W edge of the tank farm. This is significant in determining the timings of explosions in various drains.
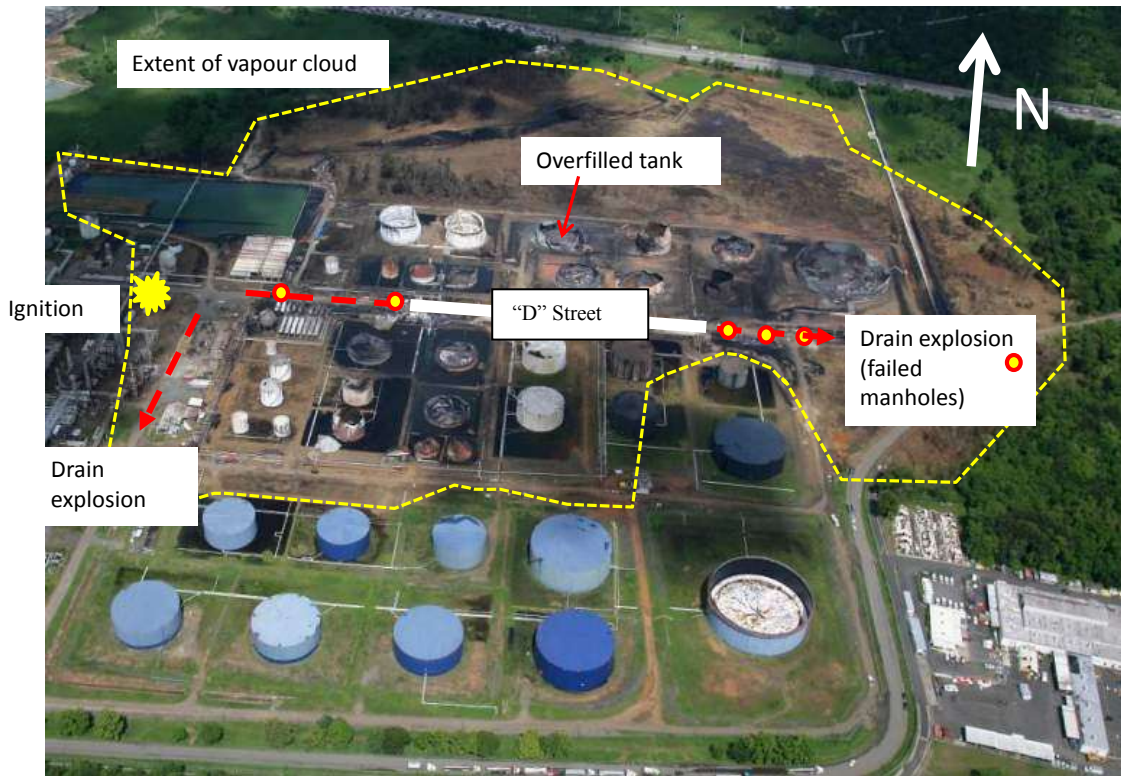
Figure 101: Location of main drain explosions
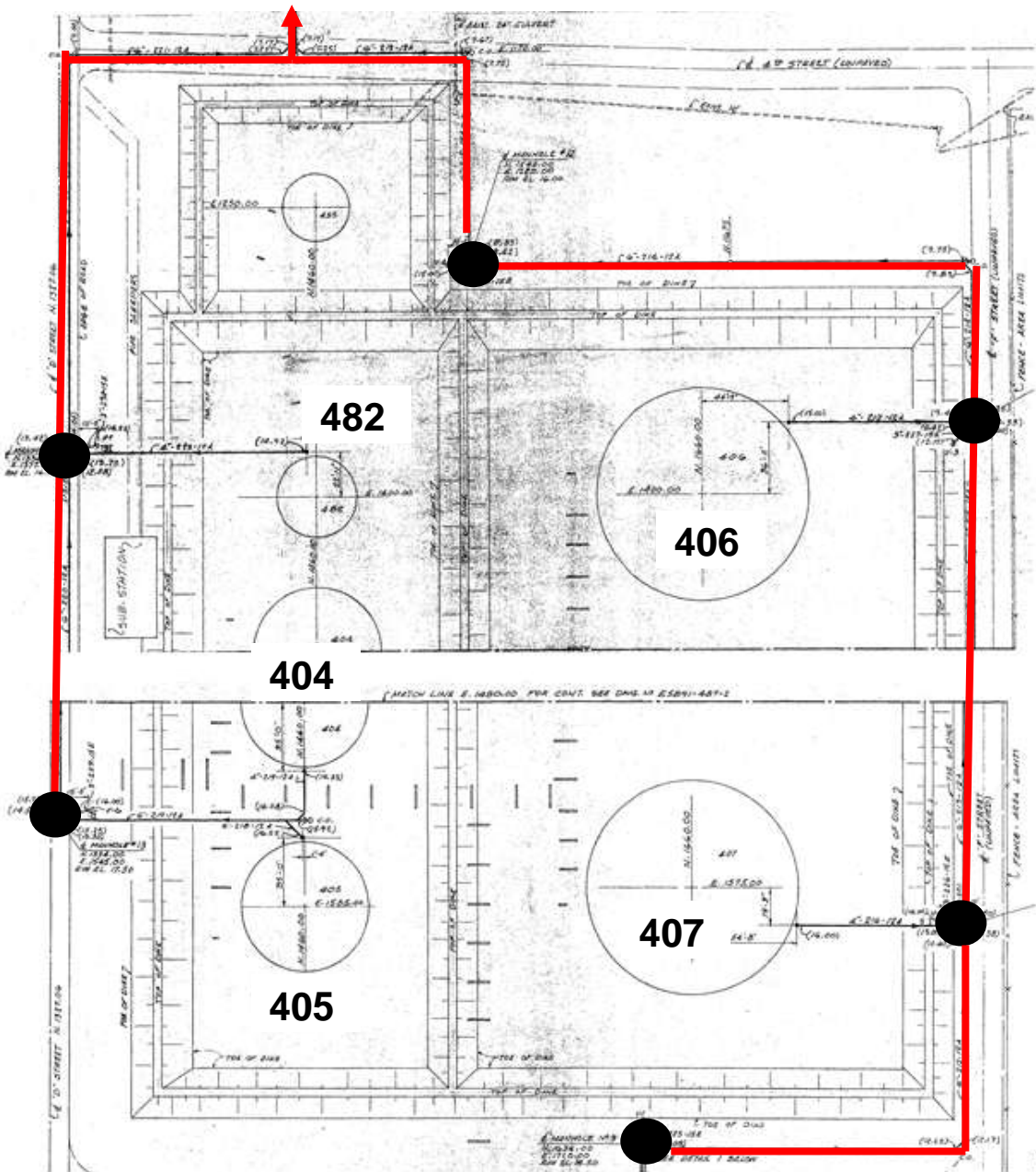
Figure 102: Drain system at the West end of "D"Street. Manholes marked as black circles.

The damage caused by the drain explosion running N-S is shown in Figure 103. This explosion occurred about 4 seconds after ignition and was clearly recorded on CCTV.

Figure 103: Track of N-S explosion in a drain

The explosion in the drains in the W end of "D" Street (Figure 102) did not break through the ground surface but displaced manhole covers. A displaced manhole cover half way along "D" Street is shown in Figure 104. At some (probably later) stage, separate drains at the E end of "D"Street also suffered an internal explosion. A displaced drain access slab near the East end of "D" Street is shown in Figure 105.

It is not known for sure when the explosion in the drains (shown in Figure 102) at the W end of "D" Street occurred. Probably it was at the same time as the N-S explosion. Pressurised flow out of the W-E drains (through the manholes) generated plumes of (non-burning) debris extending more than a hundred feet into the air. Several of these debris plumes became visible on CCTV when light levels increased after transition to a severe explosion (8 seconds after ignition). There was no apparent change in the shape of the plumes as light levels increased which suggests the drain explosion had occurred several seconds earlier. This is consistent with the idea that explosion propagated simultaneously through both of the drain systems in the W part of the site (Figure 101).

Figure 104: Displaced drain cover half way down "D" Street

Figure 105: Displaced drain slab at the East end of "D" Street.

5.5.2.3   Main on–site area affected by a severe explosion

The main area on the site showing signs of high overpressures is shown in Figure 106 (red line). The number of pressure indicators in the bunds is small and the level of burn damage is generally high so the progress of a severe explosion in many of the bunds is not proved.
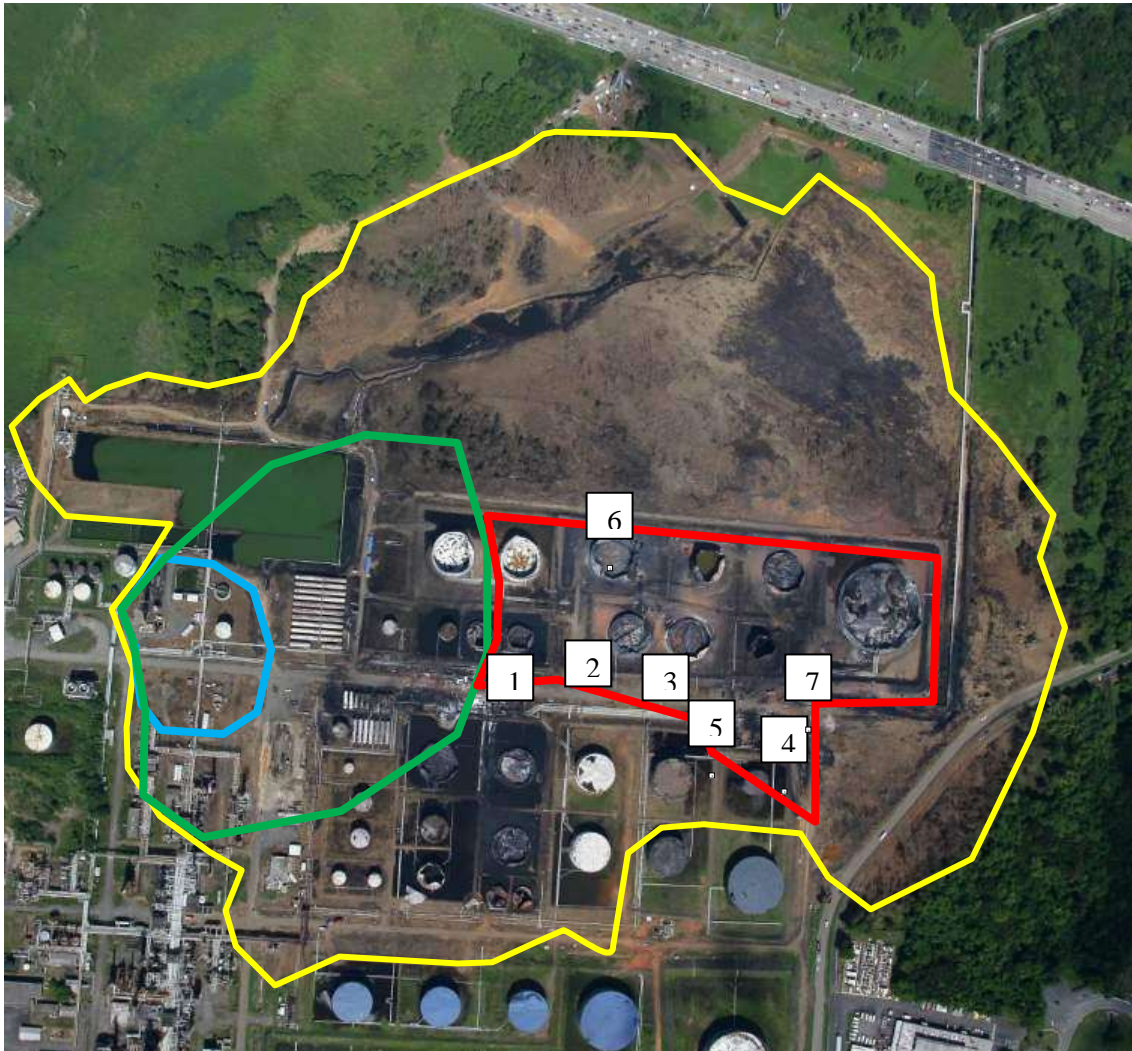
Figure 106: Main on-site area affected by a severe explosion (red line). Approximate locations of seven pressure indicators are shown

The pressure indicators numbered 1 to 7 are shown in Figure 107 to Figure 113.

Figure 107: Depressed steel cover indicating moderate to high overpressures (marked as No. 1 in Figure 106)

This location is very close to the area where there was transition to a severe explosion. It is possible that the pipework visible here was directly involved in the phase of the explosion leading to transition.
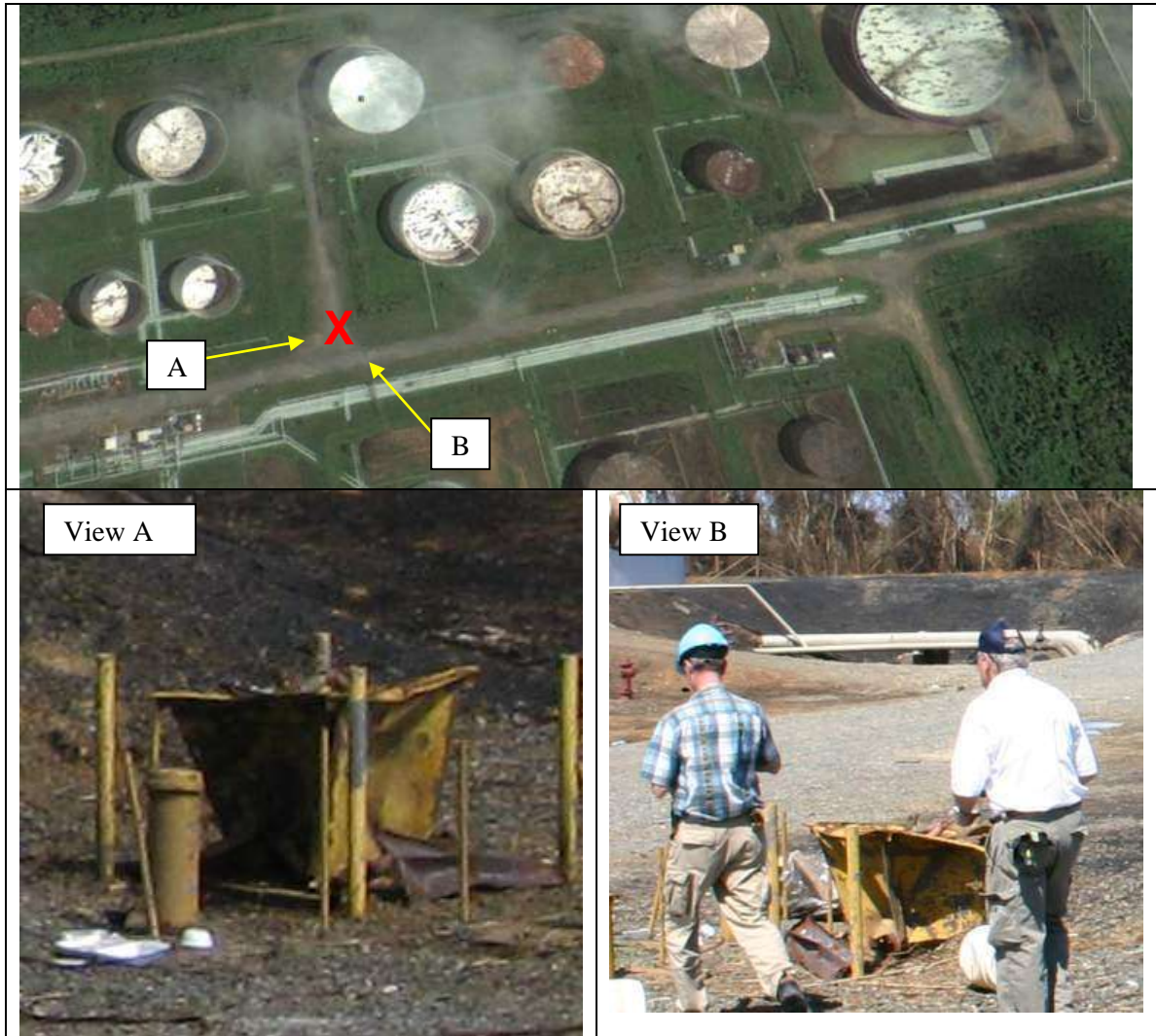
Figure 108: Crushed steel box indicating moderate to high overpressures (marked as No. 2 in Figure 106).

Figure 109: Crushed steel box indicating moderate to high overpressures (marked as No. 3 in Figure 106)

Figure 110: Crushed exhaust indicating moderate to high overpressures (marked as No. 4 in Figure 106)

Figure 111: Displaced pipe supports indicating moderate to high overpressures (marked as No. 5 in Figure 106)

Figure 112: Tree fall and tank damage indicating high overpressures to the north of the overfilled tank (marked as No. 6 in Figure 106)

There was a severe explosion in the area immediately to the N of Tank 409 – where the cloud was at its deepest. This pattern of local drag damage reflecting sharp changes in cloud depth is similar to that near the Buncefield lagoon - shown in Figure 36.

Figure 113: Deformed handrail indicating high overpressures (marked as No. 7 in Figure 106)

5.5.2.4 Damage to the boundary fencing

Sections of fencing damaged by pressure are shown in Figure 114. Some examples of damage with the corresponding locations are shown in Figure 115 and Figure 116.

Figure 114: Sections of CAPECO Boundary fence damaged by explosion

Overall boundary fencing around the site shows signs of a fairly severe explosion. There are no examples of continuous curvature of posts or top poles that might indicate a detonation.

Typical steel posts used for this application are 50mm o.d. with wall thickness 2mm. Plastic deformation of this type of post is analysed in Section 11.6.

Figure 115: Section of boundary fence

Figure 116: Section of boundary fence

5.5.2.5   Tree damage

Figure 117 shows tree damage close to the E edge of the cloud. Tree and post fall is inwards towards the main site i.e. assuming the explosion spread from the site, the directional evidence conforms to the pattern observed at Buncefield and Jaipur where there were no sharp changes in cloud depth. The pattern of tree fall could also have been simply caused by intense local explosions in the densely congested areas on the eastern fringes of the site.

Figure 118 shows tree damage just outside the NE corner of the site. There are a few clumps of very dense vegetation (bamboo) in this area. General stripping of fine branches shows there has been a severe explosion but directional evidence is mixed.

Figure 119 shows tree damage in wider parts of the wetland N of the site. There is an area of lower damage close to the point of ignition (bottom right hand corner) that fits in with the general pattern of damage on the site - Figure 120. It appears that once a severe explosion was initiated it progressed into a large proportion of the rest of the cloud – irrespective of the ground cover.

Although there is widespread stripping of finer branches in the area affected by the severe explosion, the proportion of felled trees in Figure 119 is fairly low away from the vicinity of Tank 409 – presumably this reflects the lower cloud depth and reduced drag impulse.

Figure 117: Directional tree and post fall near the E edge of the site

Figure 118: Tree damage close to the NE corner of the site

Figure 119: Tree damage in the wetlands to the N of the site – evidence of high pressure damage in burned area, except in the area in the bottom right corner

Figure 120: Approximate area apparently affected by low pressure (green) and high pressure (red). The remainder is not known or mixed.

Note some objects in the green area were affected by blasts from adjacent areas or by local effects such as explosions in drains.

5.5.3   CCTV evidence

5.5.3.1   *Camera locations and views*

Two cameras provided very useful information about progress of the flame during the explosion. The locations and fields of view are shown in Figure 121. The frame rate in the copy of the video made available by the FBI was 50 Hz. A video superimposing the explosion on a daytime view was also made available.

Camera 1 is fixed and the explosion images can be overlaid on those taken during the day (when the site layout is obvious) to obtain information about the location of events during the

explosion. Camera 2 pans significantly during the course of the explosion. Fortunately there are a number of fixed features in the explosion images that can be used to provide an accurate angular scale. This is illustrated in Figure 122 and Figure 123.
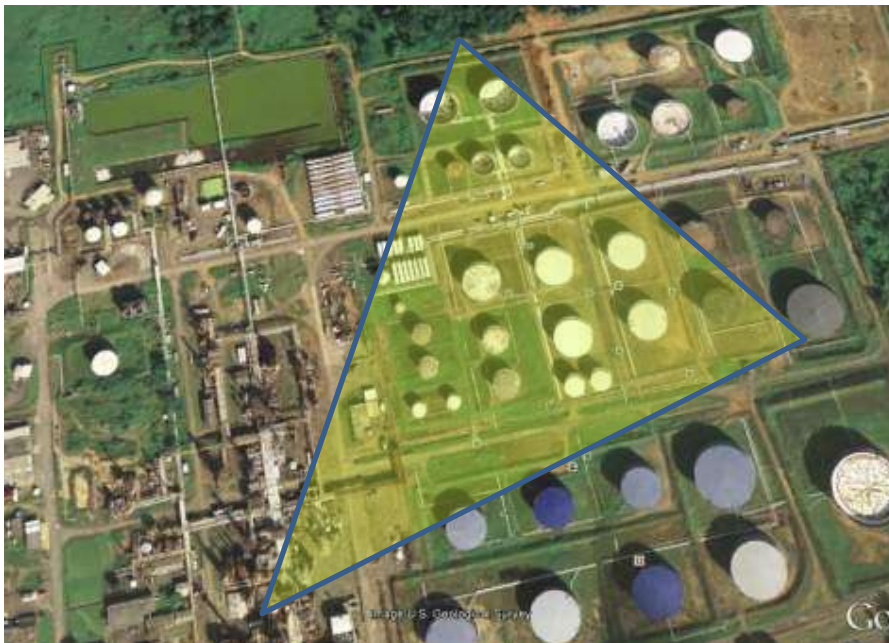
Camera 1: On flare stack
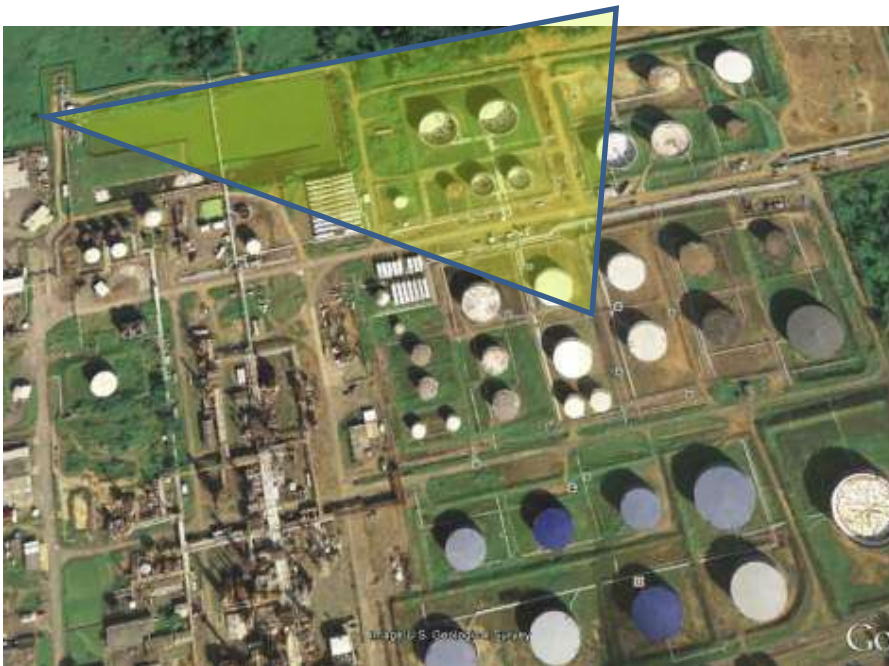
Camera 2: West end of lagoon

Figure 121: Location and approximate field of view of CCTV cameras
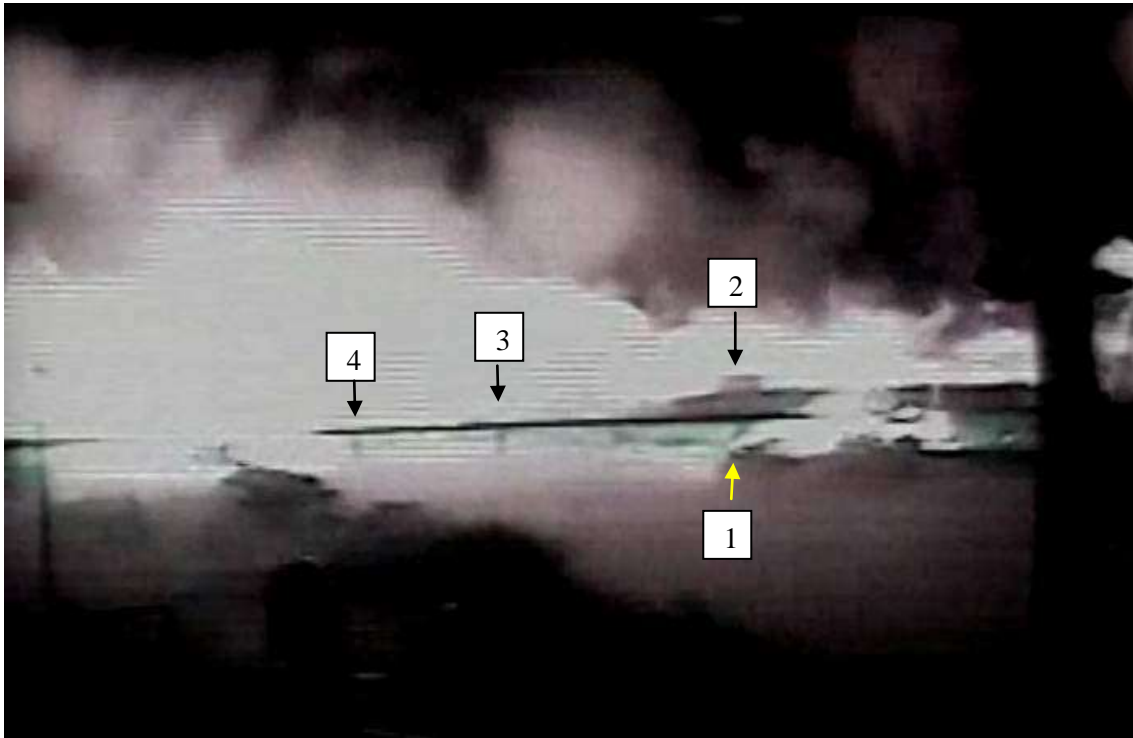
Figure 122: Examples of features used to locate video view

Figure 123: Corresponding features on satellite image

5.5.3.2   *Explosion Time line*

Table 17 shows a basic timeline for the events shown on the CCTV records. Detailed CCTV evidence about each of these stages is then presented. Interpretation of this kind of information requires great care: it is not always clear whether a given bright area corresponds to a flame or scattering of light from a separate source. Light can be scattered from solid objects, from debris plumes and from clouds of condensed water droplets. Water droplets can be created by evaporative cooling or by rarefaction during the passage of pressure waves.

.

Table 17: Time line for the explosion

Time code(s)	Time after ignition (s)	Event /phase
22:59	0	Ignition
22:59 to 23:03	0 - 4	Early stages of fire spread
23:03	4	Explosion in drain system
23:03 to 23:07.8	4 – 8.8	Low speed flame spread towards the vapor source
23:07.0	8	Secondary ignition at East end of "D" Street
23:07.8	8.8	Transition – first strong shock
23:08.00	9	First highly emissive explosion
23:08 to 23:08.5	9 - 9.5	Fast flame spread through the deep cloud around Tank 409
23:08.5 – 23:13	9.5 - 14	Continued flame spread to the East and North
23:11 – 23:13	12- 14	Developing smoke plume visible
23:15 (approx.)	16	End of explosion

5.5.3.3 *Ignition and early stages of flame spread*

The cameras do not yield much other than the timing of the ignition. The images are typically blurred and over-exposed as the cameras struggle to adjust their focus and aperture.

5.5.3.4 *Explosion in the drain system*

A typical image showing the extension of flame along the line of the N-S drain (Figure 103) is shown in Figure 124.

Figure 124: Drain explosion (Camera 1)

5.5.3.5 Low speed flame spread towards the vapor source

Images showing relatively slow flame spread through the cloud towards the deeper areas of the cloud are shown in **Figure 125.**
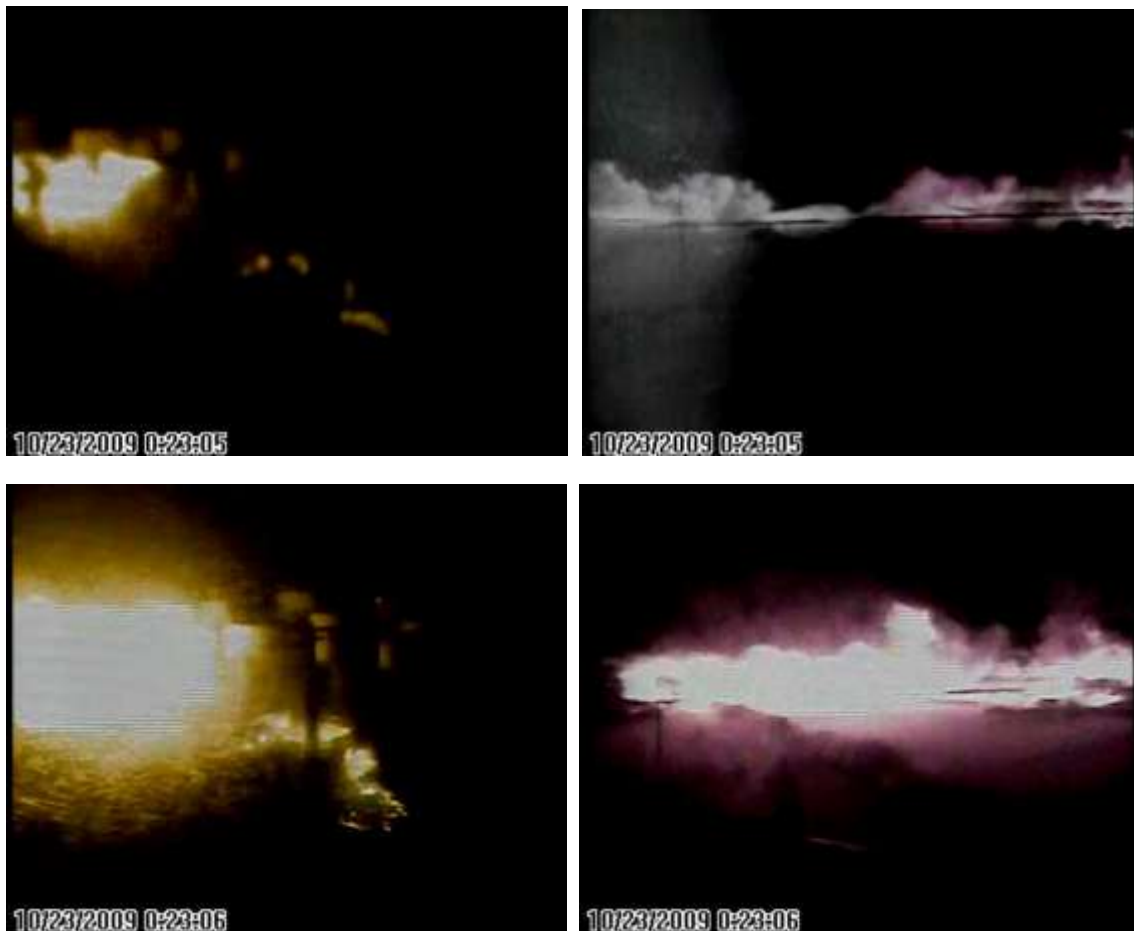
Camera 1	**Camera 2**

Figure 125: Slow flame spread prior to transition

At 23:07.00 a secondary ignition occurs near the East end of "D" Street. The location of this point of ignition can be determined by overlaying the daytime image and using a satellite shot (Figure 127 and Figure 128). The best fit is an electrical equipment station on the north side of D" Street – close to Tank 605. Some views of this area are shown in Figure 129.
.

Camera1

Figure 126: Secondary ignition towards the East end of "D" Street.

Figure 127: Location of ignition near the East end of "D" Street

Figure 128: Corresponding satellite image

Figure 129: Two views of the potential secondary ignition site near Tank 605

Above March 2012, Below October 2009

5.5.3.6   Transition – the first strong shock from the open explosion

At time 23:07.8 there is a rapid change in the image recorded by both cameras (between consecutive frames). There is a large established pool fire in the foreground in Camera 2 so the light from the intensified explosion is less obvious. In the case of Camera 1 there is more scattered light from the real targets near ground level – including debris plumes and the water droplets in the vapor cloud. There is also some flaring of the image around bright spots – because of dirt on the lens.
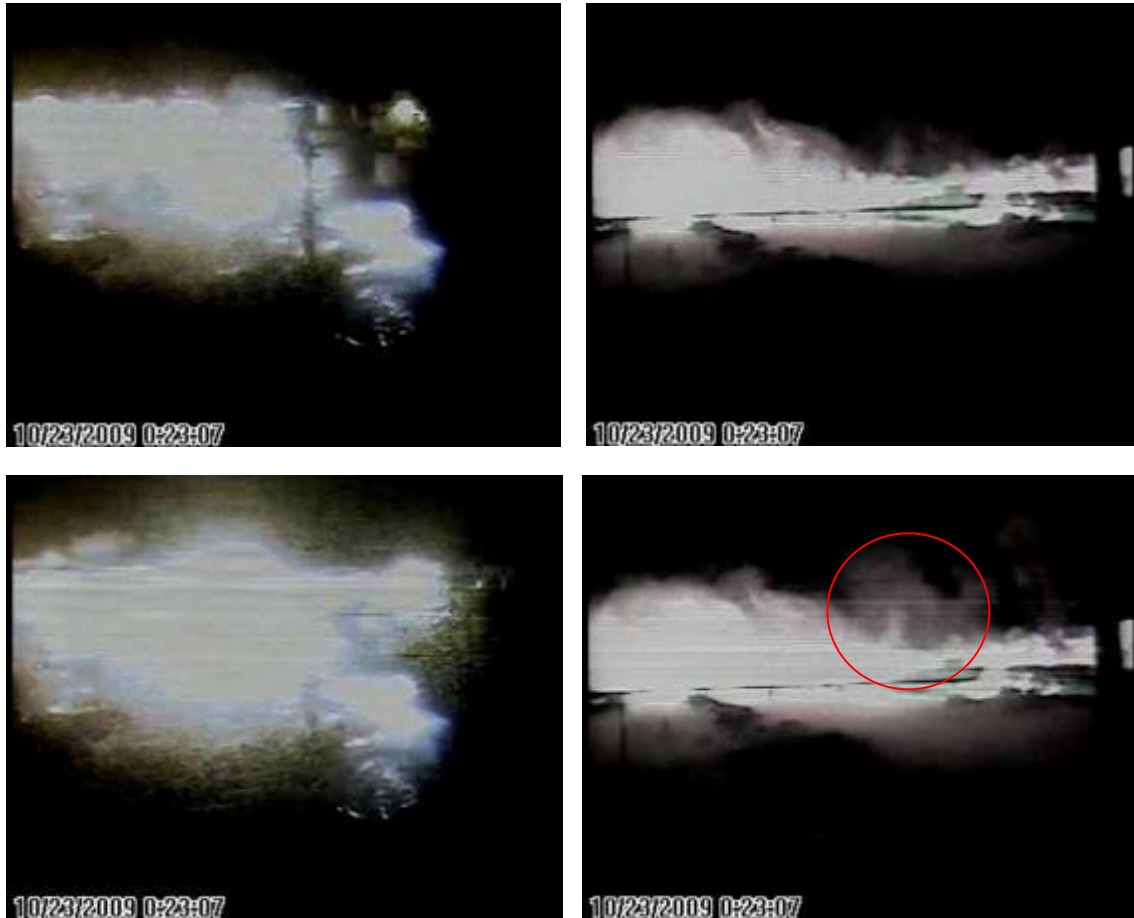
Camera 1   Camera 2

Figure 130: Transition – first violent explosion in the open cloud. Consecutive frames before and after the event shown

Fixed points in the Camera 2 view allow the direction of the point of transition to be determined (Figure 131). It is not possible identify the direction of the point of transition in the corresponding Camera 1 view so the location along the indicated direction is not proved. Support for the suggested point of transition comes from two sources:

1. The next (highly emissive) phase of the explosion – 200ms later - can be identified on both cameras and the location fixed by triangulation – see next section. One would expect the point of transition to be quite close.

Page | 159

2. The Camera 1 view cuts out 56 frames after transition. This corresponds to a time of 1.12 seconds during which a shock would travel 392 m (at 350 m/s). The distance from the point of transition indicated in Figure 131 to Camera 1 is around 395m. If the first powerful open explosion occurred at the location shown in Figure 131 then the resulting shock waves would have arrived at Camera 1 at the time when recording of images stopped.

Figure 131: Line defining possible locations for transition. Most likely location indicated as the intersection of yellow and red dashed line.

Figure 132 shows the CCTV images after transition. The debris plumes left over from explosions in drains are illuminated by an increasing amount of light. These features become more distinct later on and the identification is based on location, shape and time-stability.

Camera 1   Camera 2

Figure 132: Debris plumes - after transition

5.5.3.7 First highly emissive event

At time 23:08 there is a further rapid change in the amount of light. This coincides with the appearance of a new bright area; which in this case is visible in both Camera images (Figure 133). The location of this bright area can be found by triangulation (Figure 134 and Figure 135).

There is another rapid extension of the bright areas in the image (a similar thing occurred at transition). It is crucially important to determine whether these extensions indicate the (ultra-rapid) propagation of flames or whether they simply correspond to additional light from the (new) events. In both cases the timings of the events and extension of bright area coincide.
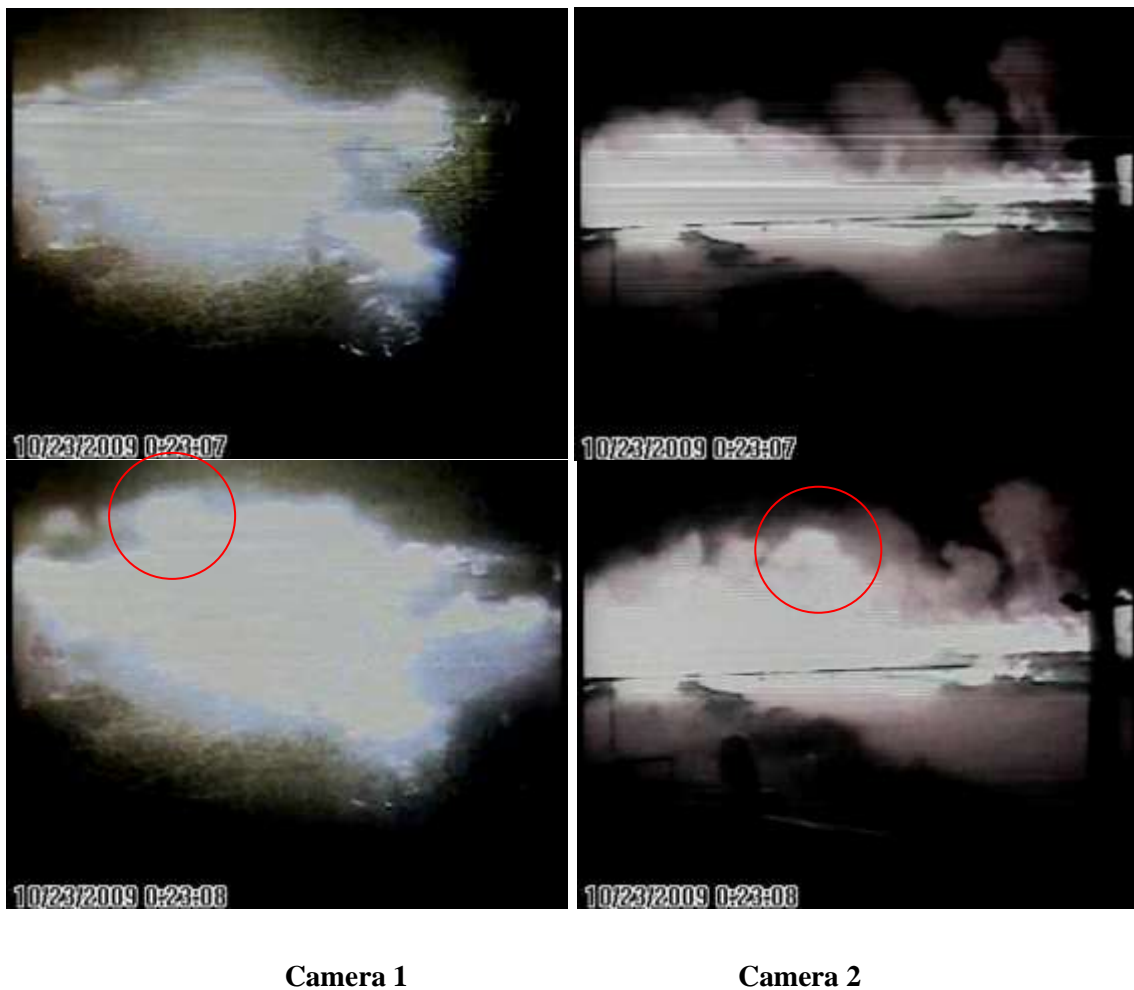
Camera 1   **Camera 2**

Figure 133: First highly emissive event – as time code changes to 23:08

Figure 134: Camera 1 view of first highly emissive event (day time image shown above)

Figure 135: Triangulation for the first emissive event – transition marked with red dot

The locations where additional light (scattered by the cloud) is observed closely correspond to the areas that would be illuminated by an elevated emissive event in the location identified by triangulation i.e. to the W of Tanks 402/403 and between Tanks 403 and 502 (Figure 136).
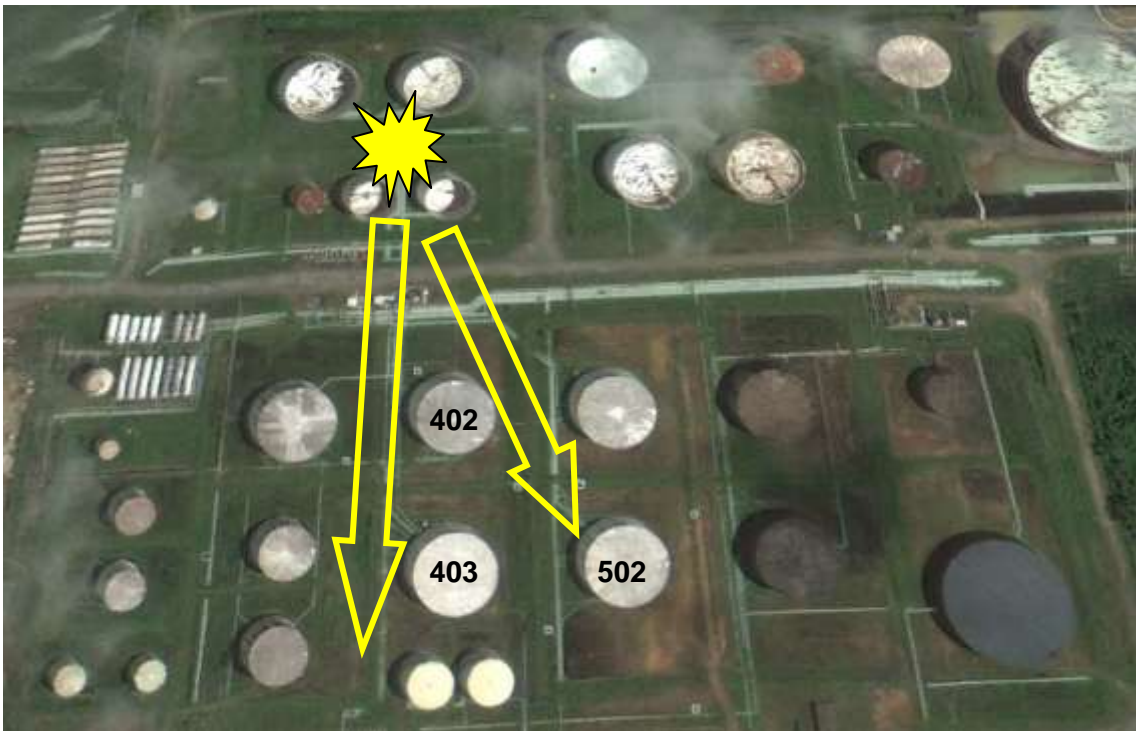
Figure 136: Areas of the cloud that were lit by the first emissive event (compare with Figure 134 - lower image)

Probably the most emissive part of the flame at transition would have been associated with the pipe rack near the S edge of the Tank 405/404 bund and would consequently be relatively low down in the bund. Light could still reach eastward to illuminate the deep vapor current flowing out of bunds into "D" Street but would be substantially blocked by the 405 bund wall from shining down into the 402 bund to the South (See Figure 130 lower image).

5.5.3.8   Further episodes of combustion in the deep area of the cloud

For 700ms after transition a succession of bright areas appear over the area covered by the deep cloud around the overfilled Tank (Tank 409). An example (600 ms after transition) is shown in Figure 137. This event is in the direction of the area just to the north of Tank 409 which was the centre of violent explosion that caused the tank and tree damage illustrated in Figure 112. No other location in this direction would have a deep enough cloud to cause such a large explosion.

Figure 137: Explosion in the deep part of the cloud to the north of Tank 409

There is a third CCTV view from the Security Cabin near the site entrance that shows that the window breaks at this building at 0:23:09.9.

Flame first spreads to the deepest part of the cloud close to Tank 409 at about 0:23:08.15 and the distance between this area and the Security Cabin is around 610m (see Figure 138). The breakage of the window is consistent with the arrival of the shock from explosion in this area of the cloud since the apparent velocity of the pressure wave is around 350 m/s.

Time delay = 1.75 seconds

Distance = 610 m

Velocity of pressure wave = 610 / 1.75 = 349 m/s

Figure 138: Location of security cabin and distance to the edge of the deepest area of cloud

Weak pressure waves start to arrive at this cabin from the violent explosions at and after transition somewhat earlier than would be expected for transmission through air. In fact pressure waves can propagate at low level (with low efficiency) more rapidly through the hot combustion productss that cover about half the distance from the point of transition to the guard house. The early pressure effects are explicable on this basis.

5.5.3.9   Continued spread of the main flame

As the flame progressed to the E and N of Tank 409 the cloud depth would have declined rapidly, as the flame moved beyond the deep area around the overfilled tank. Camera 1 cut out (probably because of the arrival of shockwaves from the post-transition explosion) and the progress of the main flame was obscured by the flames in the foreground of the Camera 2 view (Figure 139).

A few seconds later the Camera 2 view shows the start of development of a large smoke plume over the pool of spilled gasoline (Figure 140). The character of the developed plume can be appreciated from the daytime view shown in Figure 89. The pre-mixed flame is continuing at this point, behind and to the left of the pool, and illuminates the fringes of the smoke plume. By 14 seconds after ignition Camera 2 has almost panned away from the fire (Figure 141). The smoke plume has developed further and the level of scattered illumination has declined – suggesting the explosion is coming to an end. A view from another (off-site) CCTV system also suggests that the explosion lasted just over 15 seconds (duration of high intensity illumination).

Figure 139: View after flame has passed deep area around overfilled tank

The pressure signature of the later stages of the explosion would have been extremely weak as positive and negative phases of pressure waves from a large number of uncorrelated constituent small explosion episodes largely cancel. This is explained in more detail in Atkinson (2011b). The large positive pulse occurs as the explosion front expands and runs into an area where cloud depth is increasing. The main negative phase follows as the cloud depth levels off or declines.

Figure 140: Smoke plume developing on left hand side. Hydrocarbon jet fire on the right hand side

Figure 141: Final images of the explosion

The arrival of the vapor flame at the W end of the lagoon (near to Camera 2) is also visible in the bottom right-hand corner of Figure 141 (red circle).

5.5.3.10   Progress of the secondary ignition

Transition of the main explosion to a severe event occurred 800 ms after the secondary ignition. At this stage the secondary explosion was still confined to the area around ignition and had not progressed far to the E or S (Figure 130).

However by 1600 ms after secondary ignition the secondary explosion had crossed the road into the congested area at the East end of "D"Street (Figure 142) and probably caused an explosion in the drains near the E end of "D" Street . The explosion itself was hidden behind tanks but it was illuminating the debris plumes left by the drain explosions.

It is not clear whether this secondary explosion or the main explosion front was responsible for spread into the densely wooded areas on the Eastern fringes of the cloud. This probably took another 3 or 4 seconds by which time Camera 1(which would have had a view) had cut out.

The damage recorded in and around these trees (Figure 117 and Figure 118) suggests that high levels of congestion caused severe local explosions in these final stages.

10/23/2009 0:23:07

1600ms after secondary ignition

10/23/2009 0:23:08

Figure 142: Locations secondary ignition (top) and illuminated debris plume(s) at the East end of "D" Street (centre). Day view (below)
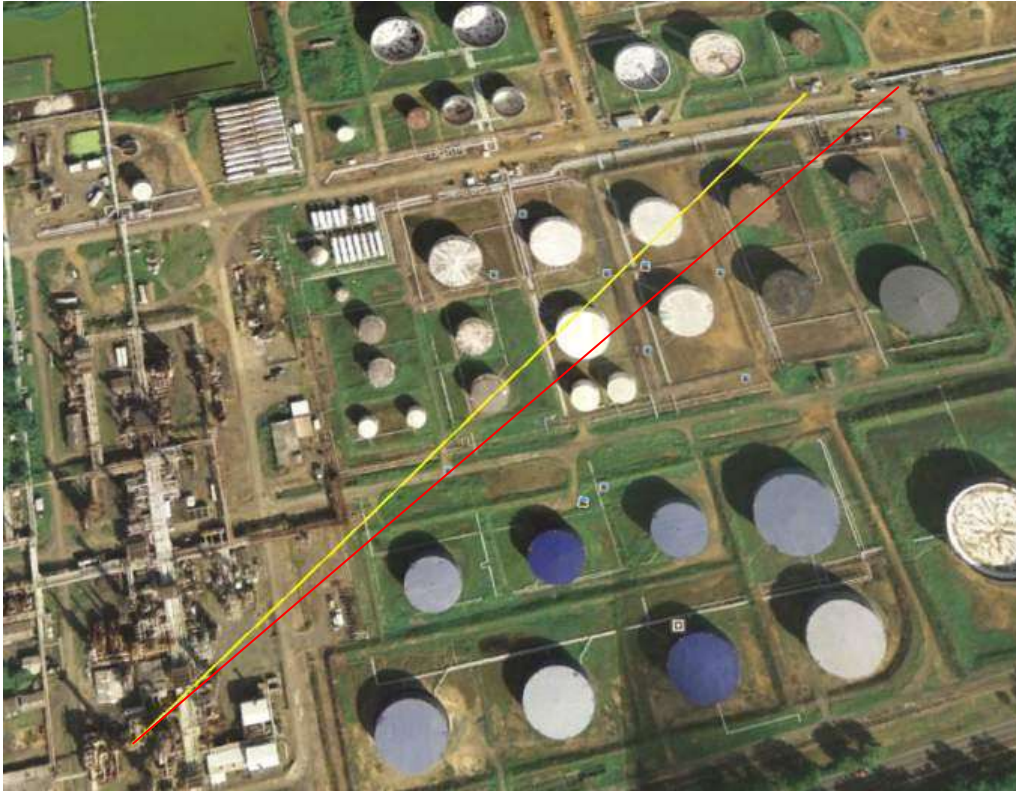
Figure 143: Satellite view showing directions indicated in Figure 142

5.5.4　　What caused transition to a severe explosion at San Juan?

The area indicated by CCTV for transition is shown in Figure 145 as a yellow circle. There was a set of pumps and associated pipework in the approach to the transition area. It is likely that significant overpressures were developed in this area and this is supported by explosion damage indicators (Figure 107). There is also pipework within the bund (Figure 145) that would have further added to the risk of transition.

Figure 144: Area where transition to a severe explosion occurred (yellow circle). Arrow indicates direction of explosion approach.

Figure 145: Close up of pipework in the area in which transition occurred

The locations of the points of transition and the first emissive explosion event are shown in Figure 146.
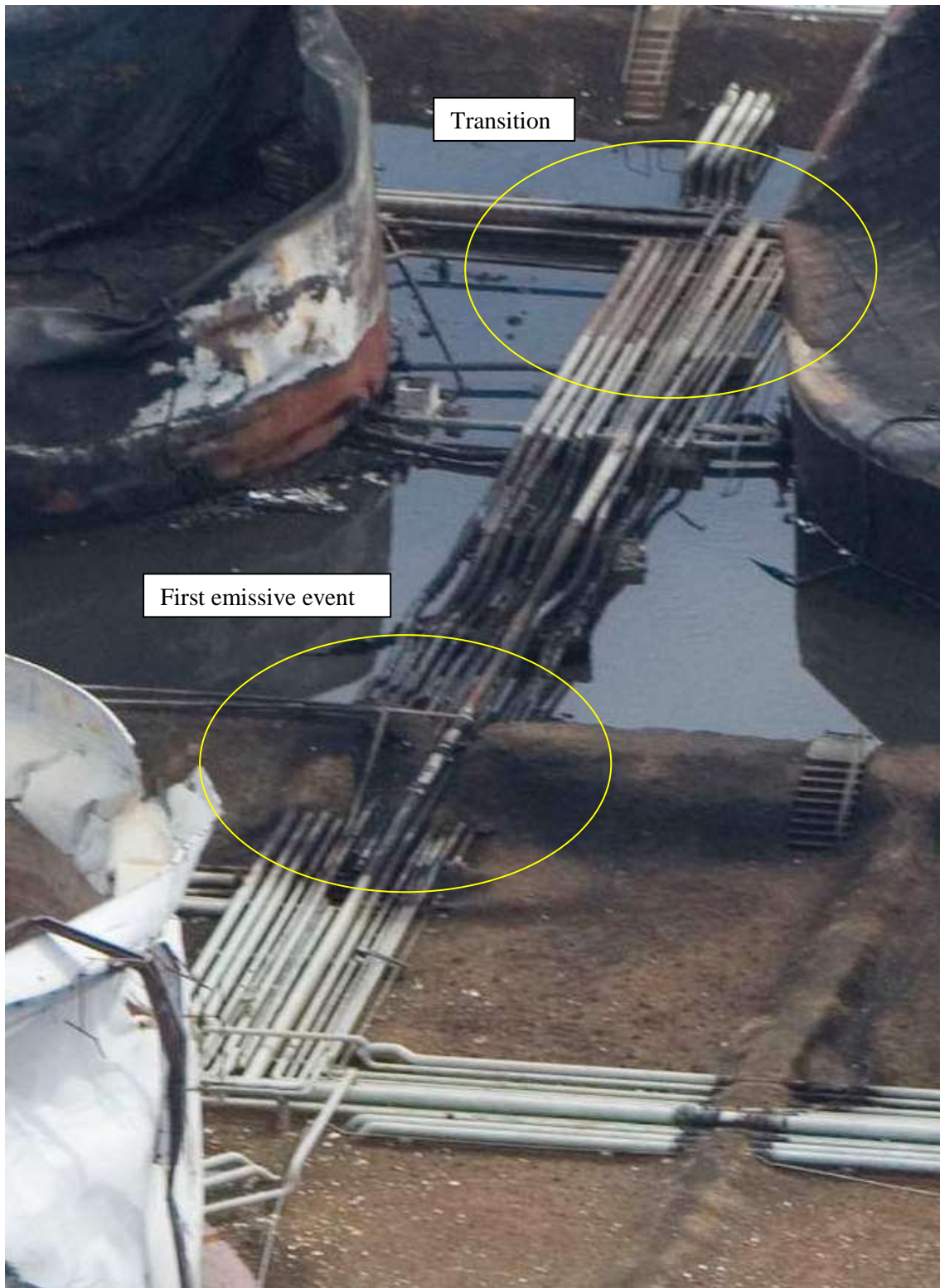
Figure 146: Locations of transition and first highly emissive explosion

It is possible that the blast that occurred at transition displaced fine material from the top of the earth bank that then mixed with the surrounding vapor. Thermal radiation would then have been able to act strongly on the unburned gas ahead of the flame. Pre-warming greatly increases the reactivity of gas when the flame arrives: for example pre-warming by 230°C increases the reactivity of propane- air to that of acetylene–air (Section 10). After a delay the volume of pre-warmed gas could have been consumed in a violent localised explosion. This would be a highly emissive event because of the speed of combustion and presence of particles.

The potential for a self-sustaining sequence of explosions of this sort is discussed in Section 10. This would explain the series of discrete explosion events visible in the Camera 2 record – as well as the relatively slow average rate of propagation. It would also explain how violent explosion episodes were sustained in uncongested areas – for example the area just to the N of Tank 409.

This kind of effect may also have been important in triggering transition in the first place – the congested area around a pump set is also separated from the transition area by an earth bank (Figure 144).

5.5.5   Alternative interpretations as DDT

The progress of an episodic explosion has been described previously (Atkinson 2011b) but it remains a controversial idea. There seems little doubt that high overpressures were sustained in open areas at San Juan and the conventional view is that this is only possible in a detonation. Notwithstanding the fact that pressure damage does not appear to correspond to a detonation, it is important to consider whether the CCTV evidence could be consistent with deflagration to detonation transition (DDT) and then propagation of a detonation around the site.

DDT would have had to occur at the edge of the main flame or the secondary ignition. There is no sign of rapid extension of the secondary flame to the E and S before or after transition so this seems unlikely. Consequently, if DDT occurred, it must have been in the same place as the transition area identified above.

The timing of DDT is another variable. Various options can be examined to see if they fit the data.

Option 1: DDT at the time of first rapid event (Figure 130)

This is the natural assumption. The extension of a bright area away from the transition area for around 200m along "D" Street occurs within one frame on Camera 1. This corresponds to a velocity well in excess of detonation velocities, so the observed extension of light must simply be light from the DDT - rather than a flame. This is a similar conclusion to the analysis above.

The next available frames (Figure 133) around 200 ms later show light around Tank 403 and a highly emissive area near Tank 407. As noted above the light could simply be a reflected light or it could be a detonation flame that has propagated about 180 m along a narrow track to the South. By this stage one would expect the detonation to have also propagated along most the length of "D" Street and to areas around and beyond the overfilled Tank 409.

Very few frames are dropped in the next 500 ms of images from Camera 2. The succession of visible events over the area covered by the deepest parts of the cloud is difficult to explain as a

detonation. In particular the shock wave visible 600 ms after transition (Figure 137) must correspond to the large explosion that occurred just to the N of Tank 409.

The average rate of propagation of the flame from the point of transition to this area is sub-sonic (as expected in an episodic explosion). If the explosion were a detonation there must have been be an extended delay between DDT and the detonation wave reaching Tank 409. Detonations cannot stand still so either the explosion had to take a very circuitous route (> 7 times longer than the most direct track) or there must have been a detonation failure followed very rapidly by another DDT. The damage to tanks and trees around Tank 409 shows that the mixture around the tank did support a violent explosion so it is difficult to understand how such delays (or failure) could have occurred.

Illumination around the overfilled tank and around the debris plume(s) at the end of "D" Street is also difficult to explain if there was DDT.

Option 2: DDT at the time of first emissive event (Figure 133)

In this case the bright track along "D"Street that appears at transition must be the result of light from a rapid acceleration in the lead up to DDT. The bright track southwards must be light following DDT (not a flame). The problems with delays in detonation propagation remain but the discrepancy in velocity is reduced to a factor of around 5. Problems explaining illumination remain. As noted previously the explosion damage also does not appear consistent with a detonation.

Option 3: DDT 600m after transition - in the area around Tank 409 or the wetlands

In this case the violent explosions and damage around Tank 405 and 407 and high levels of illumination in the 600 ms period after transition in this area are very difficult to explain.

5.5.6   Conclusions about the explosion mechanism at San Juan

The San Juan CCTV records are a very rare opportunity to observe the progress of a large severe VCE. The evidence strongly points to transition close to Tank 405. There is some significant congestion in this area but not more than one might expect to find in many LNG sites and fuel depots. This suggests that a wide range of sites might be at risk of transition to a severe VCE; which is in line with the observation that there are few records of very large pre-mixed clouds that burned as flash fires rather than severe VCEs.

For LNG sites, the issue would be releases of LPG from refrigerant systems rather than release of LNG due to the relatively low burning velocity of methane.

It is true that the explosion at San Juan progressed for around 250m through some congested areas without making a transition. But it does not follow that this early phase was a meaningful example of a large cloud burning as a flash fire: the part of the cloud that burned in this way would have all have been shallow, because **it did not contain the source of vapor**. Whether the source of pre-mixed vapor is a tank over-fill or some sort of spray it is almost inevitable that there will a substantial deep area around the source. For transition to occur probably requires a minimum cloud depth of around 2.5 - 3m.

Gravity driven clouds that extend for many hundreds of metres from source will generally have a central area where the cloud depth is substantial and any significant congestion and/or

confinement in this area runs a high risk of triggering transition to a severe explosion that will propagate into uncongested areas.

The incident suggests that there is value in keeping plant elements that may introduce congestion (like fire pumps and large intersecting pipe racks) well away from potential sources of vapor.

The evidence is also consistent with the progress of an episodic deflagration across large parts of the site. The average flame speed was subsonic – especially in the shallower parts of the cloud away from the source – but there were periods of rapid flame spread producing a sequence of violent explosions.

There were highly congested areas on the eastern fringes of the cloud. It is not clear whether the high overpressures developed here were the result of a continuing episodic explosion or a fast quasi-steady deflagration. Judging by the damage to fencing around the adjacent military facility it seems unlikely that there was DDT and an extended detonation in these areas.

5.6   BRENHAM, TEXAS

Time and date:	07:00 7th April 1992
Location	Brenham, Texas, USA
Company	MAPCO Natural Gas Liquids, Inc
Narrative :	Highly volatile hydrocarbons (LPG) escaped from an underground storage cavern when it was overfilled. There was no wind and an extensive vapor cloud accumulated, tracking down shallow valleys around the source. A severe vapor cloud explosion occurred damaging builldings over an area of about three square miles. There were three fatalities – all members of the public.
Incident Cause	The capacity of the storage cavern was not known accurately. The operators had also lost track of the net amount that had been pumped in, because the system of balancing receipts and deliveries was defective. The well-head safety system was inoperative because of brine sensing lines had been isolated. This system was not fail safe.
Category Categorize incident cause (e.g. operator error, equipment malfunction, material failure, construction error, design error, weld failure)	Design error Operator error

Source Term	Type of release (e.g. gas, evaporating liquid or a gas-liquid (two phase) flow)	Description of equipment/pi ping	Hole size or pipe diameter if it was a guillotine failure	Substance(s) released	Release pressure and temperature
	2 phase gas/liquid flow – gas exited via a brine pond	Storage cavern and associated well-head pipework	Not known NTSB estimated release rate from cloud size (burned area) 3000-10,000 barrels (400-1360 m3)	LPG	Not known accurately. Witness reported fountain of liquid reached height of 50ft

Release	Quantity released	Migration of substance from release source	Duration of release

	3000-10,000 barrels (400-1360 m3)	Gravity driven		Approx 60 minutes	
Cloud development	Cloud footprint	Depth and influence of topography under and near the vapor cloud.	Surface roughness	Substance which formed a vapor cloud	Near field dispersion
	Approx 625,000 m^2 (150 acres)	Vapor accumulated in shallow valleys	Rural – some wood land	LPG	Vertical jet 2 phase LPG issuing up through a brine pond
Weather conditions	Atmospheric stability		Temperature	Wind speed	
	Stable		About 12˚C (52 F)	See data below Figure 149	
Ignition	Ignition strength		Source of ignition	Ignition location	
	Not known		Not known	Not known	
Explosion severity	Overpressure		Distance of flame travel	Flame speed	
	3.5 – 4 on the Richter scale		Approx. 1000m	Not known directly. Overpressure indicates detonation, fast deflagration (FD) or episodic deflagration (ED).	
Consequences	Fatalities, injuries, health effects, property damage within and outside of the plant property. Heavy damage – structural collapse Moderate damage- cladding loss, cracking of vulnerable masonry, purlin deformation Light damage - cladding damage, window breakage,			Blast damage to plant and other structures within and outside of cloud footprint.	
	See Figure 147 Houses destroyed to within about 1000m (3300ft) of the cloud edge. Houses damaged to within about 2000m (6600ft) of the cloud edge.			Plant badly damaged by fire	

| Mitigating Measures	Cloud mitigation measures	Performance and/or reasons for poor performance		
	Vapor barrier surrounding site	Not installed		
	On-site vapor fencing	Not installed		
	Active vapor dispersal	Not installed		
	Vapor detection	Installed but response involved an operative travelling to the site to investigate.		
Facility Information	Other Hydrocarbons at Facility	Quantity stored (is amount >10,000 lbs?)	Type of storage vessel/container	End product or used for a process
	No	300,000 barrels (approx. 40,000 m^3)	Cavern	End product
	Characteristics of the area where the event occurred	Urban, rural, suburban	Industrial, residential	Proximity to ports/marine
	Rolling hills	Rural	Scattered residential	Inland
	Facility description	Category (refinery, petrochemical, gas processing, upstream)	Number of similar facilities worldwide	
	Storage (cavern)	Terminal and distribution		
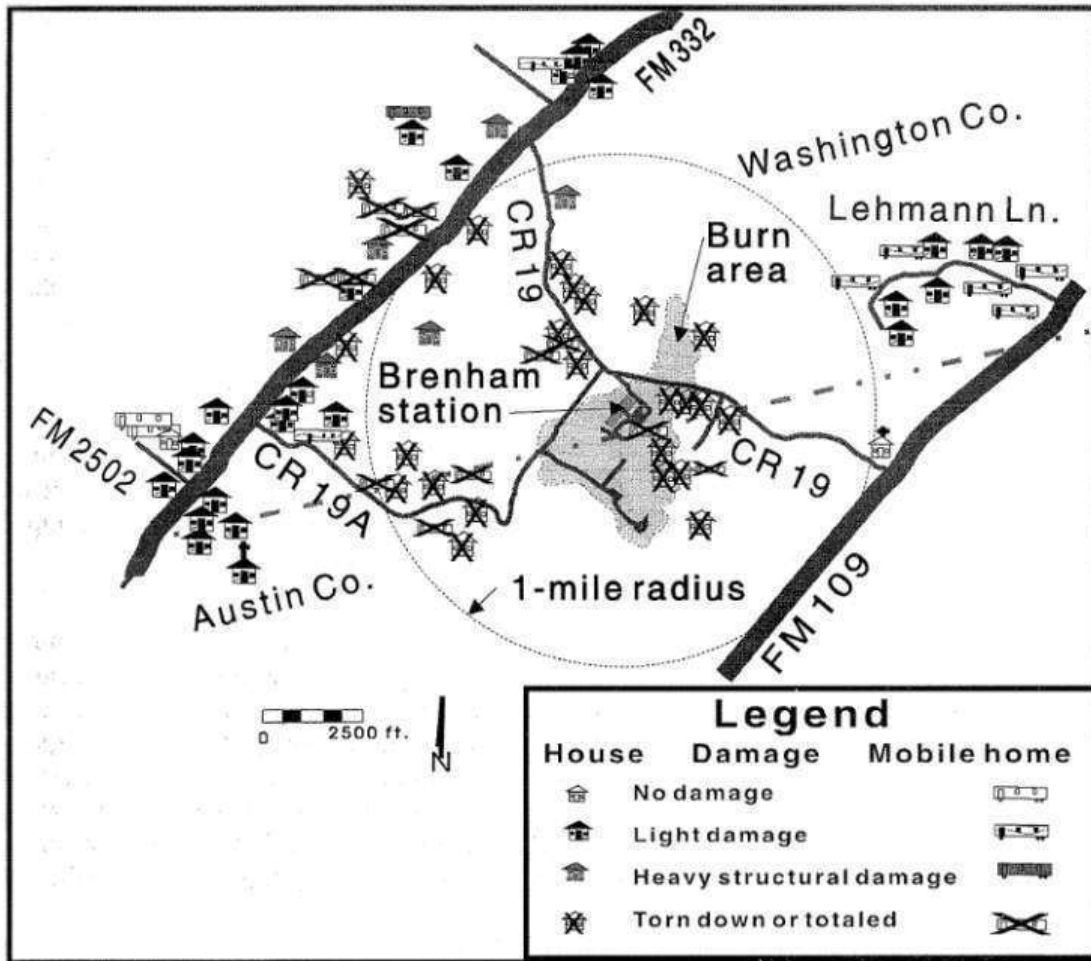
Figure 147: Building damage around the site

Figure 148: Approximate area covered by cloud (Area shown 625,000 m^2)
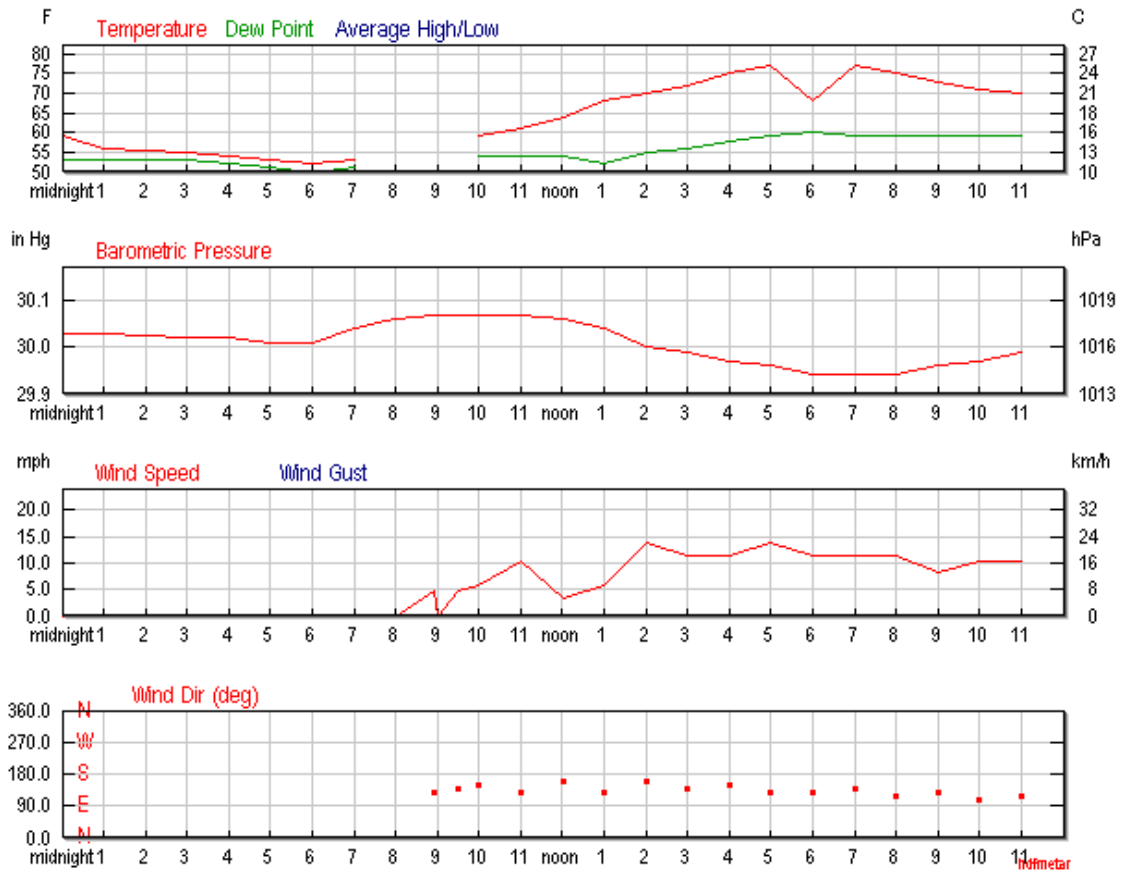
Figure 149: Weather conditions (explosion around 7:00 am)

5.7 UFA

Time and date:	01:14 am 4th June 1989
Location	Near Ufa (Ural mountains)
Company	Trans-Siberian pipeline
Narrative :	The pipeline was 1852 km long carrying pressure liquefied petroleum products from Siberian for processing in European Russia. Pipeline diameter was 700 mm and it was buried to a depth of 1.2- 1.5m. The design flow rate was 116-120 kg/s and the working pressure was 38 bar. The pipe suffered complete rupture which would have resulted in initial discharge from both ends. When pipeline operators detected a drop in pressure they increased the pumping rate to attempt to sustain the flow. The release was apparently sustained for at least 3 hours. A very large vapor cloud accumulated. The release was smelled in villages up to 7km away prior to the explosion. The ignition occurred as two trains passed each other within the cloud. 1224 people on the trains were killed or severely injured. The blast affected area extended to an area of around 2.5 km^2.
Incident Cause	The causes of the rupture were not determined. There could have been an installation fault that made the pipe susceptible to progressive damage by thermal cycling and hydraulic shocks. The same pipeline had apparently failed 4 months previously in another location – causing another powerful explosion but no casualties.
Category Categorize incident cause (e.g. operator error, equipment malfunction, material failure, construction error, design error, weld failure)	Material failure

Source Term	Type of release (e.g. gas, evaporating liquid or a gas-liquid (two phase) flow)	Description of equipment/piping	Hole size or pipe diameter if it was a guillotine failure	Substance(s) released	Release pressure and temperature
	Two phase flow	700mm diameter pipeline	Complete rupture	Propane 41% n-butane 25.6 % iso-butane 16% + other light hydrocarbons	Pipeline working pressure 38 bar

Release	Quantity released	Migration of substance from release source	Duration of release	

	Not known directly. Back calculations from blast and fireball characteristics suggest 2,000-10,000 tonnes (Makhviladze, and Yakush, 2005)	Flow of vapor strongly influenced by topography. But the fact that the gas was smelled at long range suggests that there was a wind blowing for at least part of the time		At least three hours	
Cloud development	Cloud footprint	Depth and influence of topography under and near the vapor cloud.	Surface roughness	Substance which formed a vapor cloud	Near field dispersion
	625 acres (2.5 km^2) (Area affected by burning and blast)	Heavy gases ran down valleys leading away from the release point	Largely Forested	LPG	Two phase jet and evaporation of rain out
Weather conditions	Atmospheric stability		Temperature	Wind speed	
	Not known		Not known	Not known	
Ignition	Ignition strength		Source of ignition	Ignition location	
	Strong		Electric train	At the point where two trains passed each other.	
Explosion severity	Overpressure		Distance of flame travel	Flame speed	
	Probably >2000mbar. Trees were knocked over. Few detailed pictures of the site are available.		Approximately 2 km	Not known directly. Overpressure indicates detonation, fast deflagration (FD) or episodic deflagration (ED).	
Consequences	Fatalities, injuries, health effects, property damage within and outside of the plant property. Heavy damage – structural collapse Moderate damage- cladding loss, cracking of vulnerable masonry, purlin deformation Light damage - cladding damage, window breakage,			Blast damage to plant and other structures within and outside of cloud footprint.	

	Heavy damage to trains within the cloud *"38 passenger cars were flattened .. as if they had been clamped in a vice"*. (Gelfand and Tsyganov)	Not in a plant. Forest flattened within the cloud.
	Windows broken in a hospital 15km from the site.	
	Approximately 500 fatalities (all on two trains)	

Mitigating Measures	Cloud mitigation measures	Performance and/or reasons for poor performance		
	Vapor barrier surrounding site	No		
	On-site vapor fencing	No		
	Active vapor dispersal	No		
Facility Information	Other Hydrocarbons at Facility	Quantity stored (is amount >10,000 lbs?)	Type of storage vessel/container	End product or used for a process
	No	N/A	Pipeline	Both
	Characteristics of the area where the event occurred	Urban, rural, suburban	Industrial, residential	Proximity to ports/marine
	Wooded hills	Rural		Inland
	Facility description	Category (refinery, petrochemical, gas processing, terminal and distribution, upstream)		Number of similar facilities worldwide
	LPG Pipeline	Distribution		

Figure 150: Part of the Ufa blast site

The sharp boundary between burned and pressure damaged forest and unaffected areas is characteristic of a low lying cloud.

5.7.1 Quantity of fuel in cloud

The estimates of 2,000 to 10,000 tonnes of fuel in the cloud given in Makhviladze and Yakush, 2005 seem too high.

If the cloud area is 2.5 km^2 (620 acres) then 2000 tonnes would correspond to a stoichiometric cloud of depth 10m and 10,000 tonnes would be a 50m deep cloud. Both seem quite high as the burned area was on a pronounced slope with a substantial overall fall.

The pattern of tree fall was similar to that at Buncefield - against the direction of flame propagation. This was explained as a consequence of the convectively driven fire wind. This is not correct. Tree fall would have been caused by the explosion: this is apparent from the fact that the edge of the burned area and the flattened area are coincident; and that the transition distance is short in both cases.

5.8 PORT HUDSON

Time and date:	10:09 pm 9th December 1970
Location	Port Hudson, Missouri
Company	Phillips
Narrative :	Just after 10.00pm on December 9th 1970 an abnormality was recorded at a LPG pipeline pumping station downstream of Port Hudson. The pipeline failed at a pressure of 942 psig. Several witnesses reported seeing a plume of white spray rising 50-80 feet into the air. Over the next 20 minutes four families evacuated their homes and moved to high ground. They observed a white cloud drifting away from the release point and settling into a valley around a group of agricultural buildings. At 10:44 there was a severe VCE but fortunately no-one was killed.
Incident Cause	Not known- probably corrosion. There had been 12 previous comparable releases on the same pipeline
Category Categorize incident cause (e.g. operator error, equipment malfunction, material failure, construction error, design error, weld failure)	Material failure

Source Term	Type of release (e.g. gas, evaporating liquid or a gas-liquid (two phase) flow)	Description of equipment/piping	Hole size or pipe diameter if it was a guillotine failure	Substance(s) released	Release pressure and temperature
	Two phase flow	LPG pipeline	Rupture	LPG	942 psi (65 bar)

Release	Quantity released	Migration of substance from release source		Duration of release
	750 barrels (102 m^3).	Light wind and gravity driven settling		24 minutes

Cloud development	Cloud footprint	Depth and influence of topography under and near the vapor cloud.	Surface roughness	Substance which formed a vapor cloud	Near field dispersion
	10 acres (40,000 m^2)	Vapor observed to settle into a shallow valley	Farmland and woods	LPG	A combination of light wind and gravitational settling

Weather conditions	Atmospheric stability		Temperature	Wind speed
	Stable		1˚C	2.5 m/s
Ignition	Ignition strength	Source of ignition		Ignition location
	Moderate/strong	Electrical equipment		Within a concrete outbuilding
Explosion severity	Overpressure	Distance of flame travel		Flame speed
	>2000 mbar (29 psi)	~500m		Witnesses report very rapid flame spread
Consequences	Fatalities, injuries, health effects, property damage within and outside of the plant property. Heavy damage – structural collapse Moderate damage- cladding loss, cracking of vulnerable masonry, purlin deformation Light damage - cladding damage, window breakage,		Blast damage to plant and other structures within and outside of cloud footprint.	
	No fatalities Buildings completely destroyed within the cloud. Trees broken and uprooted. Moderate damage to arrange of 2000 ft (600m). Analysis of insurance claims from property owners around the site suggested that the proportion of structures suffering window damage at a range of 1, 2, 3, 4 and 5 miles was (respectively) 97.3%, 75%, 57.7%, 38.4% and 30%		Not a plant	

Mitigating Measures	Cloud mitigation measures	Performance and/or reasons for poor performance		
	Vapor barrier surrounding site	No		
	On-site vapor fencing	No		
	Active vapor dispersal	No		
Facility Information	Other Hydrocarbons at Facility	Quantity stored (is amount >10,000 lbs?)	Type of storage vessel/container	End product or used for a process
	No	N/A	Pipeline	End product
	Characteristics of the area where the event occurred	Urban, rural, suburban	Industrial, residential	Proximity to ports/marine

	Woods and farmland	Rural	Agricultural. Scattered farmsteads	Inland
	Facility description	Category (refinery, petrochemical, gas processing, terminal and distribution, upstream)		Number of similar facilities worldwide
	LPG pipeline	Distribution		

Further Reading:

Burgess, D.S and Zabetakis, M.G., *Detonation of a flammable cloud following a propane pipeline break.* U.S. Bureau of Mines, Report of Investigation 7752.

5.9 NEWARK, NEW JERSEY

Time and date:	12:10 am 7th January 1983
Location	Newark, New Jersey
Company	Texaco
Narrative :	Tank 67 at the Texaco storage site was a 80 foot diameter, 50 feet high gasoline tank. Between 6:50 pm on January 6th and 12:10 am on Jan 7th it was scheduled to be filled by pipeline at a rate of 5000 GPM (315 litres/s). Shortly before midnight two operators approached the tank and discovered that it was overflowing. The wind was "very light, nearly still" at the time of the incident Figure 151. At about 12:10am there was a severe explosion. One employee was killed and 24 were injured. There was serious damage to storage tanks, road vehicles, rail tankers and a several industrial buildings.
Incident Cause	Tank overfill. There was no high level alarm to alert on-site staff or automatic shut-down when the tank was full (allowed in NFPA code 30)
Category Categorize incident cause (e.g. operator error, equipment malfunction, material failure, construction error, design error, weld failure)	Operator error and design error played a part but this type of incident is fundamentally a code error.

Source Term	Type of release (e.g. gas, evaporating liquid or a gas-liquid (two phase) flow)	Description of equipment/piping	Hole size or pipe diameter if it was a guillotine failure	Substance(s) released	Release pressure and temperature
	Evaporating liquid	Tank 80 ft wide 50 ft high	Overfill	Gasoline	Ambient was -2˚C

Release	Quantity released	Migration of substance from release source	Duration of release
	Fill rate was 315 l/s but it is not known how long the overfill went on for.	Reported damage to tanks suggests the vapor cloud extended at least 1200 ft (370 m) to the North.	Not known – but more than 15 minutes

Cloud development	Cloud footprint	Depth and influence of topography under and near the vapor cloud.	Surface roughness	Substance which formed a vapor cloud	Near field dispersion
	Not known Reach of the cloud was probably 300-400m	Not known	Mixed Industrial	Gasoline vapor	

Weather conditions	Atmospheric stability		Temperature	Wind speed
	Stable		-2˚C	nil

Ignition	Ignition strength	Source of ignition	Ignition location
	Not known	Incinerator	On neighbouring site – approximately 275m from source

Explosion severity	Overpressure	Distance of flame travel	Flame speed
	>2000 mbar (29 psi)	>275m	Not known directly. Overpressure indicates detonation, fast deflagration (FD) or episodic deflagration (ED).

Consequences	Fatalities, injuries, health effects, property damage within and outside of the plant property. Heavy damage – structural collapse Moderate damage- cladding loss, cracking of vulnerable masonry, purlin deformation Light damage - cladding damage, window breakage,	Blast damage to plant and other structures within and outside of cloud footprint.
	1 fatality Heavy damage to structures in the cloud - approx. 400m. Moderate damage to surrounding industrial buildings – range not known	Empty tanks flattened or badly damaged on the site.

Mitigating Measures	Cloud mitigation measures	Performance and/or reasons for poor performance
	Vapor barrier surrounding site	No
	On-site vapor fencing	No
	Active vapor dispersal	No

| Facility Information	Other Hydrocarbons at Facility	Quantity stored (is amount >10,000 lbs?)	Type of storage vessel/container	End product or used for a process
	Gasoline, LPG and oil	26 tanks - typical size 5 million gallons	Floating roof tank	End product
	Characteristics of the area where the event occurred	Urban, rural, suburban	Industrial, residential	Proximity to ports/marine
	Mixed Industrial/rail/port	Urban	Industrial	Port
	Facility description	Category (refinery, petrochemical, gas processing, terminal and distribution, upstream)		Number of similar facilities worldwide
	Fuel storage terminal	Distribution		10,000
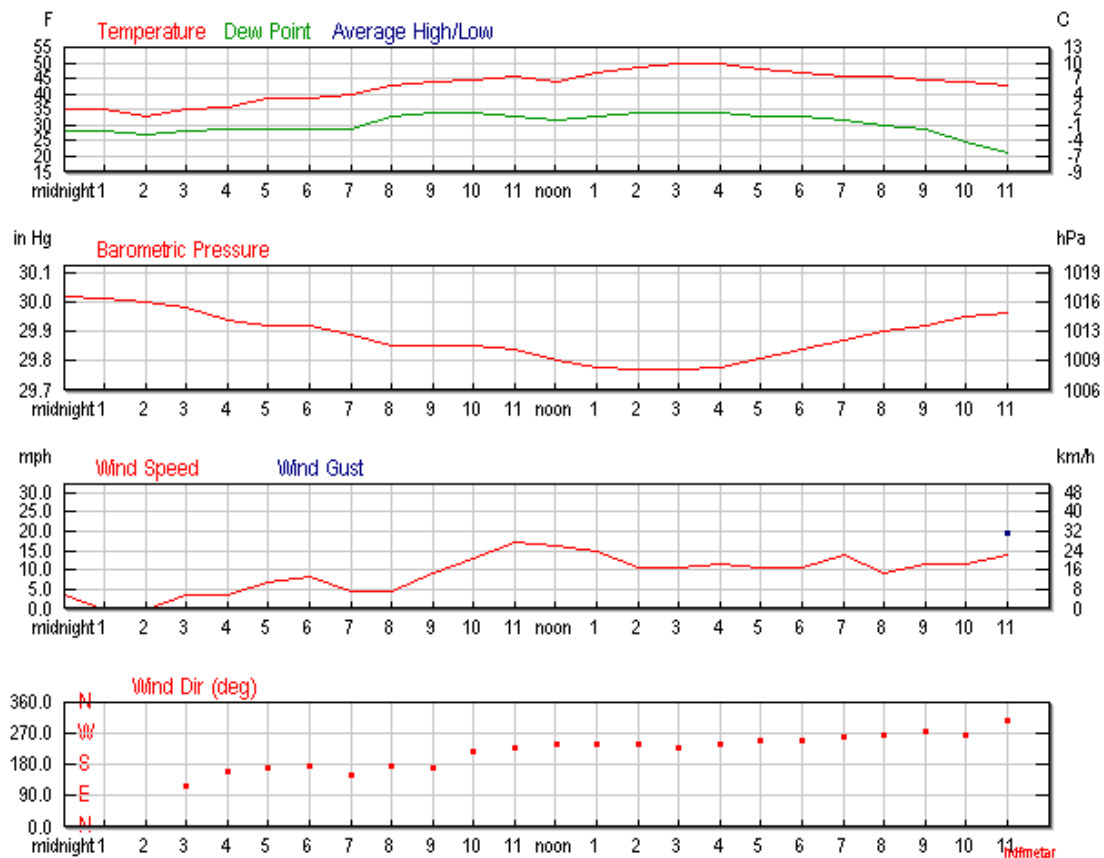
Figure 151: Relevant weather data

5.9.1 Cloud development at Newark

Unfortunately the duration of the overfill is not known and it is consequently not possible to use the incident to test models of dispersion.

Further reading

Bouchard, J.K. *Gasoline storage tank explosion and fire Newark NJ Jan 7th 1983*, National Fire Protection Association, Fire Investigation Report.

5.10 ST HERBLAIN

Time and date:	04:00am 7th October 1991
Location	St Herblain (nr Nantes)
Company	
Narrative :	The gasoline depot had a capacity of 80,000 m^3 (21 million gal). There was an adjacent lorry park used by various gasoline tankers. At the time of the incident the atmospheric conditions were: Temperature: 5˚C Wind speed: <1m/s Stable temperature gradient Humidity 100% At around 4am a large leak developed in a union fitting at the foot of a gasoline tank filled to a height of 9m. A 25,000 m^3 vapor cloud developed over a period of 20 minutes – the observed depth was around 1.5m. When the cloud ignited there was a severe VCE. Flame appeared to have accelerated along a line of adjacent parked gasoline tankers. Window breakage (50%) extended to 700m
Incident Cause	Spray release from a failed seal
Category Categorize incident cause (e.g. operator error, equipment malfunction, material failure, construction error, design error, weld failure)	Material failure

Source Term	Type of release (e.g. gas, evaporating liquid or a gas-liquid (two phase) flow)	Description of equipment/piping	Hole size or pipe diameter if it was a guillotine failure	Substance(s) released	Release pressure and temperature
	Evaporating liquid	Union with seal suitable for aromatics <30%. Used for gasoline with 55% aromatic content	12" line – Hole size not known – probably approx. 10% area	Gasoline	Ambient temperature 5˚C
Release	Quantity released	Migration of substance from release source		Duration of release	

	Not known	Gravity driven		20 minutes
Cloud development	Cloud footprint	Depth and influence of topography under and near the vapor cloud.	Surface roughness	Substance which formed a vapor cloud	Near field dispersion
	17,000 m² 4.2 acres	Site fairly flat. Vapor flow affected by bunds	Not known	Gasoline	Spray directed upward
Weather conditions	Atmospheric stability		Temperature	Wind speed	
	Stable		5˚C	< 1m/s	
Ignition	Ignition strength	Source of ignition		Ignition location	
	Moderate	Possibly gas fired water heater		Truck washing station	
Explosion severity	Overpressure	Distance of flame travel		Flame speed	
	29 psi or more	About 100m		Not known directly. Overpressure indicates detonation, fast deflagration (FD) or episodic deflagration (ED).	
Consequences	Fatalities, injuries, health effects, property damage within and outside of the plant property. Heavy damage – structural collapse Moderate damage- cladding loss, cracking of vulnerable masonry, purlin deformation Light damage - cladding damage, window breakage,			Blast damage to plant and other structures within and outside of cloud footprint.	
	Heavy blast damage onsite (within or very close to cloud) affecting: 15 tankers and 4 cars Changing rooms and offices Fencing Moderate damage to other tanks on site and to port warehouses at a range of 220m Window damage: 50% at 700m 75% at 320m			Loss around $20M (in 1991) Piping deformed	
Mitigating Measures	Cloud mitigation measures	Performance and/or reasons for poor performance			

	Vapor barrier surrounding site	Not present		
	On-site vapor fencing	Not present		
	Active vapor dispersal	Not present		
Facility Information	Other Hydrocarbons at Facility	Quantity stored (is amount >10,000 lbs?)	Type of storage vessel/container	End product or used for a process
	Furnace fuel oil Diesel	80,000 m^3 (21 million gal).	Pipework from gasoline tank	End product
	Characteristics of the area where the event occurred	Urban, rural, suburban	Industrial, residential	Proximity to ports/marine
	Port area	Urban	Industrial	Marine
	Facility description	Category (refinery, petrochemical, gas processing, terminal and distribution, upstream)		Number of similar facilities worldwide
	Fuel depot	Terminal and distribution		10,000

Figure 152 shows a line of tankers that investigators identified as the trigger for transition to a severe explosion.

Figure 152: Line of blast damaged tankers within the cloud area

Further Reading

Lechaudel, J.F. and Mouilleau Y., *Assessment of an accidental vapor cloud explosion - A Case Study: St Herblain 7th October 1991*. Loss Prevention and Safety Promotion in the Process Industries Vol 1, p377.

5.11   NAPLES

Time and date:	21st December 1985 (5:00am)
Location	Naples
Company	AGIP
Narrative :	The site stored gasoline, diesel and fuel oil with a total capacity of 100,000 m³ (730,000 barrels). The incident occurred during a transfer of gasoline from a tanker in the Bay of Naples to the site. Gasoline overflowed through the floating roof of the tank for about 90 minutes – spilling about 700 tons (1.5M pounds) of fuel.

In very light or nil wind conditions the vapor spread to cover an area of 49,000m² (12 acres). The site was highly confined by walls, buildings and an embankment to a mean height of around 8 metres (26 feet). The site included 37 storage tanks, two buildings, loading gantries and some rail tankers.

When ignition occurred a severe VCE destroyed all of the buildings and equipment of the site. The VCE was followed by a fire that lasted a week.

Three people were killed on the site and two local residents died when their home collapsed. |
| Incident Cause | Overfill. Process failure not known in detail |
| Category
Categorize incident cause (e.g. operator error, equipment malfunction, material failure, construction error, design error, weld failure) | Not known |

Source Term	Type of release (e.g. gas, evaporating liquid or a gas-liquid (two phase) flow)	Description of equipment/piping	Hole size or pipe diameter if it was a guillotine failure	Substance(s) released	Release pressure and temperature
	Evaporating liquid	Floating roof tank and pipe from ship.	Full bore overfill	Gasoline	Ambient pressure and temperature

Release	Quantity released	Migration of substance from release source	Duration of release
	700 tons (1.5M pounds)	Gravity current	90 minutes

	Over 90 minutes. 130 kg/s (286 pounds/s)			
Cloud development	Cloud footprint	Depth and influence of topography under and near the vapor cloud.	Surface roughness	Substance which formed a vapor cloud Near field dispersion
	49,000 m^2 (12 acres)	Site surrounded by walls and embankment to an average height of 8m (26 feet)	Urban	Gasoline Tank overfill
Weather conditions	Atmospheric stability		Temperature	Wind speed
	Stable (Winter night)		8˚C	low
Ignition	Ignition strength	Source of ignition		Ignition location
	Not known	Not known		Not known
Explosion severity	Overpressure	Distance of flame travel		Flame speed
	>2 bar (29psi)	About 200m		Not known directly. Overpressure indicates detonation, fast deflagration (FD) or episodic deflagration (ED).
Consequences	Fatalities, injuries, health effects, property damage within and outside of the plant property. Heavy damage – structural collapse Moderate damage- cladding loss, cracking of vulnerable masonry, purlin deformation Light damage - cladding damage, window breakage,			Blast damage to plant and other structures within and outside of cloud footprint.
	Five fatalities. 3 on-site and 2 in an off-site building collapse. Heavy explosion damage on the site – also severe fire damage Window frames and roofs damaged to 600m. Majority of glass shattered to 1000m.			Site destroyed. Blast damage obscured by a very prolonged and severe fire. Minor damage (windows) to a distance of 5 km.

Mitigating Measures	Cloud mitigation measures	Performance and/or reasons for poor performance

	Vapor barrier surrounding site	Yes – vapor cloud confined to the site. The elements that confined the cloud were not built for this purpose		
	On-site vapor fencing	No		
	Active vapor dispersal	No		
Facility Information	Other Hydrocarbons at Facility	Quantity stored (is amount >10,000 lbs?)	Type of storage vessel/container	End product or used for a process
	Diesel	100,000 m^3 730,000 barrels	Atmospheric storage tank	End product
	Characteristics of the area where the event occurred	Urban, rural, suburban	Industrial, residential	Proximity to ports/marine
	Standard ship supplied fuel storage site	Urban	Residential close by	Port close by
	Facility description	Category (refinery, petrochemical, gas processing, terminal and distribution, upstream)		Number of similar facilities worldwide
	Tanker terminal	Terminal and distribution		10,000

5.12   BATON ROUGE, LOUISIANA

Time and date:	12:35 24th December 1989
Location	Baton Rouge, Louisiana, USA
Company	Exxon
Narrative :	A loss of power on the morning of Christmas Eve 1989 to Entergy's 230 KV power grid serving a large radius of Baton Rouge — including the Exxon refinery / chemical complex which sits aside the Mississippi River — caused all facility systems to go into a "Fail Safe" mode. In this fail safe mode process safety design parameters caused various components of the process and transfer systems to default to wide open or fully closed positions to manage process variables such as flow, levels, pressures, and temperatures throughout the facility. An open valve resulting from this fail-safe procedure ultimately led to the chain of events in this Baton Rouge incident. Thermal expansion of a C3 and lighter product on an 8-inch, high-pressure product line caused a failure releasing 1,500 pounds of hydrocarbons per second in a vapor/mist form. The release lasted approximately 2.5 minutes before ignition. An estimated 225,000 pounds of released hydrocarbon vapor created a cloud 1,000-1,500 feet in circumference and approximately 80 feet in height/depth. The blast measured 3.2 on a Richter scale 75 miles away in New Orleans.
Incident Cause	Power failure to the site put systems into a fail-safe mode, which resulted in an 8" valve automatically opening and releasing ethane and propane
Category Categorize incident cause (e.g. operator error, equipment malfunction, material failure, construction error, design error, weld failure)	Design error

Source Term	Type of release (e.g. gas, evaporating liquid or a gas-liquid (two phase) flow)	Description of equipment/piping	Hole size or pipe diameter if it was a guillotine failure	Substance(s) released	Release pressure and temperature
	Evaporating liquid	8" high pressure product line	8"	Ethane and Propane	"High pressure"

Release	Quantity released	Migration of substance from release source	Duration of release	
	225,000 pounds		150 seconds	

Cloud development	Cloud footprint	Depth and influence of topography under and near the vapor cloud.	Surface roughness	Substance which formed a vapor cloud	Near field dispersion
	4.1 acres			Ethane and Propane	

Weather conditions	Atmospheric stability		Temperature	Wind speed
	Stable Data from Baton Rouge Metropolitan Airport (3.5 miles Northeast) shown below		-1.7-0 degC	1.5 – 2.1 m/s NNW

Ignition	Ignition strength	Source of ignition	Ignition location
	Not known	Not known	Not known

Explosion severity	Overpressure	Distance of flame travel	Flame speed
	3.2 on Richter scale 75 miles away in New Orleans	Not known	Severe explosion

Consequences	Fatalities, injuries, health effects, property damage within and outside of the plant property. Heavy damage – structural collapse Moderate damage- cladding loss, cracking of vulnerable masonry, purlin deformation Light damage - cladding damage, window breakage,	Blast damage to plant and other structures within and outside of cloud footprint.
	1 employee fatality 7 injured	

Mitigating Measures	Cloud mitigation measures	Performance and/or reasons for poor performance
	Vapor barrier surrounding site	Not known if present
	On-site vapor fencing	Not known if present
	Active vapor dispersal	Not known if present

Facility Information	Other Hydrocarbons at Facility	Quantity stored (is amount >10,000 lbs?)	Type of storage vessel/container	End product or used for a process
	Characteristics of the area where the event occurred	Urban, rural, suburban	Industrial, residential	Proximity to ports/marine
	Flat floodplain	Urban	Residential	Inland Next to Mississippi river
	Facility description	Category (refinery, petrochemical, gas processing, terminal and distribution, upstream)		Number of similar facilities worldwide
	Refined crude oil into petroleum products and had a capacity of 503,000 barrels-per-day	Refinery		≈650

Figure 153: Site boundary

Hourly Weather History & Observations

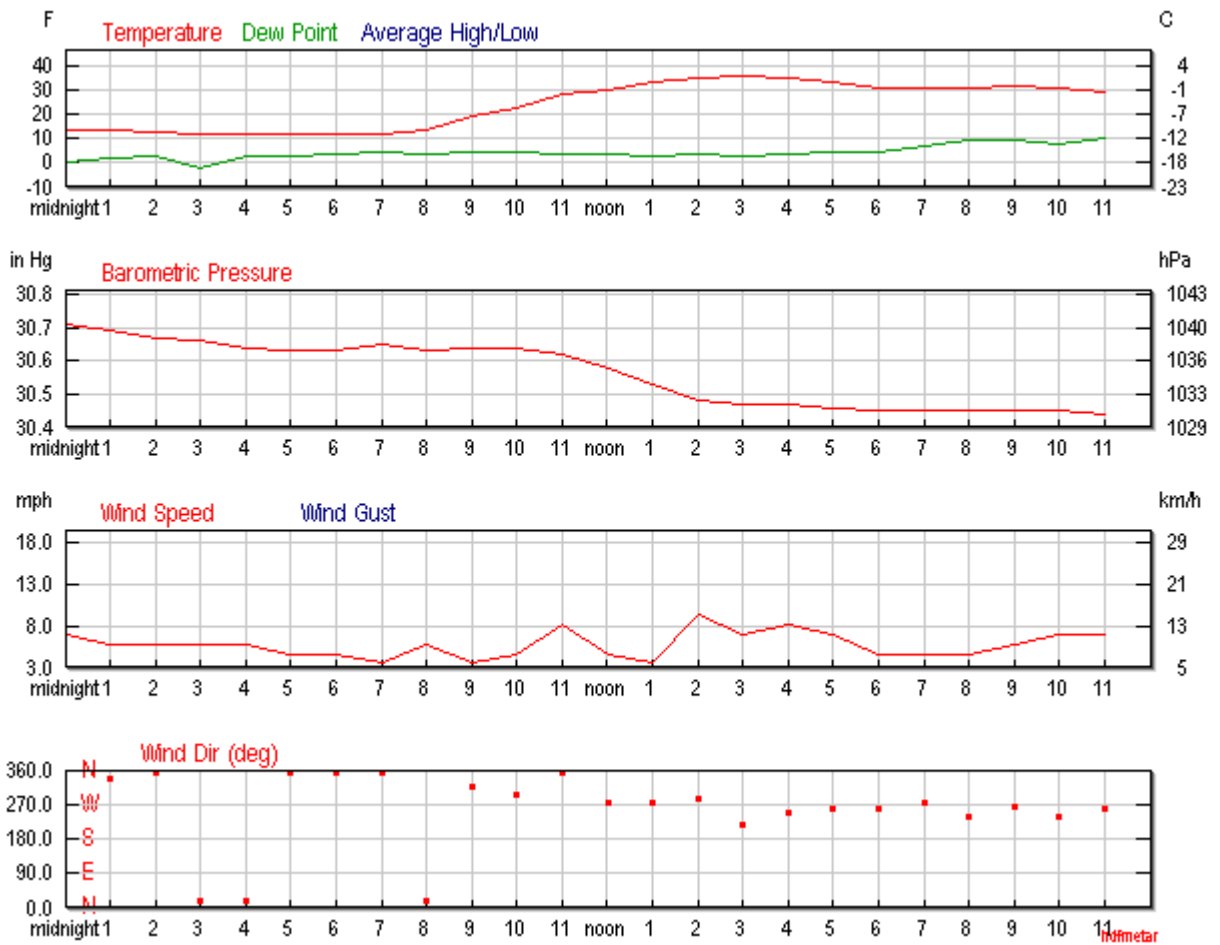| Time(CST)	Temp.	Dew Point	Humidity	Pressure	Wind Dir	Wind Speed	Conditions
12:00 AM	-10.6 °C	-18.3 °C	54%	1039.8 hPa	NNW	11.1 km/h /3.1 m/s	Clear
1:00 AM	-10.6 °C	-17.2 °C	59%	1039.3 hPa	NNW	9.3 km/h /2.6 m/s	Clear
2:00 AM	-11.1 °C	-16.7 °C	64%	1038.6 hPa	North	9.3 km/h /2.6 m/s	Clear
3:00 AM	-11.7 °C	-19.4 °C	54%	1038.0 hPa	NNE	9.3 km/h /2.6 m/s	Clear
4:00 AM	-11.7 °C	-16.7 °C	67%	1037.6 hPa	NNE	9.3 km/h /2.6 m/s	Clear
5:00 AM	-11.7 °C	-16.7 °C	67%	1037.3 hPa	North	7.4 km/h /2.1 m/s	Clear
6:00 AM	-11.7 °C	-16.1 °C	70%	1037.2 hPa	North	7.4 km/h /2.1 m/s	Clear
7:00 AM	-11.7 °C	-15.6 °C	73%	1037.7 hPa	North	5.6 km/h /1.5 m/s	Clear
8:00 AM	-10.6 °C	-16.1 °C	65%	1037.3 hPa	NNE	9.3 km/h /2.6 m/s	Clear
9:00 AM	-7.8 °C	-15.6 °C	54%	1037.6 hPa	NW	5.6 km/h /1.5 m/s	Clear
10:00 AM	-5.6 °C	-15.6 °C	46%	1037.6 hPa	WNW	7.4 km/h /2.1 m/s	Clear
11:00 AM	-2.8 °C	-16.1 °C	36%	1036.8 hPa	North	13.0 km/h/ 3.6 m/s	Clear
12:00 PM	-1.7 °C	-16.1 °C	33%	1035.6 hPa	West	7.4 km/h /2.1 m/s	Clear
1:00 PM	0.0 °C	-16.7 °C	28%	1033.7 hPa	West	5.6 km/h /1.5 m/s	Clear
2:00 PM	1.1 °C	-16.1 °C	27%	1032.2 hPa	WNW	14.8 km/h/ 4.1 m/s	Clear
3:00 PM	1.7 °C	-16.7 °C	25%	1031.8 hPa	SW	11.1 km/h /3.1 m/s	Clear
4:00 PM	1.1 °C	-16.1 °C	27%	1031.7 hPa	WSW	13.0 km/h/ 3.6 m/s	Clear
5:00 PM	0.0 °C	-15.6 °C	31%	1031.3 hPa	West	11.1 km/h /3.1 m/s	Scattered Clouds
6:00 PM	-1.1 °C	-15.6 °C	33%	1031.0 hPa	West	7.4 km/h /2.1 m/s	Scattered Clouds
7:00 PM	-1.1 °C	-14.4 °C	36%	1031.2 hPa	West	7.4 km/h /2.1 m/s	Clear
8:00 PM	-1.1 °C	-13.3 °C	40%	1031.2 hPa	WSW	7.4 km/h /2.1 m/s	Scattered Clouds
9:00 PM	-0.6 °C	-13.3 °C	38%	1031.0 hPa	West	9.3 km/h /2.6 m/s	Mostly Cloudy
10:00 PM	-1.1 °C	-13.9 °C	38%	1031.0 hPa	WSW	11.1 km/h /3.1 m/s	Mostly Cloudy
11:00 PM	-2.2 °C	-12.8 °C	45%	1030.6 hPa	West	11.1 km/h /3.1 m/s	Unknown

Daily Weather History Graph

Figure 154: Daily Weather History Graph

5.13   BIG SPRING, TEXAS

Time and date:	08:10, 18th February 2008 (Monday)
Location	Interstate 20 and Refinery Road, Big Spring, Howard County, Texas , USA
Company	Alon Israel Oil Co. Ltd.
Narrative :	The refinery is a basic fuels refinery, serving West Texas by processing crude oil from the area, and shipping the refined products offsite, via pipeline, rail car and tanker truck. Alon is located on the northeast edge of the city of Big Spring, but outside the city limits.

There was an explosion measuring 2.1 on the Richter scale

The resulting fire started in the propylene plant and threatened the alkylation plant where hydrofluoric acid (HF) is used and stored as part of the cracking process for propane.

The fire was contained to four, refined product, aboveground storage tanks: two tanks contained gasoline and the other two tanks contained asphalt. The fire created a large, black smoke plume, which reached approximately 6500 feet in height as it drifted slowly to the east-northeast away from Big Spring along I-20.

The refinery personnel were evacuated, as well as non-essential personnel at the nearby Sid Richardson Carbon Black Plant, but there was no community evacuation of Big Spring. Four personnel and one person driving a car on interstate-20 were injured but none of the individuals suffered life threatening injuries.

Alon USA emergency responders and other firefighting response crews extinguished the fire at 17:30 hours after using a combination of firefighting foam and water. |
| **Incident Cause** | A faulty weld on a pump casing within a propylene splitter unit (PSU) allowed liquid propylene to escape and reach an ignition source. |
| **Category**
Categorize incident cause (e.g. operator error, equipment malfunction, material failure, construction error, design error, weld failure) | Weld failure |

Source Term	Type of release (e.g. gas, evaporating liquid or a gas-liquid	Description of equipment/piping	Hole size or pipe diameter if it was a guillotine failure	Substance(s) released	Release pressure and temperature

	(two phase) flow)				
	Evaporating liquid	Pump casing	Not known	Liquid propylene	Not known
Release	Quantity released	Migration of substance from release source		Duration of release	
	Not known	Not known		Not known	
Cloud development	Cloud footprint	Depth and influence of topography under and near the vapor cloud.	Surface roughness	Substance which formed a vapor cloud	Near field dispersion
	Not known	Not known	Not known	Propylene/propane	Not known
Weather conditions	Atmospheric stability		Temperature	Wind speed	
	Two temperature inversion layers at ground level and at 2500 m (8200 ft) Data from Big Spring McMahon-Wrinkle Airport (7.5miles West) Clear		2.0degC	Calm (nil wind)	
Ignition	Ignition strength	Source of ignition		Ignition location	
	Not known	Not known		Not known	

Explosion severity	Overpressure	Distance of flame travel	Flame speed	
	Measured 2.1 on the Richter scale, pressure pulse duration estimated at 0.5 secs	Not known	Not known	
Consequences	Fatalities, injuries, health effects, property damage within and outside of the plant property. Heavy damage – structural collapse Moderate damage- cladding loss, cracking of vulnerable masonry, purlin deformation Light damage - cladding damage, window breakage,		Blast damage to plant and other structures within and outside of cloud footprint.	
	5 people were hospitalised Heavy damage – Not clear Moderate damage – Not clear Light damage – 13km		Pictures knocked off walls 45 miles away	

Mitigating Measures	Cloud mitigation measures	Performance and/or reasons for poor performance		
	Vapor barrier surrounding site	Not known if present		
	On-site vapor fencing	Not known if present		
	Active vapor dispersal	Not known if present		

Facility Information	Other Hydrocarbons at Facility	Quantity stored (is amount >10,000 lbs?)	Type of storage vessel/container	End product or used for a process
	Propylene/propane	162,300 – 192,000kg (357,000 – 423,000 lbs)	Not known	Process fluid
	Characteristics of the area where the event occurred	Urban, rural, suburban	Industrial, residential	Proximity to ports/marine
	An uneven hilly landscape with many valleys	Suburban	Residential 1-2 miles away	Inland
	Facility description	Category (refinery, petrochemical, gas processing, terminal and distribution, upstream)		Number of similar facilities worldwide
	Refinery capacity 70,000 barrels-per-day	Refinery		≈650

Figure 155: High level inversion. There was also a ground level inversion during the leak

Figure 156: Overview of site giving some idea of the area affected by the cloud

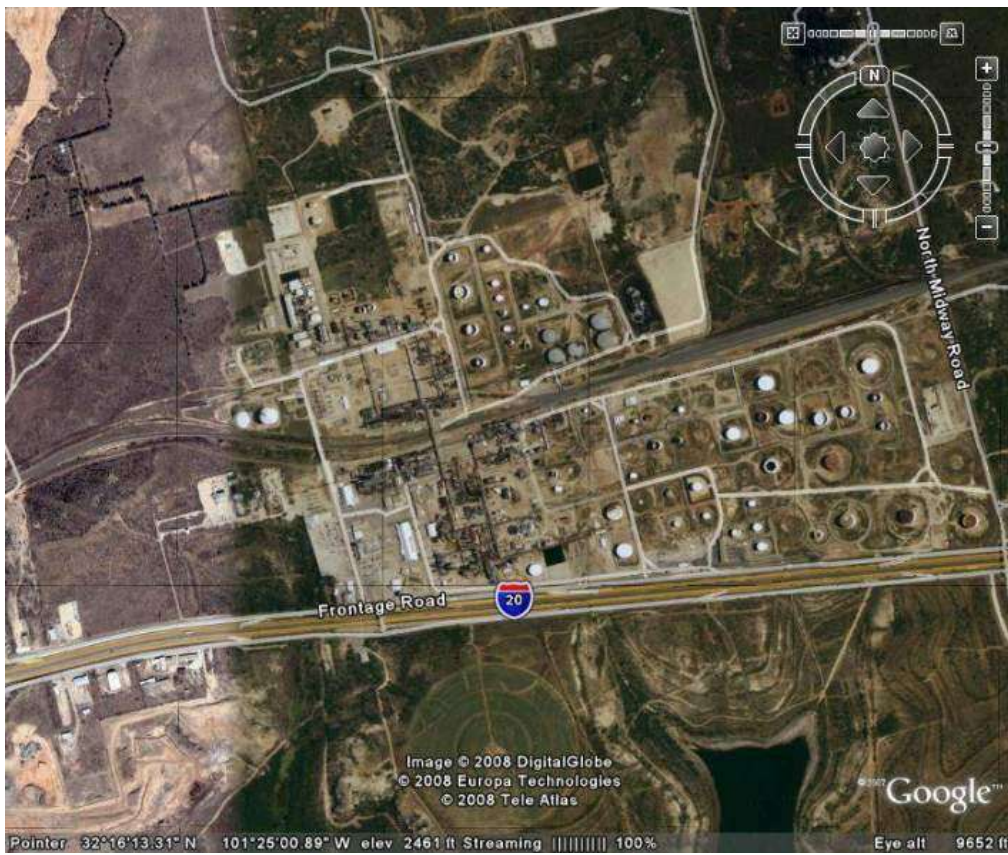**Figure 157: Further view of site and smoke plumes**

Figure 158: Plan view of site

Hourly Weather History & Observations

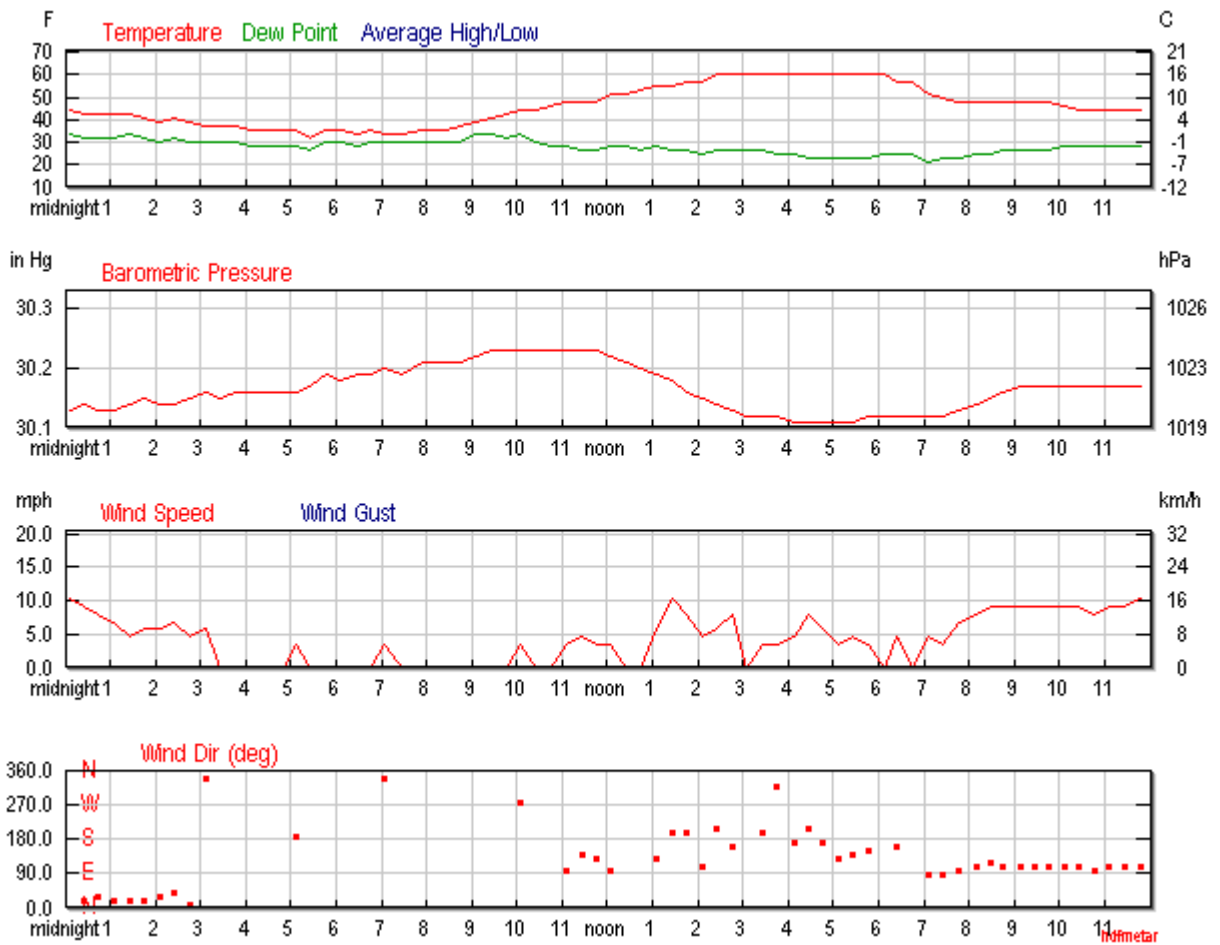| Time(CST)	Temp.	Dew Point	Humidity	Pressure	Wind Dir	Wind Speed	Conditions
12:06 AM	7.0 °C	1.0 °C	66%	1020.2 hPa	North	16.7 km/h/ 4.6 m/s	Clear
12:25 AM	6.0 °C	0.0 °C	66%	1020.5 hPa	NNE	14.8 km/h/ 4.1 m/s	Clear
12:45 AM	6.0 °C	0.0 °C	66%	1020.2 hPa	NNE	13.0 km/h/ 3.6 m/s	Clear
1:05 AM	6.0 °C	0.0 °C	66%	1020.2 hPa	NNE	11.1 km/h/ 3.1 m/s	Clear
1:26 AM	6.0 °C	1.0 °C	70%	1020.5 hPa	NNE	7.4 km/h/ 2.1 m/s	Clear
1:46 AM	5.0 °C	0.0 °C	70%	1020.9 hPa	NNE	9.3 km/h/ 2.6 m/s	Clear
2:06 AM	4.0 °C	-1.0 °C	70%	1020.5 hPa	NNE	9.3 km/h/ 2.6 m/s	Clear
2:26 AM	5.0 °C	0.0 °C	70%	1020.5 hPa	NE	11.1 km/h/ 3.1 m/s	Clear
2:46 AM	4.0 °C	-1.0 °C	70%	1020.9 hPa	North	7.4 km/h/ 2.1 m/s	Clear
3:06 AM	3.0 °C	-1.0 °C	75%	1021.2 hPa	NNW	9.3 km/h/ 2.6 m/s	Clear
3:26 AM	3.0 °C	-1.0 °C	75%	1020.9 hPa	Calm	Calm	Clear
3:46 AM	3.0 °C	-1.0 °C	75%	1021.2 hPa	Calm	Calm	Clear
4:08 AM	2.0 °C	-2.0 °C	75%	1021.2 hPa	Calm	Calm	Clear
4:25 AM	2.0 °C	-2.0 °C	75%	1021.2 hPa	Calm	Calm	Clear
4:50 AM	2.0 °C	-2.0 °C	75%	1021.2 hPa	Calm	Calm	Clear
5:06 AM	2.0 °C	-2.0 °C	75%	1021.2 hPa	South	5.6 km/h/ 1.5 m/s	Clear
5:25 AM	0.0 °C	-3.0 °C	80%	1021.6 hPa	Calm	Calm	Clear
5:47 AM	2.0 °C	-1.0 °C	81%	1022.2 hPa	Calm	Calm	Clear
6:05 AM	2.0 °C	-1.0 °C	81%	1021.9 hPa	Calm	Calm	Clear
6:29 AM	1.0 °C	-2.0 °C	81%	1022.2 hPa	Calm	Calm	Clear
6:45 AM	2.0 °C	-1.0 °C	81%	1022.2 hPa	Calm	Calm	Clear
7:05 AM	1.0 °C	-1.0 °C	87%	1022.6 hPa	NNW	5.6 km/h/ 1.5 m/s	Clear
7:27 AM	1.0 °C	-1.0 °C	87%	1022.2 hPa	Calm	Calm	Clear
7:53 AM	2.0 °C	-1.0 °C	81%	1022.9 hPa	Calm	Calm	Clear
8:05 AM	2.0 °C	-1.0 °C	81%	1022.9 hPa	Calm	Calm	Clear
8:25 AM	2.0 °C	-1.0 °C	81%	1022.9 hPa	Calm	Calm	Clear
8:46 AM	3.0 °C	-1.0 °C	75%	1022.9 hPa	Calm	Calm	Clear
9:07 AM	4.0 °C	1.0 °C	81%	1023.2 hPa	Calm	Calm	Clear
9:26 AM	5.0 °C	1.0 °C	76%	1023.6 hPa	Calm	Calm	Clear
9:47 AM	6.0 °C	0.0 °C	66%	1023.6 hPa	Calm	Calm	Clear
10:05 AM	7.0 °C	1.0 °C	66%	1023.6 hPa	West	5.6 km/h/ 1.5 m/s	Clear
10:26 AM	7.0 °C	-1.0 °C	57%	1023.6 hPa	Calm	Calm	Clear
10:45 AM	8.0 °C	-2.0 °C	50%	1023.6 hPa	Calm	Calm	Scattered Clouds
11:05 AM	9.0 °C	-2.0 °C	46%	1023.6 hPa	East	5.6 km/h/ 1.5 m/s	Mostly Cloudy

Figure 159: Daily Weather History Graph

5.14   GEISMER, LOUISIANA

Time and date:	08:30 13th June 2013 (Thursday)			
Location	Geismar, Louisiana, USA			
Company	Williams Olefins Inc.			
Narrative :	Little information is currently available on this incident. A large explosion occurred at the Williams Olefins plant in which 2 workers were killed and 114 were injured. Unconfirmed sources suggest the point of failure may have been a ruptured heat exchanger. The plant does have a history of accidental flammable gas releases of various sizes. The incident is still under investigation by both the OSHA and CSB.			
Incident Cause	Rupture within a heat exchanger			
Category Categorize incident cause (e.g. operator error, equipment malfunction, material failure, construction error, design error, weld failure)	Material failure			
Source Term	Type of release (e.g. gas, evaporating liquid or a gas-liquid (two phase) flow)	Description of equipment/piping	Hole size or pipe diameter if it was a guillotine failure	Substance(s) released Release pressure and temperature
	Evaporating liquid			Propylene (75%), Ethylene, Benzene
Release	Quantity released	Migration of substance from release source	Duration of release	
	14,146 kg (31,186 lb)			
Cloud development	Cloud footprint	Depth and influence of topography under and near the vapor cloud.	Surface roughness	Substance Near field which dispersion formed a vapor cloud

Weather conditions	Atmospheric stability		Temperature	Wind speed
	Data from Baton Rouge Metropolitan Airport (21 miles North) Scattered clouds		28degC	Nil wind at 7am. Inversion may have persisted at the site	Westerly
Ignition	Ignition strength	Source of ignition		Ignition location
Explosion severity	Overpressure	Distance of flame travel		Flame speed
Consequences	Fatalities, injuries, health effects, property damage within and outside of the plant property. Heavy damage – structural collapse Moderate damage- cladding loss, cracking of vulnerable masonry, purlin deformation Light damage - cladding damage, window breakage,			Blast damage to plant and other structures within and outside of cloud footprint.
	2 plant workers were killed 114 injured			

Mitigating Measures	Cloud mitigation measures	Performance and/or reasons for poor performance		
	Vapor barrier surrounding site	Not known		
	On-site vapor fencing	Not known		
	Active vapor dispersal	Not known		
Facility Information	Other Hydrocarbons at Facility	Quantity stored (is amount >10,000 lbs?)	Type of storage vessel/container	End product or used for a process
	Ethylene Benzene Propylene			

Characteristics of the area where the event occurred	Urban, rural, suburban	Industrial, residential	Proximity to ports/marine
Flat topography, situated the floodplain of the Mississippi river	Suburban, 2.5 miles from closest residential area	Industrial	Inland
Facility description	Category (refinery, petrochemical, gas processing, terminal and distribution, upstream)		Number of similar facilities worldwide
The plant produces ethylene and propylene amongst other products through the steam cracking of propane and ethylene	Petrochemical		

Figure 160: Fire following explosion

Figure 161: Overview of area in which explosion occurred

Figure 162: Post blast photo of the heat exchanger which ruptured catastrophically

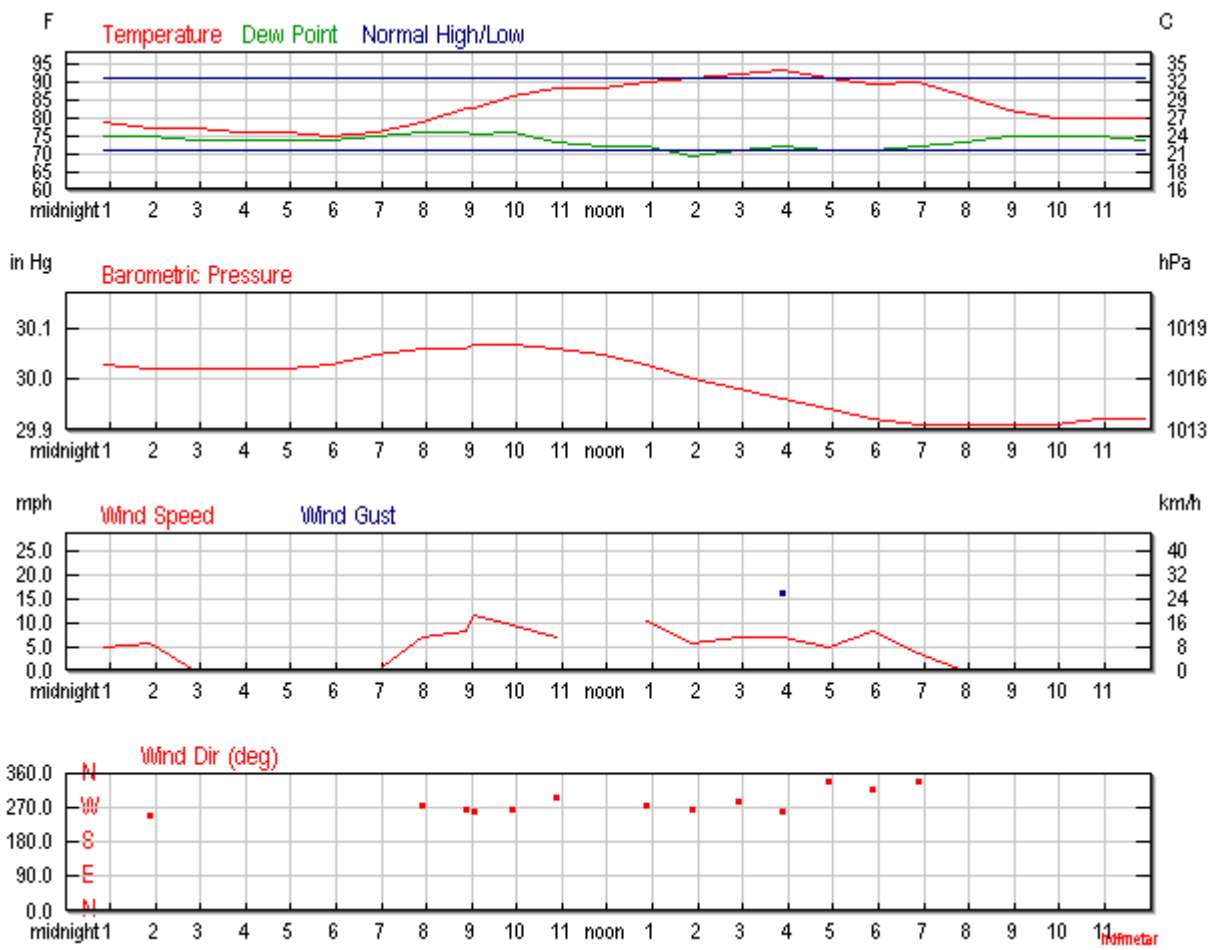| Time(CDT)	Temp.	Dew Point	Humidity	Pressure	Wind Dir	Wind Speed	Conditions
12:53 AM	26.1 °C	23.9 °C	88%	1016.9 hPa	SW	7.4 km/h /2.1 m/s	Clear
1:53 AM	25.0 °C	23.9 °C	94%	1016.6 hPa	WSW	9.3 km/h /2.6 m/s	Clear
2:53 AM	25.0 °C	23.3 °C	90%	1016.5 hPa	Calm	Calm	Clear
3:53 AM	24.4 °C	23.3 °C	94%	1016.4 hPa	Calm	Calm	Clear
4:53 AM	24.4 °C	23.3 °C	94%	1016.6 hPa	Calm	Calm	Clear
5:53 AM	23.9 °C	23.3 °C	96%	1016.9 hPa	Calm	Calm	Partly Cloudy
6:53 AM	24.4 °C	23.9 °C	97%	1017.5 hPa	Calm	Calm	Scattered Clouds
7:53 AM	26.1 °C	24.4 °C	90%	1017.9 hPa	West	11.1 km/h /3.1 m/s	Scattered Clouds
8:53 AM	28.3 °C	24.4 °C	79%	1018.0 hPa	West	13.0 km/h/ 3.6 m/s	Mostly Cloudy
9:03 AM	28.0 °C	24.0 °C	79%	1018.2 hPa	West	18.5 km/h/ 5.1 m/s	Mostly Cloudy
9:53 AM	30.0 °C	24.4 °C	72%	1018.1 hPa	West	14.8 km/h/ 4.1 m/s	Mostly Cloudy
10:53 AM	31.1 °C	22.8 °C	61%	1017.7 hPa	WNW	11.1 km/h /3.1 m/s	Mostly Cloudy
11:53 AM	31.1 °C	22.2 °C	59%	1017.5 hPa	North	-	Mostly Cloudy
12:53 PM	32.2 °C	22.2 °C	55%	1016.9 hPa	West	16.7 km/h/ 4.6 m/s	Partly Cloudy
1:53 PM	32.8 °C	20.6 °C	48%	1015.9 hPa	West	9.3 km/h /2.6 m/s	Partly Cloudy
2:53 PM	33.3 °C	21.7 °C	50%	1015.0 hPa	WNW	11.1 km/h /3.1 m/s	Scattered Clouds
3:53 PM	33.9 °C	22.2 °C	50%	1014.3 hPa	West	11.1 km/h /3.1 m/s	Unknown
4:53 PM	32.8 °C	21.7 °C	52%	1013.6 hPa	NNW	7.4 km/h /2.1 m/s	Scattered Clouds
5:53 PM	31.7 °C	21.7 °C	55%	1013.0 hPa	NW	13.0 km/h/ 3.6 m/s	Partly Cloudy
6:53 PM	32.2 °C	22.2 °C	55%	1012.6 hPa	NNW	5.6 km/h /1.5 m/s	Partly Cloudy
7:53 PM	30.0 °C	22.8 °C	65%	1012.6 hPa	Calm	Calm	Partly Cloudy
8:53 PM	27.8 °C	23.9 °C	79%	1012.6 hPa	Calm	Calm	Partly Cloudy
9:53 PM	26.7 °C	23.9 °C	85%	1012.8 hPa	Calm	Calm	Clear
10:53 PM	26.7 °C	23.9 °C	85%	1013.2 hPa	Calm	Calm	Clear
11:53 PM	26.7 °C	23.3 °C	81%	1013.0 hPa	Calm	Calm	Clear

Hourly Weather History & Observations

Figure 163: Daily Weather History Graphs

5.15   LA MEDE

Time and date:	05:20, 9th November 1992 (Monday)
Location	La Mede, Martigues, France
Company	Total
Narrative :	The explosion occurred at the fluid catalytic cracking unit (FCCU). Six operators were killed and two seriously injured. The FCCU and surrounding process units were severely damaged resulting in the refinery being shut down for months. The origin was a 25 cm^2 break in the 8" by-pass of the absorber stripper column cooler; an amount of about 15 tons of LPG and light naphtha was released within 10 minutes, covering an area of 14000 m^2 including Gas Plant, Cryogenic, Propene and Merox units before being ignited on the FCC main furnace. There were eight people on shift in the unit: 6 died, one was very seriously injured, and one slightly injured. The total loss including loss of production is estimated at \$600,000,000. Subsequent fires created a domino effect leading to further loss of containment and escalation. Some fires continued to burn for up to 3 days until their sources were exhausted.
Incident Cause	A section of bypass pipework failed through internal corrosion, which had been uniformly thinned. The pipework had been in service for 36 years but was not regularly inspected as it was a bypass.
Category Categorize incident cause (e.g. operator error, equipment malfunction, material failure, construction error, design error, weld failure)	Material failure

Source Term	Type of release (e.g. gas, evaporating liquid or a gas-liquid (two phase) flow)	Description of equipment/piping	Hole size or pipe diameter if it was a guillotine failure	Substance(s) released	Release pressure and temperature
	Evaporating liquid	Absorber stripper reflux cooler bypass line	80 x 20cm (2.5 x 0.64 ft) crack/ opening	LPG, light Naphtha	40˚C (104 F) 10bar (145 psi)

Release	Quantity released	Migration of substance from release source	Duration of release	

	12 tonnes (26,400 ft) 70,000 m^3	Gravitational slumping		10 minutes
Cloud development	Cloud footprint	Depth and influence of topography under and near the vapor cloud.	Surface roughness	Substance which formed a vapor cloud	Near field dispersion
	14,000 m^2	Gas cloud height varied between 4-6m		LPG, light Naphtha
Weather conditions	Atmospheric stability		Temperature	Wind speed
			≈5degC	
Ignition	Ignition strength	Source of ignition		Ignition location
		Open flame		Furnace F301
Explosion severity	Overpressure	Distance of flame travel		Flame speed
	Phase 1: Phase 2: 0.6bar (8.7 psi) Phase 3: 2-3bar (29 – 43 psi)	100 m (328 ft)		Phase 1: 5-10 m/s Phase 2: 10-200 m/s Phase 3: 2000 m/s
Consequences	Fatalities, injuries, health effects, property damage within and outside of the plant property. Heavy damage – structural collapse Moderate damage- cladding loss, cracking of vulnerable masonry, purlin deformation Light damage - cladding damage, window breakage,		Blast damage to plant and other structures within and outside of cloud footprint.	
	Six employee fatalities One employee seriously injured One employee minor injuries 37 others suffered minor injuries Heavy damage – 35 m (115 ft) Moderate damage – 200 m (656 ft) Light damage – 4000 m (13,100 ft)		Vast damage caused to plant although it is unclear from the literature what was damaged by blast and what was damaged by subsequent explosions and fire	

Mitigating Measures	Cloud mitigation measures	Performance and/or reasons for poor performance
	Vapor barrier surrounding site	Not known if present

|	On-site vapor fencing	Not known if present		
	Active vapor dispersal	Not known if present		
Facility Information	Other Hydrocarbons at Facility	Quantity stored (is amount >10,000 lbs?)	Type of storage vessel/container	End product or used for a process
		FCCU (4,800 tonne)		
	Characteristics of the area where the event occurred	Urban, rural, suburban	Industrial, residential	Proximity to ports/marine
	An open rocky dale	Rural	Industrial	<0.5miles to port
	Facility description	Category (refinery, petrochemical, gas processing, terminal and distribution, upstream)		Number of similar facilities worldwide
	Refines crude oil into petroleum products: An FCCU producing up to 29,700 bbl/d; An atmospheric distillation unit producing 136,000 bbl/d; A vacuum distillation unit producing 47,500 bbl/d; A visbreaking unit producing 22,000 bbl/d; A reforming unit producing 23,400 bbl/d.	Refinery		≈650
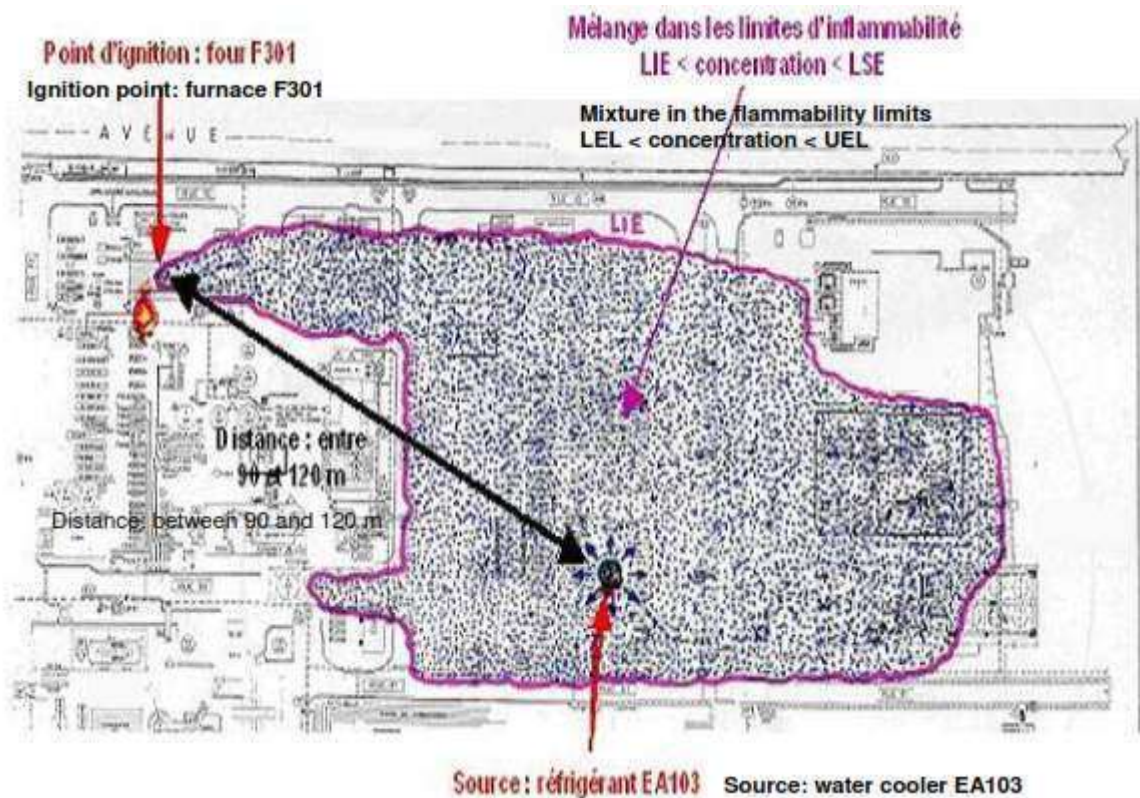
Figure 164: Gas cloud propagation diagram
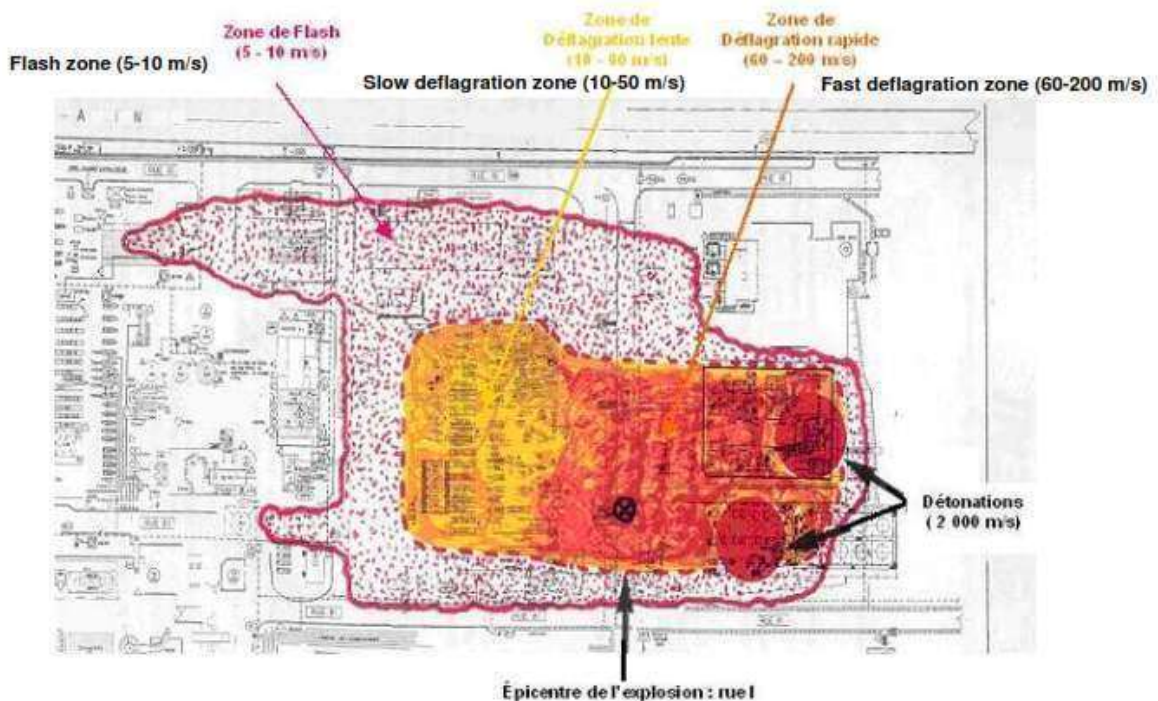
Figure 165: Illustration of the different phases of explosion

The following description has been taken from a research report on the incident (ARIA Report 3969).

Three successive phases could be identified during the initial explosion. The other explosions resulted from the cascade effects.

The initial "flash" travelled at a low speed of around 5 to 12 m/s. Both air blast effect and over pressure was absent as long as the fire front did not encounter an obstacle. The involved surface was around 3,300 m². The flammable volume represented a volume of around 13,500 m³. The first phase can be compared to the functioning of a wick.

The second phase involved the deflagration phenomenon. The presence of a gas concentration gradient within the cloud, disturbances due to the various obstacles and the partial confinement accelerated the slow deflagration into a fast one (speed estimated at approx. 200 m/s) and hastened the UVCE phenomena. The overpressure generated by the deflagration was weak at around 0. 6 bar (9 psi) and the surface in question was approximately 7,200 m². The flammable volume was about 44,000 m³ and contained nearly 3.6 tonnes (7900 lb) of gaseous hydrocarbons.

Lastly, the shock wave from the gas plant compressed the cool gas in the cryogenic unit and amplified by the local phenomena of focusing and reflection, locally triggered one or several detonations (speed > 330 m/s). The weight of the cloud at this stage was relatively low (less than 200 kg or 440 lb of gaseous hydrocarbons). The supersonic spherical waves collided with the propagation of rapid deflagration from the gas plant probably at passage I, the zone designated as the epicentre of the explosion. The over pressure generated is in the order of 2 to 3 bar (29 – 43 psi). The surface in question is estimated at 3,400 m² and the flammable volume represented around 13,500 m³.

Figure 166: Crack in 8" bypass line

The shock wave resulting from the first explosion in its two successive phases shattered structures (positive over pressure – impulse) and then drew in light structures (depression - negative phase). The explosion was accompanied by a rain of debris of which some were projected as far as 135 m (440 ft) from their initial location (such as the fairing of the cooling tower weighing 340 kg or 750 lb). The resulting cascade effects ripped out and destroyed various piping networks, the metal structure of the GT A12 turbo-alternator unit and caused the resulting fire and set fire to the B20 and C24 tanks.

The explosions secondary to the main one resulted from the indirect cascade effects. In fact, some piping networks weakened by the mechanical and/or thermal effects of the initial explosion gave in and resulted in new explosions.

Figure 4 - Vue sur la salle de contrôle à 09h00

Figure 167: View of the control room at 0900 hours

Figure 5 - Vue sur la section cryogénie

Figure 168: View of the cryogenic unit

Figure 6 - Vue sur le bac B20

Figure 169: View of Tank B20
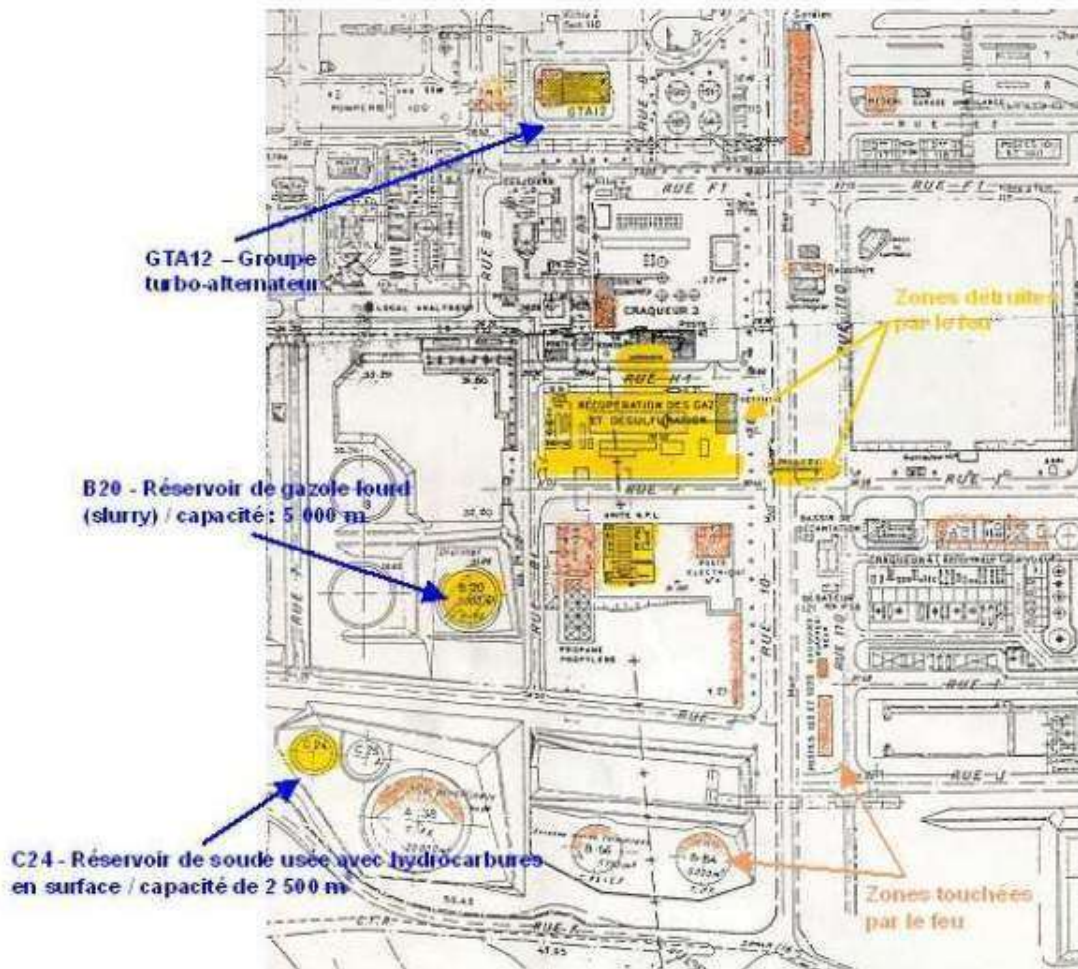
Figure 7 - Illustration des zones sinistrées

Figure 170: Illustration of damage zones

Figure 8 - Installations détruites par l'explosion

Figure 171: Installations destroyed by the explosion

Table 18: Damage observed at La Mede

Table 1
Some damages observed

Observation point	Effects	Incident pressure (kPa)	Distance (m)
Cryogenic unit	mechanical ruptures	50-100	epicentre area
Propene unit	mechanical ruptures and projectile	50-100	epicentre area
Gantry pipe and pipelines	over balancing	40-55	epicentre area
Gas plant	bending of a column	40-70 70	20
Electrical Station 42	all walls breaking down	40-80	35
Electrical Station 40	all walls arched	30-50	50
Locker room	breaking down	30-50	50
Control room	large eardrum rupture	40-90 50	80
Tanks A38, C24, C25, B14, B56	deformation and displacement	15-25	150-170
Technical building	inside, structural damages and glass windows projection	8-12	200
Neighbouring habitations	glass windows breakage	5-7	700
La Mède	about 50% glass windows breakage	2-3	1000-1400
Commercial Center	large windows breakage	1-2	2100
Martigues, Jonquières and Ferrières	more than 10% of windows breakage	1-2	3500-4500
Martigues, LEP lieu-dit Brise-Lames	several windows breakage	1,5-3	3700
Martigues swimmingpool	several bays windows breakages	1,5-3	3900
Châteauneuf-les-Martigues	bay window breakage	0,5-1,1	4000

5.16   NORCO, LOUISIANA

Time and date:	03:37, 5th May 1988
Location	1205 River Rd, Norco, Louisiana, USA
Company	Shell Oil Company
Narrative :	An explosion occurred in the fluid catalytic cracking unit (FCCU) of an oil and gas refinery. The explosion appeared to be the result of corrosion of an 8" vapor line, under 270 psi pressure, which ran from a 10" header that originated as the main overhead vapor line from the depropaniser column. The apparent instantaneous line failure released ≈17,000 pounds of hydrocarbon vapor over around ≈30 seconds. A possible ignition source could have been the unit's superheater furnace. The damage pattern indicated that the explosion was probably an aerial explosion with an epicentre located in the area between the depropaniser and the FCCU control room. 7 employees were killed as a direct result of the blast and a further 19 were injured to varying degrees as a direct result of the explosion.
Incident Cause	Corrosion of an 8" vapor line that originated as the main overhead vapor line from the depropaniser column.
Category Categorize incident cause (e.g. operator error, equipment malfunction, material failure, construction error, design error, weld failure)	Material failure

Source Term	Type of release (e.g. gas, evaporating liquid or a gas-liquid (two phase) flow)	Description of equipment/piping	Hole size or pipe diameter if it was a guillotine failure	Substance(s) released	Release pressure and temperature
	Vapor	8" vapor line		Propane	270 psi (18.6 bar)

Release	Quantity released	Migration of substance from release source	Duration of release
	17,000 pounds		30 seconds

Cloud development	Cloud footprint	Depth and influence of topography under and near the vapor cloud.	Surface roughness	Substance which formed a vapor cloud	Near field dispersion
Weather conditions	Atmospheric stability		Temperature	Wind speed	
	Data from New Orleans Airport (12miles East) Clear		18.3	13.0km/h Northerly	
Ignition	Ignition strength	Source of ignition		Ignition location	
		Superheater furnace			
Explosion severity	Overpressure	Distance of flame travel		Flame speed	
Consequences	Fatalities, injuries, health effects, property damage within and outside of the plant property. Heavy damage – structural collapse Moderate damage- cladding loss, cracking of vulnerable masonry, purlin deformation Light damage - cladding damage, window breakage,			Blast damage to plant and other structures within and outside of cloud footprint.	
	7 employees killed, 19 injured				

Mitigating Measures	Cloud mitigation measures	Performance and/or reasons for poor performance		
	Vapor barrier surrounding site	Not known if present		
	On-site vapor fencing	Not known if present		
	Active vapor dispersal	Not known if present		
Facility Information	Other Hydrocarbons at Facility	Quantity stored (is amount >10,000 lbs?)	Type of storage vessel/container	End product or used for a process

|	Gasoline Ethylene Ethane Propane Isobutane Butane Methyl ethyl ketone Secondary butyl alcohol Crude epichlorohydrin			End product End product
	Characteristics of the area where the event occurred	Urban, rural, suburban	Industrial, residential	Proximity to ports/marine
	Immediately adjacent to town of Norco	Urban	Residential	Inland but next to Mississippi river
	Facility description	Category (refinery, petrochemical, gas processing, terminal and distribution, upstream)		Number of similar facilities worldwide
	Refines crude oil into petroleum products and had a capacity of 220,000 barrels-per-day	Refinery		≈650
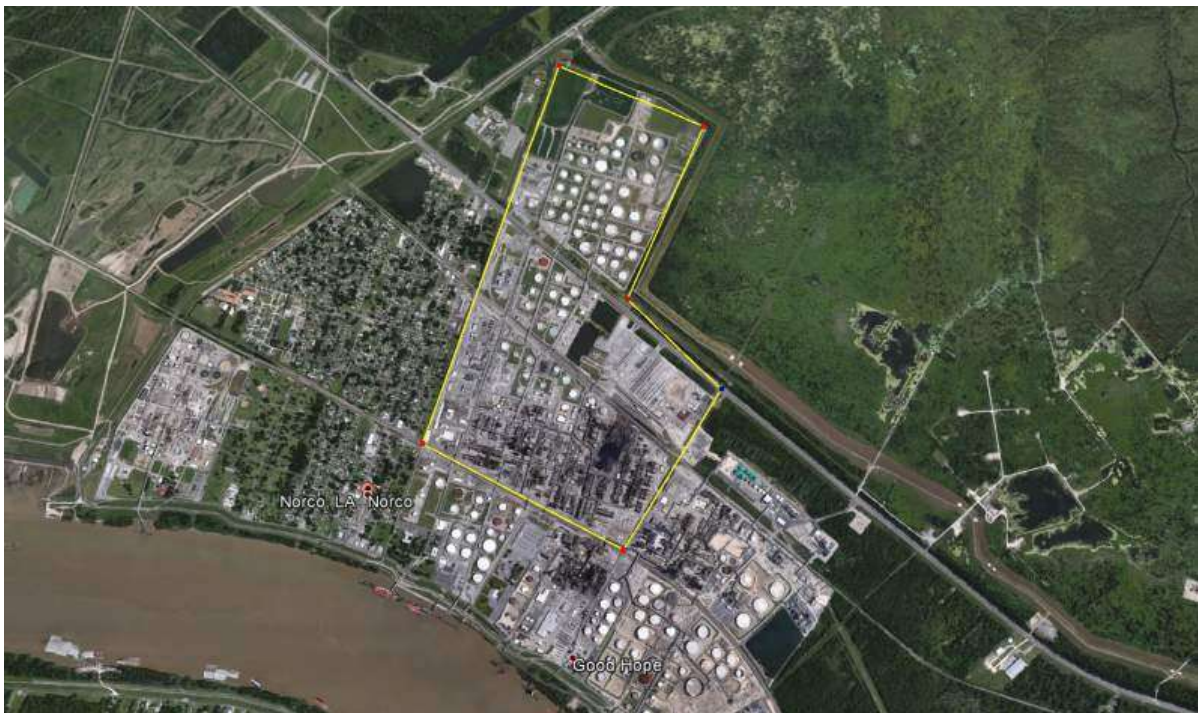
Figure 172: Site boundary

Figure 173: Explosion damage

Hourly Weather History & Observations

Time(CDT)	Temp.	Dew Point	Humidity	Pressure	Wind Dir	Wind Speed	Conditions
12:00 AM	**21.1** °C	**13.9** °C	63%	**1019.3** hPa	North	**16.7** km/h /**4.6** m/s	Clear
1:00 AM	**20.0** °C	**13.3** °C	65%	**1019.4** hPa	North	**14.8** km/h /**4.1** m/s	Clear
2:00 AM	**19.4** °C	**12.8** °C	66%	**1019.4** hPa	NNW	**13.0** km/h /**3.6** m/s	Clear
3:00 AM	**18.3** °C	**12.8** °C	70%	**1019.2** hPa	North	**13.0** km/h /**3.6** m/s	Clear
4:00 AM	**18.3** °C	**12.8** °C	70%	**1019.3** hPa	North	**11.1** km/h /**3.1** m/s	Clear
5:00 AM	**17.2** °C	**13.3** °C	78%	**1019.8** hPa	NNW	**9.3** km/h /**2.6** m/s	Clear
6:00 AM	**15.6** °C	**12.8** °C	83%	**1020.1** hPa	North	**9.3** km/h /**2.6** m/s	Clear
7:00 AM	**15.6** °C	**13.3** °C	86%	**1020.7** hPa	NW	**7.4** km/h /**2.1** m/s	Clear
8:00 AM	**21.1** °C	**14.4** °C	65%	**1021.2** hPa	NNE	**13.0** km/h /**3.6** m/s	Clear
9:00 AM	**23.3** °C	**13.3** °C	53%	**1021.5** hPa	NNW	**13.0** km/h /**3.6** m/s	Clear
10:00 AM	**24.4** °C	**11.7** °C	45%	**1021.8** hPa	NNW	**14.8** km/h /**4.1** m/s	Clear
11:00 AM	**25.0** °C	**12.2** °C	45%	**1022.0** hPa	NW	**18.5** km/h /**5.1** m/s	Clear
12:00 PM	**25.6** °C	**12.2** °C	43%	**1021.8** hPa	NW	**22.2** km/h /**6.2** m/s	Clear
1:00 PM	**26.1** °C	**11.1** °C	39%	**1021.4** hPa	NW	**14.8** km/h /**4.1** m/s	Clear
2:00 PM	**27.2** °C	**10.6** °C	35%	**1020.9** hPa	North	**24.1** km/h /**6.7** m/s	Clear
3:00 PM	**27.2** °C	**10.6** °C	35%	**1020.4** hPa	North	**22.2** km/h /**6.2** m/s	Clear
4:00 PM	**27.8** °C	**10.6** °C	34%	**1019.6** hPa	NNW	**22.2** km/h /**6.2** m/s	Clear
5:00 PM	**27.8** °C	**11.7** °C	37%	**1019.3** hPa	NW	**18.5** km/h /**5.1** m/s	Clear
6:00 PM	**26.7** °C	**10.6** °C	36%	**1019.1** hPa	NW	**18.5** km/h /**5.1** m/s	Clear
7:00 PM	**25.6** °C	**11.1** °C	40%	**1019.0** hPa	WNW	**16.7** km/h /**4.6** m/s	Clear
8:00 PM	**22.2** °C	**12.2** °C	53%	**1019.2** hPa	NNW	**13.0** km/h /**3.6** m/s	Clear
9:00 PM	**21.1** °C	**12.2** °C	57%	**1019.8** hPa	NW	**11.1** km/h /**3.1** m/s	Clear
10:00 PM	**18.3** °C	**13.9** °C	75%	**1020.3** hPa	NNW	**7.4** km/h /**2.1** m/s	Clear
11:00 PM	**16.7** °C	**11.7** °C	72%	**1020.4** hPa	North	**5.6** km/h /**1.5** m/s	Clear
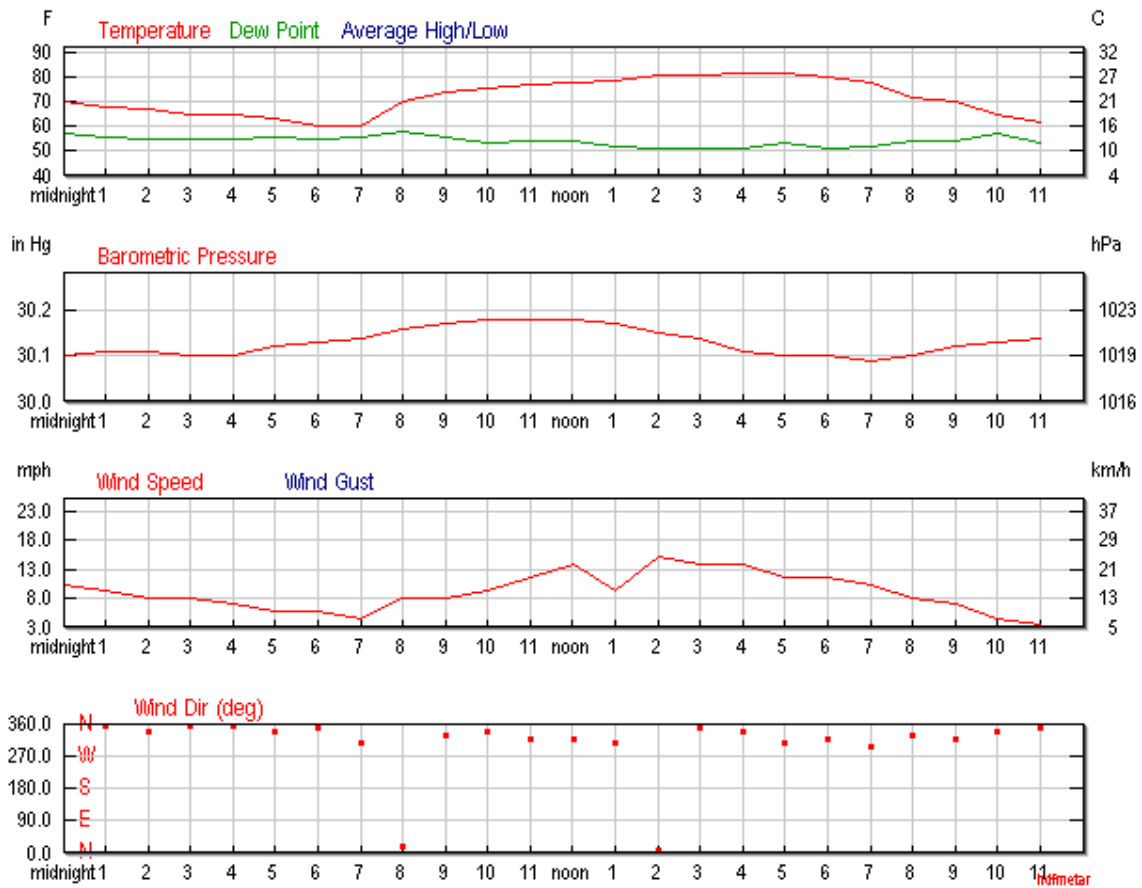
Figure 174: Daily Weather History Graph

5.17   PASADENA, TEXAS

Time and date:	≈13:00 23rd October 1989
Location	Phillips Petroleum Houston Chemical Complex, Pasadena, Texas, USA
Company	Phillips Petroleum
Narrative :	During the course of operations at the Phillips Petroleum Houston Chemical Complex in Pasadena, Texas, on October 23, 1989, an explosion and ensuing fire occurred which resulted in 23 known dead and one missing. In addition, more than 100 other people were injured in varying degrees. Metal and concrete debris was found as far as six miles away following the explosion.
Incident Cause	The release was attributed to the accidental opening of an un-blanked process line to atmosphere during maintenance. This accidental opening was a result of deviation from well understood and established procedures. It was established that Phillips corporate safety procedures and standard industry practice require backup protection in the form of a double valve or blind flange insert whenever a process or chemical line in hydrocarbon service is opened. Phillips, however, at the local plant level, had implemented a special procedure for this maintenance operation which did not incorporate the required backup.
Category Categorize incident cause (e.g. operator error, equipment malfunction, material failure, construction error, design error, weld failure)	Operator error

Source Term	Type of release (e.g. gas, evaporating liquid or a gas-liquid (two phase) flow)	Description of equipment/piping	Hole size or pipe diameter if it was a guillotine failure	Substance(s) released	Release pressure and temperature
	Gas	Settling leg No.4 of Plant V, reactor 6	10" pipe diameter	Ethylene and/or isobutene	700psi (48barg)

Release	Quantity released	Migration of substance from release source	Duration of release	
	85,000lbs		Thought to be 60-90 seconds	

Cloud development	Cloud footprint	Depth and influence of topography under and near the vapor cloud.	Surface roughness	Substance which formed a vapor cloud	Near field dispersion
				Ethylene and/or isobutene	

Weather conditions	Atmospheric stability		Temperature	Wind speed
	Data from Ellington Field, TX (12km South)		30degC	≈18km/h 0km/hr until 10am

Ignition	Ignition strength	Source of ignition	Ignition location
		Unknown	

Explosion severity	Overpressure	Distance of flame travel	Flame speed
	4.0 on the Richer scale		

Consequences	Fatalities, injuries, health effects, property damage within and outside of the plant property. Heavy damage – structural collapse Moderate damage- cladding loss, cracking of vulnerable masonry, purlin deformation Light damage - cladding damage, window breakage,	Blast damage to plant and other structures within and outside of cloud footprint.
	23 fatalities 314 injured Heavy damage – 750ft Moderate damage – Light damage – 3-4miles Property damage estimated at $1.4 billion	Severe damage to plant although specifics are not known

Mitigating Measures	Cloud mitigation measures	Performance and/or reasons for poor performance
	Vapor barrier surrounding site	Not known if present
	On-site vapor fencing	Not known if present
	Active vapor dispersal	Not known if present

Facility Information	Other Hydrocarbons at Facility	Quantity stored (is amount >10,000 lbs?)	Type of storage vessel/container	End product or used for a process
	Characteristics of the area where the event occurred	Urban, rural, suburban	Industrial, residential	Proximity to ports/marine
	Situated on banks of Buffalo bayou, flat wetland	Suburban	Industrial	Next to Buffalo bayou, 15km from closest port
	Facility description	Category (refinery, petrochemical, gas processing, terminal and distribution, upstream)		Number of similar facilities worldwide
	Polyethylene plant	Petrochemical		
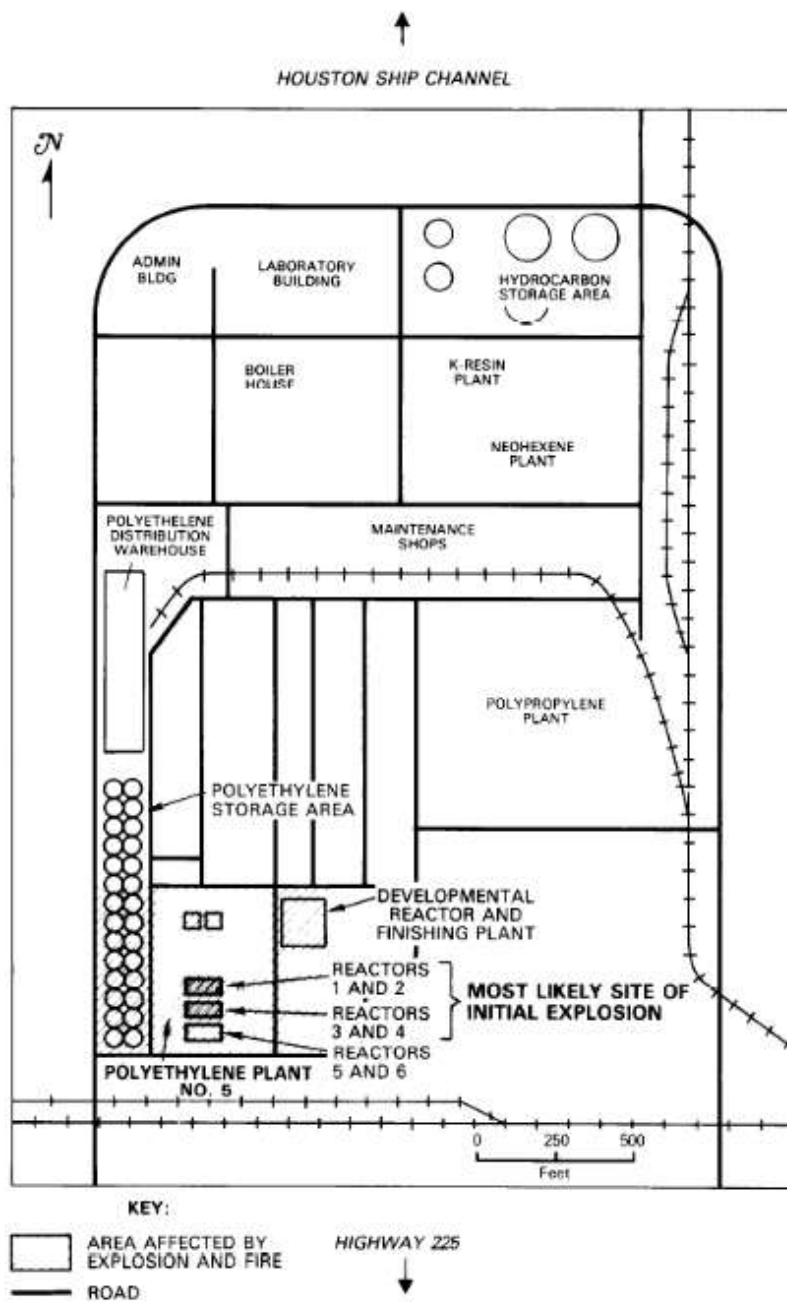
Figure 175: Site plan
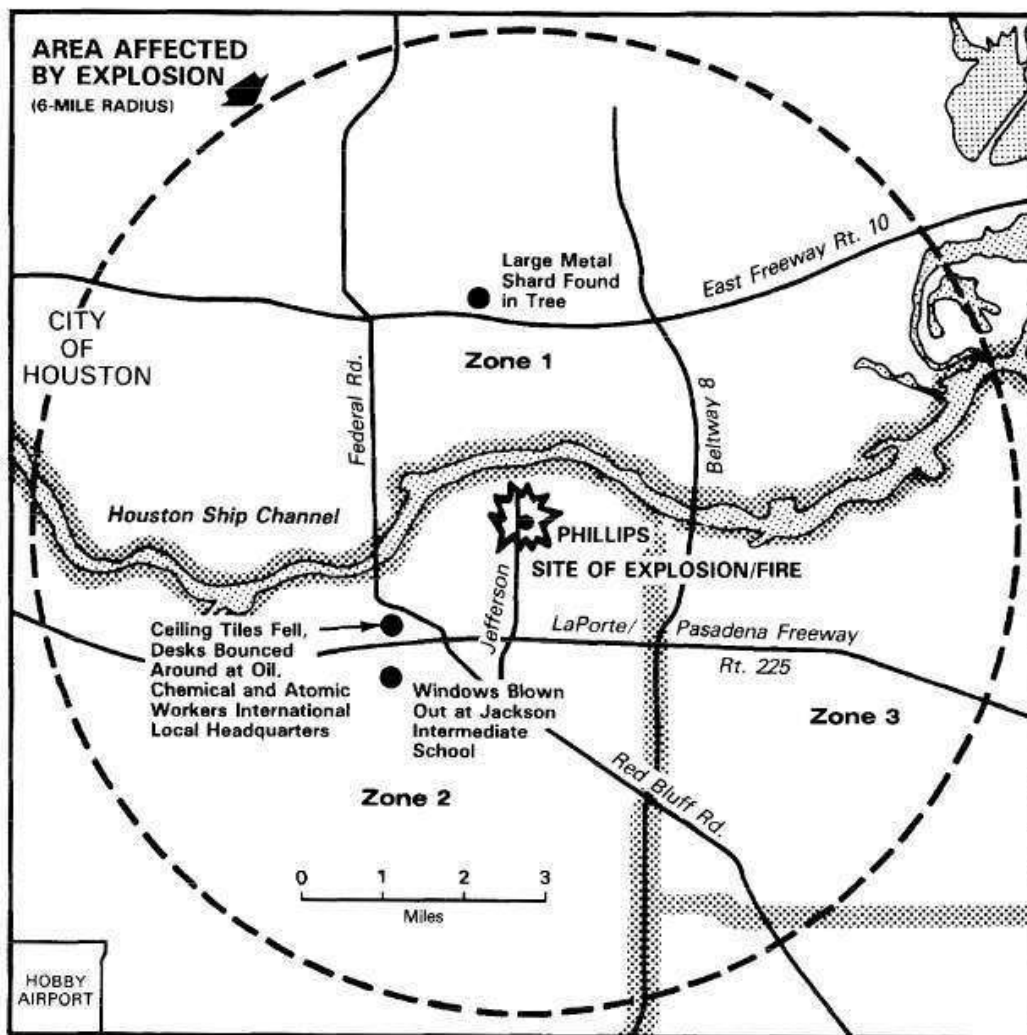
Figure 176: Area affected by explosion

Figure 177: Site boundary

1. Aerial view of the Phillips plant taken prior to the explosion.

Figure 178: Aerial view prior to incident

2. Aerial photo of complex as seen from north to south. Arrow at top points to the north edge of the staging area for responding mutual aid equipment. Arrow pointing to building shows were GATX terminal Chief Goyer was located when blast occurred. Area of origin thought to be near center (arrow).

Figure 179: Explosion damage: View North to South

3. Aerial photo of complex as seen from east to west. Arrow points to berm to west of the property. This appears to actually be a bank for a large holding pond but served well as a protective berm.

Figure 180: Explosion damage: View East to West

7. View from south to north. Personnel and equipment near structure are working on victim recovery.

Figure 181: Explosion damage: View South to North

9. View from southwest corner toward north/northeast. Metal fatigue clearly visible in remaining superstructure.

Figure 182: Explosion damage: View towards North/Northeast
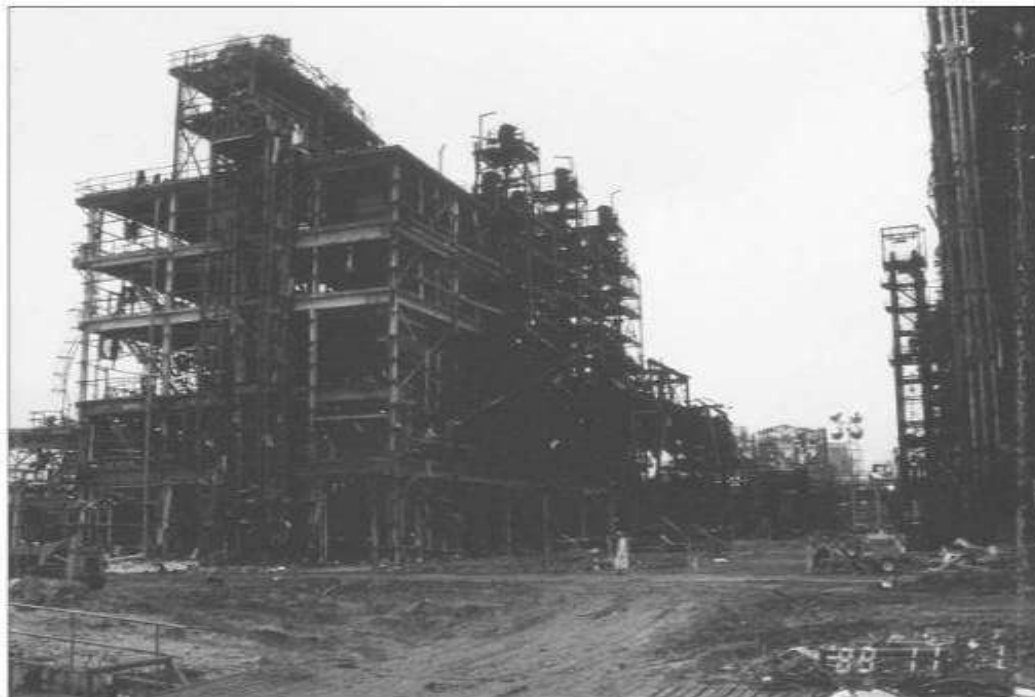
11. View is from south to north. Cleared area is to the west side of the tower. The cleared area in the center was designed in a like manner to the left side of this frame before the explosion.

Figure 183: Explosion damage: View South to North

12. View of tower and cleared area from south to north. The tower was listing to the west and north and was reported to be approximately 14 degrees out of plumb.

Figure 184: Explosion damage: View of tower

16. View of the plant from west to east. This view has the south side to the right.

Figure 185: Explosion damage: View of plant West to East

18. Silo holding areas to the northwest of the main blast area. The blast wave partially flattened the silo sides.

Figure 186: Explosion damage: Silo area

Hourly Weather History & Observations

Time(CDT)	Temp.	Dew Point	Humidity	Pressure	Wind Dir	Wind Speed	Conditions
12:00 AM	**18.3** °C	**15.0** °C	81%	**1022.4** hPa	South	**7.4** km/h /**2.1** m/s	Clear
1:00 AM	**18.3** °C	**15.0** °C	81%	**1022.1** hPa	South	**5.6** km/h /**1.5** m/s	Clear
2:00 AM	**18.3** °C	**15.0** °C	81%	**1022.1** hPa	Calm	Calm	Clear
3:00 AM	**17.2** °C	**15.0** °C	87%	**1021.7** hPa	Calm	Calm	Clear
4:00 AM	**17.2** °C	**15.0** °C	87%	**1021.4** hPa	Calm	Calm	Clear
5:00 AM	**16.7** °C	**15.0** °C	90%	**1021.4** hPa	Calm	Calm	Clear
6:00 AM	**17.2** °C	**15.0** °C	87%	**1021.7** hPa	Calm	Calm	Clear
7:00 AM	**16.7** °C	**15.0** °C	90%	**1022.4** hPa	Calm	Calm	Scattered Clouds
7:19 AM	-	-	N/A%	**1022.6** hPa	Calm	Calm	Scattered Clouds
8:00 AM	**17.2** °C	**15.0** °C	87%	**1022.9** hPa	Calm	Calm	Scattered Clouds
9:00 AM	**23.3** °C	**17.8** °C	71%	**1023.6** hPa	ESE	**1.9** km/h /**0.5** m/s	Mostly Cloudy
10:00 AM	**27.2** °C	**18.3** °C	58%	**1024.1** hPa	SSE	**14.8** km/h/ **4.1** m/s	Scattered Clouds
11:00 AM	**28.3** °C	**17.8** °C	53%	**1024.1** hPa	SSE	**14.8** km/h/ **4.1** m/s	Mostly Cloudy
12:00 PM	**28.3** °C	**17.2** °C	51%	**1023.7** hPa	South	**16.7** km/h/ **4.6** m/s	Mostly Cloudy
1:00 PM	**30.6** °C	**17.2** °C	44%	**1022.9** hPa	SSE	**18.5** km/h/ **5.1** m/s	Mostly Cloudy
2:00 PM	**31.1** °C	**16.1** °C	40%	**1021.9** hPa	SE	**18.5** km/h/ **5.1** m/s	Scattered Clouds
3:00 PM	**31.1** °C	**16.1** °C	40%	**1021.4** hPa	SSE	**18.5** km/h/ **5.1** m/s	Scattered Clouds
4:00 PM	**30.0** °C	**15.6** °C	41%	**1021.2** hPa	SSE	**16.7** km/h/ **4.6** m/s	Scattered Clouds
5:00 PM	**29.4** °C	**15.0** °C	41%	**1021.6** hPa	SSE	**18.5** km/h/ **5.1** m/s	Scattered Clouds

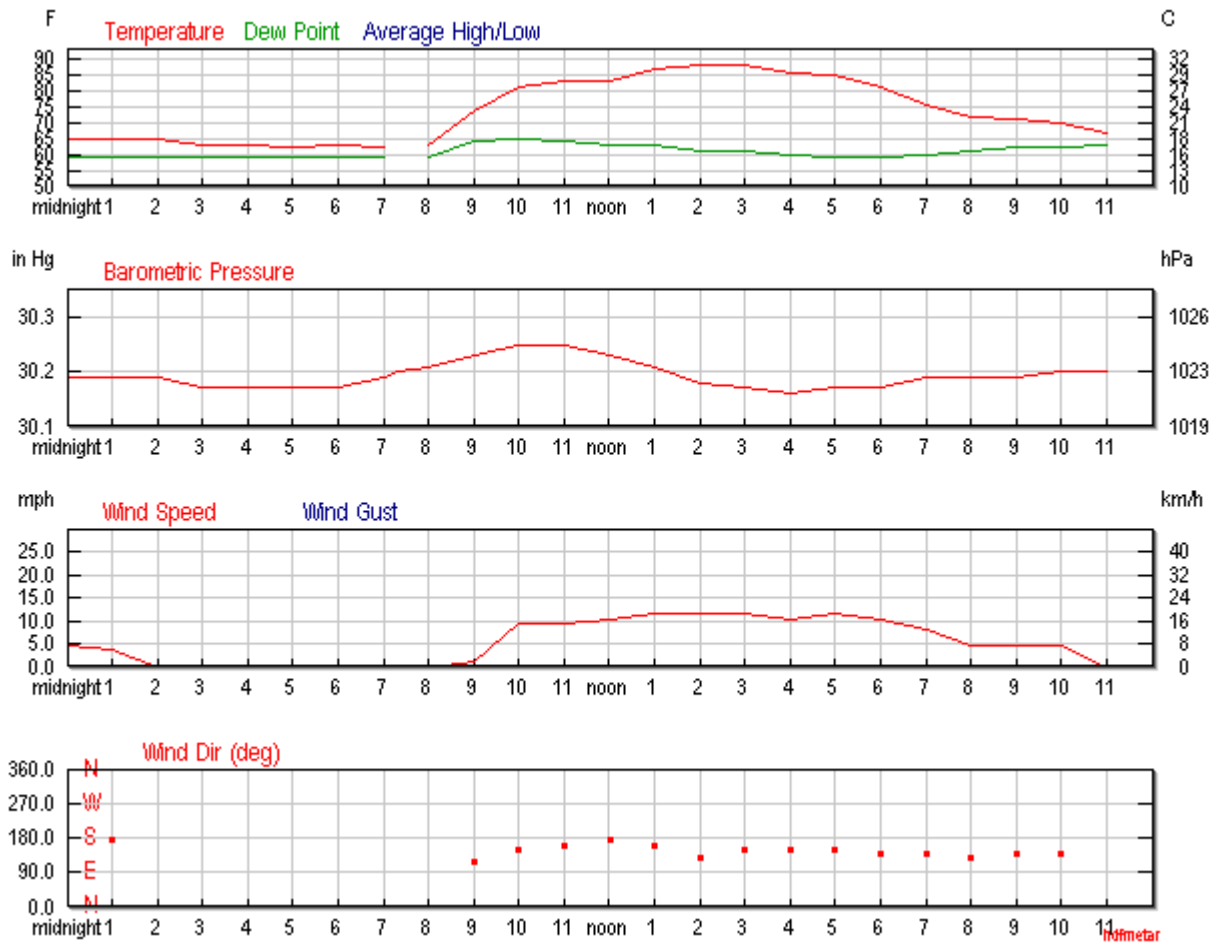| Time(CDT)	Temp.	Dew Point	Humidity	Pressure	Wind Dir	Wind Speed	Conditions
6:00 PM	27.2 °C	15.0 °C	47%	1021.6 hPa	SE	16.7 km/h/ 4.6 m/s	Scattered Clouds
7:00 PM	24.4 °C	15.6 °C	58%	1022.1 hPa	SE	13.0 km/h/ 3.6 m/s	Scattered Clouds
8:00 PM	22.2 °C	16.1 °C	68%	1022.2 hPa	SE	7.4 km/h /2.1 m/s	Mostly Cloudy
9:00 PM	21.7 °C	16.7 °C	73%	1022.4 hPa	SE	7.4 km/h /2.1 m/s	Scattered Clouds
10:00 PM	21.1 °C	16.7 °C	76%	1022.7 hPa	SE	7.4 km/h /2.1 m/s	Scattered Clouds
11:00 PM	19.4 °C	17.2 °C	87%	1022.7 hPa	Calm	Calm	Scattered Clouds

Figure 187: Daily Weather History Graph

5.18   SKIKDA, ALGERIA

Time and date:	18:40, 19th January 2004
Location	Skikda LNG Plant, Skikda, Algeria
Company	Sonatrach
Narrative :	On January 19th, 2004, Unit 40 at the Skikda LNG plant exploded. Within seconds, the adjacent Units 20 and 30 also exploded in an apparent chain reaction. The blast spread outward, damaging surrounding structures and facilities — including a nearby power plant, one of the berths at the Skikda harbour and numerous homes and other buildings in the community.
Incident Cause	A leak (probably mixed refrigerants) occurred in the semi-confined area between train 40's control room, boiler, and the liquefaction area.The air intake to the boiler's firebox ingested the fuel-air mix, causing more heat to be generated within the boiler and raising the internal pressure. After the boiler's pressure relief valve activated, and the operators turned off the supply fuel to the boiler, the air intake fan ingested hydrocarbon/air mixture within the flammable limits, which led to an explosion within the boiler. Access to primary evidence is limited but photographs of crushed cars similar to those at other VCEs suggests that a severe explosion was sustained into open areas.
Category Categorize incident cause (e.g. operator error, equipment malfunction, material failure, construction error, design error, weld failure)	Not known

Source Term	Type of release (e.g. gas, evaporating liquid or a gas-liquid (two phase) flow)	Description of equipment/piping	Hole size or pipe diameter if it was a guillotine failure	Substance(s) released	Release pressure and temperature
	Evaporating liquid/gas	Either: Fuel gas exchanger, fuel gas compressor, fuel gas flash drum or LNG pumps		Probably LPG	
Release	Quantity released	Migration of substance from release source	Duration of release		

Cloud development	Cloud footprint	Depth and influence of topography under and near the vapor cloud.	Surface roughness	Substance which formed a vapor cloud	Near field dispersion
				Probably LPG	

Weather conditions	Atmospheric stability		Temperature	Wind speed
	Calm			Nil wind

Ignition	Ignition strength	Source of ignition	Ignition location
		Gas/steam explosion/flame in boiler	Boiler

Explosion severity	Overpressure	Distance of flame travel	Flame speed

Consequences	Fatalities, injuries, health effects, property damage within and outside of the plant property. Heavy damage – structural collapse Moderate damage- cladding loss, cracking of vulnerable masonry, purlin deformation Light damage - cladding damage, window breakage,	Blast damage to plant and other structures within and outside of cloud footprint.
	26 employees killed 74 injured Heavy damage – 0.1km Moderate damage – 1km Light damage – 2km	Damage to trains 30 and 20 in operation Subsequent fires within plant

Mitigating Measures	Cloud mitigation measures	Performance and/or reasons for poor performance
	Vapor barrier surrounding site	Not known if present
	On-site vapor fencing	Not known if present
	Active vapor dispersal	Not known if present

Facility Information	Other Hydrocarbons at Facility	Quantity stored (is amount >10,000 lbs?)	Type of storage vessel/container	End product or used for a process
	LNG	308,000 m^3		End product
	Characteristics of the area where the event occurred	Urban, rural, suburban	Industrial, residential	Proximity to ports/marine
	Flat land on coast with mountains to south	Suburban	Industrial	Next to port
	Facility description	Category (refinery, petrochemical, gas processing, terminal and distribution, upstream)		Number of similar facilities worldwide
	LNG liquefaction plant	Gas processing		17 (at time of incident)

Figure 188: View of plant before incident

Figure 189: Site boundary

Figure 190: Plan of surrounding area
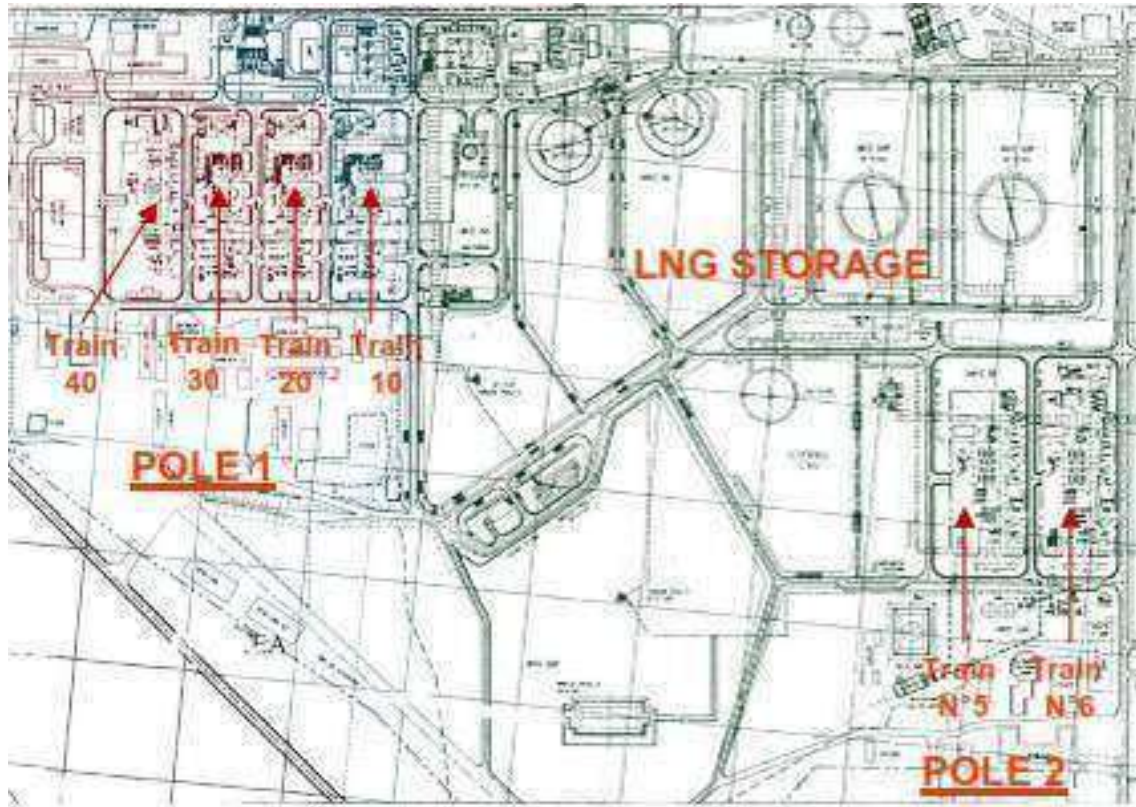
Figure 191: More detail plan of LNG liquefaction and storage

Figure 192: Trains on fire
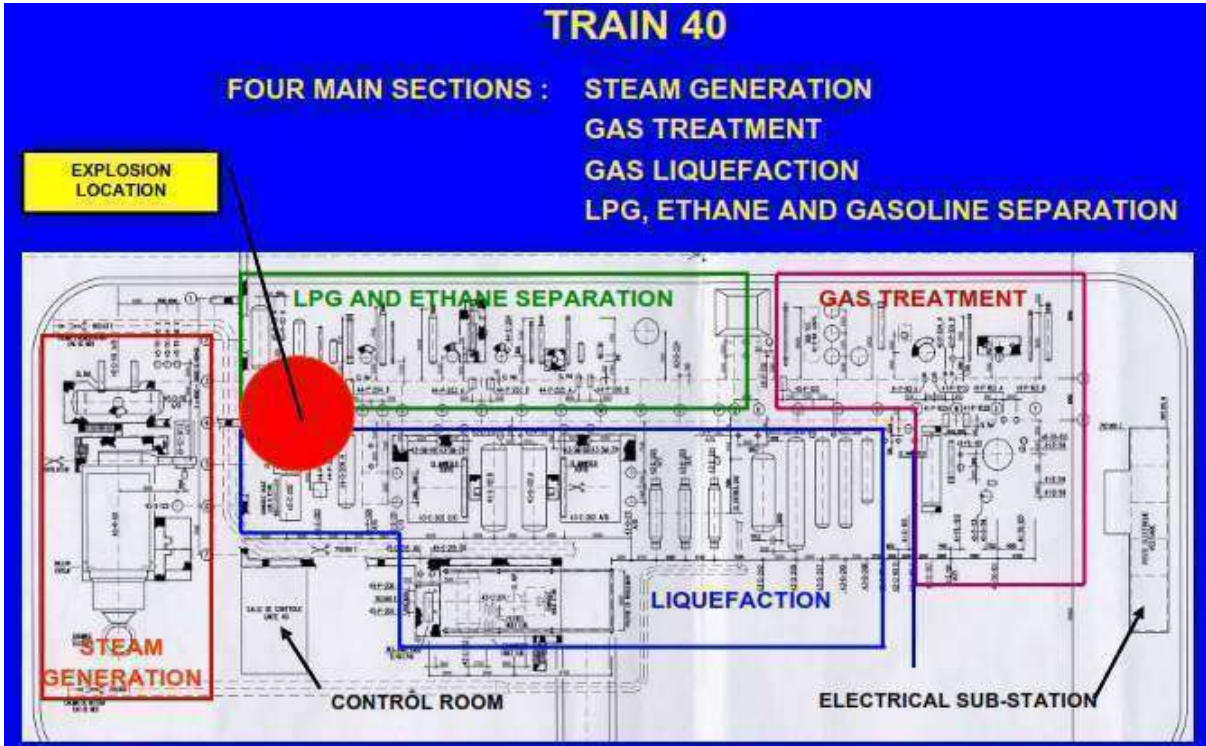
Figure 193: Liquefaction train process diagram
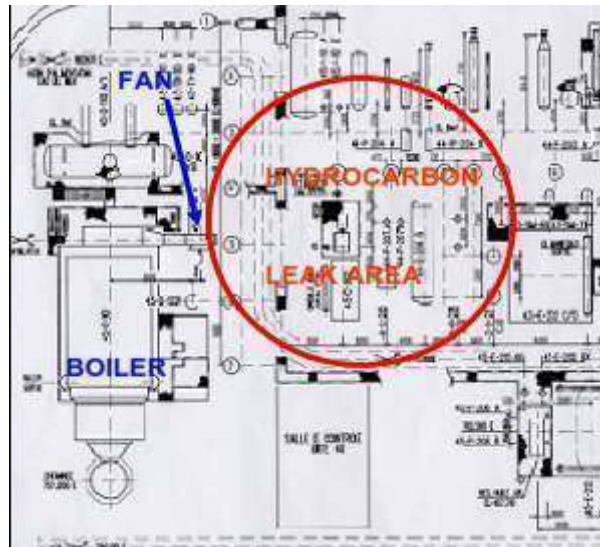
Figure 194: Leak area
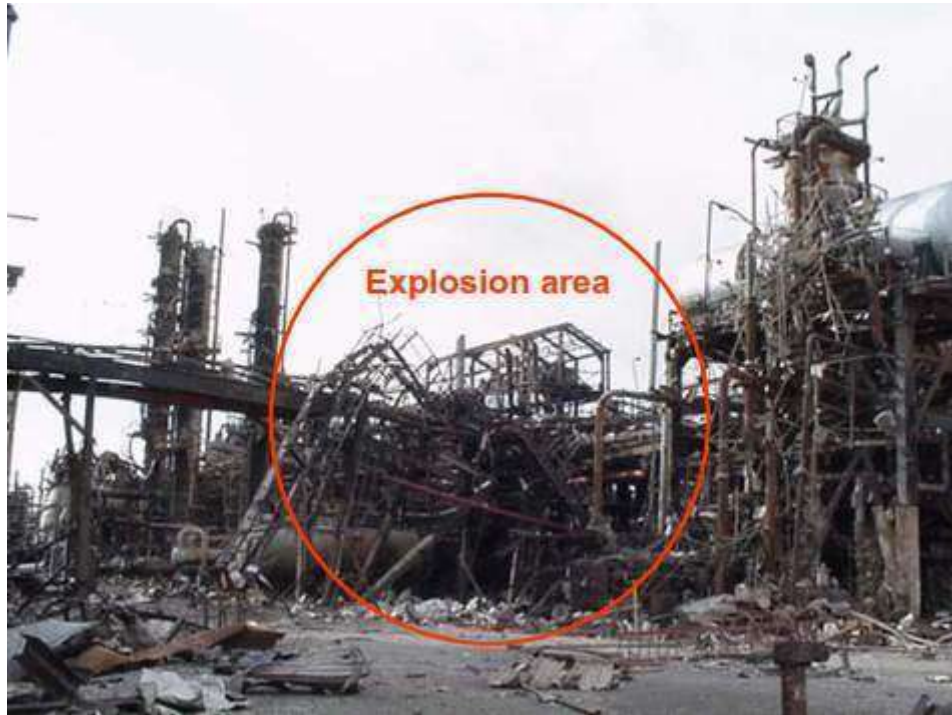
Figure 195: Train 40 after incident

Figure 196: Damage areas off-site
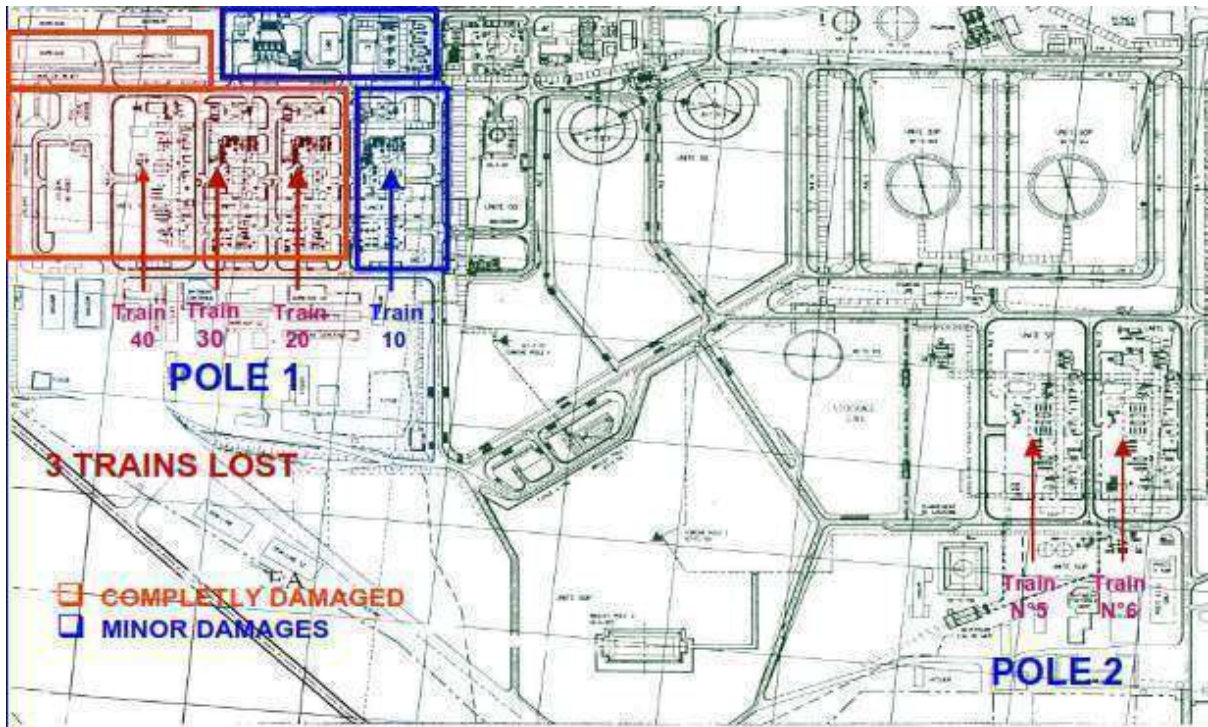
Figure 197: Damage in LNG plant

Figure 198: Train 40 and part of Train 30

Figure 199: Train 40 and part of Train 30

Figure 200: Collapsed maintenance building near Train 40

Figure 201: Damage to plant

5.19 LPG PIPELINE AND STORAGE INCIDENTS

HSE have published a review of U.S. pipeline incidents 1970 – 2000 (Casella 2002). This includes a section on flashing liquids most of which were LPG. Of 12 major incidents in this category, investigated by the NTSB, 8 incidents involved delayed ignition and the development of a vapor cloud.

A summary of these 8 incidents is shown in Table 19.

Table 19: Summary of 8 US pipeline incidents 1970 - 2000

| Location	Time	Release	Wind	Ignition delay (mins)	VCE/ Flash	Burn area
Austin, Texas	22nd Feb 1973,	1.5"Gap (10.7 " pipe)	Nil	10-15	Flash	720 x 18m Downhill - along a roadway.
Brenham, Texas	7th April 1992	Storage cavern overfill	Nil	~30	VCE	Equivalent Radius about 450m
North Blenheim, NY	March 13th 1990	¾" gap (8.6" pipe)	Nil	<10	Flash	Approx 1000m x 150m Downhill - along a valley
Donnellson, Iowa	4th August 1978	33" Rupture (8.6" pipe)	Nil[1]	A few	Flash	Equivalent radius about 350 m
Ruff Creek Pennsylvania	July 20th 1977	10" x 3/16"" Crack (12.7" pipe)	Nil	90	Flash	1200 m x 90m Downhill – along a valley
Devers, Texas	12th May 1975	70" Rupture (8.6" pipe)	2.2 m/s	7	Flash	305m (cross wind) 244 m (downwind)
Lively , Texas	August 24th 1996	13" rupture (8.6 " pipe)	2 m/s	15	Flash	450m x 90m (cloud spread approximately perpendicular to wind direction)
Port Hudson, Missouri	9th December 1970	80" x 4"Crack (8.6" pipe)	2.5m/s [2]	22	VCE	Approx 500m (downwind/downhill) x 150m

[1] Based on cloud shape and wind records at Des Moines
[2] May have been nil because of local topography. The cloud was confined in a valley – but this led away from the source in approximately the same direction as the (light) wind at altitude.

Remarkably 5 of these 8 incidents occurred in nil wind conditions. All of the other 3 incidents occurred in low winds and clearly showed the effects of terrain: in 2 cases (Devers,TX and Lively, TX) the cloud spread further in a cross-wind direction than in the direction of the wind. The single case (Port Hudson) in which the cloud spread roughly downwind, this direction also corresponded to a downhill direction into a pronounced valley –witnesses described the cloud accumulating in this valley. Given the season and time of the release it is highly likely that the wind speed in this valley was in fact nil.

Page | 253

Only 2 of these incidents caused vapor cloud explosions whilst 6 were consistent with flash fires. This contrasts with gasoline overfill incidents where all of the recorded incidents that caused very large clouds (cloud radius > 200m) have resulted in explosions.

Part of the reason for this difference may be the potential for very rich clouds to be formed in low wind speed conditions for an LPG release. It is difficult to distinguish between a flash fire that (initially) progresses over the top of a rich cloud and a flash fire in a pre-mixed cloud that is flammable through its full depth.

Dispersion in all of the 8 cases listed in Table 19 involved vapor movement with entrainment heavily restricted by buoyancy effects. Four of the six flash fires involved nil/low-wind dispersion in which the cloud concentration is likely to have been quite similar and potentially above the UFL over a wide area.

HSE Research Report RR036 also provides estimates of release rate for the incidents. In nil wind cases where the depth and homogeneity of the cloud can be estimated, the reported cloud sizes are consistent with very rich (>UFL) mixtures. A review of dispersion in these cases would be useful and is planned by HSE.

Overall the incident history suggests that large clouds are generally associated with very light or zero winds. If such a cloud develops the risk of a VCE is probably less than 50%. It may be that there is a significant probability that, even if a large LPG cloud accumulates in very light or nil wind conditions, it will be too rich to undergo transition to a VCE. This is clearly of relevance to the assessment of risk at LNG sites.

6 DISCUSSION RELEVANT TO VAPOR CLOUD DEVELOPMENT

6.1 INCIDENTS IN NIL/LOW-WIND CONDITIONS

An important finding from the review is that a high proportion of vapor cloud incidents occurred in nil/low wind conditions. By the term "nil/low wind" we mean a wind that was so weak close to the ground that it did not significantly affect the gravity driven transport of released vapor. Rather than moving downwind, the vapor in these cases spread out in all directions and or followed any downward slopes around the source.

The dispersion conditions in the incidents reviewed are summarised in Table 20.

In 50% of the cases (12/24) there is clear evidence from the well-documented transport of vapor in all directions and/or meteorological records that the vapor cloud formed in nil/low-wind conditions.

In a further 21% (5/24), the pattern of vapor transport suggests nil/low-wind conditions but there is insufficient data available to be sure.

In the remaining 29% (7/24) vapor dispersion appears to have occurred in light or moderate winds. These tend to be very large releases that were ignited very quickly.

At first sight these results are surprising because nil/low-wind weather conditions are relatively rare: in the UK they usually correspond to stable conditions that develop at night in high pressure weather systems. The overall frequency is around 5%. This frequency will vary on a site by site basis around the world but the frequency is always fairly low. Notwithstanding such low frequencies, incidents in nil/low wind conditions apparently make up the majority of historical records of the most serious VCEs.

One explanation for this is that a wider range of smaller losses of containment (with much higher frequency) have the potential to cause a disaster in these conditions, if the releases are not stopped and the vapor is allowed to accumulate around the source.

The potential importance of nil/low-wind conditions in an overall risk assessment is illustrated by results shown in Table 21 and Table 22. This is a simple test case of 2" liquid release from a 30,000 gallon tank containing propane at 288K. Windy dispersion modelling used DRIFT[7]. In nil/low-wind case the average cloud depth was assumed to be 2m.

In windy conditions - F2 and D5 in the Pasquill classification scheme (Pasquill 1961) - the contour defining the lower flammable limit (LFL) reaches a maximum extent within a period of less than 100 seconds. In nil/low-wind conditions the cloud continues to grow throughout the time that the tank takes to empty (which is 350 -1500 seconds).

If the density of ignition sources is constant in the area around the tank, the chances of ignition in nil/low-wind conditions will be much greater for this type of release – because the area covered by the cloud is much larger. This illustrates why nil/low-wind conditions dominate records of major vapor cloud incidents even though the weather frequency is low.

---

[7] *www.hse.gov.uk/research/rrhtm/rr629.htm*

Table 20: Summary of vapor transport conditions in the incidents reviewed

(mass release rates/durations included for non-pipeline failures – where known)

Incidents that occurred in nil/low–wind conditions		Vapor release rate (kg/s)	Duration prior to igniton (s)
Brenham, TX	LPG Storage	100	3600
Newark, NJ	Gasoline storage	35	>900
Big Spring, TX	Refinery	NK	NK
San Juan, Puerto Rico	Gasoline storage	50	1560
Skikda, Algeria	LNG facility	~10	<300s
Buncefield, UK	Gasoline storage	19	1380
Amuay, Venezuela	Refinery LPG storage	67	4080
Jaipur	Gasoline storage	34	4500
Austin , TX	LPG pipeline		
North Blenheim, NY	LPG pipeline		
Donnellson, IA	LPG pipeline		
Ruff Creek, PA	LPG pipeline		
Incidents that probably occurred in nil/low-wind conditions			
Port Hudson, MO	LPG pipeline		
St Herblain, France	Gasoline storage	NK	1200
Geismer, LA	Petrochemicals	NK	
Naples, Italy	Gasoline storage	20	5400
La Mede, France	Refinery	25	600
Incidents that occurred in light or moderate winds			
Baton Rouge, LA	Refinery	681	150
Norco, LA	Refinery	257	30
Pasadena, CA	HDPE	643	60
Flixborough, UK	Petrochemicals	670	45
Devers, TX	LPG Pipeline		
Lively, TX	LPG Pipeline		
Ufa, USSR	LPG Pipeline		

Table 21: Approximate vapor cloud size (2" horizontal release aligned with wind)

30,000 gallon tank containing propane at 288K. Release rate 32kg/s (507 gpm)

	Weather	Area (acres) above LFL Calculated with DRIFT
	F2	2.5
	D5	0.74
	Nil/low wind	151

Table 22: Approximate vapor cloud size (2" vertical release)

30,000 gallon tank containing propane at 288K, Release rate 32kg/s (507 gpm)

	Weather	Area (acres) above LFL Calculated with DRIFT
	F2	0.14
	D5	nil
	Nil/low wind	151

This study suggests that risk assessments and emergency planning should consider the potential for releases in nil/low wind conditions. Although these conditions are relatively rare, a much wider range of releases can cause large clouds with a high risk of ignition.

6.2   WHAT COUNTS AS NIL/LOW-WIND?

Normally nil/low-wind conditions develop in stably stratified atmospheric conditions and are easily recognised. The density gradient near the ground is sufficient to suppress turbulent mixing in the lowest part of the atmosphere. This occurs when the Richardson number is greater than about 0.25.

$$Ri = \frac{g\Delta\rho h}{\rho_0 u^2} > 0.25$$

$\Delta\rho$ is the (total) density difference across the stably stratified boundary layer

ρ_0 is the ambient density

h is the depth of the stable layer

Page | 257

u is the speed of the overlying airflow

g is the gravitational acceleration

This is illustrated by Figure 202which shows momentum flux (caused by turbulent transport) as a function of Richardson number (Grachev et al, 2013). Turbulent transport collapses for Ri >0.25.
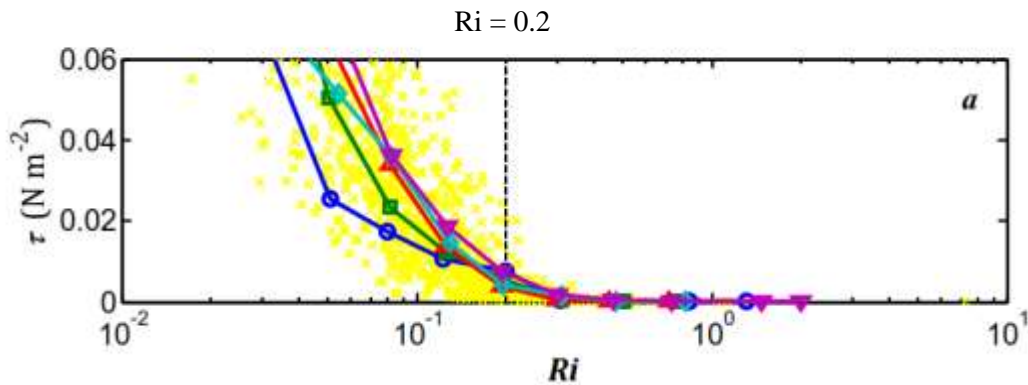
Figure 202: Momentum flux ($\rho<u'w'>$) as a function of Richardson number over a period of 11 months. Coloured lines are average values at different elevations between 2.2m (blue) and 18.2m (magenta).

Typical values in a stable boundary layer are $\Delta\rho / \rho_0$ = 0.01 and h = 30m (100 ft). For Ri > 0.25 implies u < 3.4 m/s.

As a rule of thumb if the overlying wind speed is 3 m/s or less the wind at ground level will drop out completely in conditions of rapid ground cooling (e.g. in clear conditions when the sun goes down).

When the stable gradient decays (normally a little while after sun rise) the overlying wind can penetrate to ground level and nil/low-wind conditions cease. Normally transitions to and out of nil/low-wind conditions occur quickly once the temperature gradient changes but stable conditions can persist for several hours.

It is possible for very low wind speeds in stable or neutral conditions to give vapor flows that are dominated by gravitational slumping and which entrain air very slowly. Work by Briggs et al (1990) on detrainment of heavy gas from depressions is useful in analysing this problem. Briggs showed that detrainment (stripping) of heavy gas from a pool in a depression occurs close to the upstream edge of the pool. As the current of air reaches the edge of the pool the boundary layer thickness (and hence the Richardson number) are necessarily small and turbulent mixing –entrainment of the heavy gas– must occur. As the mixing layer thickens the Richardson number increases until at some point it is large enough for further entrainment to be suppressed. Normally this thickening occurs fairly close to the upstream edge and there is no entrainment over the rest of the pool.

Briggs found that the rate of (volume) detrainment per unit width of pool exposed to the crosswind was

$$V = 0.05 \frac{U^3}{g'}$$

U is the flow speed over the surface

g' is the reduced density g' = g. Δρ/ρ

Note this detrainment rate is not a function of the downwind length of the pool of heavy gas – as detrainment only occurs close to the upstream edge.

The flow is illustrated in Figure 203.
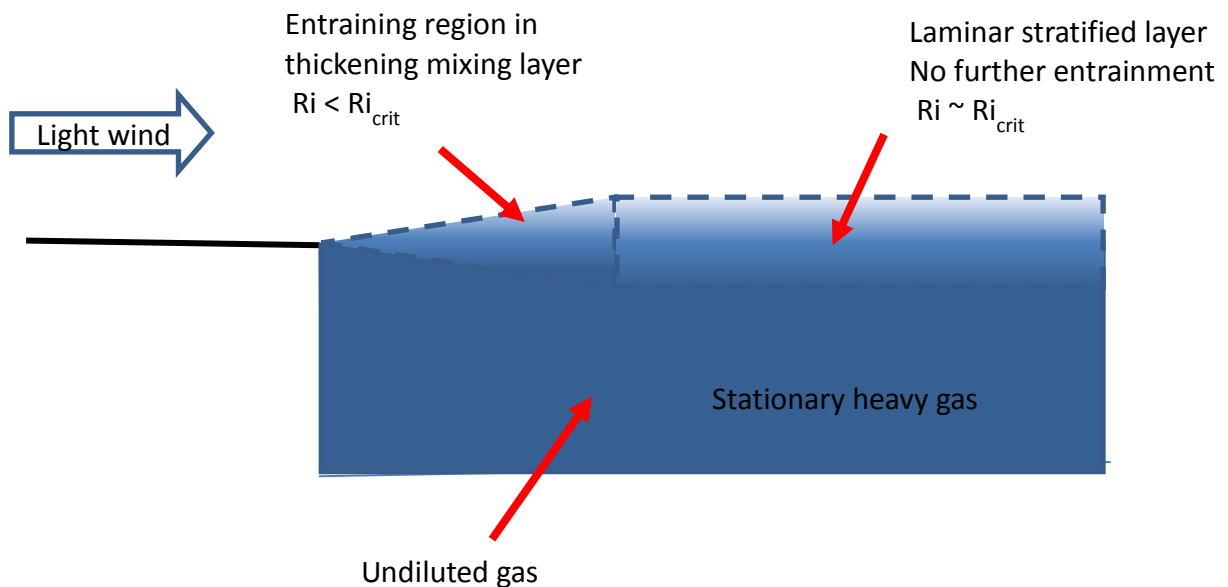
Figure 203: Detrainment of a heavy gas by a light wind

Brigg's detrainment formula can be used to estimate the critical Richardson number at which entrainment stops:

Assume that the gas volume fraction and velocity vary linearly across the mixing layer which is of depth h. Integrating the product of volume fraction and flow speed across the layer gives the volume flux D of detrained gas (per unit width).

D= Uh/6

The depth h will stop increasing when $Ri = g'h/U^2 = Ri_{crit}$

Substituting for h from the equation above gives $Ri_{crit} = g' \, 6D \, / \, U^3$

Comparing with the Brigg's formula gives Ri_{crit}= 0.05 x 6 = 0.3

A typical range value for the density difference in a vapor cloud is $\Delta\rho/\rho = 0.05$ to 0.1 which leads to $g' = 0.5$ to 1.

A typical value for the depth of the whole heavy layer is $h = 2m$. The condition for laminar (non-entraining) flow in a stratified layer in the top 25% of the gas flow (with undiluted heavy gas flow beneath) is $h = 0.5m$

Substituting into the formula $Ri_{crit} = g'h/U^2 = 0.3$ gives an upper limit of wind speed of

$U < 0.9$ m/s for $g' = 0.5$ m/s^2
$U < 1.3$ m/s for $g' = 1$ m/s^2

Low wind speeds (< 1.3 m/s) are consequently required to allow gravity driven vapor transport with minimal dilution.

For wind speeds above about 2.5 m/s the mixing layer will not be able to deepen sufficiently to prevent entrainment over the bulk of the pool and the heavy gas will rapidly disperse.

Note these limits on wind speed apply at the top surface of the heavy gas flow – i.e. a height of about 2m. Wind speed data is normally recorded at a height of 10m and there can be a significant drop in speed closer to the ground - depending on the roughness length. For roughness length 0.1m (which is typical of general agricultural land with a few scattered obstacles) the ratio of wind speeds at a height of 10m and 2m is U(10m)/ U(2m) ~1.5.

The condition for 75% of the gas cloud to remain undiluted (based on wind speeds measured at 10m) becomes:

U (10m) < 0.9 x $1.5 = 1.35$ m/s   for $g' = 0.5$ m/s^2
U (10m) < 1.3 x $1.5 = 1.95$ m/s   for $g' = 1$ m/s^2

6.3   TIMESCALE FOR CLEARANCE OF UNIGNITED VAPOR CLOUDS

The timescale T for removal of a cloud by detrainment is

$$T = \frac{V_{total}}{D.W}$$

V_{total} is the total volume of the cloud and W is the width (across the wind)

D is the detrainment rate.

Assuming cloud width and length (parallel with the wind) are similar L= W and the initial depth is H then the Briggs equation for detrainment rate gives

$$T = \frac{1}{0.05} \frac{g'HW}{U^3}$$

Typical values for a vapor cloud containing 25 -50 tonnes of gas at a flammable concentration would be:

g' = 0.75   H = 2m   W = 500m

Such clouds might accumulate for wind speeds U under about 1.5 m/s

The minimum timescale for detrainment of such a cloud would be about

$$T = \frac{1}{0.05} \frac{g'HW}{U^3} = \frac{1}{0.05} \frac{0.75 \times 2 \times 500}{1.5^3} = 4400 \sec$$

The time would be longer if the wind speed was lower.

Stable conditions that normally allow such low wind speeds at ground level (in the UK) typically arise at dusk and persist until just after sunrise. If detrainment has not already removed the cloud by sunrise, then the cloud will quickly disappear soon after; as the ground level wind picks up and entrainment starts across the full extent of the surface.

6.4   ASSSESSMENT OF VAPOR TRANSPORT IN NIL/LOW-WIND CONDITIONS

Since the incident HSE and others have developed a reasonably complete understanding of the various important stages of vapor cloud production during overfilling:

- Liquid outflow;
- Fragmentation in the liquid cascade;
- Entrainment of air;
- Heat and mass transfer between fuel and air;
- Splashing;
- Near field air entrainment;
- Interaction between vapor currents and bunds;
- Long-range dispersion.

Some useful general methods have been developed that can be used to estimate the cloud *volume* (at a given time). These methods are described in FABIG Technical Note 12 (Atkinson and Pursell, 2013). This note also provides simple approximate methods for estimating cloud volume in the case of spray releases. Examples of the use of these methods in various incidents are given in Section 5.

The cloud depth in the Buncefield case was around 2m with roughly symmetrical spread from the source. Assuming this cloud geometry (i.e. a circular with constant depth 2m) allows the radius to be calculated from the cloud volume. For reasonably level, unconfined sites this allows an estimate to be made of the range of a vapor cloud as a function of time. More details are given in FABIG TN12.

7 DISCUSSION RELEVANT TO VAPOR CLOUD EXPLOSION

7.1 THE IMPORTANCE OF PUBLIC ACCESS TO INCIDENT DATA

In carrying out this review it has become clear that very little information is publicly available on the majority of significant vapor cloud explosions. Often a very small number of press photographs are all that is available and these are generally selected for their visual impact and do not allow any useful lessons about the nature of dispersion or explosion to be learned. Detailed investigation reports and primary evidence are typically not in the public domain.

This lack of information is particularly unfortunate because fundamental understanding of the mechanisms that operate in VCEs is incomplete. We do not fully understand the range of conditions which can lead to severe explosion or what the effects on and off sites might be. This means our ability to assess and control risk is limited; it is vital that we continue to learn through proper analysis of incidents.

Archival of primary evidence as well as summaries of contemporary conclusions is also important. For example this project has included a review of forensic records from the Flixborough explosion: forty years after the incident these unpublished data can be much more fully understood because we now have access to the results of recent large scale detonation tests and a much better understanding of the development and explosion characteristics of non-spherical clouds. The old data turns out to be of great interest in illustrating the kind of damage to be expected in a detonation.

As part of this project digital archives of hundreds of photographs from a number of significant incidents (including Flixborough) have been created. In the future these will hopefully be available to those able to derive more value from them. Undoubtedly the understanding of VCEs would progress more rapidly if process data and detailed photographs of incidents were generally available.

An important objective of the project was to use the data that we collected to advance current understanding of VCEs. The key issues that we have considered are:

1. How do we gauge the severity of an explosion from forensic evidence?

2. What mechanisms operate to allow severe explosions in open areas? If we see severe pressure damage in these areas does it imply that the cloud detonated or are there other possibilities?

3. How can we start to predict what the course of an explosion will be on a given site? What changes would be needed to reduce the probability of the most damaging kinds of explosion?

7.2 FORENSIC EVIDENCE ON VAPOR CLOUD EXPLOSIONS

Forensic techniques for the interpretation of blast effects have improved greatly in the last ten years – especially for low lying vapor clouds. Pressure-impulse diagrams are now available for some standard objects like drums and steel boxes that are sensitive to over-pressure (crushing) damage. It is possible to identify severe explosion (defined here as those generating overpressures in excess of 2000 mbar or 29 psi) with confidence by examining such objects.

Detonation tests have also demonstrated the type of damage to be expected in this type of explosion.

In low-lying clouds over relatively flat open areas the direction of breakage of trees and posts gives a useful indication of the direction of explosion propagation. This type of analysis has been used in some of the cases reviewed to identify the location of the point of transition where a flash fire accelerated to become a severe explosion.

The review has uncovered a new means of discriminating between different types of severe explosion based on examination of slender columnar objects such as lamp posts, scaffold tubes, fence posts etc. In detonation tests and some vapor cloud explosions these objects display a characteristic pattern of distributed plastic deformation which leads to continuous curvature along the length rather than concentration of plastic deformation in "hinges". This behaviour is associated the very high impulsive loads experienced during the normal impingement of a detonation. These loads accelerate lightweight spars on a time scale that is short compared with the transit of (elastic) flexural waves from points of restraint. Continuously curvature is very easy to spot in incident photographs and if it can be established that a spar has not been affected by a prolonged fire it is a very good indicator that detonation has occurred. Fast deflagrations do not produce the highly impulsive forces required.

Additional detonation testing of a range of common types of beam elements would be extremely valuable. A large number of different specimens could be examined in a single large scale test.

Variables to be studied should include:

Beam section and thickness
Beam length
Types of restraint
Cloud depth

Parallel finite element modelling of these elements is also practical with current technology and if successful this would provide a means to extend understanding to different types of beam without further testing.

Calculation of the impulsive loading associated with detonation shock reflection and detonation failure from first principles would be desirable but may be difficult and uncertain. An understanding of the impulsive forces that apply may have to be developed from comparisons between experiments and finite element modelling.

7.3 EXPLOSION MECHANISMS IN OPEN AREAS

In many of the incidents reviewed there was clear forensic evidence that a severe explosion had propagated into open uncongested areas. This was a feature of all of the large vapor cloud incidents for which detailed primary evidence was available and is very likely to have been the case in almost all of the incidents.

This observation challenges the normal assumptions made in blast damage assessment using (for example) the Multi-Energy Method (Van den Berg 1985) in which it is normally assumed that high overpressures are only sustained in congested areas.

The regular occurrence of severe explosions extending to the whole cloud has been recognised in the years since Buncefield. There has been a general presumption that this means that all such incidents were detonations. This is the only established theory that allows sufficiently rapid burning to be sustained in open areas. The results of this review cast doubt on this presumption: there are serious discrepancies between the effects of experimental detonation on a variety of objects and what has been observed at most VCE incidents. For example, as noted above, normal impact by a detonation typically leaves slender column-like objects with continuous curvature. No objects with this type of deformation have been observed at the sites presumed to have been detonations: Buncefield, Jaipur, Amuay and San Juan. Similar discrepancies have been noted for all of the other types of damage reviewed in Section 9.

It is consequently appropriate to critically examine the assumption that has underpinned VCE assessment for the last 30 years namely that (unless DDT occurs) high overpressures are confined to congested areas. The data suggests that severe explosions can progress by a different mechanism: one that has not yet been observed in experimental tests on congestion arrays in gas tents. There is a large gap between the scale of clouds in real incidents and available test data and it was always possible that very-large scale phenomena might have been missed.

The data suggests that this new type of explosion is episodic in nature. Rapid phases of burning are punctuated by pauses. The overall rate of progress of the flame is sub-sonic. This effect is shown directly in CCTV footage of the explosion at San Juan.

It is suggested in Section 10 that, at very large scale, radiation may play a key role in driving explosions. Pressure waves from a severe localised explosion may disturb particles on the ground and other surfaces. Thermal radiation impacting on such   re-suspended particles would lead to pre-warming of the surrounding gas and the development of an area ahead of the flame where gas is warmer and consequently more reactive. Warming of propane/air by 230°C increases the laminar flame speed to that of acetylene/air. At some point this warmed gas could react violently – producing a localised explosion capable of re-elevating more particles and sustaining the episodic combustion.

7.4   TRANSITION TO SEVERE EXPLOSIONS

The transition to a severe (but not detonative) explosion regime seems to involve some degree of congestion or confinement. Based on the incidents studied the following may act as triggers: confined explosions in buildings (e.g. pump houses), dense vegetation, pipe racks and other moderately congested plant. The extent and density of congestion required is substantially less than that required for DDT.

There are very few, if any, reports of very large premixed gasoline clouds (R>200m) which have burned slowly as flash fires. Notwithstanding the lack of pressure effects such flash fires could cause deaths or injuries and would certainly leave a huge burned area. It seems likely that a high proportion of such occurrences would be reported. The lack of such reports suggests that if a very large cloud develops in the context of a fuel depot, the probability of a severe explosion is high.

Our observations of the circumstances under which transition has occurred in the past provide an explanation for this: the density of pipework and other plant and the type of buildings that have provided triggers for transition are typical of fuel storage sites and could be expected in almost all sites. Again the conclusion is that if a very large cloud develops in a normal site it is

appropriate to assume that the risk of transition to a severe (non-detonative) explosion is high (close to unity). With careful design and operation of sites it may be possible to reduce the risk of such transition but currently we lack the fundamental understanding required to specify what level of control of congestion and confinement is needed.

The evidence at Flixborough strongly suggests that DDT occurred in highly confined and congested areas in this case, and that the resulting detonation propagated widely through the extensive cloud around the plant, causing massive damage. Avoiding the potential for DDT by appropriate plant layout remains a priority.

In contrast with gasoline overfill incidents where all of the recorded incidents that caused very large clouds (R>200m) have resulted in explosions, there are several recorded cases of large LPG clouds form pipeline failures that apparently progressed as flash fires throughout.

Part of the reason for this difference may be the potential for very rich clouds to be formed in low wind speed conditions for an LPG release. It is difficult to distinguish between a flash fire that (initially) progresses over the top of a rich cloud and a flash fire in a pre-mixed cloud that is flammable through its full depth.

Where these clouds formed in nil/low-wind conditions (and the depth and homogeneity can be estimated) the reported cloud sizes are consistent with very rich (>UFL) mixtures. A review of dispersion in these LPG cases would be useful and is planned by HSE.

Overall the incident history for pipeline failures suggests that large clouds are generally associated with very light or zero winds. If such a cloud develops the risk of a VCE is probably less than 50%. It may be that there is a significant probability that, even if a large LPG cloud does accumulate in very light or nil wind conditions, it will be too rich to undergo transition to a VCE. This is clearly of relevance to the assessment of risk at LNG sites. Additional experimental and modelling work would be useful to establish what kinds of LPG spray releases in nil/low-wind conditions result in clouds within the flammable range.

8   CONCLUSIONS

1. A high proportion of the major vapor cloud incidents studied occurred in nil/low wind conditions. This reflects the fact that relatively small but sustained leaks can accumulate near the source and build a substantial cloud. Nil/low wind conditions are relatively rare but so are very large leaks that are needed to build a big cloud in windy conditions.

2. In nil/low wind conditions the cloud spreads through the action of gravity. The flammable zone has reached >500 m from the source on several occasions (e.g. Amuay, Jaipur, San Juan). The flow of vapor is strongly affected by site topography. Well away from the source an increase of ground elevation of more than two metres is often sufficient to arrest cloud spread.

3. In principle risk assessments (or regulation) and emergency planning should consider both windy and nil/low-wind cases – considering different types of release together with the weather conditions in which they could produce large clouds.

4. Different approaches to mitigation may be appropriate if nil/low-wind scenarios are considered. For example: detection of gas plumes in windy conditions generally requires a large number of closely spaced devices and the chances of limiting maximum cloud size and risk of ignition by shut-down are low – because the cloud reaches its maximum size very quickly. Investment in such systems may not be warranted. On the other hand, in nil/low-wind conditions the cloud develops slowly and can be reliably detected by a small number of sensors. Shut-down on detection may be a key element of a site's safety planning.

5. The problem of nil/low-wind dispersion is generally better defined and easier to solve than the more familiar dispersion in low winds. Approximate methods suitable for fairly level sites are also available (FABIG Technical Note 12: Atkinson and Pursell, 2013). These methods require no specialist software and assessors require a minimum of training. Some examples of application of these methods in incident analysis are given in this report.

6. In many cases high pressure effects extended to a high proportion of the cloud and were not confined to areas where there was congested pipework or vegetation. There are very few, if any, reports of very large premixed gasoline clouds (R>200 m) which have burned slowly as flash fires. Notwithstanding the lack of pressure effects such flash fires could cause deaths or injuries and would certainly leave a huge burned area. It seems likely that such occurrences would be reported. The lack of such reports suggests that if a very large cloud develops in a normal industrial context, the probability of a severe explosion is high.

7. The regular occurrence of severe explosions extending to the whole cloud has been recognised in the years since Buncefield. There has been a general presumption that this means that such incidents are detonations. That was the only established theory that allows sufficiently rapid burning to be sustained in open areas.

8. Results of detonation tests cast doubt on this assumption. There appear to be serious discrepancies between the effect of experimental detonation on a variety of objects and what has been observed at most VCE incidents. For example, normal impact by a detonation typically leaves slender column-like objects with continuous curvature i.e. plastic deformation distributed along their length rather than being concentrated in a

hinge. This unusual type of deformation is caused by the extreme shortness and severity of the impulse associated with a detonation. No objects with this type of deformation have been observed at the sites presumed to have been detonations: Buncefield, Jaipur, Amuay and San Juan. Further detonation testing and finite element (FE) analysis of this type of object would be valuable (see Section 11).

9. Continuous curvature and other characteristic types of detonation damage can be seen in photographs taken within the area covered by the vapor cloud at Flixborough. They are not observed outside this area. It is very likely that high levels of congestion and confinement led to a detonation in this case - which then propagated to affect a high proportion of the cloud around the plant.

10. It is appropriate to critically examine the assumption that has underpinned VCE assessment for the last 30 years namely that (unless DDT occurs) high overpressures are confined to congested areas. The data however suggests that severe explosions can progress by a different mechanism: one that has not yet been observed in experimental tests on congestion arrays in gas tents. There is a large gap between the scale of clouds in real incidents and available test data.

11. The data also suggests that this new type of explosion is episodic in nature. Rapid phases of burning are punctuated by pauses. The overall rate of progress of the flame is sub-sonic. This effect is shown directly in CCTV footage of the explosion at San Juan.

12. It is suggested in Appendix 2 (Section 10) that, at very large scale, radiation may play a key role in driving explosions. Pressure waves from a severe localised explosion may disturb particles on the ground and other surfaces. Thermal radiation impacting on such re-suspended particles would lead to pre-warming of the surrounding gas and the development of an area ahead of the flame where gas is warmer and consequently more reactive. Warming of propane/air by 230°C would increase the laminar flame speed to that of acetylene/air. At some point this warmed gas could react violently – producing a localised explosion capable of re-elevating more particles and sustaining the episodic combustion.

13. The transition to a severe (but not detonative) explosion regime seems to involve some degree of congestion or confinement. Based on the incidents studied the following may act as triggers: confined explosions in buildings (e.g. pump houses), dense vegetation, pipe racks and other moderately congested plant.

14. The incident history for LPG pipeline failures suggests that even if a very large cloud develops and is ignited, the risk of a VCE is probably less than 50%. This appears to be because some clouds are very rich or even over the UFL. It may be that there is a significant probability that, even if a large LPG cloud does accumulate in light or nil-wind conditions, it will be too rich to undergo transition to a VCE. This is clearly of relevance to the assessment of risk at LNG sites.

15. Over the last 30 years the number of gasoline storage sites has outnumbered LNG export sites by a factor of several hundred. Unsurprisingly there have been too few major VCE incidents to base a regulatory approach solely on statistics from LNG sites. It will be necessary to use experience on failure rates, dispersion and explosion effects from other types of site. A detailed review of the specific circumstances of one or more LNG sites would be useful to assess the frequency and consequences of a range of

incidents. Such a review would provide the basis for regulation of sites and the specification of appropriate mitigation measures.

9 APPENDIX 1: EXPLOSION DAMAGE TO COMMON OBJECTS

9.1 LIGHT WEIGHT STEEL ELEMENTS E.G. FENCE POSTS, LAMP POSTS SCAFFOLDING TUBES ETC.

Light weight steel elements in detonation tests showed characteristic continuously curved shapes – i.e. plastic strain was distributed along the whole length of the element - Figure 204 and Figure 205. The continuously curved shapes indicate that the timescale of pressure rise is much shorter than the natural frequency of vibration. Figure 206 illustrates the development of continuous curvature in a weak strut exposed to an impulsive force. The zone where plastic deformation occurs starts at the support(s) and moves across the element. This leaves plastic bending strain across the full width.

Figure 204: Continuous curvature of an upright member from an angle iron frame that has been exposed to a detonation. Angle size 50 x 50 x 6 mm - which is typically used for end, 2-way or corner strainer fencing supports. 40 x 40 x 5 mm section is typical for intermediate supports.

Figure 205: Continuous curvature of an upright member from an angle iron frame that has been exposed to a detonation Angle size 50 x 50 x 6mm

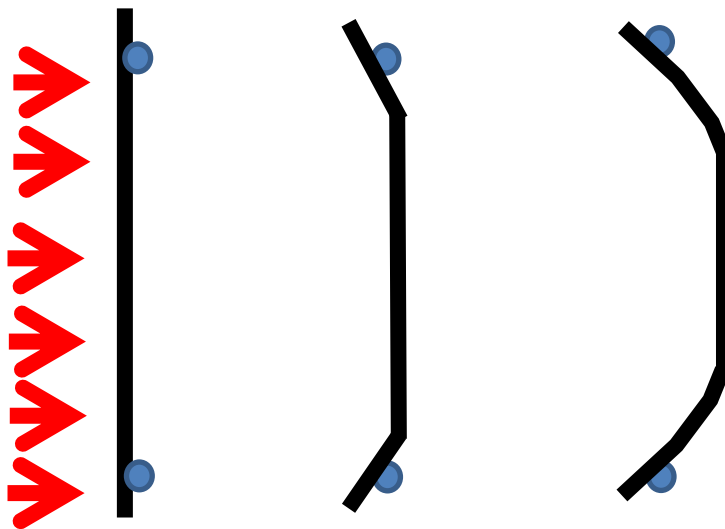*The image has been stretched on the right to show curvature more clearly.*

Figure 206: Progress of a zone of plastic formation away from the points of restraint**.**

Continuous curvature was observed in various fence posts, barrier poles, lamp posts, scaffold poles etc. across the area covered by the cloud at Flixborough and has been illustrated in Section 5.4. The damage in this incident is entirely consistent with a detonation extending to all of the accumulated cloud

On the other hand, no continuously curved steel struts, posts, pipes etc. have been recorded at the Buncefield, Jaipur or Amuay sites. This is a strong negative statement; which is difficult to document for such large complex sites without reproducing hundreds of images. Typical damage to some exposed, lightweight steel structures is shown in Figure 207 to Figure 215.

Figure 207: Lightweight open steel structures in the centre of the Jaipur explosion – there no evidence of continuously curved steels that were observed in detonation testing.

Figure 208: Lightweight open steel structures in the centre of the Jaipur explosion – there was no evidence of continuously curved steels that were observed in detonation testing. Figure 208 does however show evidence of a severe explosion: the observed crush damage to an electrical connection box would require a pressure of at least 2 bar (29 psi).

Figure 209: Lagoon area prior to incident - cloud depth at the level of the site road in the foreground was 4 - 4.5 m (13.1 – 14.7ft) – from CCTV records.

(note fence posts bordering road and hand rail at the top of ladder)

Figure 210: Fence posts in the lagoon area where the Buncefield cloud was deepest. Two water pipes had been installed beyond the fence since the prior view shot above.

Figure 211: A light weight hand rail fully exposed to explosion in one of the lagoon area.

Figure 212: Fallen but unbent fence posts in one of the areas close to the overfilled tank where the Buncefield cloud was deepest (4-4.5 m)

(HERAS fencing by the road post-dates the explosion)

Figure 213: Light-weight steel structure (bike shelter) at Buncefield. The explosion approached across an open area and struck the shelter at right angles to the horizontal cross beams.

Figure 214: A process control area in a deep area of the Buncefield cloud. Numerous straight lightweight pipes, spars and frames.

Figure 215: Mono-modal failure of hand rail on a bridge above the cloud at Amuay.

9.2 BUILDING DAMAGE

Forensic assessment of the damage to buildings directly exposed to vapor cloud explosions is of direct interest in determining the likely consequences of future explosions. It can also shed light on the explosion mechanism.

9.2.1 Buildings outside the cloud

A number of large commercial buildings were damaged by the explosions at Buncefield and Jaipur. Large portal frame warehouses are the most straightforward to analyse and they are also very vulnerable to relatively low pressures. Relatively minor damage resulting in loss of weather-tightness may necessitate recladding and force the occupier to relocate.

At both Buncefield and Jaipur single compartment warehouse structures at ranges between 100 to 500 m (328 - 1640 ft) from the cloud edge all showed mono-modal venting i.e. a single large opening in a wall or in the roof (but not both). A number of different buildings were analysed by Atkinson (2011a). Figure 216 shows a large warehouse about 300 m (984 ft) from the cloud edge. The explosion has opened a hole in the front of the building facing the explosion. The roof and sidewalls of this building were substantially undamaged and (apart from the end bays) did not have to be replaced.

Figure 216: Pressure damage to a large warehouse 300 m (984 ft) from the edge of the Buncefield cloud.
(Picture taken after the remains of cladding had been removed from the front wall)

This pattern of mono-modal venting is characteristic of response to pressure that ramps up over many hundreds of milliseconds. This is what is observed if the explosion front moves towards the building at a speed well below the speed of sound.

Explosions that progress faster than the speed of sound produce shocks: pressure at a building increases discontinuously when the shock arrives and then decays. In this case venting is generally multi-modal.

Figure 217 shows an example of damage caused by such a discontinuous rise in pressure. These are views of a warehouse 640 m (2100 ft) from the solid phase explosion at Tianjin in August 2015 – seismic analysis suggested this explosion had 21 tonne TNT equivalence. Damage to the building is multi-modal: several walls and the roof have opened up and all would certainly require replacement. The blast wave for this case and the Buncefield warehouse are compared later in this section - Figure 219.

Figure 217: Side and top views of a warehouse 640 m (2100 ft) from the Tianjin explosion

The explanation for mono-modal venting is simple: if the pressure rises slowly the first failure mode that opens a large vent allows pressurisation of the interior by an internal shock. The differential pressure between the building interior and exterior falls and no further venting modes become active. This cannot occur for a shock loading: numerous venting modes may operate simultaneously.

Figure 216 (after removal of the cladding) shows the nature of the failure and the extent of deformation in the Buncefield warehouse. The wall of the warehouse cannot yield faster than the velocity of air in the incident pressure wave and the maximum extent of deformation D_{max} allows a calculation of the minimum impulse required I_{min}.

$$I_{min} = \rho c D_{max}$$ ρ is the air density, c is the speed of sound

This equation links the displacement of a weightless and completely unrestrained body to the impulse of the incident blast wave.

Figure 218 shows a calculated detonation pressure at a distance of 300 m (984 ft) from the edge of a circular vapor cloud of 200 m (656 ft) radius (Fluid Gravity, 2009). The depth of the cloud is such that the impulse is consistent with the deformation in Figure 216. Also shown is the pressure wave generated by an episodic deflagration (Atkinson 2011b); again the cloud depth has been chosen to match the impulse indicated by deformation.

Typical design pressures for wind loading of large warehouses are of order 1000 Pa. This means that without substantial venting, and pressurisation of the interior, all of the sides and the roof of the warehouse would be expected to fail or to be badly damaged. The detonation loading shown in Figure 218 would therefore be expected to produce the kind of multimodal damage shown in Figure 217: the Buncefield detonation loading and solid phase blast are compared in Figure 219.

On the other hand the slowly increasing pressure wave generated by the episodic deflagration allows full operation of a single venting mode; an internal shock can then propagate through the empty building and this would explain why the side-walls and roof were spared the effects of rising external pressure.
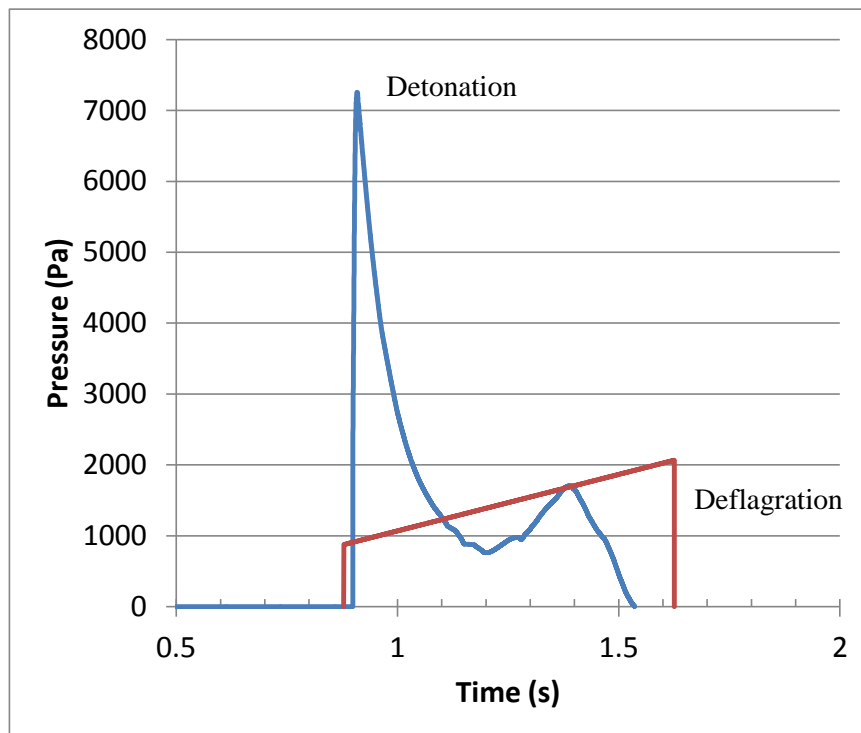

Figure 218: Incident pressure profiles with positive impulses sufficient to cause observed deflection of wall.
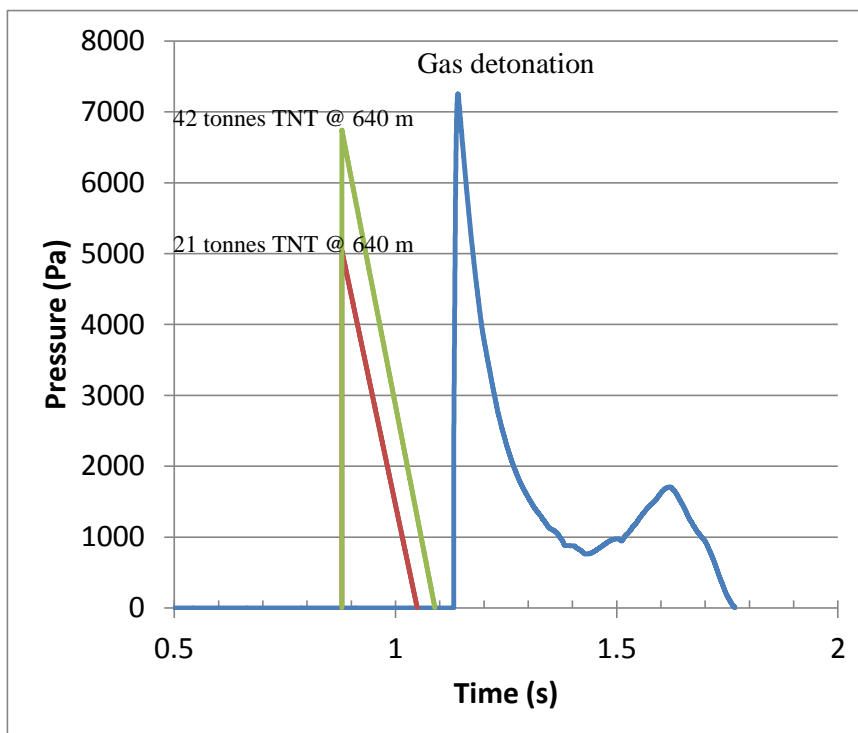
Figure 219: Detonation pressure pulse compared with TNT blasts from 21 and 42 tonnes TNT (46,300 and 92,600 lb)

9.2.2 Buildings within the cloud

Buncefield provided an example of a much stronger building that could again indicate whether the incident pressure increased discontinuously (shock loading) or increased more slowly as the explosion approached (Weidlinger Associates, 2009; SCI, 2009). Figure 220 shows a general view of the Northgate Building after the blast.

Figure 220: Northgate building after the blast

The elements of particular interest are the top level cladding panels. These are not restrained by a floor slab and in the northern part of the building failed as shown in Figure 221. In the southern part larger diameter reinforcing steels were used and deformations were much reduced.
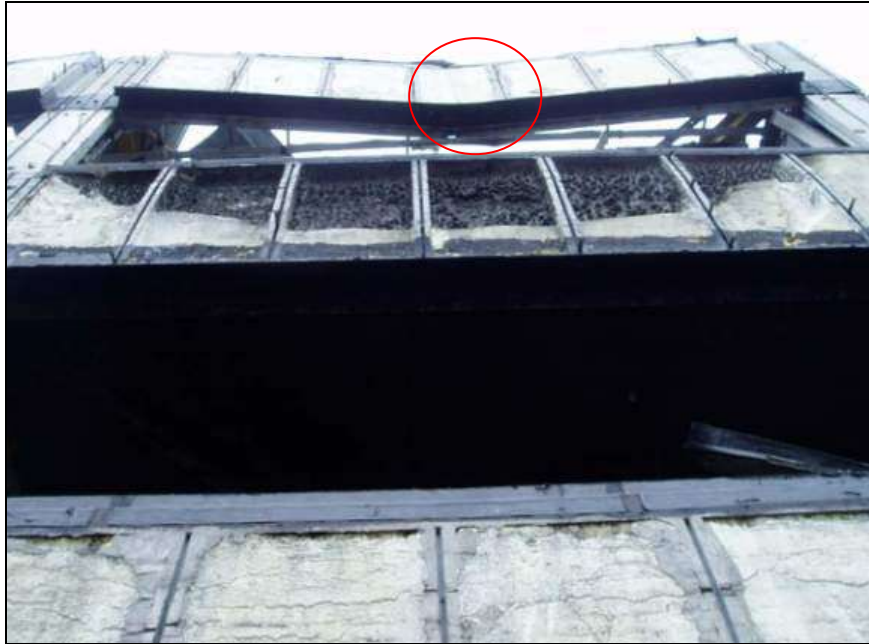

Figure 221: Failure of top level cladding panels – single central crack (circled) as a result of mono-modal failure

Finite element modelling of the response of these panels to various blast waves was undertaken. One case was the pressure variation expected in a detonation - calculated for the specific building geometry using a hydrocode (Fluid Gravity, 2009; SCI, 2009).

The observed failures could only be reproduced with a pressure loading that increased gradually over around 200 milliseconds – matching the natural fundamental frequency of the panel. Shock loading would have produced multimodal failure including cracking of the panels at the supports (Figure 222).
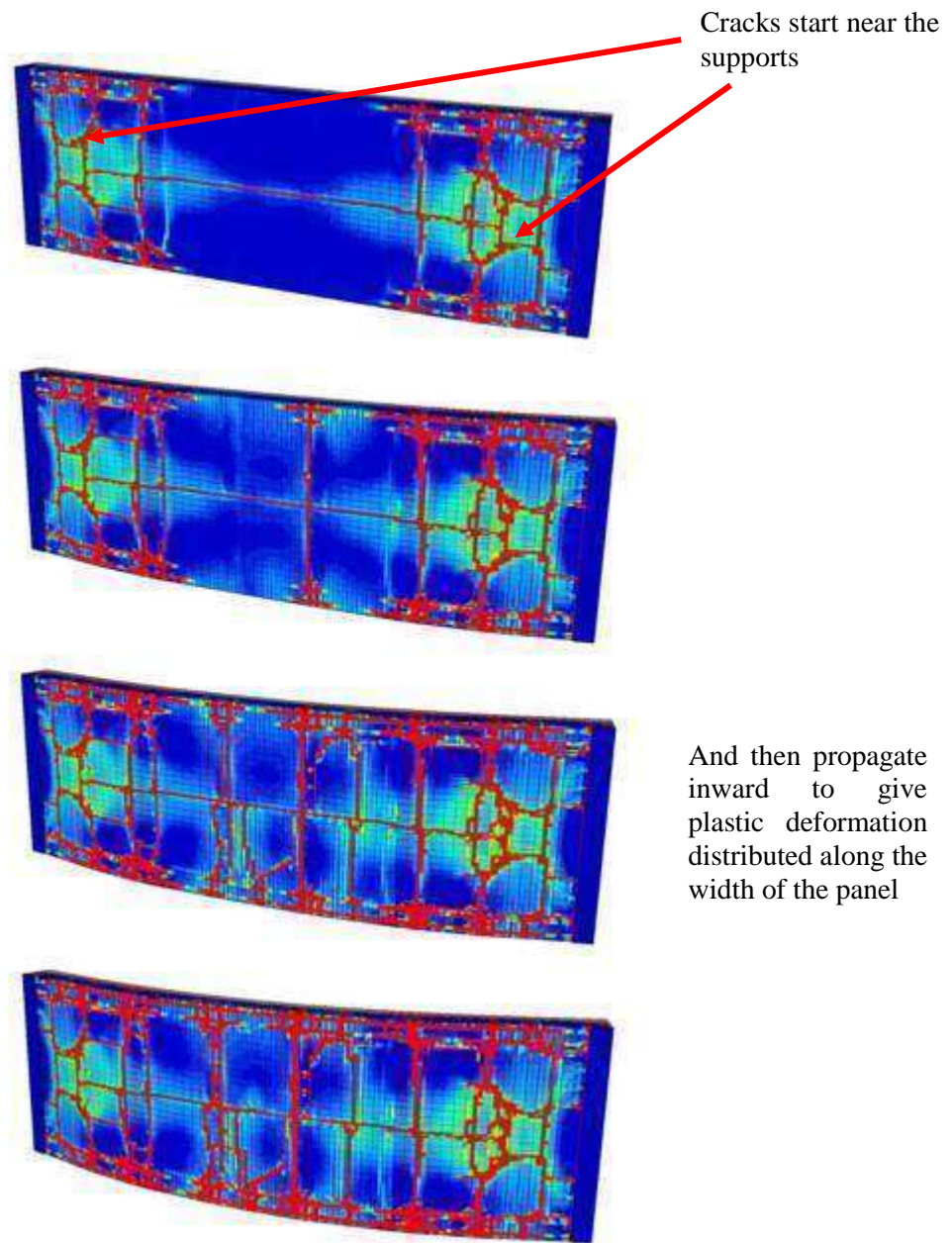
Cracks start near the supports

And then propagate inward to give plastic deformation distributed along the width of the panel

Figure 222: Multi-modal cracking predicted in the cladding panel if subjected to detonation loading (snapshots at 20 ms intervals).

This is particularly strong evidence against a detonation as CCTV evidence shows the cloud engulfing the lowest part of the building and there is clear evidence of a local severe explosion all along the base of the wall (Crushed cars, masonry stripped from steel columns). There is consequently less uncertainty in calculating the pressure wave associated with detonation than for distant buildings.

The time variation of the derived pressure wave that could explain the observed damage to the two types of panel was again consistent with an episodic deflagration.

9.3 DAMAGE TO DRUMS

Steel drums are generally standard items with a high level of symmetry. When standing upright the main variable is fill level. It is useful to compare the behaviour of drums in detonation tests with those recorded in photographs from incident sites.

9.3.1 Near-full drums

Figure 223 shows the form of a drum after a detonation test. The bending of the drum crimped rim, and downwards deflection of part of the drum top to make a flap at the front, has been caused by the extremely high forces exerted on the upstream face during the detonation. Reflected pressures at the moment of impact are generally in the range 35-40 bar (507 -580 psi).

The drum wall, crimp and top are light – elements would travel several metres in response to the forwards impulse, if unconstrained. Consequently the extent of deformation has not been limited by inertia: in fact the detonation has pulled down the front section of the drum top until it almost touches the sidewall.

Explosion direction

Figure 223: Near full drum in a detonation test

If any drum with this type of deformation were recovered at the site of a VCE it would be extremely good evidence for a detonation.

Large numbers of near full drums were involved in explosions at Jaipur and some at Buncefield. A typical damage pattern is shown in **Figure 224**

Figure 224 also shows the deformation of a drum in a static compression test at an overpressure of just over 2 bar (29 psi).

The damage observed in the incident drum in

Figure 224 (and other drums at Jaipur) matches that to be expected in a strong deflagration where the overpressure was around 2 bar (29 psi). Although dozens of near full upright drums were exposed to the explosion at Jaipur, none showed the characteristic downward deflection of a flap of the drum top at the front that would indicate exposure to a detonation.

Figure 224: Drum damage

(Left) Near full drums from Jaipur   (Right) 2 bar (29 psi) static test

9.3.2   Empty drums

The damage to empty drums in a detonation test is shown in Figure 225.

Again very high reflected pressures on the upstream face of the drum have driven this face inward producing very large flaps in the top and bottom rim. The deformation has gone so far that these flaps are almost touching close to the original drum centre plane. The drum top and bottom no longer individually lie in a plane and are certainly not parallel.

There are small tears in the downstream face where strain levels are particularly high. The internal pressurisation and damage to the rim have also led to failure of a large part of the crimp as the external pressure fell.

Damage to the drum is grossly asymmetric and it is immediately obvious from what direction the detonation struck the drum.

Explosion direction

Figure 225: Damage to an empty drum in a detonation test

This type of failure has not been observed in any incident to date without substantial congestion (Buncefield, Jaipur, Amuay). Typical behaviour for an empty drum involves much less extreme deformation of the drum sides that is partially reversed when the external pressure relaxes (Figure 226).

The ends of the drum remain parallel. It is not clear from which direction the explosion approached the drum and there is no overwhelming asymmetry in damage.

Inward doming of the ends of the drum is visible in some shots and this was also observed in static pressure tests at a pressure of around 2 bar (29 psi) - Figure 227.

Significant displacement of drums also generally occurs.

Higher levels of damage are to be expected for unstoppered empty drums; because shape recovery after the explosion will be less complete.

Figure 226: Remains of empty drums involved in incidents

(Top)   Buncefield (2005)
(Centre)   Amuay Refinery (2012)
(Bottom) Jaipur (2009)

Figure 227: Deformation of the end of a drum in a static pressure test at just under 29 psi

9.3.3   Summary

In the case of both near-full and empty drums, the damage observed at incidents at Buncefield, Jaipur and Amuay corresponds to that expected for a fast deflagration or episodic deflagration with pressures of a few bar (a few tens of psi).

Substantial deformation of the crimped rims out of plane and asymmetric damage associated with very high reflected pressures on the upstream face would be good indicators that a detonation had occurred (e.g. Figure 223 and Figure 225). No examples of such deformation have been recorded at Buncefield, Jaipur or Amuay.

9.4   DRAG DAMAGE TO BOXES AND SIGNS ON STANDS

This section deals with the effects of drag forces on the steel frames supporting lightweight objects such as metal boxes and signs.

Figure 228 shows the variation in directional dynamic pressure in a 3m deep stoichiometric propane cloud (SCI, 2009). Directional dynamic pressure is calculated as

$$P_d = \frac{1}{2}\rho U |U| \qquad \qquad |U| \text{ is the (positive) magnitude of velocity}$$

The drag force on an exposed object can be calculated by multiplying the dynamic pressure by the frontal area and a drag coefficient. The drag coefficient is shape dependent but normally of order 1 for boxes and sheets normal to the flow.

The maximum drag force in the positive direction (in the direction of detonation propagation) is about 30 times the force associated with the reverse flow. However, the reverse flow lasts very much longer and in fact the total net drag impulse is backwards.
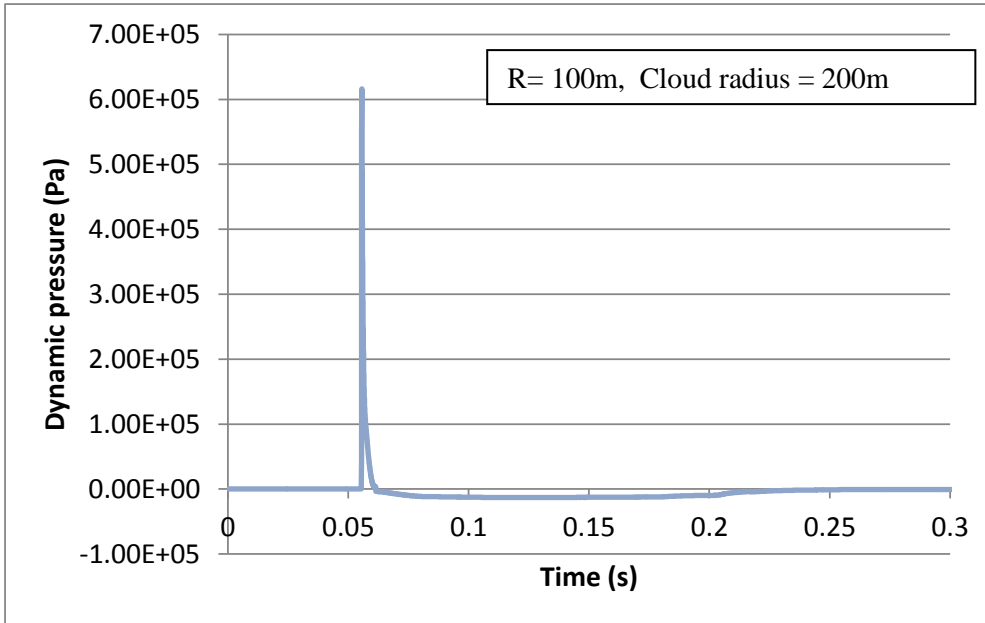
Figure 228: Forwards and reverse drag forces in a detonation (Fluid Gravity, 2009)

The variation of overpressure in a strong *deflagration* is more variable depending on whether the flame is quasi steady or episodic. Results for a steady flame (overpressure 1.5 bar – 22 psi) illustrate the key features (SCI, 2009) Figure 229.
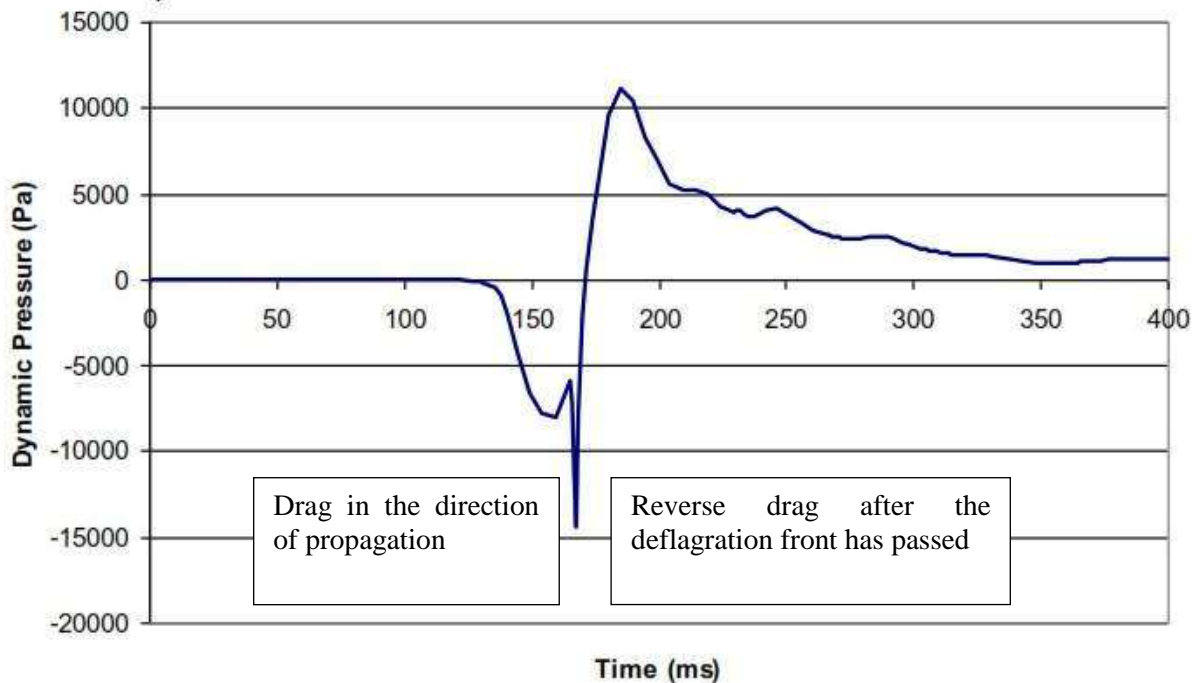

Figure 229: Drag forces in a fast deflagration - *note the deflagration is travelling in the direction of negative values of x.*

Again the net drag impulse is backwards but in this case the maximum sustained reverse drag force is *greater* than the forwards drag: rather than 30 times less as was the case for detonations.

Figure 230 compares the two explosion mechanisms. The direction of propagation has been matched in this case.
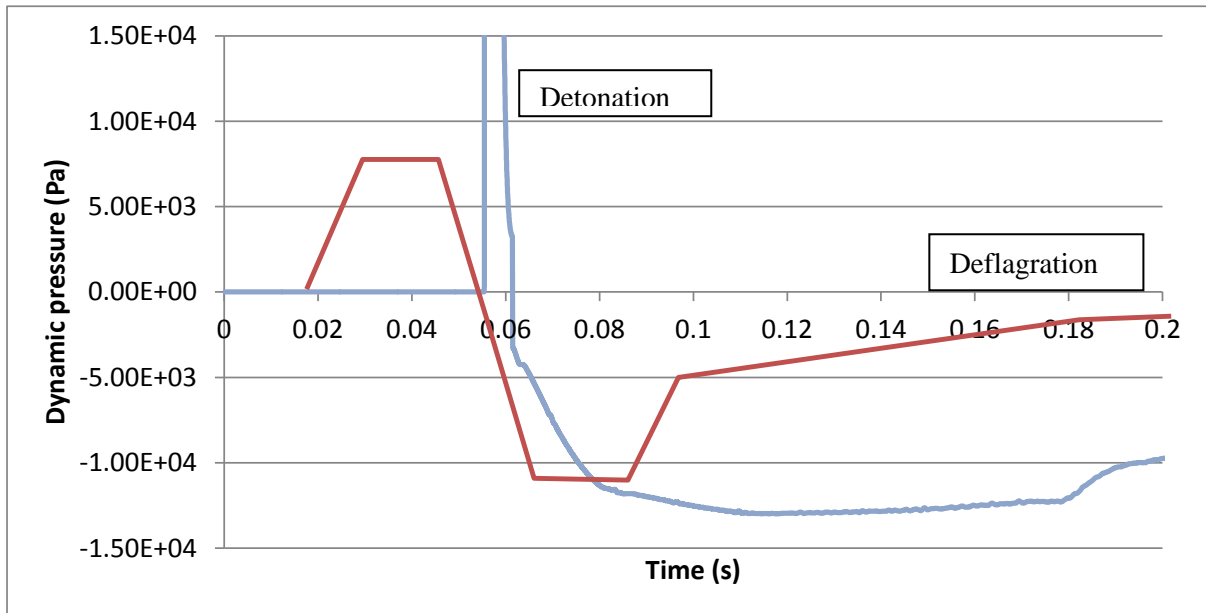

Figure 230: Approximate comparison of drag forces in detonation and deflagration regimes (References included in previous figures)

Although the forward drag in a detonation is short lived it can produce substantial deflections in relatively light objects. Table 23 shows some example deflections for some unrestrained rigid objects over the period of the positive impulse.

Table 23: Example deflections of unrestrained objects due to detonation

Unrestrained object	Displacement by positive drag (m) (over the period of the positive impulse)
Steel sheet 1 mm thick	2.5
Steel sheet 3 mm thick	0.85
Steel sheet 6 mm thick	0.425
Steel box 600 x 600 x 150 mm - wall 1.3 mm thick	0.65
Steel box 300 x 300 x 150 mm - wall 1.3 mm thick	0.5
Timber pole diameter 10 mm 500 kg/m^3	5
Timber pole diameter 20 mm	2.5
Timber pole diameter 50 mm	1.0
Timber pole diameter 100 mm	0.5
Timber pole diameter 200 mm	0.25

:

If objects are restrained (e.g. by stands) deflections are reduced. Figure 231 shows the final forwards deformation of a steel box subjected to an experimental detonation (depth 3m).

Figure 231: Deformation in the support frame of a 600 x 600 x 150 mm steel box subject to a detonation

The box support frame has deformed forwards plastically with hinges immediately below the box. This damage would have been done immediately after the impact of the detonation front by a combination of drag forces and short lived asymmetry in overpressure between the front and rear of the box. This initial displacement occurs so quickly that inertial restraints on the lower part of the stand raise the bending moment just below the box above the yield point. The stand has also deflected further forwards with plastic hinges at the lowest point of the stand – where the bending moment of sustained forwards forces is greatest. There is no sign that the (much lower) reverse drag forces have produced any permanent backward deflection.

The forwards drag force in a detonation is much larger than the reverse force and the forwards impulse is sufficient to cause rapid plastic deformation. This means that we would expect to see three types of response to drag forces in a detonation - Figure 232.
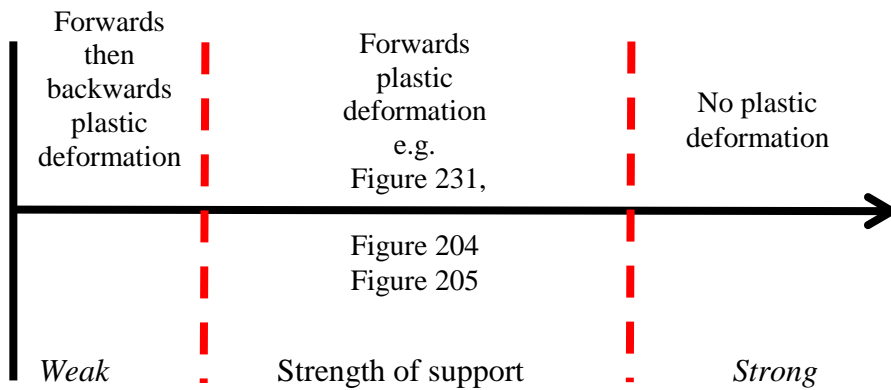
Figure 232: Schematic showing the types of deformation to be expected in a detonation

In contrast the forwards drag force in a *deflagration* is smaller than the reverse force and the forwards impulse is also less than the reverse impulse. This means that we would expect to see only two types of response to drag forces in a deflagration: backwards deflection or no deflection - Figure 233.
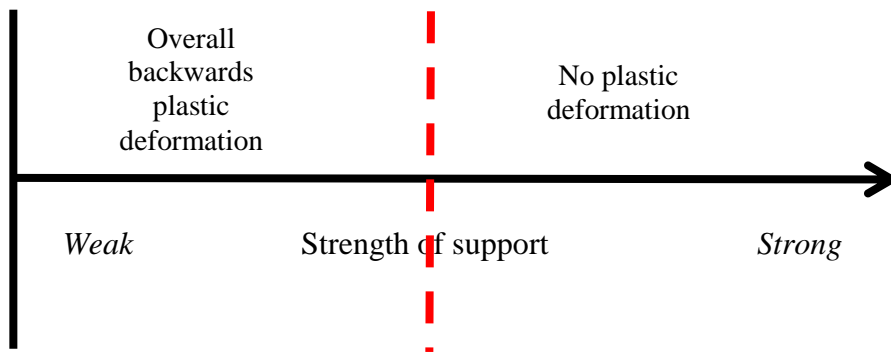
Figure 233: Schematic showing the types of deformation to be expected in a deflagration.

9.4.1   Evidence from incidents

In general metal support frames within the Buncefield and Jaipur explosions were all deflected backwards. Examples are shown in Figure 234, Figure 235 and Figure 236 below.

Figure 234: Backwards deflection of a steel support frame at Jaipur
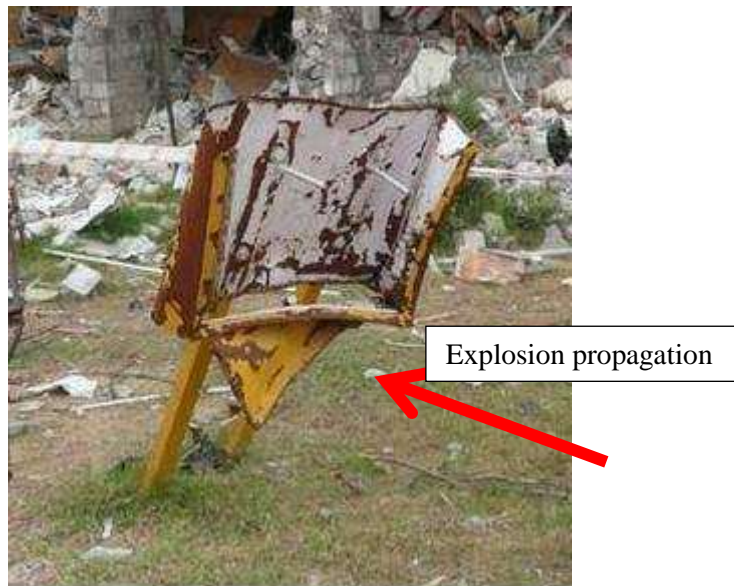
Figure 235: Backwards deflection of a steel support frame at Jaipur

Figure 236: Backwards deflection of a steel support frame at Jaipur

The only exceptions to this are frames that support weakly connected boxes or sheets on the upstream face of a stand. The forwards impulse is transmitted to the stand but the reverse flow breaks the connections, greatly reducing the backwards impulse. Such objects can be left with positive displacements. An example is shown in Figure 237.

Figure 237: Forward deflection of a steel frame at Buncefield

The bending of a support stand at the midpoint visible in the detonation test (Figure 231) is only possible (perpendicular to the plane of any bracing) under extremely high impulsive load. Multi-modal failures of this sort have not been observed at any of the sites.

9.4.2　　　Summary
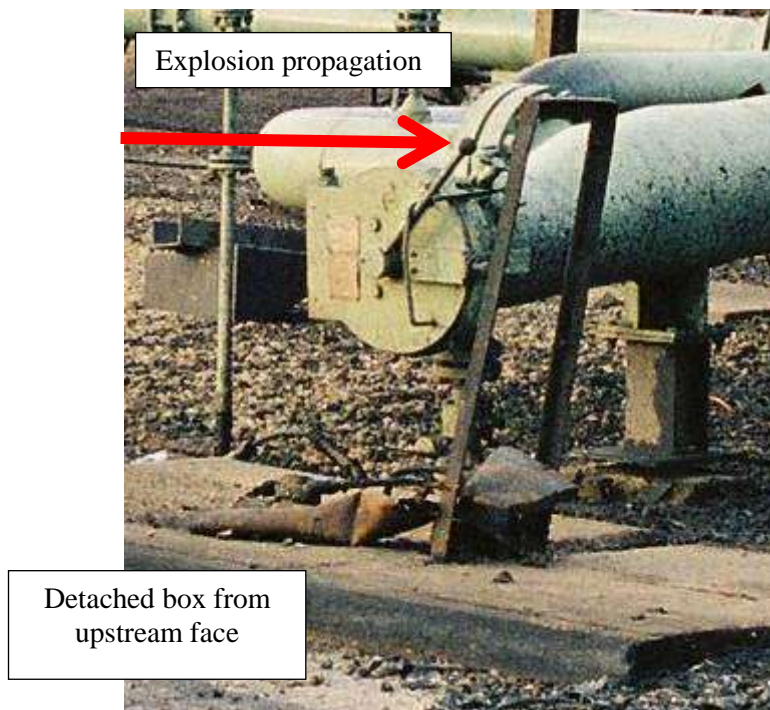
Overall the pattern of failure of steel stands within explosions conforms closely to that to be expected in a strong steady or episodic deflagration (Figure 233). Stands with a positive deflection or multi-modal failures would be good evidence for a detonation (Figure 231). Both were observed in the detonation test but neither has been observed at the sites of large VCEs.

9.5　　　EFFECTS OF VCES ON VEHICLES AND SKIPS

The structural effects of a detonation on larger objects such as cars are complex and more difficult to interpret than those for simpler, more symmetrical object such as drums.

Figure 238 and Figure 239 shows the effects of an experimental detonation on the side of a car facing the oncoming explosion and the side facing away from the explosion.

Figure 238: Damage to the side of a car facing oncoming detonation

Figure 239: Damage to the side of a car facing away from a detonation

The asymmetry in damage to the two sides of the car is obvious, for example:

1. On the upstream side tyres have been completely displaced whilst on the downstream side there have not.
2. On the upstream side the door frames and sills have been substantially displaced inwards whilst on the downstream side some of these elements appear to have been displaced slightly outwards.

As was the case for drums, this asymmetry is a result of very high reflected pressures (35-40 bar, 507- 580 psi) on the upstream face.

No clear asymmetry in damage to cars has been recorded in incident photographs. Typical shots of damaged cars are shown in Figure 240 and Figure 241.

Car damage in a detonation (Flixborough) is illustrated in Figure 242.

Figure 240: Car damaged in Buncefield VCE

Figure 241: Car damaged in Buncefield explosion – explosion direction left to right

Figure 242: Car damaged by a detonation at Flixborough

The bodywork of some of the vehicles in the Jaipur explosion suffered high levels of damage. Possibly this reflects the fact that some vehicles may have been left with open windows and hence filled with gas prior to the explosion.

Figure 243 shows damage to a car subject to a pressure of around 1000 mbar (14.5 psi) in an explosion chamber (Pritchard et al., 2006). The damage is less severe than observed for the incident vehicles. This is consistent with the conclusion drawn from deformed drums: that the explosion pressure was greater than 2000 mbar (29 psi).

Figure 243: Car subject to 1 bar (14.5 psi) overpressure in a reinforced explosion chamber

Some simpler objects have been observed that give a clearer indication of the degree of asymmetry in loading during the explosion. The skip shown in Figure 244 was almost exactly side-on to the explosion and located in an open location. The final deflections of the upstream and downstream faces are quite similar.

This type of object has not been subject to detonation testing but based on the observed deformations in the car one would expect that deflection of the upstream face would be substantially larger than the downstream face if the skip were impacted by a detonation.

This skip shows an anomalous multi-modal failure in the top stiffening bar. This bar is not particularly strong, given the large loaded area of the side of the skip. The natural frequency of this bar will be particularly low because its effective mass is greatly increased by the mass of the sides and side reinforcement bars. These greatly increase the effective mass of the top bar without significantly contributing to increased stiffness. The natural period of vibration of this element of the skip probably corresponds to the rise time of the pressure load.

Figure 244: Deformation of a skip exposed to VCE from the side (the skip has been rolled over onto the upstream face)

Figure 245: Location of skip prior to the explosion

10   APPENDIX 2: RADIATIVE HEAT TRANSFER IN LARGE SCALE EXPLOSION PROPAGATION

This Appendix considers the propagation of premixed gas mixtures contaminated with finely divided solid material. The mass loading of solid material is so small that it only slightly increases the heat capacity of the flammable mixture but it absorbs thermal radiation over a characteristic distance of L.

Such solids would increase the absorption of thermal radiation ahead of the flame and will generally also increase the emissivity of the flame after they pass through the flame front. (Figure 246 and Figure 247).

Figure 246: Flame propagating through clean pipe array

Figure 247: Flame propagating through pipes contaminated with soot at 500 mg/m^2

10.1   HEAT TRANSFER MECHANISMS IN EMISSIVE LAMINAR FLAMES

The temperature gradient in a stoichiometric laminar hydrocarbon flame is approximately 6 x 10^6 °C /m which corresponds to a conductive heat transfer rate of approximately 300 kW/m^2. The upper limit on forwards radiative heat flux from an emissive flame (corresponding to the adiabatic flame temperature) is approximately 1400 kW/m^2 – a typical figure for large flames would be 1000 kW/m^2- see Section 10.6.

For wide flames the total rate of heat transfer to unburned gas ahead of an emissive laminar flame would be dominated by radiation. Any theory aimed at calculating the flame speed from first principles would have to account for radiation.

This result is not of direct practical significance because very large flames do not remain laminar.

10.2   HEAT TRANSFER MECHANISMS IN TURBULENT FLAMES IN ARRAYS OF OBSTACLES

As an example, consider a flame propagating through a series of grids made up of obstacles size r_0 and spacing r_0. As unburned gas is forced through the arrays ahead of the flame at a speed U_{ug} turbulent eddies are induced with a length scale of r_0. The magnitude of root mean square turbulent velocity u' induced in such a case is approximately.

$$u' \approx \frac{U_{ug}}{4} \qquad \text{(Gardner et al 1998)}$$

This corresponds to a turbulence intensity in the flow of unburned gas of 25%.

If backward movement of the unburned gas is constrained e.g. the flame is propagating in a tube, then the forwards flow of gas is related to the observed flame speed U_f as

$$U_{ug} = \frac{E-1}{E} U_f \qquad \text{Where E is the flame expansion ratio.}$$

If the flame is propagating in the open where neither burned nor unburned gas are constrained, then the forwards flow of gas is related to the observed flame speed U_f as

$$U_{ug} = \frac{\sqrt{E}-1}{\sqrt{E}} U_f \qquad \text{(Atkinson 2012)}$$

In this latter case (flame spread in the open) the magnitude of induced turbulent velocities is related to the observed flame speed as approximately

$$u' \approx \frac{U_f}{7}$$

Development of the turbulence in the flow of unburned gas produces eddies with a range of smaller sizes with kinetic energy cascading down to smaller scales. Assuming that the turbulence is roughly homogeneous and isotropic at least in the later stages of this process then the flow of kinetic energy should correspond to the cascade described by Kolmogorov (Poinsot and Veynante, 2005). The energy flux from one scale to another is constant along scales and is given by the dissipation rate (per unit mass). This can be estimated from the ratio of the kinetic energy of the initial eddies (per unit mass) to their timescale.

$$\varepsilon \approx \frac{u'^2}{r_0 / u'} \approx \frac{u'^3}{r_0}$$

At smaller sales the strength of eddies is related to their scale and the dissipation rate as

$$\varepsilon \approx \frac{u'(r)^3}{r}$$

The characteristic time for dissipation of eddies of size r is

$$\Delta t \approx \frac{r^{2/3}}{\varepsilon^{1/3}}$$

The scale of the smallest eddies corresponds to a size at which viscous dissipation dominates eddy decay rather than transfer of energy to smaller scales. This Kolmogorov scale occurs when

$$r_{min} \approx \left(\frac{\upsilon^3}{\varepsilon}\right)^{1/4} \qquad \upsilon \text{ is the kinematic viscosity}$$

If the flame speed in the open is about 100 m/s and the length scale of obstacles (r_0) is 1m then the Kolmogorov scale in the unburned gas is about 10 mm. It increases with increasing scale as $r_0^{1/4}$ and decreases with flame speed as $U_f^{-3/4}$. In such a flow the turbulent velocities associated with the primary eddies and all smaller scales down to the Kolmogorov scale are greater than the laminar flame speed. This means the flame front is greatly deformed during the process of eddy break up to produce a distributed reaction zone where a folded and refolded flame encloses unburned pockets of gas at a range of sizes.

In a case where the unburned gas is loaded with fine particles, thermal radiation from the burned gas within the reaction zone is absorbed by pockets of unburned gas at a range of scales. Assuming for simplicity that an unburned pocket is spherical (radius r), then in time Δt thermal radiation increases the temperature of unburned gas in pocket by an amount

$$\Delta T = \frac{f.I}{\rho C_p} \cdot \frac{4\pi r^2}{4/3\pi r^3} \cdot \Delta t = \frac{3f.I}{\rho C_p r} \cdot \Delta t$$

f is the proportion of the incident thermal radiation absorbed by the pocket. This is a function of the mass loading of particles and the pocket size. If the pocket size is greater than L (characteristic distance for thermal absorption) then f will approach 1.

I is the characteristic thermal radiation within the emissive flame – a typical value would be 1000 kW/m^2 – Section 10.6.

The time available for absorption of radiation is equal to the lifetime of the pocket which is related to its size by

$$\Delta t \approx \frac{r^{2/3}}{\varepsilon^{1/3}}$$

The total average change in temperature of gas within the pocket (radius r) over its lifetime is therefore

$$\Delta T = \frac{3f.I}{\rho C_p} \cdot \frac{1}{\varepsilon^{1/3}.r^{1/3}}$$

The relationships between dissipation rate, turbulent velocity and flame speed in the example case are:

$$\varepsilon \approx \frac{u'^3}{r_0} \qquad \text{and} \qquad u' \approx \frac{U_f}{7}$$

The average temperature rise in unburned gas because of thermal radiation is therefore

$$\Delta T = \frac{21.f.I}{\rho C_p} \cdot \frac{1}{U_f} \cdot \left(\frac{r_0}{r}\right)^{1/3}$$

Many common dusts such as rust, soot and finely divided cellulose have high absorption cross-sections for thermal radiation (typical wavelength 1 um). For example, if such materials were in the form of 10 μm radius spherical particles at a concentration of 100 g/m³ then the typical radius of a pocket having f=0.5 would be around 100 mm.

Substituting these values gives an idea of effect on the temperature of unburned gas that could be expected.

$$\Delta T = \frac{21.f.I}{\rho C_p} \cdot \frac{1}{U_f} \cdot \left(\frac{r_0}{r}\right)^{1/3} = \frac{21(0.5).10^6}{1.2.(1000)} \cdot \frac{1}{100} \cdot \left(\frac{r_0}{0.1}\right)^{1/3} = 190.r_0^{1/3} \ ^\circ C$$

If the size of the primary eddies is large i.e. $r_0 \geq 1$ m then this temperature increase in the unburned gas can be substantial i.e. $\geq 190\ ^\circ$C (374 F).

Smaller particles would have similar effects at lower mass concentrations: 1 μm radius spherical particles would give f=0.5 for a 100 mm (8") radius pocket at a mass concentration of around 10 g/m³. At a mass loading of 50 g/m³ of such particles, a 100 mm pocket would absorb almost all incident thermal radiation f~1. In this case

$$\Delta T = \frac{21.f.I}{\rho C_p} \cdot \frac{1}{U_f} \cdot \left(\frac{r_0}{r}\right)^{1/3} = \frac{21(1).10^6}{1.2.(1000)} \cdot \frac{1}{100} \cdot \left(\frac{r_0}{0.1}\right)^{1/3} = 380.r_0^{1/3} \ ^\circ C$$

This would be a temperature rise of >380 °C for an array of large obstacles ($r_0 \geq 1$ m)

Non spherical particles (e.g. flakes) would also lead to higher cross-sections for thermal absorption per unit mass.

10.2.1   Effects of heating of unburned gas on laminar flame speed

The laminar flame speed of all hydrocarbons increases sharply with the temperature of the unburned gas (Poinsot and Veynante, 2005). Figure 248 shows the laminar speed of propane as a function of unburned gas temperature.
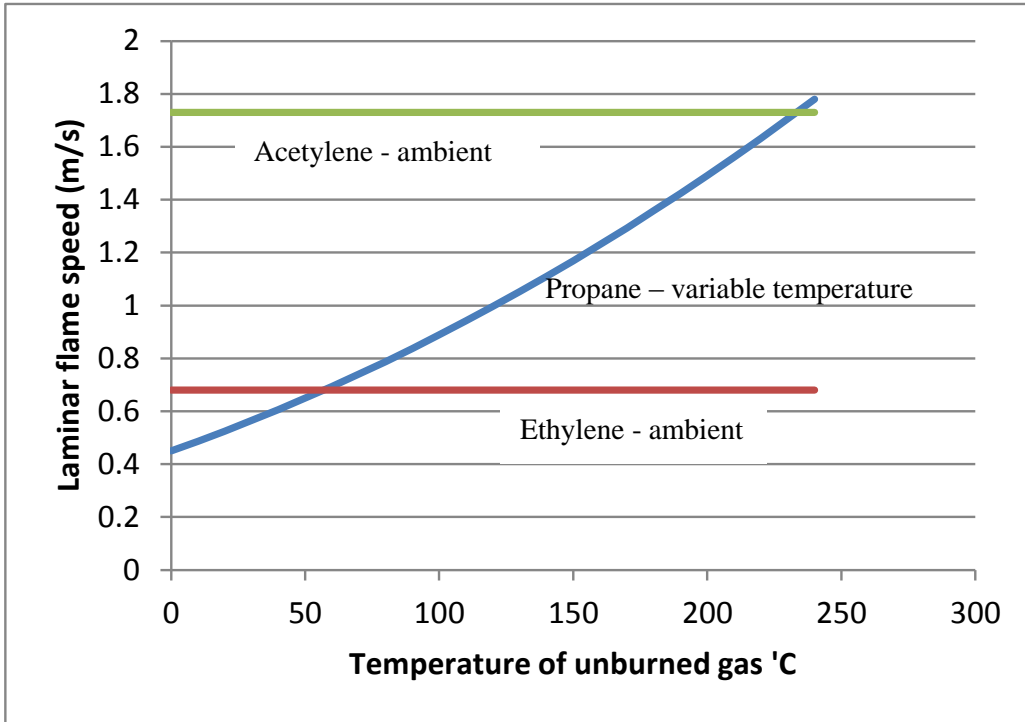
Figure 248: Laminar flame speed as a function of unburned gas temperature for propane

If the temperature of the unburned gas is increased by around 60 ˚C the reactivity of the gas increases to that of ethylene. If gas is pre-warmed to around 230 ˚C the laminar flame speed increase to that of acetylene.

This analysis suggests that if premixed gas is mixed with fine particles then the burning of gas within a distributed reaction zone will proceed much more rapidly than would be the case in the absence of particles. As for the laminar case, any theory aimed at calculating the flame speed from first principles should account for radiation if there is contamination with fine particles.

10.2.2   Effects of increased reactivity on explosion severity

It is well known that increases in reactivity of gas produce substantial increases in the severity of an explosion in a given array. Similarly, for reactive gases such as ethylene or acetylene, severe explosions can develop in much less congested environments.

This is illustrated by the effect of changes in reactivity on the steady flame speed in lightly congested open arrays and the level of congestion that leads to flame runaway to severe explosion. A simple theory for predicting steady flame speeds in described in Atkinson (2012). Empirical data, for example that shown in Figure 249, suggest that the turbulent burning velocity (at low values of Karlowitz number) is

$$S_T = 17 \cdot \left(\frac{S_L}{S_L^0} \right)^{0.75} \cdot u'^{0.5}$$

S_L is the laminar burning velocity and S_L^0 is a reference laminar burning velocity (0.45 m/s)
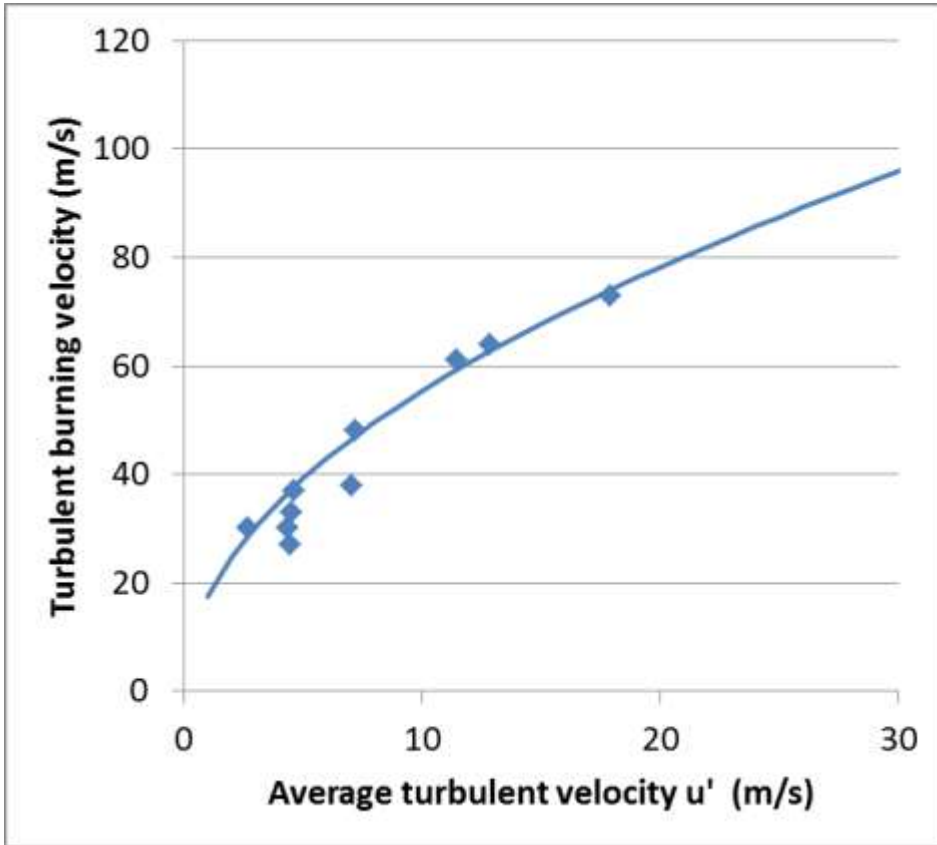u' is the turbulent velocity in the unburned gas

Figure 249: Burning velocity data at low Karlowitz numbers (Gardener et al 1998)

This expression for S_T depends on S_L and u' in a similar way in the turbulent burning relationship proposed by Bray (1990) and used in FLACS which is $S_T \propto u'^{0.412}.S_L^{0.784}$.

The turbulent velocity in the unburned gas depends on the speed of the unburned gas flowing past obstacles which is simply related the burning velocity. For flames in the open

$$U_{ug} = \left(\sqrt{E}-1\right)S_T \qquad \text{and} \qquad u' = t \cdot \left(\sqrt{E}-1\right) \cdot S_T$$

t is the turbulent intensity in the unburned gas i.e. $t = u'/U_{ug}$

Solving these equations gives the turbulent burning velocity

$$S_T = 17^2 \cdot \left(\frac{S_L}{S_L^0}\right)^{1.5} \cdot t \cdot \left(\sqrt{E}-1\right)$$

And for the (steady) flame speed

$$U_f = \sqrt{E} \cdot 17^2 \cdot \left(\frac{S_L}{S_L^0}\right)^{1.5} \cdot t \cdot \left(\sqrt{E}-1\right)$$

Figure 250 shows these results for propane and for propane preheated to 100 ˚C and 200 ˚C (212 – 392 F). This simple analysis is only applicable at low flame speeds where the flow is close to incompressible. Extension to higher flame speed (Atkinson 2015b) shows that where the simple theory predicts flame speeds over about 150 m/s the explosions run away to severe and no steady flame is possible.
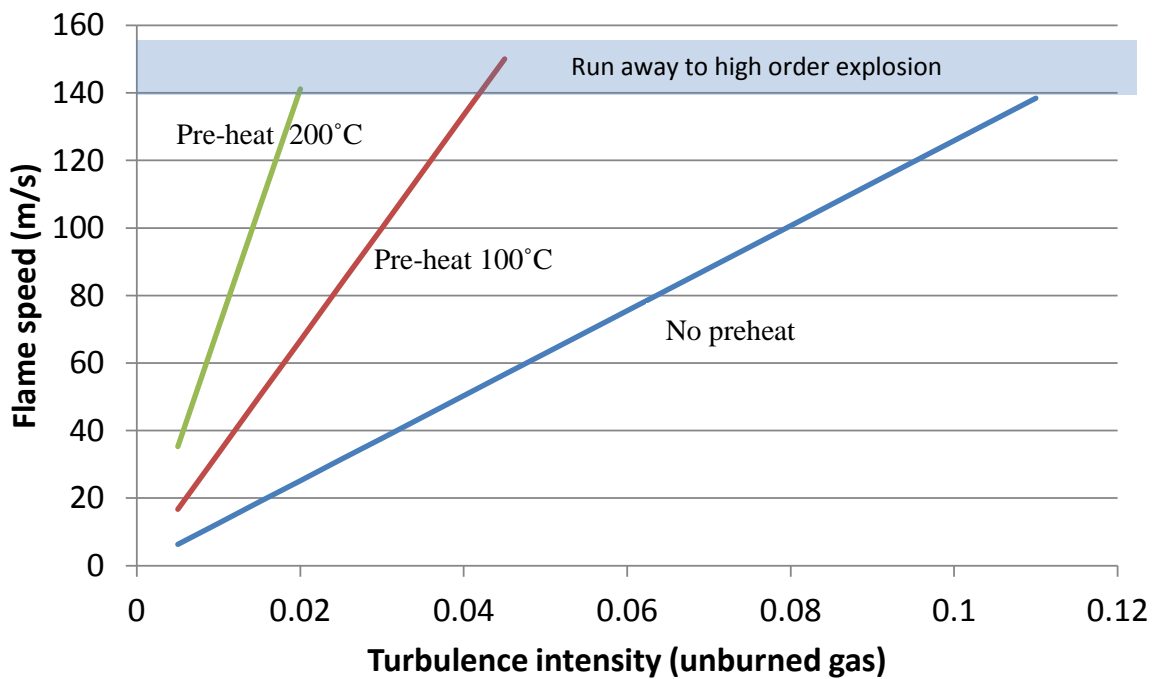
Figure 250: Steady flame speed as a function of turbulence intensity (E= 7). *Note in this case the height and width of the explosion front is assumed to be much greater that the thickness of the reaction zone – so there is no side venting. For narrower arrays the flame speed would be lower for a given turbulent intensity.*

This analysis shows that for propane at ambient temperature relatively high turbulence intensities are required to produce a severe explosion. This corresponds to relatively densely packed arrays of congestion elements.

On the other hand, if the unburned gas is pre-warmed then much lower turbulence levels will lead to explosions that will run away and produce severe overpressures

10.3   HEAT TRANSFER IN EXPLOSIONS PROPAGATING IN THE OPEN

One effect of blasts is to re-elevate dust that has accumulated on the ground. Figure 251 shows a sequence of images from a gas explosion in a plastic tent showing the formation of a layer of dust and the roll up of vortices in the boundary layer above the ground to form a large scale dust cloud ahead of the flame.
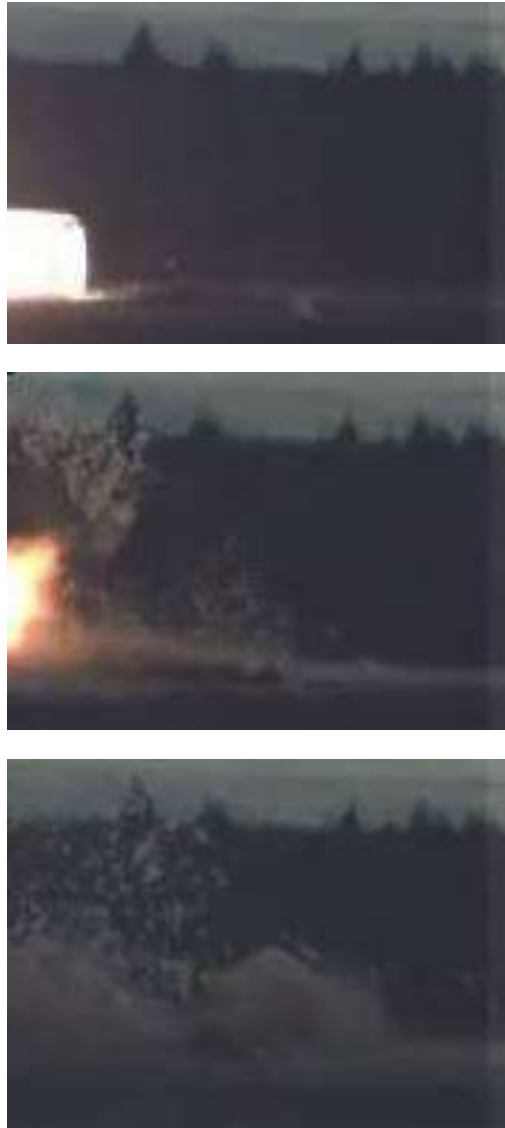

Figure 251: Re-elevation of dust caused by a gas explosion

Pressure waves will also raise dust from other surfaces e.g. vegetation, pipework etc.

When this occurs ahead of a flame that continues to propagate (at less than the speed of sound) there is a heating effect on the dust and the part of the gas cloud with which it is mixed.

Figure 252 shows a schematic of the heating of a dust layer above a surface. In this case the width of flame is assumed to be large so that a two-dimensional calculation is appropriate. A component of the incident radiant flux is normal to the dust layer and is effective in raising its temperature as the flame approaches.
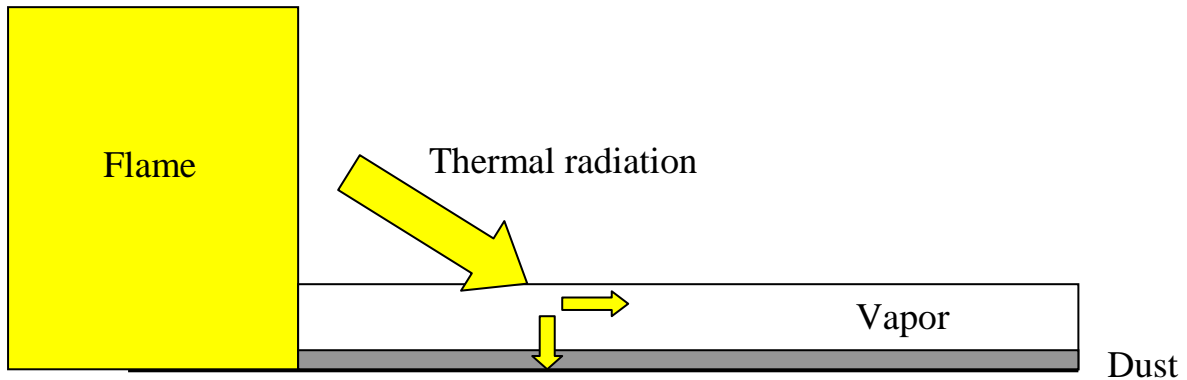
Figure 252: Schematic of radiative heating of dust and gas ahead of the flame front

Table 24 shows the final temperature rise dust layers of various depths as a flame approaches. It is assumed that the dust concentration is sufficient to fully absorb incident radiation and that the dust does not thermally decompose. This is reasonable for most minerals but not appropriate for finely divided organic matter over a temperature of about 350 ˚C (662 F). Also shown are temperature rises for isolated volume of dust of various sizes – such a volume might correspond to dust displaced from a leaf. Temperature rises are larger because such a target will absorb both components of the incident radiative flux. Heat losses have been neglected.

In all of these calculations the depth of the vapor cloud is 2m and expansion ratio is 7. The surface emissive power of the flame is assumed to be 1000 kW/m^2 (See 10.6)

Table 24: Temperature rises ahead of the flame caused by thermal radiation

Temperature rises in a dust layer above the ground		
Depth of dust layer	100 mm (8")	200 mm (16")
Temperature rise before arrival of the flame	430 ˚C	215 ˚C
Temperature rises in a dust volume (e.g. displaced from a leaf)		
Size of dust pocket	100 mm (8")	200 mm (16")
Temperature rise before arrival of the flame	834 ˚C	417 ˚C

It is clear that where dust is elevated by pressure waves running ahead of the flame then the gas through which the explosion propagates will be strongly heated in a layer above the surface. Flame propagation through such a layer would be greatly increased by the increased reactivity of the gas. For example a temperature rise of 230 ˚C raises the reactivity of propane to that of acetylene. The surface layer of gas is also typically associated with the highest levels of turbulence.

Similarly if dust is shaken from vegetation ahead of the flame, the gas with which it mixes may be substantially heated by the time the flame arrives. When the flame arrives, this gas will be combusted more quickly.

If the vapor cloud is deeper the reach of high thermal intensities form the burned layer will increase and the flame will advance proportionally faster.

10.4   IMPLICATIONS FOR EXPLOSION ANALYSIS

Contamination of pre-mixed gas clouds with fine particulates leads to pre-heating of unburned gas within a distributed reaction zone. This accelerates burning within the flame and increases the effective turbulent burning velocity. Consequently contamination with fine particulates may lead to a severe explosion in lightly congested environments where this would not occur for uncontaminated gas.

In large vapor clouds it is common for the release or early stages of the explosion to produce flows that disturb dust on the ground or on elevated structures or vegetation. For example the explosion may start in a congested or confined area and generate a pressure of many hundred millibars (several psi) without undergoing DDT. The effect of such an explosion would be to disturb dust in nearby areas and the explosion will then propagates through a gas cloud that may be heavily contaminated with dust.

Re-elevation of dust deposits is part of the normal sequence of events in dust explosions: usually an initial localised event raises dust that supports much more widespread and violent secondary explosions. The quantities of dust required for a dust explosion are typically larger than those that would be required to accelerate the burning of pre-mixed gas clouds.

An explosion model that does not include the effects of dust contamination on the development of explosions may significantly underestimate the severity of an incident.

Unfortunately these phenomena will not be easy to study because the effects only become really import in very extensive clouds. Table 25 compares the temperature rise in a 0.2 m (8 in) sized dust volme ahead of an explosion in a wide 2 m (6.5 ft) deep cloud (such as that at Buncefield) and in a 2 x 2 m (6.5 x 6.5 ft) gas tent test.

Table 25: Comparison of radiative effects in a large VCE and in a typical test geometry

Type of gas cloud	Temperature rise
Large pancake cloud 2m (6.5 ft) deep	417 ˚C
Gas tent 2m (6.5 ft) across	40 ˚C

In the test geometry the effects of radiation on flame propagation will be relatively small and may be confused with variations in ambient temperature in the tent.

Experiments at a substantial size will be required to provide experimental validation of the theory presented here.
.

10.5 INSTABILITY IN BURNING OF VAPOR CLOUDS CONTAMINATED WITH DUST

Combustion of clouds contaminated with particles is more likely to proceed in an unstable manner than is the case for uncontaminated clouds. The temperature of unburned gas will increase throughout a distributed reaction zone which may lead to a phase of rapid burnout and potentially a localised peak in pressure. When pre-heated gas has been consumed the rate of burning will fall until another distributed reaction zone forms. This means that there may be episodes of very rapid burning and localised high pressures even if the overall speed of the flame is sub-sonic. In this case the pressure waves associated with episodes of rapid burn-out would travel ahead of the flame front and could provide the means to re-elevate dust in the unburned gas. This mechanism could explain the damage observed in a number of large VCEs (Buncefield, Jaipur) in which flames apparently travelled at sub-sonic speeds (on average) but showed evidence of widespread episodes of more rapid combustion.

Special conditions are required to recover forensic evidence of variations in explosion pressure over a few metres. A uniform set of indicators are required that respond differently to pressures in the range approximately 1-5 bar (14.5- 72 psi) and these indicators must not be moved by the explosion.

Figure 253 shows a set of drums of lube oil at Jaipur. These were in an open storage area, well away from site roads and the point of ignition. The location was roughly 150 m (492 ft) from the source of vapor and a similar distance from the outer edge of the cloud. The explosion passed along the line of drums from left to right. Deformation of the drums is largest in a set of four or five drums in the centre of the set – corresponding to higher overpressures in an area two or three metres across. Variations in overpressure are unlikely to be caused by large horizontal gradients in cloud fuel concentration because, over the long period of time during which the cloud accumulated, these would be removed by buoyancy driven flows.

Figure 253: Evidence of rapid horizontal variations in explosion pressure at Jaipur.

10.6 SURFACE EMISSIVE POWER OF PREMIXED FLAMES

The flame front is approximately two-dimensional if its width is very much greater than its height.

Assume the combustion occurs in a circular zone as shown in Figure 254 and the flame is fully emissive. The temperature of the flame is less than the adiabatic flame temperature because of radiative losses from the reaction zone.
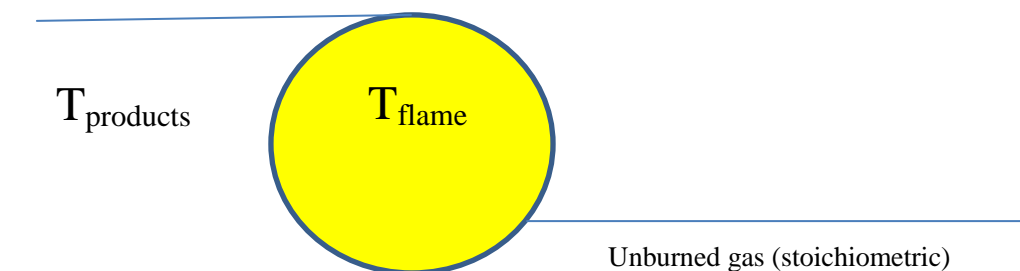

Figure 254: Schematic of a two-dimensional premixed flame – moving left to right

If the emissive zone is as shown the rate of radiative loss is $I_{flame}. \pi E.L = \sigma T_{flame}^4. \pi E.L$

This should equal the rate of heat loss from products i.e.

$\sigma T_{flame}{}^4 . \pi E.L = Cp. \rho VL(T_{adiabatic} - T_{products})$

Substituting for $T_{products}$ using $T_{flame} \sim (T_{adiabatic} + T_{products})/2$

$\sigma T_{flame}{}^4 . \pi E.L = Cp\, 2\rho VL(T_{adiabatic} - T_{flame})$

This equation gives the variation of flame surface emissive power with flame speed shown in Table 26. The following inputs were used

$\epsilon = 7$ (Expansion ratio)
$C_p = 1000$ J/kg/K
$T_{adiabatic} = 1980$'C

Also shown are corresponding results for a three-dimensional flame in a square test tunnel dimension L x L. In this case the reaction zone is assumed to be a cylinder with diameter and length of $E^{1/2}$ L.

Table 26: Variation of surface emissive power with flame speed

2D flame				
Flame speed (m/s)	150	100	50	25
Flame emissive power (kW/m^2)	1202	1110	907	675
3D flame				
Flame speed (m/s)	150	100	50	25
Flame emissive power (kW/m^2)	1110	997	773	550

These prediction fit with the Buncefield JIP measurements of surface emissive power of around 600 kW/m^2 for an emissive flame (seeded with soot) travelling with speed of roughly 20 m/s (SCI, 2014).

11 APPENDIX 3: PLASTIC DEFORMATION OF SCAFFOLD POLES, FENCE POSTS AND STREET LAMPS

There are two requirements for a beam to show distributed plastic deformation (continuous curvature) rather than concentration of plastic deformation in an area where the moment is highest.

1. Duration of the impulse.
2. Magnitude of energy transfer

11.1 DURATION OF IMPULSE

The duration must be so short that there is insufficient time for transfer of force (by transverse flexural waves) along the beam to the place where the moment of forces exerted at the beam supports is greatest.

The fundamental frequency of a beam simply supported (pinned) at both ends is

$$f = \frac{1.57}{L^2}.\sqrt{\frac{EI}{m}}$$

L is the length of the beam
E is the elastic modulus
I is the moment of area of the beam
m is the beam mass per unit length

11.1.1 Example 1: A steel scaffolding tube

Outside diameter	48mm	
Wall thickness	4mm	(I= 1.3 x 10^{-7} m^4 , E =200 GPa)
Mass per unit length	4 kg	
Length	2 m	

Calculated frequency f = 31.4 Hz   (ω = 197 s^{-1} – angular frequency)

Period of oscillation T_o= 32 ms.

For transfer of momentum along the beam to be negligible the duration of the impulsive load should be much less than the period of oscillation $T_{impulse} \ll T_o$.

Another way of looking at this is via the inward speed of flexural waves from the supports. These waves are dispersive i.e the wave speed a function of wavelength.

$$c_{wave} = \sqrt[4]{\frac{\omega^2 EI}{m}}$$

The fundamental angular frequency is most appropriate in this equation as it corresponds to waves that bend the beam with maximum deflection at the point of maximum moment.

In the above example

$$c_{wave} = \sqrt[4]{\frac{\omega^2 EI}{m}} = 126 \text{ m/s}$$

The time taken for these waves to travel from the support to the centre of the beam (a distance of 1m) is 8ms. If a scaffold pole like this is bent by an impulse briefer than this then the strain will be distributed along its length; rather than being concentrated around the point of maximum imposed moment (the mid-point in this example). The impulse associated with drag forces from a 3m deep detonation is short enough to satisfy this criterion.

11.2 MAGNITUDE OF ENERGY TRANSFER

If a short impulse transfers momentum to the beam much more quickly than momentum can be redistributed along the beam by flexural stiffness then central parts of the beam initially accelerate as they would if unrestrained.

If the dynamic pressure impulse is M then the momentum transfer P to the beam (per unit length) is

$$P = M.A.C_d$$

    A is the cross section of the beam in the (normal) flow per metre of length
    C_d is the drag coefficient[8]

In addition to the drag on the beam based on undisturbed dynamic pressure, there are two additional effects which may significantly increase or even dominate the momentum and energy transfer:

1. Shock reflection on the upstream face of the beam. This raises the upstream pressure by about 20 bar (290 psi) for a short period.
2. Failure of the detonation immediately behind the beam. The area affected by detonation failure may extend beyond the width of the obstacle especially if obstacle width and detonation cell size are comparable. The pressure in this area will decline by about 18 bar (261 psi). The duration of this additional impulse depends on the extent of the detonation failure.

---

[8] *The maximum Mach number is around 0.8. An average (approximate) value of Cd = 1.4 has been chosen. Gowen,F.E. and Perkins E.W. (1953), **Drag of a circular cylinder at a wide range of Reynolds and Mach Number**, NACA Technical note 2960.*

The calculation presented below is based only on drag forces with dynamic pressure calculated in the undisturbed flow and corresponds to a lower limit on the momentum transfer[9].

The energy accumulated by the beam (per unit length) is

$$E = \frac{P^2}{2m} \qquad \text{m is the mass per unit length}$$

Calculations for detonation in a 3m deep stoichiometric propane/air cloud by Fluid Gravity gave a dynamic pressure impulse of 580 Pa.s (with a duration of 4-5ms).

11.2.1   Example 1: Steel scaffold pole (as above)

Outside diameter	48mm	$A = 0.048 \text{ m}^2/\text{m}$
Mass per unit length	4 kg	
C_d	1.4	

The momentum transfer per unit length is 0.048 x 1.4 x 580 = 39 N.s/m

Energy accumulated during the positive phase (per metre) = $39^2/8$ = 190 J/m

11.3   ENERGY REQUIRED FOR DEFORMATION TO THE ELASTIC LIMIT

The energy required for elastic bending of a beam to a (uniform) curvature of κ is

$$E \text{ (per metre)} = \frac{1}{2}\kappa^2.E.I$$

κ is the reciprocal of the radius of curvature, E the elastic modulus and I the moment of area

For a tube plastic deformation first occurs when

$$\kappa = \frac{\varepsilon_{yield}}{r_{tube}} \quad \text{where } \varepsilon_{yield} \text{ is the yield strain (approx. 0.002 for steel)}$$

11.3.1   Example 1: Steel scaffold pole (as above)

Outside diameter   48mm

ε_{yield} = 0.002

$\kappa_{yield} = \dfrac{0.002}{0.024}$ = 0.083   (Radius of curvature = $1/\kappa$ = 12 metres)

I= 1.3×10^{-7} m^4

E =200 GPa

Energy (per metre) require to bend to the elastic limit = 89 J/m

---

[9] *Preliminary FE work by the Steel Construction Institute suggest that the drag impulse may be too slow to produce continuous curvature and that more impulsive pressure forces associated with the impinging detonation must play an important role (Private Communication, 2015).*

Energy input from drag forces (Section 11.2) exceeds the amount required to flex the scaffold pole to the elastic limit. Some permanent plastic deformation is to be expected for a 3m deep detonation.

11.4 EXAMPLE 2: STEEL ANGLE IRON (RESTRAINED AT BOTH ENDS)

Dimensions (section)	40 mm x 40 mm x 5 mm thick
Length	2 m
Mass density	2.9 kg/m
I (second moment of area)	5.5 x 10^{-8} m^2

$$f = \frac{1.57}{L^2}.\sqrt{\frac{EI}{m}} = 24.1 \text{ Hz} \qquad (\omega = 151 \text{ s}^{-1})$$

$$c_{wave} = \sqrt[4]{\frac{\omega^2 EI}{m}} = 96 \text{ m/s}$$

Flexural waves at the fundamental frequency take about 10 ms to travel from supports to the middle of the post. Shock loading much quicker than this will produce distributed curvature. The impulse associated with drag forces from a 3m deep detonation may be short enough to satisfy this criterion. Impulsive forces due to shock reflection would definitely be quick enough.

Response to a detonation in a 3m deep cloud (Positive drag impulse 580 Pa.s)

> Momentum transfer per unit length is 0.056 (max width) x 1.4 x 580 = 45.5 N.s/m
> Energy accumulated during the positive phase (per metre) = 45.5^2/5.8 = 356 J/m

The energy required for elastic bending of the angle iron to a (uniform) curvature of κ is[10]

$$\text{E (per metre)} = \frac{1}{2}\kappa^2 .E.I = \frac{1}{2}.\ 0.124^2 .\ 2 \text{ x} 10^{11} \text{ x } 5.5 \text{ x } 10^{-8} = 84 \text{ J/m}$$

Energy input from drag forces substantially exceeds the amount required to flex the angle iron to the elastic limit. Some permanent distributed plastic deformation is to be expected for a 3m deep detonation and for significantly shallower clouds.

If the length of the equal angle iron section is L and thickness is t, then the energy absorbed from the drag impulse is proportional to L/t and the energy required to bend to the plastic limit is proportional to Lt. The ratio of these quantities is consequently proportional to$1/t^2$. The tendency to continuous curvature is therefore independent of L and decreases with thickness as $1/t^2$.

---

[10] *assuming that the mode of bending is such that maximum distance to the neutral plane is 16mm*

For example the analysis above suggests the ratio of kinetic energy accumulated to that required for plastic deformation in 40 x 40 x 5mm angle would be 356/84 = 4.2 for a 3m deep detonation. For the 50 x 50 x 6mm material used in detonation tests (Figure 204 and Figure 205) the ratio would be 4.2 x (52/62) = 2.9. Again plastic deformation is to be expected and this fits the experimental evidence.

Angle iron 50 x 50 x 6mm is a very common choice for the main bearers in chain link fencing 40 x 40 x 5mm is used for intermediate supports. The degree of restraint in this case depends on the angle at which the detonation strikes the fence and the type of top bracing. Different wave speeds and frequencies apply if the posts are effectively cantilevered

11.5 EXAMPLE 3: STEEL TUBULAR STREET-LIGHT SUPPORT

Outside diameter	76mm
Wall thickness	3mm
Length	6m
Mass density	5.4 kg/m
I (second moment of area)	4.6 x 10^{-7} m^2

Response to a detonation in a 3m deep cloud (Positive drag impulse 580 Pa.s)

Momentum transfer per unit length is 0.076 x 1.4 x 580 = 61.7 N.s/m
Energy accumulated during the positive phase (per metre) = 52.9^2/10.8 = 352 J/m

The energy required for elastic bending of the street-light support to a (uniform) curvature of κ is

$$E \text{ (per metre)} = \frac{1}{2}\kappa^2.E.I = \frac{1}{2} . 0.053^2 . 2 \times 10^{11} \times 4.6 \times 10^{-7} = 129.2 \text{ J/m}$$

In this case the energy input is again in excess of that required to bend to the elastic limit.

11.6 EXAMPLE 4: STEEL TUBULAR FENCE POST

Outside diameter	50mm
Wall thickness	2mm
Length	2m
Mass density	2.4 kg/m
I (second moment of area)	8.7 x 10^{-8} m^2

Response to a detonation in a 3m deep cloud (Positive drag impulse 580 Pa.s)

Momentum transfer per unit length is 0.05 x 1.4 x 580 = 40.6 N.s/m
Energy accumulated during the positive phase (per metre) = 40.6^2/4.8 = 343 J/m

The energy required for elastic bending of the street-light support to a (uniform) curvature of κ is

$$\text{E (per metre)} = \frac{1}{2}\kappa^2 . E.I \quad = \frac{1}{2} . \ 0.08^2 . \ 2 \text{ x} 10^{11} \text{ x } 8.7 \text{ x } 10^{-8} = 55.7 \text{ J/m}$$

In this case the energy input is again well in excess of that required to bend to the elastic limit.

Much shallower clouds producing briefer positive impulses would be sufficient to bend posts like this.

11.7   RESEARCH REQUIREMENT

Detonation testing of a range of common types of beam element – including those considered above- would be extremely valuable. A large number of different specimens could be examined in a single large scale test

Variables to be studied should include:

Beam section and thickness
Beam length
Types of restraint
Cloud depth

Parallel finite element modelling of these elements is also practical with current technology and if successful this would provide a means to extend understanding to different types of beam without further testing.

Calculation of the impulsive loading associated with detonation shock reflection and detonation failure from first principles would be desirable but may be difficult and uncertain. An understanding of the impulsive forces that apply may have to be developed from comparisons between experiments and finite element modelling.

12   REFERENCES

ARIA (undated), *Explosion de gaz dans les unités craquage catalytique et gas plant d'une raffinerie Le 9 novembre 1992,La Mède [Bouches du Rhône] France*, ARIA report No. 3969

Atkinson (2006), *Buncefield Investigation: Forensic examination of an emergency pumphouse,* HSL Report FS/06/11.

Atkinson, G., Gant, S.E., Painter, D., Shirvill, L.C. and Ungut, A. (2008) *Liquid dispersal and vapor production during overfilling incidents*. Proc. IChemE Hazards XX Symposium & Workshop, Manchester, UK.

Atkinson G.T. (2011a) *Blast damage to storage tanks and steel clad buildings*. Process Safety and Environmental Protection, Vol. 89, No. 6, pp. 371-381.

Atkinson G.T. (2011b) *Buncefield: A violent, episodic vapor cloud explosion* . Process Safety and Environmental Protection, Vol. 89, No. 6, pp. 371-381.

Atkinson, G. (2012) *Effects of constraints on gas flow on the severity of vapor cloud explosions*, IChemE Symposium 158.

Atkinson, G. and Gant, S.E. (2012) *Buncefield Investigation – Liquid Flow and Vapor Production*, HSE Research Report RR936, HSE Books: Sudbury. Available from http://www.hse.gov.uk/research/rrhtm/rr936.htm.

Atkinson, G. and Coldrick, S. (2012a) *Vapor cloud formation – Experiments and modelling*, HSE Research Report RR908, HSE Books: Sudbury. Available from http://www.hse.gov.uk/research/rrhtm/rr908.htm.

Atkinson, G. and Coldrick, S. (2012b*) Buncefield Research Phase 2, Work Package 2: Vapor cloud formation (Final Report),* FP/12/18, July 2012. Available from http://www.fabig.com/Files/FABIG/BEM_JIP_Phase_II-WP2-Final_Report.pdf.

Atkinson, G. and Pursell, M. (2013) *FABIG Technical Note 12 - Vapor cloud development in over-filling incidents*, April 2013. Available from http://fabig.com/video-publications/TechnicalGuidance#,

Atkinson, G. (2014) *Assessment of explosion severity at small scale LNG sites,* HSL Report MH/14/66. Available from HSL.

Atkinson G., Coldrick S., Gant S.E. and Cusco, L. (2015) a *Flammable vapor cloud generation from overfilling tanks: Learning the lessons from Buncefield,* Journal of Loss Prev., Vol 35, p329-338.

Atkinson, G. (2015)b *Explosion assessment at small LNG sites*, IChemE Hazards XXV Conference.

Bray K.N.C. (1990). *Studies of the turbulent burning velocity*, Proc. R. Soc. Lond. A, 431, 315–335.

Briggs, G.A., Thompson, R.S. and Snyder, W.H., (1990), Dense gas removal from a valley by crosswinds, J. Haz. Mat., Vol **24**, p.1-38.

Buncefield Major Incident Investigation Board (2007) *The Buncefield Incident – 11th December 2005 – The Final Report of the Major Incident Investigation Board, Vol. 1.*, ISBN 978-07176-6270-8. Available from http://www.buncefieldinvestigation.gov.uk, accessed 19 August 2013.

Casella (2002), *Report on a second study of pipeline accidents using the Health and Safety Executive'srisk assessment programs MISHAP and PIPERS,* HSE Research Report RR036.

Chen, A (2013), Structural Response to Vapor Cloud Explosions, PhD Thesis, Department of Civil and Environmental Engineering, Imperial College London, UK.

CSB (US. Chemical Safety and Hazard Investigation Board) 2015, *Caribbean Petroleum Tank Terminal Explosion and Multiple Tank Fires (October 23rd 2009) – Final Investigation Report*

Coldrick, S., Gant S.E., Atkinson G.T. and Dakin, R. (2011) *Factors affecting vapor production in large scale evaporating liquid cascades*. Process Safety and Environmental Protection, Vol. 89, No. 6, pp. 371-381.

Davis, S.G., Groethe, M.A., Engel, D., and van Wingerden, K. 2016 *Large Scale Testing - Development of Advanced CFD Tools for the Enhanced Prediction of Explosion Pressure Development and Deflagration Risk on Drilling and Production Facilities,* Offshore Technology Conference, OTC-27290-MS.

DNV (2013) Phast Version 7 Software, DNV Software, London, UK. Available from http://www.dnv.com/software, accessed 19 August 2013.

Drysdale, D. (1986) An Introduction to Fire Dynamics , John Wiley and Sons, Chichester.

Fluid Gravity (2009), "*Further pancake cloud detonation results*" Fluid gravity Client Report CR106/09.

Gant, S.E., Heather, A.J. and Kelsey, A. (2007) *CFD modelling of evaporating hydrocarbon sprays.* Health & Safety Laboratory Report CM/07/04. Available from HSL: Buxton.

Gant S.E. and Atkinson G. (2011) *Dispersion of the vapor cloud in the Buncefield Incident,* Process Safety and Environmental Protection, Vol. 89, No. 6, pp. 391-403.

Gant, S.E. and Atkinson, G. (2012) *Flammable Vapor Cloud Risks from Tank Overfilling Incidents,* HSE Research Report RR937, HSE Books: Sudbury. Available from http://www.hse.gov.uk/research/rrhtm/rr937.htm, accessed 19 August 2013.

Gardner, C.L., Phylaktou, H. and Andrews, G.E. (1998) *Turbulent Reynolds number and turbulent flame quenching influences on explosion severity with implications for explosion scaling*, IChemE Symposium Series No. 144. pp. 279–292, Paper 23.

Gelfand,B.E and Tsyganov S.A., (undated), *Gas pipeline accident in Bashkir autonomous Soviet Republic (Near the City of Ufa)"* Private Communication.

Grachev, A., Andreas, E., Fairall, C., Guest, P. and Persson, P. *The Critical Richardson Number and Limits of Applicability of Local Similarity Theory in the Stable Boundary Layer,* Boundary-Layer Meteorology: Volume 147, Issue 1 (2013), Page 51-82.

Harris, R.J. and Wickens, M.J. (1989) *Understanding vapor cloud explosions – an experimental study*. 55th Autumn Meeting of the Institution of Gas Engineers, Kensington, U.K.

Horton, R.E. (1967) *Weir experiment, coefficients and formulas,* Water-Supply and Irrigation Paper No. 200, US Geological Survey.

Johnson, D.M., (2012) *Characteristics of the vapor cloud explosion at the IOC terminal in Jaipur.* Global Congress of Process Safety, Chicago, April 2012.

Makhviladze,G.M. and Yakush, S.E. (2005) *Large unconfined fires and explosions,* , Proc of Comb. Inst., Volume 29, p195-210.
MoPNG Committee (2010) (constituted by Govt. of India) *Independent Inquiry Committee Report on Indian Oil Terminal Fire at Jaipur on 29th October 2009;* completed 29th January 2010. Available from http://oisd.nic.in, accessed 19 August 2013.

Pasquill, F. (1961). The estimation of the dispersion of windborne material, The Meteorological Magazine, vol 90, No. 1063, pp 33-49.

Poinsot, T. and Veynante, D. (2005) *Theoretical and Numerical Combustion*, Pub.R.T. Edwards Inc.

Pritchard D. K., Blanchard R. J., Hedley D. and Eaton G. T., (2006) *Buncefield investigation: Blast damage assessment,* Report Number EC/06/69.

SCI (2009). *Buncefield Explosion Mechanism Phase 1,* Research Report RR718 HSE Books, Sudbury (http://www.hse.gov.uk/research/rrhtm/rr718.htm).

SCI (2014) *Dispersion and Explosion Characteristics of Large Vapor Clouds Volume 1 – Summary Report,* Steel Construction Institute, SCI Document ED023

Van den Berg, A.C 1985 The multi-energy method: A framework for vapor cloud explosion blast prediction, Journal of Hazardous Materials, Volume 12, Issue 1, , Pages 1-10

Weidlinger Associates (2009) "*Characterising the response of reinforced concrete cladding panels to vapor cloud explosions*", Report DES07021_090225_v2.0